Evaluation Of Finite Element Analysis Techniques Applied To A Floating Offshore Wind Turbine

Mohamed Abdalla Mohamed Almherigh

School of Computing, Science & Engineering

University of Salford, Salford, UK

Ph. D Thesis

Submitted in Partial Fulfilment of the Requirements of the Degree of Doctor of Philosophy, January 2005

Abstract

The work presented here is a research thesis of the Ph. D programme in The School of Computing, Science & Engineering at The University of Salford UK. The work presents the evaluation of using explicit finite element techniques for structural non-linear dynamic analysis of a floating offshore wind turbine used for harnessing wind kinetic energy and converting it to electricity. The LS-DYNA3D explicit finite element analysis programme is used in performing the evaluation of the analysis and in creating a full scale model typical to the one evaluated. The developed model (case study) is a 1.4MW power rated floating 3 blades turbine elevated at 46.5 m above main sea level a top a tripod lattice steel tower firmly resting on a moored floating concrete hull buoy, positioned on a concrete circular disk. The mooring cables supporting the floating units in the multi unit farm are designed to share seabed anchoring piles for economic reasons. The model is intended for use in moderately deep waters of up to 500m. The State-of-the-art report is presented concerning wind energy technology, floating offshore wind structures and important features of the LS-DYNA3D code. The theoretical basics for service loads experienced by the floating wind turbine are explored and the loads are quantified. The Verification and validation work on developed small models is presented to ensure confidence in the developed full scale model and the evaluation of the finite element techniques which may be applied to such structures. Development of full scale model, material properties, loads and boundary conditions are presented. Recommendations both for this model and future development are accordingly made.

Acknowledgements

The work presented here is a research based theses for a Ph. D degree programme in the School of Computing, Science & Engineering at The University of Salford, Salford, Manchester, UK under the supervision of Dr. Laurence Weekes of Civil Engineering.

My sincere thanks go to my supervisor, Dr. L. Weekes for his numerous guidance, encouragement and valuable comments throughout the process of the research work, Dr. Weekes help, availability and positive attitude were highly valuable and was accountable friend whenever needed during the work time period.

Thanks and appreciations are extended to El-Fateh University, Tripoli, Libya for providing the financial support for this research degree work.

Worm thanks go to the academic staff, my post graduate colleges, administrative staff and technicians of The School of Computing, Science & Engineering at The University of Salford, Salford UK for any help I received.

Sincere thanks and appreciations go to my *wife* and my '*three daughters and three sons*' for their patience, help and encouragement during the period of this work.

Thanks also extended to the support team of the software providers LSTC and ETA both US based, for any feedback or help throughout the research course.

Table of Contents

Content **Page**

Content **Page**

Content Page

Content **Page**

Content Page

Content **Page**

List of Tables

Number	Title	Page
Table 4-1	Stability positions for buoyant 2-D box	97

List of Figures

CHAPTER I

Introduction

1.1 Background

The industrial revolution led to the inventions in all fields of technology this is in turn led to a cycle of "more chasing more" which resulted in more demand for energy, thus as more fossil fuels are consumed contributing to the already existing environmental problems, this leads Mankind to the dead lock of running out of fuel. Possibly the main problem is the fact that these resources are non-renewable. The coal, oil and natural gas resources that are used today took millions of years to form and cannot easily be replaced. At the present usage rate, known reserves of coal will be gone in 200 years, natural gas in 55 years, and oil in 50 years. Unless alternative sources of energy are found, there will be no energy left to run the machine that became crucial to human existence. Since wind is free and renewable resource that is also a clean, non-polluting form of electricity, there are many advantages to using it as a form of energy. Unlike other forms of power wind plants emit no air pollutants or greenhouse gases and can be located on land that is also used for grazing and farming or offshore. Wind power is domestic, reliable and can create more jobs at no environmental costs, a prescription mostly needed for growing economy.

The work reported here is an attempt to address the energy demand issue from a structural point of view by looking closely and in detail to the possibility of application of advanced finite element techniques for analysis of the yet most comprehensive kind of support for wind energy converters. The model to be investigated in this work is based on the float concept employing a state-of-the-art Finite Element Code namely LS-DYNA3D. Hopefully the outcome of this work will result in major improvements in the analysis and design approaches employed for offshore wind industry particularly its structural and hence economical performance.

The work presented shall include (i) the evaluation of non-linear dynamic analysis techniques available in the explicit code as applied to a floating offshore wind energy converter (ii) calculation of aerodynamic and hydrodynamic service loads expected to be experienced by the full scale

floating offshore wind turbine (iii) the development of a full scale model using LS-DYNA3D explicit finite element code. The good features included in the explicit code such as ALE, non-reflecting boundaries, constraint joints, contacts, multi-materials, initial volume fraction or geometry features and the flexibility in creation and application of load curves are explored and employed in the investigation. The fact that the focus is on structural engineering does not necessarily prevent from highlighting related issues which are crucial at the design stage and therefore reflected as factors directly influencing the analysis process. The evaluation of the analysis it self is aimed to address gaps in this field of structural engineering leading if possible to the avoidance of conservatism in the design approaches which is the key in economical performance, and constitutes new horizons of challenges in structural design for such harsh offshore environment.

1.2 Structure of the Report

- **In Chapter II, a state-of-the-art-report is presented introducing wind energy concepts and terminology, with special emphasis being put on the offshore wind energy and floating wind converters, its benefits and reasons. The explicit finite element analysis code 'LS-DYNA3D' and its suitability for this type of analysis, previous analysis as well as standards are addressed. Conclusions and findings of this report paving the way to the rest of the thesis are presented.**

- **In Chapter III, LS-DYNA3D the code used in the work is introduced, its main features and capabilities are pinpointed, theoretical formulation of the service aerodynamic and hydrodynamic loads and conditions are deeply discussed and developed in a concept leading to their quantification.**

- **In Chapter IV, relevant features of the LS-DYNA3D code applied in the verification work and buoyancy of floating bodies are presented and deeply investigated. Theoretical calculation for buoyancy of characteristic verification developed 2-D model is presented, the model**

is analyzed and the results from the two approaches are compared. Further 3-D models are developed, analyzed and presented to give more confidence in the used features in the code and the methodology used. Conclusions and relevant critical discussion is presented.

- **In Chapter V the developed detailed full scale floating wind converter is presented, the gravity, aerodynamic and hydrodynamic loads anticipated to affect the model once in service are calculated and presented in a format acceptable to the LS-DYNA3D code and ready for the analysis phase.**

- **In Chapter VI discussions, conclusions and recommendations for future work extracted from the thesis are addressed.**

- **List of the references and consulted literature throughout this thesis and related to it are presented.**

- **The appendices regularly called in the thesis text are presented. Appendix-A1 showing important theoretical background of LS-DYNA3D code related to the analysis. Appendix-A2 presents material and element properties, constraints, coupling functions used in creating the different parts of the full scale model. Appendix-A3 presents the theoretical basis used for the formulation of aerodynamic loads for wind turbine analysis. Appendix-A4 presents a MathCAD sheet formulation of the 'Grüneisen equation of state' for internal pressure initiation in the water part.**

CHAPTER II

State-Of-The-Art Report

2.1 Introduction:

The word engineering is lost some where between science and technology. Science, engineering, technology and innovation are very closely linked and interrelated. Wind energy, however as a part of engineering is no exception from this interrelated process.

Wind energy, therefore, has two parts: the "know what" or 'simply knowledge' and the "know how" or 'process'. The first part, is the growing body of facts, experience and skills in this field of application, while, the second part is the creative process that applies knowledge and experience to find likely solutions, which uses experience and informed judgement to decide on the best solution.

In fact wind turbines are never installed so that conventional power stations can be closed prematurely; building wind farms, avoids the need to build new fossil fuel or nuclear power plants. Expanding the use of wind energy will increase energy diversity and improve the security of electricity supply, thereby reducing the international political risks and environmental damage (global warming due to greenhouse gases and acid rain due to sulphur and nitrogen emissions) associated with fossil fuels, the volatility of oil and gas prices, and hazards associated with nuclear power and depleting natural resources.

Despite its good reputation as renewable, green, sustainable, reliable and available energy, wind energy only recently has proven to be economically feasible and commercially competitive with other sources of energy, (a vital reason for consumers to convert to it). Wind energy coincides well with periods of peak electricity demand, which often peaks on cold, windy, winter days in the northern hemisphere just when wind turbines are at their most productive.

Due to the mentioned factors, and adding to that, less maintenance and operational requirements are needed; wind energy is perfect for farms, remote communities, islands and isolated locations that are not connected to utilities,

(areas where wind mechanical energy was in use for pumping water for decades).

2.2 Where Does Wind Energy Come From?

In physics the word energy is defined, as the amount of work a physical system is capable of performing. According to the well known principle of conservation of energy, energy cannot be consumed, destroyed or created. Energy however, may be converted or transformed into different forms: The kinetic energy of moving air molecules may be converted to rotational energy by the rotor of wind turbine, which in turn may be converted to electrical energy via an attached generator. Whenever energy is converted from one form to another, part of the energy from the source is converted to heat energy. Therefore, the use of the common expression of energy loss is absolutely wrong but rather, means that part of the energy from the source cannot be used directly in the next link of the energy conversion system, due to its conversion to heat. In fact most if not all mechanical systems, e.g. rotors, gearboxes and generators are never 100% efficient, because of heat losses due to friction in the bearings, or friction between air molecules. As fossil fuels burned, loosely speaking, the global potential for future energy conversion is reduced. Since the vast majority of wind turbines produce electricity, usually their performance is measured in terms of the amount of electrical energy they are able to convert from the kinetic energy of the wind. This energy is measured in kilowatt hours (kWh) or megawatt hours (MWh). Based on the reality, that energy cannot be created but only converted into different forms, wind turbines should be rather called wind converters, although the word turbine is widely used throughout the literature and is understood to have the same meaning as converter.

Power is energy transfer per unit of time; electrical power is measured in watt (W) or its multiplications. Power may be measured at any point in time, whereas energy has to be measured during a certain period of time, e.g. a second, an hour, or a year. The expression "horsepower" used in rating engines gives an intuitive idea that power defines how much "muscle" a motor

or a generator has, whereas, energy tells how much "work" a generator or motor performs in a certain time.

Wind energy is an indirect form of solar energy. Between 1-2% of the solar radiation that reaches the Earth is converted into energy in the wind, Hartwig and Goerge [77], Carlin et al [116]. Winds result from an unequal heating of the earth's surface, causing cooler dense air to circulate to replace warmer, lighter air. While some of the Sun's energy is absorbed directly into the air, most of the energy in the wind is first absorbed by the surface of the Earth and then transferred to the air by convection.

Seasonal variations in the speed and direction of the wind result from the seasonal changes in the relative inclination of the Earth towards the Sun, which in turn changes the patterns of differential heating. Daily, or diurnal, variation is caused by differential heating of local regions, such as adjacent land and oceans.

This air movement is complicated by a number of global scale factors such as the Earth's rotation, continents, oceans and topology. Airflow is rarely smooth, with most places experiencing fairly rapid changes in wind speed and direction. The wind speed also increases with the height above the ground, due to the frictional drag of the ground, vegetation and buildings. It is clear that any plans to harness the wind must take into account these variables.

2.3 Energy of the Wind:

The power in the wind is proportional to the cube of the wind speed or velocity $(\frac{1}{2}\ \rho A\ V^3)$ **as will be discussed later. It is therefore essential to have a detailed knowledge of the wind and its characteristics if the performance of wind turbines is to be estimated accurately. As is well known, the highest wind velocities are generally found on hilltops, exposed coasts and out at sea. Various parameters need to be known of the wind, including the mean wind speed, directional data, and variations about the mean in the short (gusts), daily, seasonal and annual variations, and variations with height. They are used to assess the performance and economics of wind plant.**

In order to create wind energy there is a process that must be completed to turn the wind into electricity. To start the process, the wind must pass over the airfoil shaped blade. It passes more rapidly over the longer or upper side of the airfoil, which creates a lower air pressure area above the airfoil. The pressure difference between the top and bottom surfaces of the blade results in a force called an aerodynamic lift. This force causes the airfoil to rise and this lift force causes rotation about the hub since the blades of the wind turbine are constrained to move in a plane with the hub at its centre. In addition to the lift force, another force called a drag force perpendicular to the lift force impedes rotor rotation. A relatively high lift-to-drag ratio is a prime objective in wind turbine design; this ratio can be varied along the length of the blade to optimize the turbine's energy output of various wind speeds, a subject of wide research activity and of concern to mechanical engineers and therefore outside the scope of this work.

The kinetic energy in a flow of air through a unit area perpendicular to the wind direction is ½ ρV^2 per unit volume or ½ V^2 per unit mass.

For an air stream flowing through an area A the mass flow rate is ρAV, therefore:

$$\text{Power, } W = (\rho AV) \times \frac{1}{2} V^2 = \frac{1}{2} \rho A V^3 \qquad 2.1$$

Where ρ is the air density (kg/m^3), V is the wind speed (m/s) and W is the power in Watts or Joules per seconds.

The air density ρ is a function of the air pressure and air temperature:

$$\rho = \rho_o \left(\frac{288B}{760T}\right) \qquad 2.2$$

Where ρ_o is the density of dry air at standard temperature and pressure (1.226 kg/m^3 at 288 K, 760mm of mercury) and T is the air temperature (K) while B is the barometric pressure in mm of mercury.

Both the pressure and the temperature are functions of height above sea level. Taking a typical density of air at sea level as 1.2 kg/m^3, the power becomes

$$W = 0.6V^3 \text{ per unit area} \qquad 2.3$$

At a wind speed V the energy is measured in watt-seconds passing through area A during time t is given by:

$$\text{Energy, } Wt = (1/2)\,\rho A V^3\, t \qquad 2.4$$

This is the total energy available for doing work on the wind turbine. Practically speaking, there is no change in the temperature of the air flowing through a wind turbine. This is also clearly the case in water turbines. In both cases the energy extracted using the change in fluid velocity, not through a change in temperature.

2.4 The World Wind Resources:

To estimate the global potential for wind energy it is necessary to know the mean wind speed over the earth's surface. This has been measured and the results are published in the form of wind atlases for countries, regions, and continents, even for the whole Globe. In fact these atlases are often depend on interpolation of wind data obtained form dispersed measuring stations, but still they can provide a useful estimate for the available wind resource for initial planning purposes, Barthelmie [18], Mathies [37] and Hartwig et al [77]. Walker et al [73] reported The World Energy Council (1994) as giving estimates of the global wind resource at about 27% of the earth's land surface experiences annual mean wind speeds higher than 5.1 m/s at 10 m above the surface. Only 4% of this area might be available for the electricity generating wind farm because of unsuitable terrain, urban areas, crop cultivation and other existing land use. Quoted from the last source assuming a generating capacity of 8 MW/km^2 and a capacity factor of 23%, it is estimated that the global potential for wind turbine power production is 20,000 TWh per year. For comparison (same source) in 1987 the total world electricity consumption was about 10,500 TWh (the prefix T stands for tetra or 10^{12}).

The mentioned estimate is for large scale grid-connected wind converters and it depends on a variety of assumptions. It does not include the potential for offshore wind energy developments or small-scale wind turbines used for water pumping or battery charging, feasible applications in wind speeds as low as 3 m/s. About 50% of the earth's land surface is exposed to mean annual wind speeds of between 4.4 m/s and 5.1 m/s quite suitable for small wind turbines (same source).

The outlook for future energy demand is that it is predicted to rise quite dramatically. It is supposed; Walker et al [73] that from 1998 to 2010 the world wide yearly electricity demand will rise by about 30% to about 20,825 TWh and by nearly 50% to about 27,326 TWh by 2020, with an annual growth of 2 percent. The former source estimated that the entire electricity demand for the earth could have been covered by the use of only 0.04% of the kinetic energy extracted from wind resources in theory. Clearly, there is a serious energy problem associated with environmental catastrophe and the only viable solution is wind energy. Based on the quoted estimation and given the renewable nature of wind, it is evident how much energy could be harvested from wind.

2.5 Vertical Wind Speed Gradient:

The wind speed at the surface is zero due to the friction between the air and the surface of the ground. The wind speed increases with height about 2 km above the ground the change in the wind speed becomes zero, Walker et al [73]. The vertical variation of the wind speeds and the wind speed profile are expressed in different functions. Two of the more common functions which have been developed to describe the change in the mean wind speed with height are based on experimental evidence, these are power exponent function and logarithmic function, Walker et al [73], Hartwig et al [77], Manwell [78]. The hub height of new generation wind energy converters is in the performance range around 1 megawatt lies over 60 metres above ground level for land based towers. The reliability of wind speed versus height must be treated with caution since they are based on extrapolation and very much dependent on the surroundings and terrain.

2.6 Wind Energy Trends:

Since the beginning of the modern wind energy era, which followed the oil crisis of the 1970s, the installation of wind turbines has regularly been considered as different nations have formulated their wind energy programmes. The arguments were and still are, based on the notion that the potential of wind energy on land in densely populated countries is limited

compared with total national energy demand, and that the countries with relatively long coastlines could increase their exploitable wind potential by installing wind turbines offshore. Yet, although wind speeds offshore are higher than those on land, integrating the converters electrical connections to the existing network will be more expensive to reduce energy loss. The challenge, therefore, is to balance those two counteracting parameters so that offshore wind energy is comparable in cost to electricity generated by land based wind turbines.

In order to sell the idea of offshore wind energy, cost reduction is the base line of all structural and technical activities; this necessitates a close consideration of:

- **Determining wind resources, in terms of speed, duration and site based on detailed measurements of near-shore and offshore areas and mountains regions.**
- **Integrating wind, wave and current loading in the structural analysis and design which will eventually lead to avoidance of over designed or conservative structure, and hence reducing the cost of the energy outcome.**
- **Careful consideration should be given to relevant environmental issues, associated with this new energy, namely, oil and gas mining, noise, military use, ship traffic routes, fishery, effects on fish and birds breeding, sand mining, erosion, visual impacts and the natural environment.**
- **Development of dedicated offshore concepts. Use low maintenance, direct-drive generator systems, transport, installation, and maintenance 'touch and go' systems, power electronics for optimal electricity transport.**

It has been recognised that the offshore waters of the British Isles are currently one of its principle energy sources, through its hydrocarbon deposits. Some of the gas accumulations in these fields are difficult to extract and utilize economically. Thus, combined use of this gas, with floating wind turbines could prove to be more economic. However, the cost of wind converters is falling and is expected to continue doing so over the coming decade and once more experience has been gained in building offshore

projects, the offshore construction industry is likely to find similar cost-savings.

2.7 Offshore Wind Energy:

Shortage of land sites in north-western Europe is one reason for this move offshore other reasons include significantly higher wind speeds than on land, and thus higher energy production at sea where wind speeds are believed to be higher than what was previously anticipated. The marine environment gives more stable winds with less turbulence and less wind shear, facilitating the design of cheaper turbines with a longer life span.

To be economic and hence competitive offshore wind parks (as they normally called) have to be as large as economically feasible, and must therefore, use large turbines. New foundation technologies, using steel rather than concrete will probably improve the economics of the offshore wind power dramatically. Wind turbines at sea would have a longer design lifetime due to lower mechanical fatigue loads due to less turbulence.

Up to now, most offshore energy installations were built in shallow waters near shorelines, so if the mentioned economy factor is to dominate, which means larger systems, the feasible choice will very likely be a floating system. The total wind power resources offshore are vast and will certainly be able to supply a significant proportion of electricity needs in an economic manner.

Generally, there are six reasons for justification of the move towards offshore wind energy:

i) Land shortage:

One of the prime reasons for offshore wind farms is the lack of suitable wind turbine sites on land; this is evident, for Europe where most if not all countries are densely populated or relatively flat landscape.

ii) Higher wind speeds:

Equally important, however, is the fact that wind speeds are often significantly higher offshore than onshore, an increase of some 20% is common, Krohn [58]. With the fact that wind energy increases with the cube of the wind speed,

the energy yield may be some 73% higher than on land, Krohn [58]. If turbines on land where to be located on good land sites, such as mountains or hill tops, where the wind speeds up significantly compared to flat terrain, in such situations, an onshore energy system is advisable.

iii) More stable winds:

In most wind turbine sites around the globe, the wind speed varies substantially, with high wind occurring rather infrequently, and low winds occurring most of the time. In most of the locations around the globe, as already mentioned, wind speeds happen to be positively correlated with peak electricity demand (more wind during the day than at night, more wind in winter than in summer). At sea, periods of complete calm are generally extremely rare, and quite short lived, thus the effective use of wind turbine generating capacity will be higher at sea than on land.

iv) More wind resources:

Offshore wind resources are enormous and ever lasting and it is believed to be several times larger than the projected energy consumption, theoretically 15 times current energy consumption world wide, Rehfeldt and Matthias [59], while for Europe, it is believed to be 8 times the current energy demand, Khün [60], the UK's offshore wind resource is equivalent to three times the current electricity usage and is some 33% of the total European potential, Pincott [64], Group [91].

v) Lower turbulence:

The temperature difference between the sea surface and the air above it is far smaller than the corresponding difference on land, particularly during the daytime. This means, that, the wind is less turbulent at sea than on land, which in turn, means lower fatigue load and thus longer serving time for turbines at sea than on land.

vi) Low surface roughness:

Another argument in favour of offshore wind power is; the generally smooth surface of water, which means that wind speeds do not increase as much with

the height above sea level as they do on land. This implies that it may be economic to use lower (and thus cheaper) towers for offshore wind turbines.

In addition to the technical and engineering advantages of offshore energy, it is the environmental factor which is the most encouraging for the future. Once again, the reduction of greenhouse and acid rain responsible gases is a genuine reason, positive impact on marine wildlife is observed and still under surveillance, which will be another decisive factor for the choice of offshore wind energy. Nevertheless, there will be additional cost due to the more expensive marine foundations, due to weather conditions access will be restricted and installations will be more expensive. Furthermore, the limited access for operations and maintenance will result in an additional penalty of reduced converter usage and hence less output.

2.8 Components of Wind Energy Converter:

Offshore wind energy system is usually made up of wind farms or parks, which vary in size according to the required energy outcome, however, due to the cost reasons, both the wind turbine and the wind farm have to be an optimum 'large' size compared to those onshore. The wind system (farm) in turn consists of a number of integrated wind turbines. A typical shallow water (bottom mounted) wind turbine is identical to land based turbine and comprises the following parts, Figure (2.2):

2.8.1 Rotor:

Consisting of a hub, blades (one, two or three) and transmission, the blades are driven by the wind driving the turbine generator as shown in Figure (2.1) and Figure (2.2). Sometimes gearing is used to increase the frequency of electricity generation, while in some designs the generator is directly shafted to the blades.

2.8.2 Nacelle:

Of the size of a small van, the nacelle is elevated up in the air to capture more wind it is the house of most of the electricity generating equipments. Providing structural support for the included equipment and rotor, the main internal

parts are: gear, drive, generator, and transformer. Sometimes gearing is eliminated due to cost reasons hence the generator is run directly. In many cases transformers are located either inside the tower or on the ground or submersed in offshore turbines. In fact deployment of the transformer some where else other than the nacelle will serve reducing the nacelle weight, hence lowering the centre of gravity of the whole system which is of utmost benefit for stability of the floating structure. Electricity is transferred (either directly or in transformed form) to the next stage using cabling to be either stored or used by grid customers.

Horizontal axis machines working on the upwind principle (to be explained later) requires a mechanism to swing them into line with the wind. Also small machines usually have a tail assembly, whereas large machines usually have a "servo mechanism" that orients them to the direction of the maximum power-yew mechanism.

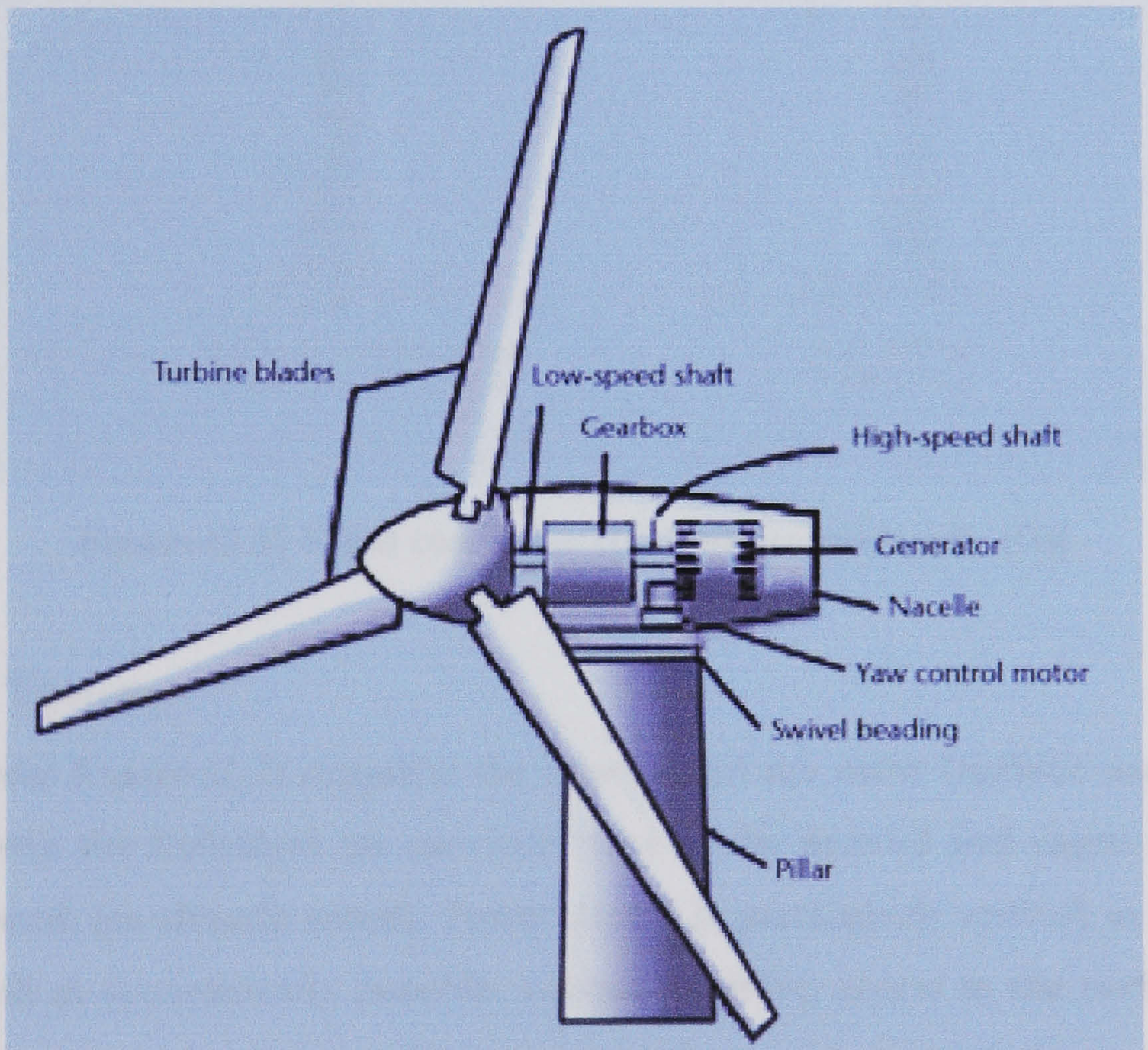

Figure (2.1) Nacelle and rotor parts, [66]

Modern wind turbines are usually equipped with mechanisms to prevent damage in excessively high winds. Large machines may have complex

arrangements to shut down generation at high wind speeds, whereas smaller systems change the blades' orientation so that they present a smaller surface to the wind and thereby reduce the speed of rotation, or otherwise use mechanical brakes. A typical nacelle is shown in Figure (2.1) and Figure (2.2).

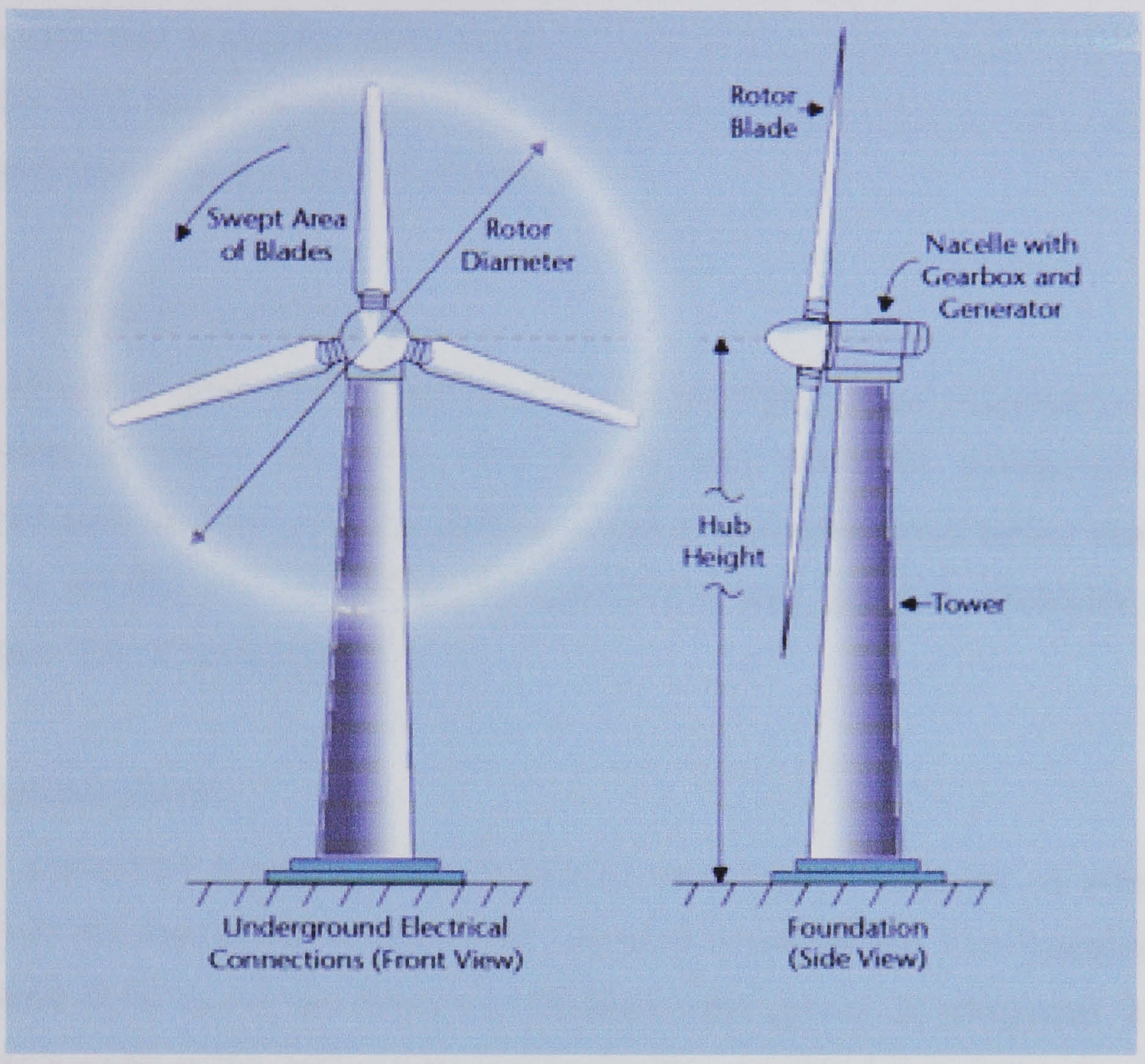

Figure (2.2) Wind converter (turbine) components, [66]

2.8.3 Tower:

The tower Figure (2.2) supports the nacelle and the rotor (turbine assembly) well above the turbulent air currents close to the ground and captures high wind speed, (as already noted). Tower design is particularly critical, as it must be as tall as economically possible, robust, enabling access to the turbine for maintenance, and yet not add unnecessarily to the cost of the system. A particularly important aspect of tower design is elimination of resonance between the frequency range of rotating blades and the resonant frequency of the tower. Towers are made from tubular steel, concrete shaft or steel lattice,

comprising the upper part of the supporting structure, which includes the foundation as well. Therefore, two types of towers are commonly used:

2.8.3.1 Tubular tower:

Most of the towers used for large wind turbines in shallow waters are shaped like a tube that is slightly wider at the bottom than at top, tubular steel towers are not only the strongest solution but are also believed to be the cheapest Rehfeldt and Matthias [59], Group [91].

2.8.3.2 Lattice steel tower:

A tower can be made out of general steel sections that are put together to form a lattice, a lattice tower is very strong and relatively inexpensive to manufacture. It does not take as much steel to manufacture a lattice than to make a tubular one, let alone, transportation and erection, Rehfeldt and Matthias [59], Group [91].

2.9 Foundations:

When assembled together, the foundation and tower, comprise of what is known as the supporting structure, as has been noted before. The foundations are found to be one of the drivers in offshore wind energy development. They account for about (16-25)% of the total cost for a shallow water offshore wind farm, Rehfeldt and Matthias [59], Group [91] and Hogler [121]. Hence, a strong incentive is given to develop cost efficient support structures. In general, two major groups can be distinguished:

- Bottom- mounted support structures.
- Floating support structures.

It is obvious, the decision of which option to use will depend on water depth. For areas of relatively moderate water depths of up to say 40-50m, the focus is placed on bottom mounted structures, while floating support structures (drawn from offshore oil and gas industry) are intended for use of exploiting deep ocean wind energy.

Since wind energy farms deployment, they have been limited to near shore shallow waters, hence only bottom mounted support structures, namely,

gravity and monopile foundations are widely used. This has led to complete domination of bottom mounted offshore turbines, and they have become synonymous with offshore wind farms. Most of the reported literature and drawbacks attributed to offshore wind energy are in fact typically for near shore bottom mounted wind farms, Vugts, [1], Swift [2], Khün [4], Martine [6], Weil [12], Khün [30] through [32], [36], [38] and [61], Cockerill [33] and [35], Ferguson [34], [35] and [42] and Zaaijar [41] and [87].

Various options for the foundations and some of their specifics are as follows:

2.9.1. Gravity foundations:

Gravity based foundations, represent the traditional solution. As the name suggests, the gravity force of a concrete caisson is used to keep the complete structure (foundation, tower and turbine) in an upright position while being exposed to the overturning moment from wave and wind impact on the turbines' rotor and the support structure itself, as shown in Figure (2.3). They are structurally designed with the objective of avoiding tension between the foundation and seabed by providing sufficient dead loads to stabilise the whole structure against overturning moment resulted from horizontal forces. This foundation type is found to be sensitive to extreme hydrodynamic loading as substantial heave loads may occur during the passage of waves, Rehfeldt and Matthias, [59], Hogler [121]. Wave heights in turn are dependent on water depths, and thus the weight of the foundation will have to be heavily increased with deeper water sites,

It is assumed that this type of foundation is commercially unfavourable in water depths in excess of 10m, while physical constraint limits its use over some 20m, Rehfeldt and Matthias [59], Hogler [121].

Gravity based support structures provide rather stiff foundation properties, thus allowing little aerodynamic damping (damping of the fore-aft motion of the structure due to the adverse changes in the aerodynamic forces on the rotor in response to support structure motion). It also allows limited tuning of the support structure's dynamic characteristics. The fatigue life of the gravity based support structure (foundation and tower) is expected to be dominated by aerodynamic loading owing to stiffness of the concrete foundation.

However, at extreme conditions at deep water sites the increased wave height hydrodynamic loading will gain in significance, Rehfeldt and Matthias [59], Group [91], Hogler [121]. The gravity based foundation requires seabed preparations to be carried out contributing to a cost increase with water depth.

The seabed must be levelled and prepared with a layer of crushed stones, in sights prone to scour, hence some kind of protection against erosion will be needed. This is done by placing boulders around the foundation base, Hogler [121]. In theory, the foundation may be easily removed after the service life, in practice however this may not be as easy as it might seem. The common technique is to build these caisson foundations in a dry dock and to float them out to the site of use after completion. To facilitate the transport, the caissons may be made hollow and ballasted on site with sand, gravel, concrete or olivine (a very dense mineral) to achieve the required weight.

Obviously, the large weight of gravity based foundations (typical weight 500-1000 tonnes) pose considerable demands on transport and installation procedures and in addition requires temporary site preparations. Also the effort for casting, formwork, and maintenance of the construction site are considerable for concrete foundations (typical diameter 12-15m). A new technology offers a similar method to that of the concrete gravity caisson. Instead of reinforced concrete it uses a cylindrical steel tube placed on a flat steel box on the seabed, Hogler [121]. Because of its relatively low weight, it could be transported and installed rapidly with a fairly light crane. The steel tube once installed is filled with olivine, to give sufficient weight for stability. In this version as well, protection against erosion is required, Rehfeldt and Matthias, [59], Group [91] and Watson Gillian [70].

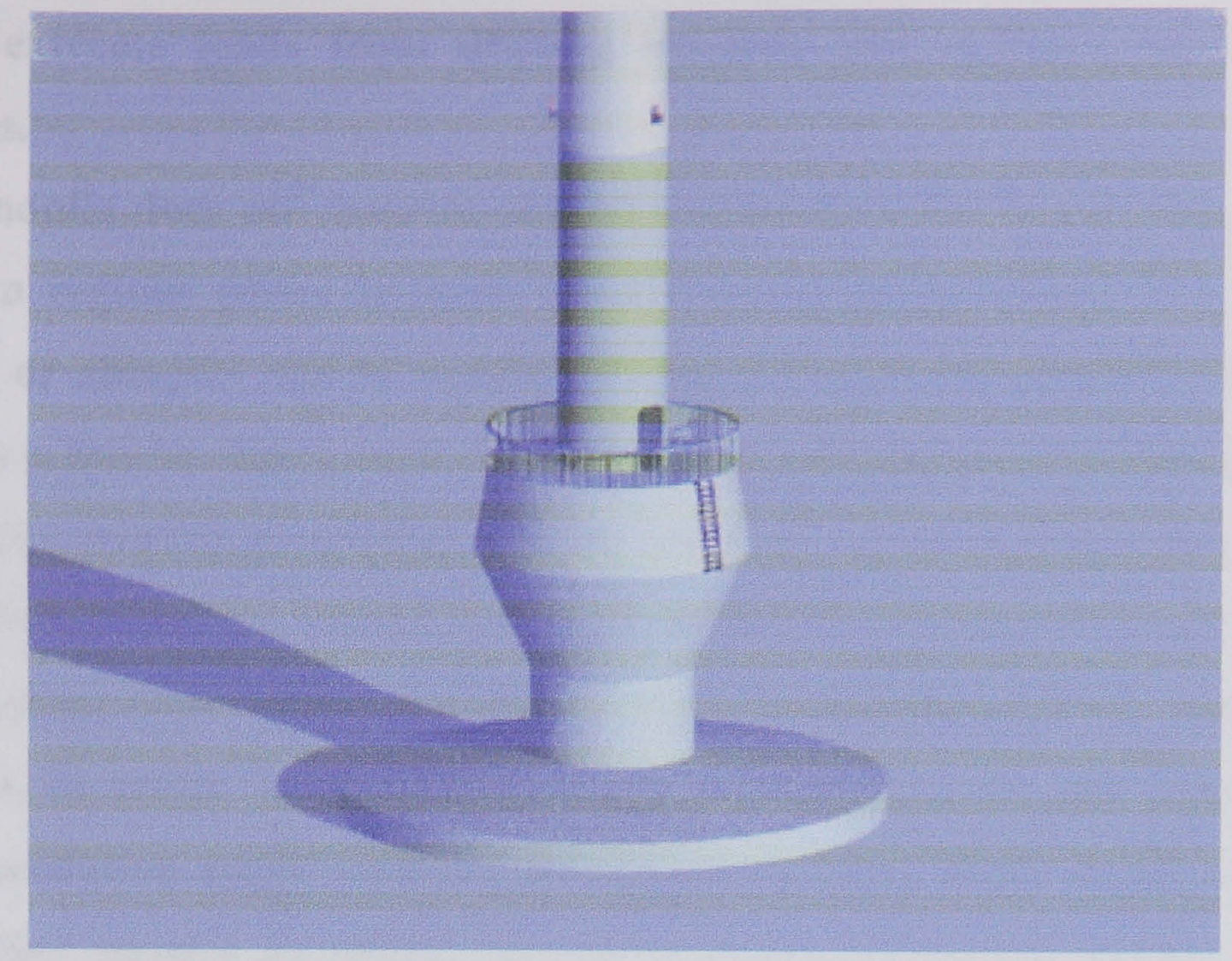

Fig (2.3) Gravity foundation, Reference [71]

2.9.2. Monopile foundation:

Piled foundations make up the most common form of offshore traditional foundations, shown in Figure (2.4). The pile, a simple steel tube, driven into the seabed by means of a vibrating or piling hammer and enables lateral and axial forces (tensile and compressive) to be transferred to the seabed. A monopile support structure would consist of the pile and the tower and possibly a connection between both. Pile diameter (typically 3-5m), weight (typically 175 tonnes), and penetration into the seabed are directly dependent on design philosophy, turbine size, and seabed soil conditions, typical values 10-25m, Watson Gillian [70], Ferguson [34]. Maximum water depth for monopile support structures is identified to be around 25m, Rehfeldt and Matthias [59], Group [91].

The monopile foundation represents a rather soft design with respect to foundation stiffness. As such it offers significant advantages with respect to aerodynamic damping and reduced dynamic response, such characteristics offer the potential of considerably reduced fatigue from aerodynamic loading (rotor) if the support structure dynamic characteristics are properly tuned. In general, the design is expected to be fatigue driven, however, in ice invested

waters, extreme loads from drifting ice may also require increased wall thickness.

The monopile does not require seabed preparation but is sensitive to scour. Hence, in regions prone to scour some form of protection such as artificial seaweed or shingles will be needed. Piling is restricted to seabed conditions with only a few boulders, as they might cause problems during piling. For very stiff seabed conditions drilling will be required. In such a case the monopile will be slotted into the drilled hole and grouted. With respect to corrosion it is worth noting that below the seabed line no coating will be used on the monopile, in order to provide adequate friction between pile and soil. For other foundation types cathodic protection is most likely to be applied by either using passive sacrificial anodes or active impressed current. No anti-fouling will be used on the monopile. Removal of the monopile from the seabed may be accomplished by cutting it some metres below mud line or by extracting it from the seabed using a vibration hammer.

Piles are relatively easier to manufacture, to transport and to erect, with only moderate increase of cost in deep waters, and very stiff soils, monopiles are well researched and dominant for near shore wind energy, Martine [6], Weil [12], Gud [26], Mathies [37], Ferguson [42], Watson [70].

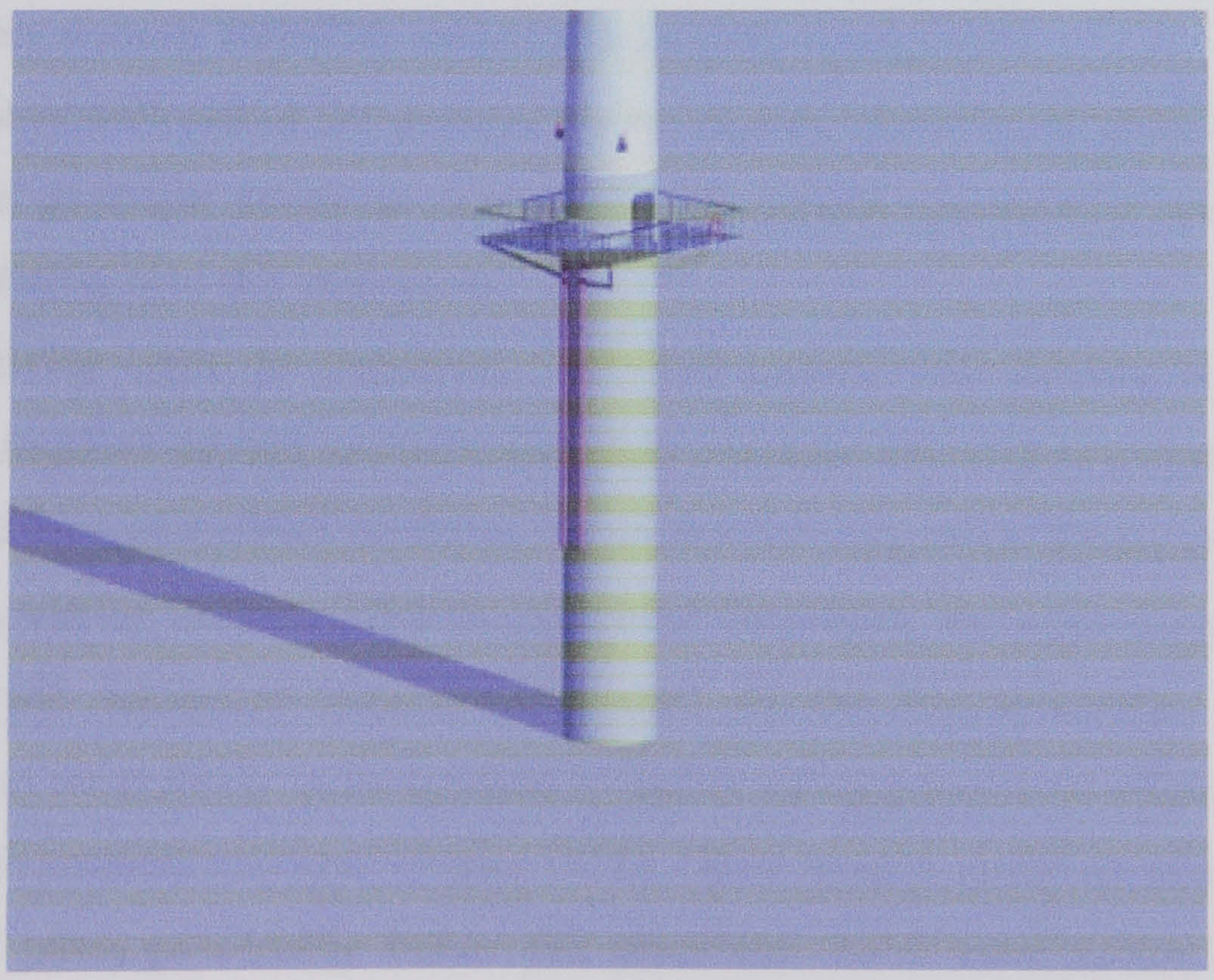

Figure (2.4) Monopile foundations, Reference [71]

2.9.3. Tripod foundation:

This type of foundation is drawn from experience with lightweight and cost efficient three-legged steel jackets for marginal offshore fields in the oil industry. The structure is made of a centre column that carries the tower and a steel space frame transferring the loads from the tower to mainly tension and compression loads in the three piles that are driven into the seabed and connected to the frame through sleeves at the three corners. The cylinder between piles and pile sleeves is filled with grout after piling to ensure a rigid connection, Figure (2.5), Rehfeldt and Matthias [59], Group [91].

The centre column has a reduced diameter at the sea level to reduce wave and ice loads, while the penetration depth is dependent on seabed conditions.

As tripod foundations represent a lightweight structure, dynamic behaviour must be carefully examined. It is a rather stiff structure with small allowance for aerodynamic damping to reduce dynamic response when compared to the monopole, Rehfeldt and Matthias [59], Group [91]. Wave loading has been shown to be insignificant in water depths down to 11m some 10–25% contribution to the over all overturning moment, Rehfeldt and Matthias [59]. Hence, as the tripod support structure is mainly governed by aerodynamic fatigue loading, the importance of wave loads becomes significant with deeper waters. Loading from ice crushing against the structure can also be the design driver in icy waters, Rehfeldt and Matthias [59], Group [91].

The tripod is well suited for greater water depths, however, in shallow water, a technical problem arises as service vessels cannot approach it without the risk of colliding into the structure.

It is relatively light to transport, but well-known and proven techniques should be applied during manufacture and erection. No seabed preparation is required, lifting and piling facilities are somewhat expensive. Below the seabed no coating will be used on piles to guard for corrosion, the reason, once again is to provide adequate friction with soil. As for the monopile, cathodic protection is most likely to be applied by either using passive sacrificial anodes or active impressed current, Hogler [121]. Once used it could be removed by cutting off piles, preferably below the mud line. As it most suited for deep

water sites away from shore, it has the potential of being useful, although it is not been known to be used until now.

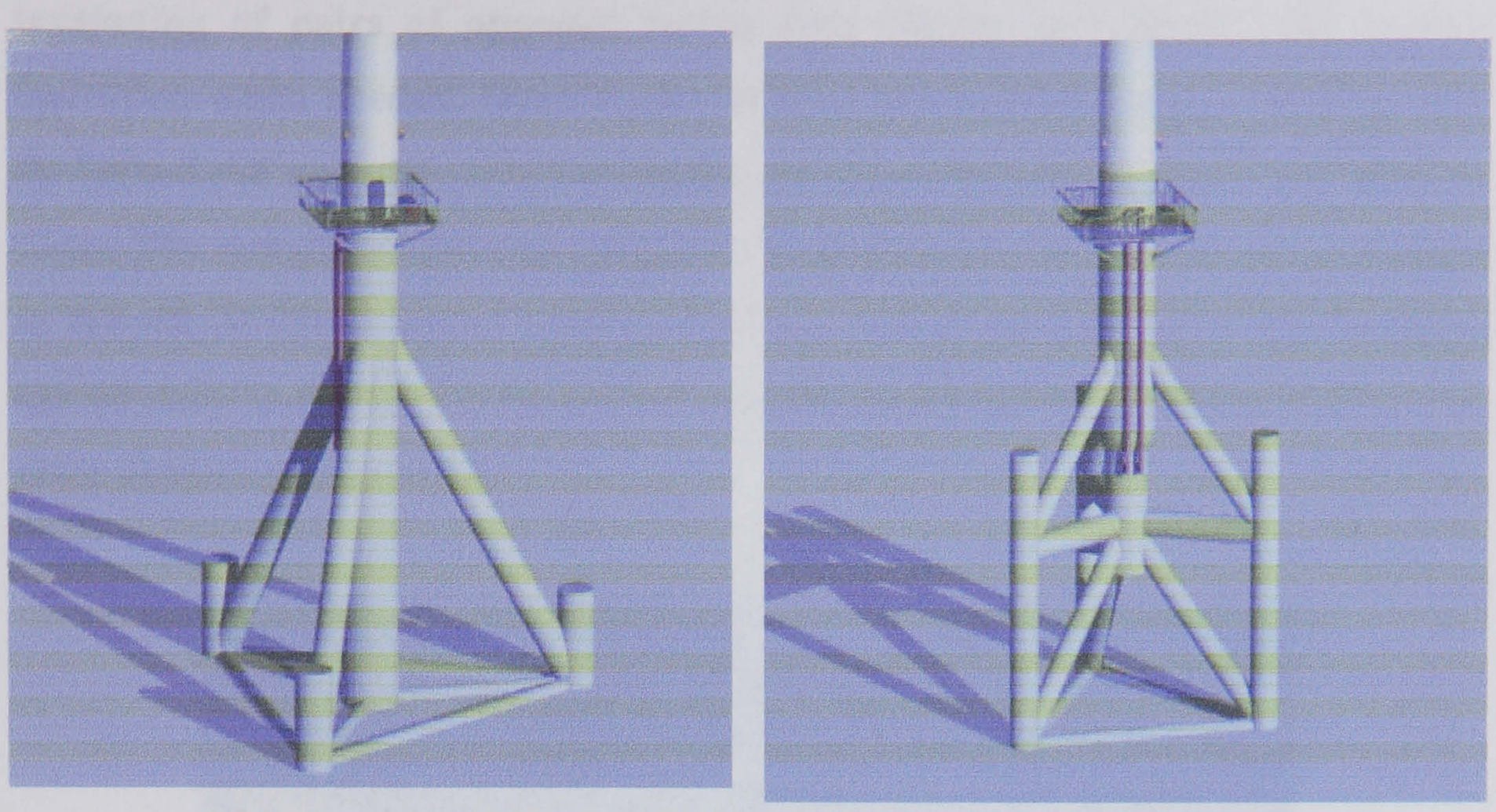

Figure (2.5) Tripod foundation, Reference [71]

2.10 Floating Support Structure:

An incentive to use floating support structures in offshore wind farm developments is the constraint to modest water depths necessary for any seabed mounted structure. This drawback can be overcome with floating support structures hence the development of offshore wind energy generating facilities could be extended to areas with water depths of up to several hundred metres. This approach has been mentioned by several references, Tong [10], Page et al [19], Henderson [43], Rehfeldt and Matthias [59], Hogler [121]. Accordingly, two feasible options for floating offshore wind farms emerged:

2.10.1The buoy type:

In the case of the buoy type system, the support structure comprises the tower, the hull and the moorings to the seabed. The tower, a tripod steel space frame, is bolted onto the deck of cylindrical buoy hull with a wider bottom disk, for improved dynamic behaviour the lattice tower could be replaced by steel tube tower, Figure (2.6). The mooring system is made up of units adaptable to

water depths then the mooring lines are connected to mooring anchors piled at the seabed. A line tensioning system is to be mounted on the deck to allow tensioning of pairs of opposite facing lines during installation and during operation when needed. Once a pair of lines has been tensioned the lines will be locked off and the winches engage on the next pair of lines and tension them. The completed floating structure including the turbine would be floated to the site of development where, in a first phase, mooring lines and anchors are already installed. Mathematical models based on this concept will be the main subject of this work.

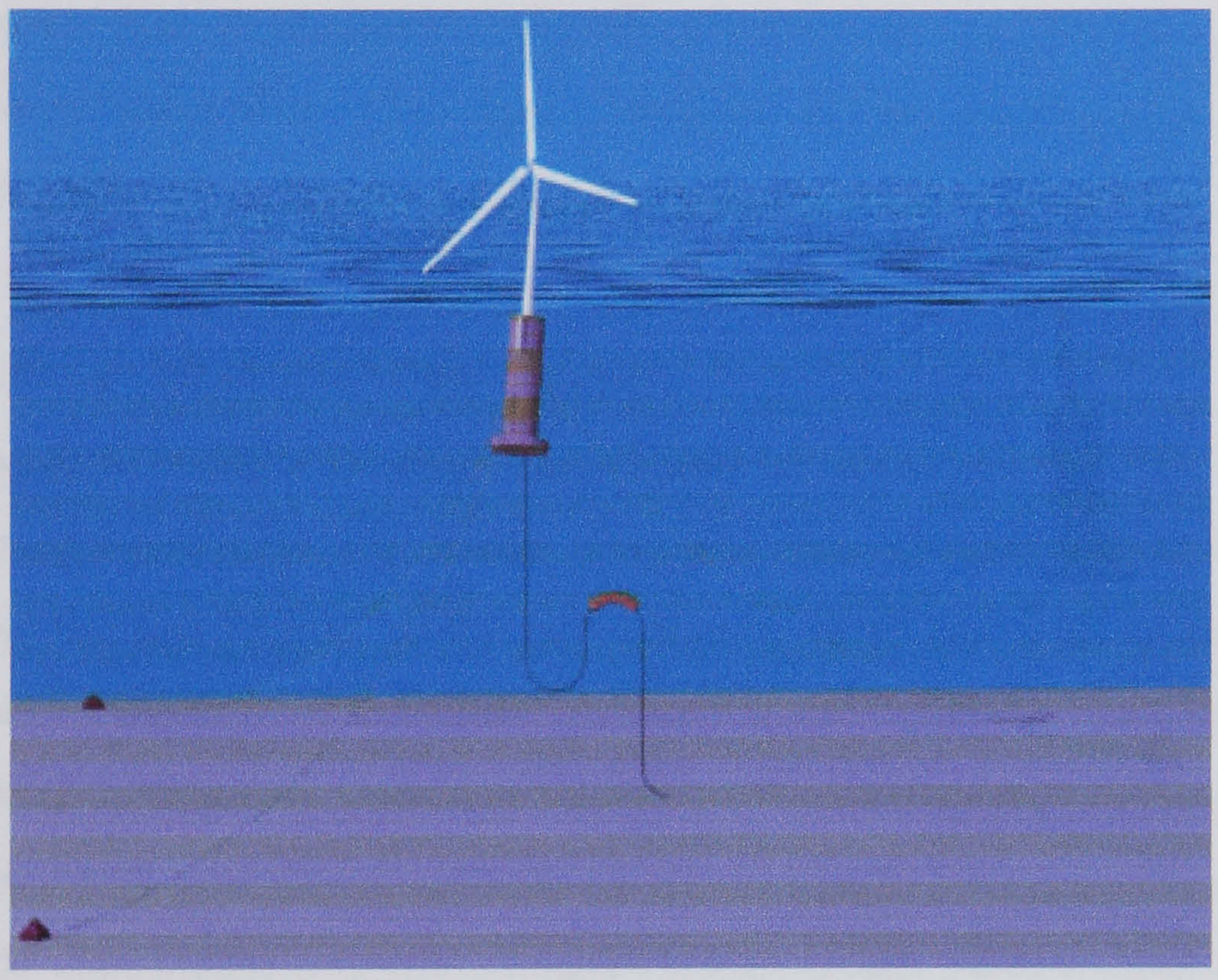

Figure (2.6) Buoy floating support structure, Reference [71]

2.10.2. The semi-submersible type:

As opposed to the afore-mentioned case the main semi-submersible support structure will be located below the water surface. This technique is well proven in the oil and gas industry, and the deep submergence of the individual hulls arranged in a larger structure lead to reduced response waves and with longer natural periods of motion. These characteristics are attributed to the wave kinematics to decay exponentially with depth. The hulls will be manufactured from reinforced concrete and braced to an overall structure capable of carrying a cluster of 3–6 multi megawatt turbines. These clusters

can adopt various shapes to comply with different optimisation targets. The complete arrangement is to be moored by catenary chains to piled anchor points on the seabed. Investigating the loads on the turbine in comparison to those found for turbines on bottom-mounted support structures has provided evidence of a dramatic increase in fatigue damage for the floating case, Rehfeldt and Matthias [59], Group [91], Hogler [121]. As already stated, floating offshore wind energy systems were directly drawn from oil and gas experience with the controversial increase in cost well justified, unlike the case for wind energy where cost reduction is the main driver. This leaves floating wind energy systems as an option that is considered to be technically feasible, but at present there is no incentive to take forward the cost for the exploration of these deep-water sites. This type of support is thoroughly investigated by Henderson [62].

2.11 Floating Offshore Wind Farms:

The principle of using a floating storage and or production towers as well as spar floating structures for many purposes was known and been in use throughout the second half of the past century. Over the final decades of the last century, a number of feasibility projects have examined the possibility of locating wind turbines on floating structures. Henderson [62], summarises the main advantages and disadvantages of the Multiple Unit Floating Offshore Wind farm (MUFOW) concept compared with single units as follows: lower installation costs (per unit), improved stability, better dynamic characteristics, easier maintenance, smaller turbine spacing, weather vamping required and limited range of water depth. Henderson [39], [43], [62] and [138] summarised a detailed work at (UCL), of the moorings, the motion response and economics of a floating wind energy concept consisting of multiple wind turbines mounted on a horizontal floating cylinder.

Henderson [62], reported work concentrated on overall concepts and investigated small unit multiple turbine devices. Various configurations were investigated with emphasis on the overall design, the conclusions were:

- Platform based turbines could be competitive with inland based schemes.

- **Depth of water was a key parameter, when considering mooring performance and competitiveness with respect to fixed designs.**

The float concept believed to be the future offshore wind turbine for deep ocean wind energy exploration, 'Garrad-Hassan/Technomare/BMT' developed this concept for the European Union and briefly reported by Tong [10], Page [19], Henderson [62], Hans [90], Group [91], Petru [92] and Hogler [121] in the period between 1992 and 94. The selected concept was a single turbine located on a large floating cylinder, though other configuration such as barge platforms; four-column semi-submersible hulls and twin turbines were also reported.

The evaluation of using an explicit finite element analysis code for analysing this optimised design is the basis for the work reported herein and will be discussed in further detail in the proceeding chapters of this thesis. In summary the concept consists of:

- **Simple tubular concrete hull buoy,**
- **Water depth between 75m and 500m,**
- **Catenaries chain or taut wire synthetic fibre eight line mooring,**
- **Shared piles anchors,**
- **Submerged or mounted 3.3/33kV transformer,**
- **Three bladed 60m diameter 1.4MW turbine,**
- **Free-yawing, downwind design at 45.6m above sea water level,**
- **High tip speed rotor.**

The estimated cost of power was 9p/KWh, Rehfeldt and Matthias [59] and Group [91] for a site in the Northern Irish Sea.

Looking at the design in greater detail, the turbine hub is located at a height of 0.75 of rotor diameter, lower than might be practised for a land-based machine, to reduce the leverage of the wind thrust turning moment. As stability is critical for this offshore concept, using a tripod lattice steel tower (transparent) further reduces the turning moment.

Free yawing was selected due to the initially perceived inability of the floating structure to provide a sufficient reactive moment. This has implication in the design for the farm and physical size which will be used.

Henderson [62] reported all the above-mentioned floating concepts and added that a group from Milan investigated single turbine concepts under a title of 'Eolomar' including toroidal or lens shaped semi-submerged floating structures. The advantage of this novel shape is its good hydrodynamic performance, but it was subsequently discarded for a lattice design due to its likely expense. Both theoretical and model testing were claimed to be performed on the float concept, however none of the results of such tests were reported in the accessible literature.

2.12 Mechanical Characteristics of Wind Energy Converter:

A wind energy system transforms the kinetic energy of the wind into mechanical then electrical energy that can be harnessed for practical use.

There are two basic designs of wind electric turbines:

- Vertical-axis, or "egg–beater" style, Figure (2.7) (a) and
- Horizontal–axis machines, Figure (2.7) (b)

Simply refer to the axis about which rotation of blades is taking place. Horizontal axis turbines are the most common in commercial use. The wind turns the blades, which spin a shaft that connects to a generator and produces electricity.

Horizontal wind turbines could be operated by one, two or three blades, with the three blades option being mostly used as 'upwind' with blades facing the wind, while the two blades option is used as 'downwind' with the rotor placed on the lee side of the tower. The whole system (turbine) is mounted on the top of a tower (concrete or steel), with its foundations piled into or bearing on seabed for shallow waters or otherwise floating for deep waters as has been discussed in previous headings.

There are three basic physical laws governing the amount of energy available from the wind (The 3 law criterion). The first states that the power generated by the turbine is proportional to the wind speed cubed, i.e. if the wind speed doubles, the power available increases by a factor of eight. The second states that the power available is directly proportional to the swept area of the blade length, i.e. doubling the blade length will increase the power by four times. The third states that there is a maximum theoretical

efficiency of wind generators of 59%. In practice, most wind turbines are much less efficient than this and different types are designed to have a maximum efficiency at different wind speeds, a matter of concern to mechanical engineers, and extensively researched.

Once electricity is produced, it has to be readily integrated into the utility grid or network by means of transformers, which could be installed inside the raising tower or somewhere near the surface.

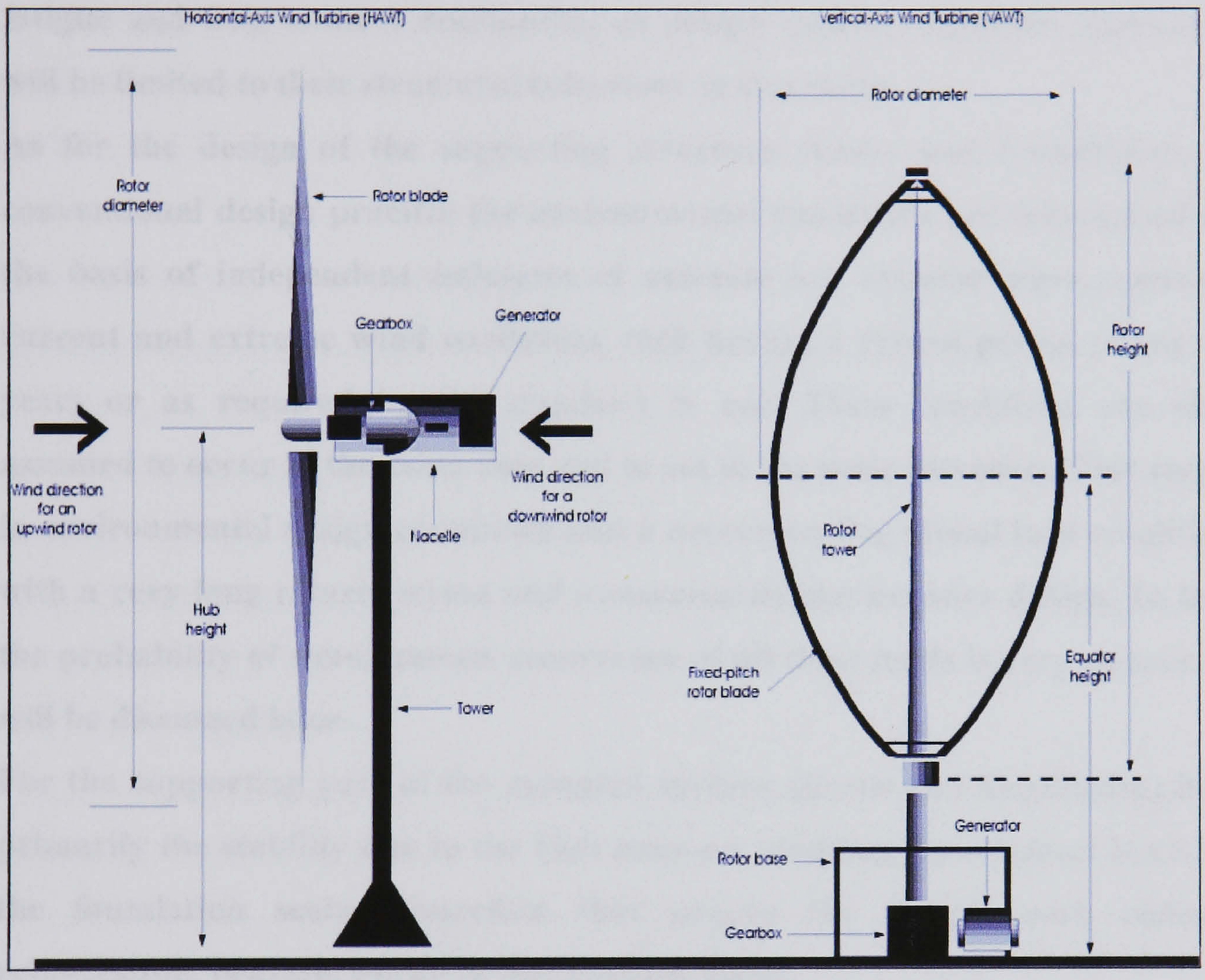

Figure (2.7) Vertical and horizontal axis wind converter (AWEA) website, 2001

2.13 Overall Design Considerations for Wind Energy Systems:

There is a long experience in offshore technology with design of large and unique fixed structures for the petroleum industry, which are built "fit for purpose" with respect to their site and function.

Transportation and installation issues are often a main design driver since these costs can be even higher than those for the manufacturing of the structure onshore. Reduction and where possible elimination of underwater

inspection and maintenance is essential due to the difficult access and the high costs associated with these operations offshore. Other important design aspects concern the safety of personnel working on or travelling to the structures, environmental impact and dismantling.

It is obvious, because of the diversity of the components, sites and materials involved in wind energy systems, that the engineering methodology of dealing with these different parts will be different. The design of the mounted components (nacelle and rotor) is a concern to mechanical engineering, with fatigue and heat control dominating as design criteria, however, discussion will be limited to their structural behaviour in this thesis.

As for the design of the supporting structure (tower and foundation), in conventional design practice the environmental conditions are determined on the basis of independent estimates of extreme ice, extreme wave, extreme current and extreme wind conditions each having a return period of say 50 years or as required by the standard in use. These conditions are next assumed to occur at the same time and to act in the same direction. This result in environmental design conditions and a corresponding global load condition with a very long return period and unnecessarily conservative design. In fact the probability of simultaneous occurrence of all these loads is very remote as will be discussed later.

For the supporting part of the mounted turbine (tower and foundation) it is primarily the stability due to the high moment resulting from lateral loads at the foundation seabed interface that govern the design, with sliding, compression, bearing, buckling and possibly shear.

In addition to the critical combination of wind, wave and current forces, affecting the support structure, fatigue due to hydrodynamic and aerodynamic damping loading is an important factor; fatigue due to aerodynamic loading is dominated by the rotor thrust and the fundamental frequency of the support structure relative to the rotor angular velocity. Fatigue due to hydrodynamic loading generally considered minor for shallow waters and will be significant for deep waters.

To insure structural integrity, safety factors must be applied to external loads, and partial material safety factors for fatigue analysis also must be applied the same arguments apply for bearing and sliding resistance of the foundation.

The primary objectives when choosing a concept for any energy generating project are: cost, safety and reliability. It is not clear which type of floating wind farm concepts will deliver these most efficiently. Floating wind farms will experience extremely hostile environments and will be subjected to a much more complicated mixture of static and dynamic effects, yet still its design is mainly preoccupied by cost reduction, unlike its rival, offshore oil and gas industry, where profit justifies innovation.

Broadly speaking, it is economic to invest a high amount of capital in order to achieve high and reliable energy output, for instance, a 30% increase in wind turbine costs results only in 10% extra energy cost, Khün et al [40] and Hogler [121].

2.14 Different Design Methodology for Offshore Wind Energy:

Although the challenges of building large offshore wind farms will be considerable, with many of the problems relating to the converter (turbine) will have previously been faced on-land, and those relating to the support structure by the offshore industry. The key point will be to know how to integrate these two technologies. In fact, the combination is not always equal to the sum of the parts, both in a beneficial and a detrimental sense, hence a cost-saving opportunities may be missed and unexpected problems may be encountered during construction and operation. Once more, avoiding unnecessary costs is especially important now when offshore wind energy aims at becoming competitive on price with traditional energy sources.

Offshore wind energy is fairly new field, almost one may think of several different design approaches for an offshore wind park depending on the already gained experience, the project size, the design philosophy, applied standards, etc. Khün [60] and Hogler [121] reported four approaches, these are identified with their order of increased consideration of offshore wind energy conversion system (OWECS) design aspects and the required experience jointly integrated and used as a basis for European design approach. These approaches are:

2.14.1 Robust or traditional design approach:

This approach makes use of the well developed offshore oil and gas technology mixed with the relatively well known onshore wind energy technology. The main objectives of the approach are the demonstration, the investigation of environmental effects and the gathering of first experience rather than high economic performance. Therefore, more or less standard onshore wind turbine designs are applied. Wind turbines and towers out of the series production are installed in a similar manner to onshore.

Furthermore, reduction of operation and maintenance costs is aimed for by well proven onshore wind turbine designs marinized by features as for instance improved corrosion protection, air–tight nacelle, built–in lifting facilities, etc.

This approach was used by Danish designers in 1990s, and though it may be applicable for the site it was designed for, it may not be feasible for large scale wind energy systems due to its limitation to sheltered waters with minimum wave loading and poor economic performance, it is evident that this approach refers to bottom mounted turbines.

2.14.2 Parallel structural design approach:

This approach was used by the Dutch and Swedish designers in 1990s and as a basis for Phase II of the (Opti–OWECS) project which is the European integrated design approach, Khün et al [40] and Khün [61]. In this approach, one may think separately of the offshore design implications for the main sub-system as wind turbine, support structure, grid, etc.

In the Dutch version of this design, monopile foundation supports a standard onshore tower and a cable laying technique with partial avoidance of a cable laying ship. Though it is considered to be success, the system aspects have not been fully considered, specifically, investigation of overall dynamics. It is however, acceptable to sheltered sites, Hogler [121].

In the Swedish version, however the support structure design intended as a small scale prototype system while installation procedures are adapted from onshore to offshore. The entire unit has been fully assembled and

commissioned prior to towing to the final destination so that in-situ work was minimised.

This approach may look promising if strong experience is available at sub-system level. Nonetheless, this procedure might not achieve the best performance that is feasible in the nearby future because of the lack of system integration in the economic optimisation and the dynamic analysis and how these features are adapted to system design, Rehfeldt and Matthias [59], Group [91].

In the aforementioned approaches, the direct mix of onshore and offshore techniques eventually led to conservative design.

2.14.3 Integrated overall design approach:

This is a developed version of the previous approaches with more consideration to particular properties of the constituents. Still, sub-system design is done in parallel based on the state-of-the-art knowledge in wind engineering and offshore technology. However, the solutions are governed by overall criteria such as: global economics, actual site conditions, entire system dynamics, transportation and installation as well as operation and maintenance strategies. This is the typical design approach for most structures.

Therefore at least the site selection, the preliminary design and a check of the final design have to be done with respect to these global criteria. Moreover, the engineers in the different disciplines involved need assistance and new tools for judging intermediate results during the design process.

2.14.4 Radical design approach:

This approach follows similar methodology to the last approach the difference however, is in the use of unconventional designs for the entire sub-system, which provide a major (economic) benefit for the entire system. In addition, the radical design approach requires that the (preliminary) design is governed by the offshore wind energy requirements rather than by adapting simply existing experience for the new situation. This might include: In wind turbine system one may think of the "ultimate wind turbine" an extremely flexible

turbine with the absolute minimum of components, an umbrella type wind turbine which adjust their shape according to the wind loading, a multi turbine concepts or no-maintenance concepts Khün [60]. Unconventional support structures are proposed by the Multi Unite Floating Offshore Wind Farm (MUFOWF) concept Khün [60] and Henderson [62], [43].

Ultimately this approach might be the most promising. However, unproven or just (large) designs, do not lend themselves well for application in the demanding offshore environment.

The experience gained during the course of the other design approaches is necessary. Therefore, the radical approach is not considered feasible at the moment but may be required for very large offshore wind farms with a capacity of several hundred megawatts.

2.15 Environmental Concerns of Wind Energy:

For the most part, wind power plants have little impact on the environment compared to other conventional power plants. The only concern with the use of the wind power is the noise produced by the rotor blades, aesthetic impacts and some times birds have been killed by flying into the rotor blades. Most of these problems have been eliminated or reduced by technological development and/or properly citing of wind plants e.g. offshore.

Offshore wind energy therefore is giving the proper solution for noise, visual impacts, moving shadows and illusion by locating wind farms in (no-mans land) high in the seas. Through proper location and alignment, other problems can eliminate some of the concerns namely: i) impact on birds either by affects on their living and feeding and hence breeding habitat or by blocking their migration roots and thus the risk of collision. ii) impacts on fish, fishery and sea mammals and marine fouling. iii) impacts on air and ship traffic roots. v) impacts on electromagnetic communications. vi) impact on seabed mining.

Fortunately, all these negative aspects are either have been addressed by the technology or under through investigation and are therefore on their way to be eliminated. Because of the public awareness and sensitivity of these issues, public acceptance is a corner stone in planning these projects, due to its political effects on decision makers, many studies were devoted to

environmental consequences of offshore wind energy some of them are completed, some are still underway, and definitely many will follow and be parallel to this energy. Among the reported literature, British Wind Energy Association [19], Metoc Plc [65], European Commission [68], Dobesch et al [69], Hans [90], Group [91, and Hogler [121], collectively they form very good background for highlighting the main environmental concerns and paving the road for more environment friendly energy.

2.16 Conversion of Wind Energy:

How can the variations in the wind velocity over a period of time be converted into an annual energy output in kilowatt-hours (kWh) for the wind turbine?

Starting from a time series of wind velocity and integrating the power in a series of small time intervals over the specified period, this can be done from a turbine power characteristic with the cumulative distribution of wind speeds. The variation of wind speed with height needs to be taken into account, then a value representing the speed at the given hub height is chosen. Depending on local wind speeds, a turbine will produce an annual average power that is some proportion of its maximum rated power, typically up to 30%. Assuming the wind turbine will be available to operate for 95% of the time, the overall annual load factor or capacity factor would then be 0.3 x 0.95 or 28.5%.

Studies relating power output (kW) to wind speed shows that optimum power is extracted between speeds of 5 m/s and 13 m/s, Walker et al [73], Manwell et al [78], Hartwig [77] and Veritas [88] and with speed below 5 m/s (usually known as the cut-in wind speed) there is not enough energy in the wind to overcome the mechanical losses within the turbine. While the number of hours per year when the wind speed exceeds 13 m/s is quite small, therefore typical speeds within the mentioned range is widely used in rotor design. The hub height wind speed at which the turbine produces its maximum or rated power is known as its rated wind speed.

There are two main techniques for limiting or regulating the power of the wind turbine. Pitch regulation rotates the wind turbine blades mechanically in order to reduce their aerodynamic efficiency, thereby lowering C_p (coefficient of performance known as 'Betz limit' discussed in Appendix-A3 of this thesis).

Stall regulation allows the blades to go into condition of aerodynamic stall when the wind speed is high; the blades are not mechanically moved. Stall regulation also reduces aerodynamic efficiency, limiting the power which must be transmitted by the drive train to the generator.

2.17 Rotor Function:

In principle there are two different types of wind energy conversion devices: those which depend mainly on aerodynamic lift and those which use mainly aerodynamic drag.

Low speed devices are mainly driven by drag forces acting on the rotor. They generally move slower than the wind, and their motion reduces rather than enhances the power extraction. The torque at the rotor shaft is relatively high. There are many types of wind rotors in use, which are dependent on the purpose and function, such as electricity generation (high speed or lift type) whereas water pumping (low speed or drag type). For the same swept area (area covered by the rotor blades motion) the power extracted by a wind turbine relaying on lift forces is generally many times greater than the power from a turbine relying on drag. Although Betz limit for energy conversion applies to any type of wind turbine despite the orientation of its axis of rotation, horizontal-axis or propeller-type turbines are more common and highly developed than the vertical-axis designs. Vertical-axis wind turbines range from the drag type such as the Savonius type and cup anemometer for measuring wind speed to high speed turbines where the blades are vertical and straight with a symmetrical airfoil profile or as curved in the classic troposkien shape. The later are usually known as the Darrieus type and the shape is such the centrifugal loads are balanced by pure tension forces in the blades, thus avoiding bending moments.

Modern vertical axis machines have several advantages: they operate independently of the wind direction, hence yawing mechanism is not required; heavy gearboxes and generating machinery may be situated at ground level; as they rotate the blades do not suffer fatigue stresses from gravitational induced forces. They also have some disadvantages: they are not self-starting; the torque fluctuates with each revolution as the blades move into and away from the wind; and speed regulation in high winds can be difficult. There has

not been enough indications in the published literature that the vertical axis wind turbines are proven to be as cost-effective as their horizontal-axis counterparts. Therefore the commercial significance of vertical-axis wind turbines is some what limited for the time being.

Whether the rotor is allowed to run at variable speed or constrained to operate at a constant speed is decided by the designer according to the employed function. For small battery charging and water pumping turbines, it is desirable to allow the rotor speed to vary. However, for the large scale generation of electricity it is common to operate wind turbines at constant speed. This allows the use of simple generators whose speed is fixed by the speed of the frequency of the network. Variable speed wind turbines are sometimes used for electricity generation but a power electronic frequency converter is then required to connect the variable frequency output of the wind turbine to the fixed frequency of the electrical system.

2.18 Finite Element Analysis of Wind Converter

2.18.1 Finite element method:

Finite element analysis or FEM is a method for numerical solutions of field problems. For the last half of the 20^{th} century, FEM was dominant in engineering analysis, as a technique that is suitable for almost any engineering problems. Armed with excellent available knowledge in the vast literature and extremely well developed computer hardware both in terms of speed and storage capacity, engineers can tackle almost any problem within human imagination using this technique of stress analysis.

The theory itself is well developed in the accessible literature Bowes [74], Cook [79], and Zienkiewicz [82], Crisfield [84] and [85], and many other books and papers. The code to be employed in the verification of the analysis of the floating wind converter and in creating full scale model in this thesis is the commercial finite element code LS-DYNA3D with a large material and element library, good contact features, good constraints and boundary conditions capabilities. Due to complexity of the model geometry and the dynamic non-linear nature of the loads and variety of materials involved an

explicit finite element codes such as LS-DYNA3D can provide the solution to many aspects of this problem.

LS-DYNA3D allows for several material models (i) elastic and plastic (isotropic or anisotropic) (ii) volumetric compaction failure (iii) thermal effects and (iii) rate dependence. The analysis capabilities include (i) transient dynamic analysis (ii) static analysis using dynamic relaxation and (iii) dynamic analysis with static initialization. The most recent (ALE) feature for fluid modelling, non-reflecting boundaries for modelling infinite quanta, multi-materials option, fluids-structure interaction algorithms, load-density function for fluid hydrostatic pressure initiation, initial volume fraction or geometry had broadened the spectrum of the code capabilities. The additional features include the impact and contact algorithms, allowing for sliding, friction, single surface contact, tied meshing for mesh grading, and tie breaking for failure. Further features such as mesh re-zoning by interactive or automatic command execution and mesh smoothing or remapping, the superior flexibility in load curves and ease in which it is implemented are highly useful. Other programme capabilities are; analysing quasi-static large geometrical and material nonlinearities problems with large deformations, the possibility of using dynamic relaxation (if needed) and the possibility of transferring geometry and results to 'ANSYS' (implicit) code, hence performing sequential or mixed time marching scheme (explicit-implicit or vice-versa) analysis. With all the mentioned features and coupled with the fact that less time and memory is needed for explicit analysis to run which can help direct the time and memory savings to dealing with structures of larger degrees of freedom (the main advantage over implicit code). Collectively all these features are equally important in the analysis of any complex model such as the floating wind turbine. The only drawback attributed to explicit methods is their conditional stability which in large models can topple the time saving option. Therefore, the LS-DYNA3D code is chosen to be used in this evaluation and in the full scale model creation. It is worth mentioning that most of the reported applications of LS-DYNA3D programme are for the car industry impact and crashworthiness simulations Kenneth [117] with some research using the code for studying bird strike to wind turbines but no evidence of using the code in analysing floating wind turbines was found.

2.18.2 Previous analysis work:

Amongst the reported literature there has been no evidence of the use of explicit codes in the analysis of floating wind converters such as the one dealt with here. Some modelling of wind converters for analysis by FEM has been reported, computer models for aerodynamic or hydrodynamic load have also been described, Andres [125] but non of them appear to have used explicit FE code. In terms of the theory, offshore structures are doing well with many books and huge number of papers dealing with offshore platforms, moored vessels and structures which are in contact with seawater, Ivan [5], Cassidy [7], Bell [8], de Santa [9], Patel [20], Various editors [22], Boss [28], Aquelet et al [67] and Chakrabarti [63]. The dominant common factor among these references is that they deal with the problem from the foundations point of view with emphasis on soil and water structure interaction.

Floating objects such as moored ships, barges, and production platforms for offshore oil and gas industry have left enormous amount of literature for analysis of such structures. The problem with most of the offshore or floating structures that it is hard to define a general solution or theory that is equally applied to attain solution they are rather designed for a purpose with all the limitations included. One of the few reported works for multi-unit floating wind farms consists of multiple wind turbines mounted on a floating long submersed horizontal cylinder, Henderson [62], [39] and [42].

The blades design benefited from the well developed technology of the aviation industry especially the helicopter blades, with the contradiction in function for that they need energy to rotate at high speeds while turbine blades produce energy when rotating at relatively lower speeds. In terms of material development, blades have gained specific improvements in stiffness, minimum weight and fatigue performance and airfoil function this again is attributed to aviation technology, Dayton [118], Raymond [119], Lance [120], Jappe [131], Richard [133] and Abbot [134].

Lobitz [123] reported a computer program for modelling a horizontal axis wind turbine models the blades as flexible beams and the tower by rigid beams, the same principle is presented in Det Norske [88]. It presents an approximation for land-based turbine behaviour, and similar work is reported

by Donghoon [126]. For modelling the whole turbine as a flexible system, Yutaka [129] reported numerical analysis of the yawing effects on wind turbine. Xu [113] proposed a model for studying the flow around the horizontal axis wind turbine and Harri [114] reported modelling of control system of variable speed turbine.

There exist many computer programs that are essentially designed for design optimization of bottom mounted (land or seabed based) wind converters, little is known about these commercial software programmes as they are intended for use by their initiators. They are listed with brief summary about each of them and reported by Andres [125].

In fact most of the available software programmes are strong in some aspects and deficient in others. General purpose explicit code is the choice here for verification of nonlinear dynamic analysis and for the creation of full scale model of floating wind converter because it provides the comprehensive features required. Nevertheless the visible drawbacks for such type of codes are their generality which means complications in their understanding, debugging and time needed to tailor the floating wind converter to fit them. Other deficiencies that they are not capable of computing hydrodynamic and aerodynamic loads needed as input for analysis, and finally they are costly to attain and to run. The main structural parts such as the steel towers and concrete float are well defined and can therefore be modelled with ease given that we can properly estimate the combined loads, Houlsby [24], Anderson [25], Ferguson [42], Watson [70], British Standards [102] through [106], Peter [94], Guner [101] and Jørgen [135].

2.18.3 Design codes and standards:

There are several design codes for offshore industry mainly intended for the oil and gas industry, while for offshore wind energy these codes are far from being useful due to the difference in action, principle and incentives for both activities. The wind energy industry so far have managed to produce only superficial guidelines which are basic and never close to what is required in a design standard. The main source to which these guidelines make reference is the IEC 61400-1 [111], which present a conservative approach for attaining safety for maintenance personal and equipments. Other standards are the

International Standard ISO [93] which contains information for wind actions on structures that are not necessarily applicable to wind turbines. Most guidelines such as the Department of Energy [53] through [57], British Standards [105], Bomel [112] and Det Norske [75] and [88], the last two are the best among these standards. Most of these standards do refer to each other and are still attached to the oil and gas industry practice which is not always compatible with the wind industry, and the same could be said about the 'American Bureau of Shipping' [83].

The common missing link in wind offshore design standards is the method of combining different environmental loads for their use in analysis. Many works has been reported based on statistical reliability methods of combining these loads, Ude [13], Bjerager et al [14], Winterstien [15] and [23], Peter [47], Tomas [92], Madsen [94], NREL [95], British Standards [96], Larsen et al [101], Hamilton [107], Hiroshi [108], Gunjit [109], Tony [110], LeRoy [124], Osamu [127], Paul [128], Cheng [139]. Det Norske [88], [115] and British Standards [96] through [100] are basically concerned with safety. The Danish approach is better in approaching the design by proposing analysis methods for wind turbines. In general the industry is still far from adopting one reliable method for integrating environmental loads in an approach reflecting their duration throughout the life of the offshore wind turbine. Instead guidelines tilt towards the conservatism inherited from offshore oil industry.

Many works have been produced concerned with the economic performance of wind energy such as Khün [4] and [40], Tong [10] and [60], Cockerill [33] and Peter [122], these are more descriptive and analytic approaches for selling the idea of wind energy economical competitiveness. Wind database information itself has started building up (though not directly available) information that is relatively well defined, Department of Energy [51], Khün [36] and [38]. A good deal of information available in text books such as Emil [86] are partly empirical and intended for use for land based structures.

Finally, to close this review it is worth noting here that there exists an enormous amount of literature online via the internet from many research and educational institutions: Delft University of Technology of the Netherlands, Risø of Denmark and University College London (UCL) are among the most active institutions in wind energy publications. As well, all wind energy

associations such as the British Wind Energy Association and American Wind Energy Associations have good websites. One of the best is the very informative website of The Danish Wind Turbine Manufacturer Association. The Danish themselves had a 50% share of the world market of wind turbines in the year 2000. All other national associations, companies and institutions involved in this technology do have similar websites that could be explored and screened for useful information.

2.19 Discussion and Conclusions:

Offshore wind energy is expected to have a number of advantages not only over other sources of energy but also over onshore wind energy as well, lower air temperature, higher air density, lower turbulence and many environmental related benefits. As the offshore installations will be some distance from the areas of human activities, it is also expected that the permitted noise level will exceed the allowed level in an onshore site, thereby allowing higher tip-speeds for offshore converters and hence more energy outcome. There are nil or very few locations that offer the energy capture opportunities found offshore.

Offshore wind farms can be developed in locations that have reasonable wind characteristics, favourable sea and seabed conditions, and be situated to avoid shipping lanes, fishing grounds, submarine services, commercial activities and must not disturb birds or marine wild life breeding habitat. Offshore wind converters will be largely installed in moderate depth waters usually less than 50m or otherwise will be mounted on floating platforms anchored to seabed.

The increased cost of offshore wind converters will include increased component costs due to the need for the marinisation of equipment, increased electrical connection costs, increased costs due to the additional ancillary equipment required for offshore installations together with the associated auxiliary power supply overheads and also increased operational and maintenance costs. In order for offshore wind generation system to be economically viable it is anticipated to be as widespread as possible.

The technical limitations to the development of offshore wind energy generators are set by the environment in which the converters are to operate.

A significant proportion of the engineering problems that must be addressed are structural issues related to the force to which the converter and its supporting structure could be subjected to; namely waves, winds, tides and currents, and the relative ease with which such problems can be overcome. From an electrical engineering prospective, seabed conditions, tides and seabed currents have an impact on the design of the cable connection to the shore. These technical considerations will limit the number of suitable sites for development of offshore wind farms, and the following considerations are drawn from this chapter:

- **Offshore wind engineering knowledge and literature, though it is mature enough by now, it is still distributed among many traditional disciplines of engineering practices; civil, mechanical, energy, ocean, wind and offshore oil and gas engineering. Wind energy is a living reality, and is one of the regarded solutions to environmental problems. Floating offshore sites offer an ideal location for commercial size wind energy where most of world wind resources are found with the least possible restrictions while stability and economy renders bottom mounted choice nonviable.**

- **The well developed design criteria for offshore oil and gas industry structures is very different both in philosophy and priorities from that of offshore wind energy structures, hence, this criteria needs to be reconstructed to fit this new technology (high value less cash) option with more knowledge from full scale tests and field measurements being incorporated into it.**

- **An integrated overall design approach, build on the available ones, need to be developed incorporating all related factors and parameters involved in this energy in a more rational way, which collectively involves all engineering disciplines related to this energy technology. The key to this task is good knowledge of wind and marine loads involved as well as analysis techniques employed in attaining the expected response hence available techniques need be explored and evaluated.**

- **Offshore wind energy is the future solution to the energy and environmental crises and currently the momentum is very high in this direction. The main challenging task for offshore wind energy is the cost reduction with the competition favouring offshore energy due to drastic rise in oil prices. Further economy could be achieved only by going for large capacity generating facilities for which the sea is the only feasible site, meanwhile, the impact on the electrical system to which it is connected needs to be closely investigated.**

- **Floating wind turbine constitutes a marriage between two technologies therefore more versatile and comprehensive analysis methodology is needed. Finite element explicit nonlinear dynamic analysis is well suited for analysing the floating moored wind converter, the main features needed for the analysis of such complex structure are employed in the technique. However, no evidence was found for using this technique in structural analysis of offshore turbine.**

- **LS-DYNA3D is an explicit nonlinear dynamic analysis finite element code it is a complete integrated and verified product which delivers the necessary algorithms and resources needed in floating wind turbine analyses. The powerful pre/post processors attached to the explicit solver are expected to fulfil the goal of evaluating its applicability to floating offshore wind turbine analysis and the creation of a full scale model.**

- **Simplified and reliable method for calculating the environmental loads expected to be experienced by the floating offshore wind turbine once in service need be explored. Namely, these are gravity, aerodynamic and hydrodynamic loads applied by the hosting environment, such method is essential for successful analysis and hence design, and therefore need to be investigated and these loads need be quantified.**

CHAPTER III

Floating Wind Turbine Design Loads

3.1 Introduction:

Wind energy technology has developed rapidly over the last few decades. Larger machines as well as new design trends have been introduced, which demand more sophisticated design tools, capable of providing more accurate predictions of loads. The need and interest of placing wind turbines in complex terrain areas has increased. In such sites, high wind speed, high turbulence levels and strong gusts are frequently present hence the weather conditions need careful considerations as they may seriously influence the reliability of wind turbines. In order to back-up further exploitation of wind energy it is important to provide the industry and the certifying institutions with computational tools capable of performing complete simulations of the behaviour of wind turbines over a wide range of different operational conditions. In the work reported herein, the LS-DYNA3D explicit code is used for analysis all loads therefore are functions of time. Important concepts and features of the code are highlighted in the next subheadings while the formulation, capabilities of the code and its application in creating the model to be verified are detailed in Appendix-A1 of this thesis.

3.2 LS-DYNA3D Explicit Code:

LS-DYNA3D is explicit code for solving three-dimensional nonlinear solid mechanics problems which run in batch mode. The pre-processor in the updated edition of the program is capable of generating or translating any complicated geometry that might be dictated, meshing and mesh refinement and reasoning are also readily available. Upon solving for stresses and displacements in either local or global coordinates, the post-processor in the program can easily interpret the results.

LS-DYNA3D is based on a finite element discretization of the three spatial dimensions and a finite difference discretization of time. The explicit central

difference method is used to integrate the equations of motion in time. The central difference method is conditionally stable, with stability governed by the 'Courant limit' on the time step Δt , Jerry [140] and Klaus [141], J. Halliquist [44].

For solid elements, this limit is essentially the time required for an elastic stress wave to propagate across the shortest dimension of the smallest element in the mesh Subramani [117], Jerry [140] and Klaus [141].

Equivalently, this maximum time step may be related to the period of the highest free vibration mode of the finite element mesh. LS-DYNA3D automatically calculates the maximum time step size at each step of the solution, thus minimizing the cost of the analysis while ensuring that stability is maintained.

LS-DYNA3D uses a lumped mass formulation for efficiency. This produces a diagonal matrix M, which renders the solution of the momentum equation.

$$Ma_{n+1} = f^{ext} - f^{int} \qquad 3.1$$

Trivial at each step, in that no simultaneous system of equations needs to be solved, f^{ext} are the applied external forces, and f^{int} are the element internal forces. The new accelerations a_{n+1} are easily found, from which the updated velocity and coordinates are calculated using the central difference integration formulas. In LS-DYNA3D the initial conditions to the transient dynamic problem are specified as initial velocities. Boundary conditions of many types ranging from constrained nodal translations and rotations to non-reflecting boundaries are prescribed easily, Jerry [140] and Klaus [141].

In an explicit code there are many small time steps hence it is important to minimize the number of operations performed at each time step. The minimization is accomplished by using elements with one point Gauss quadrature (Gauss-Legendre Integration) for the element numerical integration. This formulation leads to spurious zero energy deformation modes the so-called "hourglass stiffness" or "hourglass viscosity" while retaining legitimate deformation modes stabilizes these spurious modes, Jerry [140]. Further discussion of this and used features of the code are left to Appendix-A1 of this thesis.

3.3 Explicit Analysis - Important Algorithms:

3.3.1. General:

For the simulation of the non-linear and time dependent behaviour of complex structures such as the floating wind energy converter dealt with here, such models have to provide high accuracy in the prediction of deformations and stability. The limiting factors of the computer simulation are usually the computer run time and the memory required to solve large scale problems. To overcome these problems LS-DYNA3D uses the dynamic explicit time integration procedure for the solution of the semi-discrete equations of motion both in transient as well as in the static conditions (dynamic relaxation). In an explicit analysis neither the element nor the system matrices are built (the solution is element based) and consequently the memory requirements are insignificant. Unfortunately, explicit methods are only conditionally stable and hence the time step size has to be smaller than a critical value, this is directly dependent on the largest frequency of the finite element discretization (smallest element). As a result in large scale problem such as the one dealt with here, extremely short time steps occurs which increase computer run time. Contrary to implicit schemes the generation and fabrication of the system matrices, which are time and memory consuming, are avoided by explicit one where lumped mass and damping matrices are employed. Working with system vectors (instead of system matrices), which may be added up by the finite element contributions for the computation of the state variables it is possible to increase the number of degrees of freedom and thus large problems can be tackled. This is the main driving reason favouring explicit algorithms for large scale and nonlinear problems. Further to that, the use of explicit schemes provides the opportunity to create a uniform software concept both for the solution of static and dynamic problems. To this end a static problem has to be transformed into a dynamic one by adding an artificial acceleration and an artificial damping. This method is known as dynamic relaxation. When static problems are solved by dynamic relaxation both the mass and damping matrices lose their physical background and become fictitious quantities which control the iteration process.

3.3.2 Dynamic relaxation for static initialization:

LS-DYNA3D contains a limited capability for performing quasistatic analysis using a dynamic relaxation algorithm. This feature is primarily intended to be used to generate a static stress solution as an initial condition for a transient dynamic analysis, but it has been applied with some success to the solution of more general static problems, J. Halliquist [44], Jerry [140] and Klaus [141].

The dynamic relaxation method is based on the observation that the long time limit of a damped dynamic solution is the quasistatic solution. Damping is introduced through a 'dynamic relaxation factor' (default=0.995) which multiplies the velocities computed at each step of dynamic relaxation solution. This factor can be adjusted by the user if required; increasing the factor decreases the effective damping while decreasing this factor increases the effective damping, J. Halliquist [44], Jerry [140] and Klaus [141].

During the dynamic relaxation solution process, 'time' is really just a parameter to describe the solution process, and does not correspond to physical time. The current implementation uses a dynamic relaxation time step equal to the standard dynamic time step. Thus if it is desired to slowly apply the static loads to minimise overshoot in the solution, then a short trial dynamic run can be made to determine the time step size. The static loads to be applied during the dynamic relaxation solution can then be applied over some number of time steps (typically 2000-5000 but problem dependent) Jerry [140], and this determines the time points to be used on the load curve controlling the static loads.

Current implementation of dynamic relaxation in LS-DYNA3D is susceptible to dynamic overshoot if static loads are applied too quickly. If only history-independent material models (such as elasticity) are used, then the resulting solution will still be correct and this overshoot behaviour is of little consequence, Jerry [140].

If history-dependent material (such as plasticity) are used, however this dynamic overshoot can cause yielding which is erroneous, and therefore an incorrect static solution is obtained. Thus the dynamic relaxation static solution capability can be used with confidence for elastic initialisation, but must be carefully used with slowly applied loads to prevent overshoot and

inaccuracy in history-dependent static problems, Jerry [140] and Klaus [141]. Dynamic relaxation is not used in this work to limit computer run time and because loads are applied gradually, therefore the forward discussion aimed at enhancing this important capability.

3.3.3. Dynamic relaxation for stresses in rotating bodies:

In many applications such as flywheel design, machine tool safety, or turbine engine containment, it is important to solve a transient dynamic problem beginning with a stress state induced by rotational motion. This problem is easily solved in LS-DYNA3D using the dynamic relaxation option for computing the initial stresses. The part of the model which is rotating should be identified, by material as receiving a body force load due to a prescribed angular velocity. These body force loads should reference a load curve which begins at zero and increases to a value coinciding with the rotational velocity, and remains constant at that value to some large time. This load curve should be marked as active for static initialization only. Initial velocities for these rotating bodies computed on their post-initialization deformed geometry may be generated by specifying on the control card the number of materials to initialize for rotational motion, and then listing these materials in their proper location, Jerry [140]. This approach will allow a smooth transition from the body-force-based calculation of the initial stresses into the transient dynamic phase where the bodies actually rotate in space. During the transient portion of the analysis, the rotating bodies may be allowed to rotate freely, or may have rotational velocities prescribed for them using load curves flagged to be active for transient dynamic analysis only. Also, other loads may be also added to the rotational body during the transient dynamic phase, such as impact with stationary object, Jerry [140].

3.4 Load Cases:

An important part of the design process for a wind turbine is its ability to withstand the various loads it will experience during its expected life. The prime purpose for this assessment is to verify that the turbine will be able to withstand these loads with sufficient safety margin. This task will be

systemised by analysing the developed model for a number of relevant load cases including combinations of environmental, operational and external conditions incorporated in it. In the design of a wind turbine, it is important to identify all load cases which are relevant. Based on evaluation of the analysis, like in this work, structural response of the structure in terms of strength, serviceability and fatigue behaviour will show any drawbacks in load assessment. Lack of statistical data, knowledge of the properties of the used materials, extreme load combinations, method of analysis etc, all could be sources of errors that will lead to failure and financial losses.

3.5 Service Conditions:

This must reflect and quantify the most significant conditions that a wind turbine is likely to experience such as;

- Normal operation and power production conditions
- Cut-in, cut-out and standstill conditions
- Transportation, installation and assembly
- Faults, maintenance, testing loads, loss of mooring conditions.

All these conditions must be quantified and reflected in the design loads together with main structural, mechanical and environmental loads the turbine might face. Design load cases to be used in this work are constructed by a combination of a relevant design situations and external environmental conditions. Such combinations reflect:

- Normal law speed standstill conditions
- Normal operation and normal external conditions
- Normal operation and extreme external environmental conditions
- Standstill condition under sever surviving environmental conditions.

Formulating the quantification of these conditions to incorporate them in the analysis phase will be the focus of the next sections.

3.6 Wind Field Presentation:

It is very important for the wind industry to accurately describe the wind conditions. Turbine designers need the information to optimise the design of their turbines and turbine investors need the information to estimate their

income from electricity generation. As is well known, the highest wind velocities are generally found on hilltops, exposed coasts and offshore. Various parameters need to be known concerning the wind, including the mean wind speed, directional data, and variations about the mean in the short term (gusts), daily, seasonal and annual variations, and variations with height. These parameters are highly site specific and can only be determined with sufficient accuracy by measurement at a particular site over a sufficiently long period.

From the point of view of wind energy, the most striking characteristic of wind resource is its variability. The wind is changing both geographically and temporally. Furthermore, this variability persists over a wide range of time scales, both in space and in time, and the importance of this is amplified by the cubic relationship to the available power. The values suggested in this work will be presented in the Chapter V of this work.

3.7 Load Types:

The external loads acting on a wind turbine are mainly wind loads. As a wind turbine consists of slender elements such as blades and tower, inertia loads will be generated in addition to the gravity loads that act on these elements. Loads due to operation such as centrifugal forces, Coriolis forces and gyroscopic forces can be of significant effect.

In most cases loads on offshore wind turbine can be classified as:

- **Aerodynamic blade loads due to wind.**
- **Gravity loads on all turbine parts.**
- **Centrifugal forces due to rotation.**
- **Gyroscopic loads due to yawing.**
- **Hydrodynamic loads on the supporting hull.**

Gravity loads on turbine blades can cause bending moments in blades in the edge wise direction. In pitch controlled blades, gravity loads will result in moments in the flap wise direction. Due to the rotational nature of blades, these gravitational moment effects will be cyclic. Eventually, the larger the rotor diameter, the greater will be the root moment, typically the blade root bending moment will follow a fourth-power law in blade diameter.

Considering that the rotor area follows a quadratic power law in rotor diameter, this forms one of the challenges in making the wind turbine larger. The adoption of the free yaw system (rotation about vertical axis) in the floating wind turbine, believed to render the gyroscopic forces (in the form of a moment) of minor significance especially for 3-blades turbine Det Norske [88], the even distribution of loads about the global vertical axis will help support this belief and is hence applied herein.

Aerodynamic, forces believed to be the most significant and will be calculated according to the Beam Element Theory some times abbreviated as BEM and Momentum Theory and will be applied as nodal forces on blades while segment pressure value is calculated and applied to nacelle shell face opposing the wind direction as segment pressure as will be discussed.

Hydrostatic water pressure is applied all round to the floating hull and addressed by the code due to body loads and water structure interaction. Wave and current effects will be superimposed linearly in the horizontal flow direction, as a kinematics velocity. Hydrodynamic forces due to wave, current and water pressure will be calculated using Morison's equation. It is used to calculate the hydrodynamic loads accordingly, as the sum of inertia forces and drag forces. The resulting force will be applied to the supporting hull as a vertical linear pressure profile, acting in the direction of flow, coincident with wind flow and normal to hull vertical axis decreasing with depth. Further formulation of Morison's equation will follow in this chapter. Meanwhile quantification of hydrodynamic loads proposed here is detailed in Chapter V of this thesis.

3.8 Aerodynamic Loads on Rotor:

Once all necessary equations have been derived from the Momentum Theory and the Beam Element theory using the approach discussed in Appendix-A3 of this thesis. Then the different control volumes (airfoil) are assumed to be independent and each strip of the blade may be treated separately and therefore the results for one radius can be computed before solving for another radius. For each control volume, the algorithm can be derived into ten steps with equations (A3. #) is referring to Appendix-A3 of this thesis:

1. **Initialise a and a' typically a = a' = 0**
2. **Compute the flow angle ϕ using equation A3.18**
3. **Assuming local pitch angle θ relative to rotor blade compute the local angle of attack α using equation A3.17**
4. **From the assumed (used) airfoil data knowing α read $C_L(\alpha) and C_T(\alpha)$ these values are empirical and based on wind tunnel tests on the airfoil they are either provided by manufactures or ready in standards a typical value of Reynolds' number (R_E) is needed.**
5. **Compute C_N and C_T coefficients from A3.19 and A3.20**
6. **Calculate solidity σ using equation A3.21 and correction factor F using equation A3.26**
7. **Calculate a and a' from A3.27 and A3.28**
8. **If a and a' has changed more than a certain tolerance relative to values assumed: go to step 2 starting with values attained for a and a' else continue.**
9. **If a > 0.3 then the simple momentum theory breaks down i.e. a must be corrected as follows:**

If $a > a_{critical} = a_c \cong 0.2$ then Glauert's correction apply and hence:

$$a=\frac{1}{2}\left(2+K(1-2a_c)-\sqrt{(K(1-2a_c)+2)^2+4(Ka_c^2-1)} \right)$$ **in which**

$$K=\frac{4F\sin^2\phi}{\sigma C_N}$$ **, calculated corrected value of a replaced previous value.**

10. Finally forces normal and tangential to rotor plane are calculated using:

$$F_N=\frac{1}{2}\rho\frac{V_0^2(1-a)^2}{\sin^2\phi}\,\mathbf{c\ C_N}$$ **= Normal force per unit length of blade and**

$$F_T=\frac{1}{2}\rho\frac{V_0(1-a)\omega\times r(1+a')}{\sin\phi\cos\phi}cC_T$$ **= Tangential force per unite length of blade**

With the terms as defined in Appendix-A3 of this work, these values are assumed acting normal and tangential to rotor swept plane orthogonal to wind flow direction. Therefore for coned blades such as is the case here, forces are transformed and applied at the cone angle of 10 degrees (in this model) abiding with the wind direction.

This is in principle the least complicated combined formulation of the Beam Element and Momentum Theories, for wind turbine blades load calculation. In order to get better results the method need to be extended and corrections some times are relevant. Simplifications and idealisations are the source of simplicity of the method over other existing methods.

From the above discussion given Reynolds' number, lift and drag coefficients for the used airfoil then for each strip at r from the blade centre knowing θ and guessing a and a', iteration till convergence is attained (a process could only be feasible through a computer based subroutine using for example MathCAD or Fortran. Assuming that convergence is attained this will give pressure values normal and tangential to the rotor swept plane and for each (r/R) chord radius ratio for the blade. Thus for different ratios of r/R the iterative operation is repeated and the corresponding pressure value is gained. Therefore blade airfoils must be chosen for which iteration is performed and resulting wind thrust will be specific for a blade with the assumed airfoil at the given strip. The final pressure or thrust profile normal to the blade and parallel to wind direction is believed to be in the form similar to that shown in Figure (3.1) but are boundary and airfoil dependent. This thrust profile is assumed to be acting uniformly over the whole rotor area, hence applying it to blades will coincide with the assumption of the Beam Element Method used for development of the approach. When this profile is reached applying it to the model could be done through creating a load curve for each r/R ring as well as the node set for all nodal forces located around this ring in the 3 blades. The thrust then applied as nodal forces for each corresponding radius.

Detailed quantification of these aerodynamic forces is developed in Chapter V of this thesis with the help of a MathCAD sheet and presented as load curves.

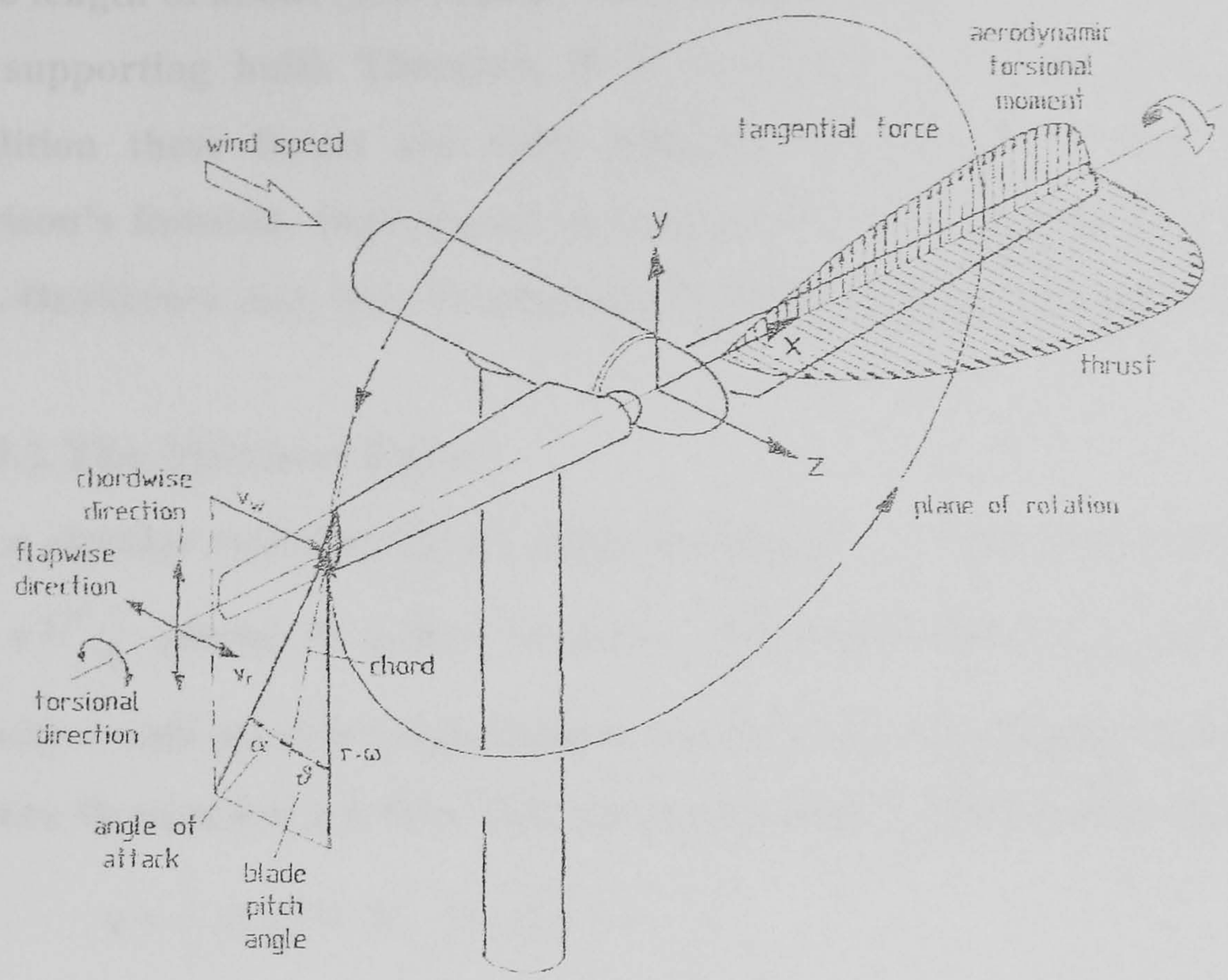

Figure (3.1) Modelling wind loads on blades, Anders [125]

3.9 Current and Wave Forces:

Waves and currents cause distributed forces on structures placed in their field. The three main categories are:

1. Drag forces caused by pressure differences between front side and rear side of the exposed structural component. The pressure differences caused by the friction between the water and the structure that may trigger separation of the boundary layer into a turbulent wake.

2. Inertial mass forces occurring in accelerating flows partly as the forces that would have accelerated the replaced water volume in an undisturbed flow and partly the force required to make the change of the flow pattern to fit with the presence of the structure.

3. Diffraction forces on the surface of structures that in the horizontal directions are not small as compared to the wavelength.

The following paragraph will focus on wave and current forces imposed on the floating hull with the cross-sectional dimension D of the hull being much smaller than the wave length L. Typically for the British North Sea waters a

wave length of about (450-560m), Nobel [142] and for D = 12.5m (diameter of the supporting hull). Therefore D is much less than 0.2L and given this condition these forces can with sufficient confidence be determined by Morison's formula, Department of Energy [56], Det Norseke [88], Lee et al [69], Henderson [62], [43], Henderson [62], Patel [20] and Various editors [22].

3.9.1 The Morison force:

For a circular cylinder, Figure (3.2) of diameter D and cross-sectional area $A = \pi D^2/4$ placed in a flow of water with mass density ρ with particle velocity v and particle acceleration a, the force per unit length of the cylinder is given by equation 3.2, Ove [72], Chakrabarti [63] and Faltinsen [136].

$$q = \frac{1}{2}\rho C_D D V_C |V_C| + \rho C_M A a_C \qquad 3.2$$

Where V_c m/sec and a_c m/sec^2 are velocity and acceleration of the water particles orthogonal to the cylinder axis respectively. The mass density ρ of the seawater is typically about 1025 kg/m^3. The values of the coefficients C_D (drag coefficient) and C_M (inertia coefficient) are partly empirical. They reflect the size of the drag force and the inertial force respectively.

This approach is conservative as it assumes hydrodynamic force on fixed installation. In this case the forces on the floating body are reduced due to the ability of the structure to move. However due to the size of the inertia (dominant force in this case) involved and the fact that the mooring will provide restraint at the stage of loading, hence the relative speed of the floating body and water particles is large enough for this assumption to provide an acceptable representation. This approach was widely mentioned to be accurate enough throughout the literature, Henderson et al [62], [43], [81], Patel [20] and Various editors [22].

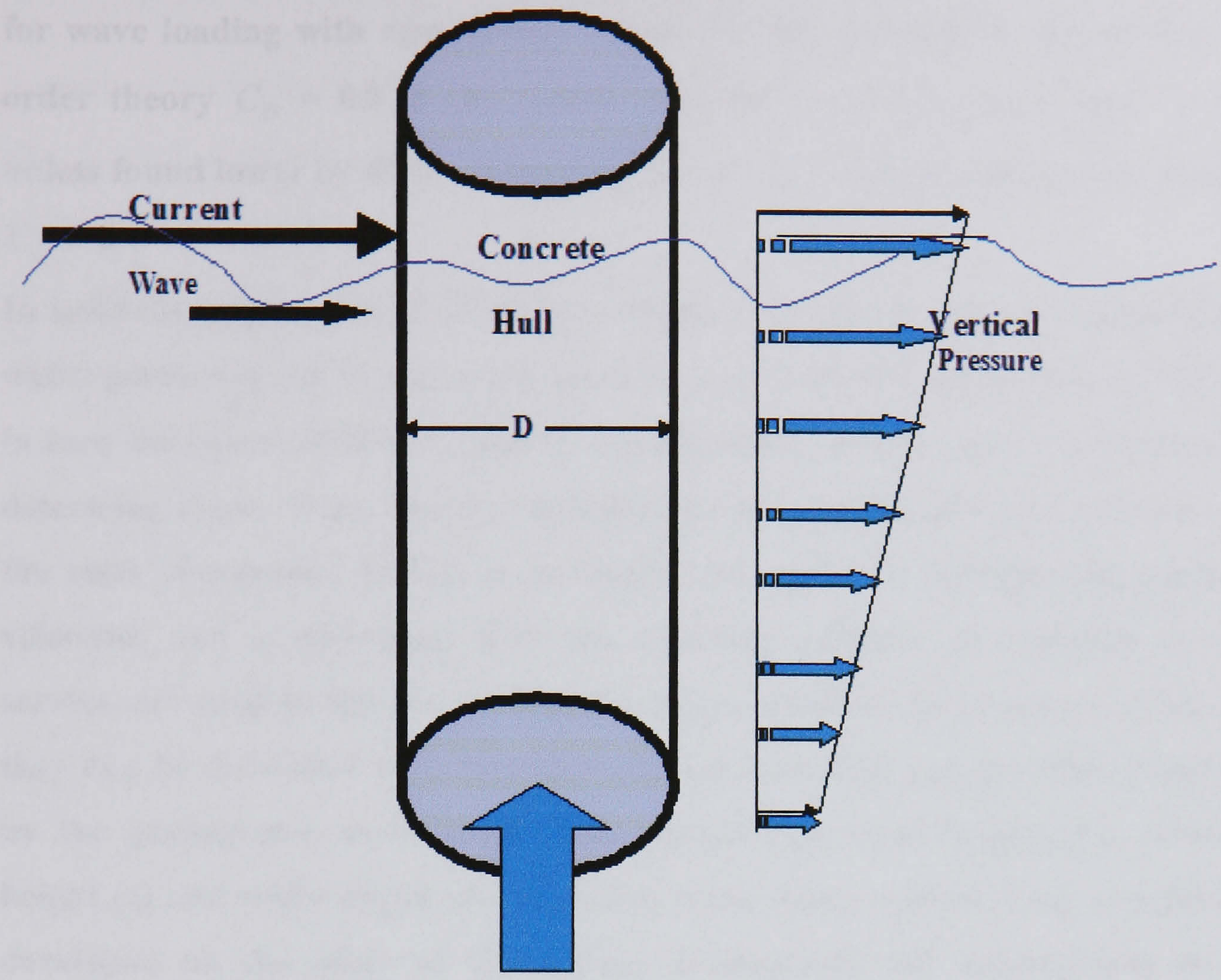

Figure (3.2) Environmental forces on hull vertical side

Detailed discussions are given for the inertia and drag coefficients throughout the fluid and hydrodynamics literature, Department of Energy [50], [53] through [57], Chakrabarti [63] and Faltinsen [136]. For the scalar drag force and mass force coefficient case the mass force coefficient C_M is typically about 2 while the drag force coefficient varies between 0.7 and 1.2. Det Norseke (DS449 1983) [88] gives the following values for circular tubes in connection with Stokes' 5th order wave theory:

$$C_M = 2.0,\ C_D = \begin{cases} 1.2\ for R \le 2.10^5 \\ .7\ for R \ge 4.10^5 \end{cases} \qquad 3.3$$

$R = \dfrac{D|V_C|}{v}$ **Is Reynolds' number the kinematics viscosity** v **is** 1.11×10^{-6} **m²/sec. For the seawater giving** $R \approx 0.9*10^6 D|V_C|$ **with** D **in meters and** V_C **in m/sec (values in between may be linearly interpolated).**

The Department of Energy [53] recommends Morison's equation to be used for wave loading with appropriate values for the coefficients. For Stokes 5th order theory C_D = 0.8 in the splash zone and = 0.6 elsewhere and C_M = 2 unless found lower by diffraction analysis are used, if Airy wave theory is used $C_D = 1$

In brief the application of Morison's equation depending on the values of the water particle speed V_c and water particle acceleration a_c in the flow direction, in turn the values of both V_c and a_c are dependent on the wave theory used to determine them. Wave theories describe the kinematics of waves of water on the basis of potential theory. In particular they serve to calculate the particle velocities and accelerations and the dynamic pressure as function of the service elevation of the waves. The waves are assumed to be long-crested i.e. they can be described by a two-dimensional flow field and are characterised by the parameters: wave height (H), period (T), wave length (L), relative height (z) and water depth (d). Different wave theories of varying complexity developed on the basis of simplifying assumptions are appropriate for a different range of wave parameters. Among the most common theories are: the linear Airy wave theory and the Stokes' fifth order theory. It is obvious that both wave and current velocity and accelerations are decaying with depth; therefore, their effect is decaying as well.

To quantify the linear distributed pressure along the hull vertical axis, a certain wave theory findings of V_c and a_c need be followed; meanwhile the values of drag and inertia coefficients are usually recommended by guidelines and mainly decided by Reynolds' number.

Based on Airy linear wave theory, the maximum horizontal particle velocity can be calculated according to Department of Energy [55] and Lee et al [69] as:

$$Vc = \frac{\pi \times H}{T} \times \frac{\cosh(k \times (z+d)}{\sinh(k \times d)} \times \cos\phi \qquad 3.4$$

Where H is the wave height in metres, T is wave period in seconds, d is the water depth in metres, z is the depth in metres at which water particle horizontal velocity in m/sec is calculated and k is empirical wave number

($k = \frac{2\pi}{L}$). The cosine term is the wave phase which is set to 1 to calculate the maximum horizontal particle velocity in m/sec.

The second part of Morison's force is the inertia which is dominant in this case. The inertia force is much dependent on water particle acceleration as well as the inertia coefficient as discussed earlier. Following Airy linear theory and previous source:

$$\mathbf{a_c} = \frac{\pi \times H \times g}{L} \times \frac{\cosh(k \times (z+d))}{\cosh(k \times d)} \times \sin\phi \qquad 3.5$$

g is acceleration due to gravity 9.81 m/sec^2 other variables as defined before and the sine term is set to 1 to calculate the maximum particle acceleration.

Having calculated the parameters involved in Morison's force either at different depths or at the water surface and bottom, a pressure profile in the shape of Figure (3.2) is established representing the vertical distributed force on the hull orthogonal to hull vertical axis. If the above dimensions were followed the resulting force will be in N/m or force per unite length of the vertical cylinder wall.

Morison's force therefore is:

F (N/m) = F_{drag} + $F_{inertia}$ acting in the discussed sense.

Quantifying this formula to create loads to apply them to the model is left to Chapter V of this thesis. For moderate depths typically between 100m and 500m this distributed pressure profile could be assumed constant on the hull for the purpose of analysis Patel [20], Boss [28] and Chakrabarti [63], the error involved is insignificant. When quantifying hydrodynamic loads reference will be made to Nobel Denton [142] and Various Editors [22] for the used parameters.

CHAPTER IV

Analysis Methodology Verification

4.1 Aims and Objectives of the Finite Element Work

The aim of the work is to produce, if possible, a detailed mathematical representation of a floating offshore wind turbine using a suitable commercial 'state-of-the-art' finite element analysis code. Simpler models have been used Det Norske [88] in the past to estimate the global behaviour of such structures, but with time, the sophistication of analysis tools available to the engineer has increased. Hence the work will explore the possibilities for modelling the detail of such a structure, examine whether the detail is relevant, and give insight into the structural performance.

The nature of the structure, materials, boundary conditions and loading (both static and dynamic) will involve complexity, and the philosophy of how all of these aspects are addressed is of the utmost importance. Explicit time integration techniques have proven to be an excellent tool for transient events such as impact, and some are highly developed in terms of modelling features. LS-DYNA3D is one of such codes and has therefore been employed in this work. The key feature that the code should be able to model, is the floating behaviour of bodies. Main features that need to be addressed are highlighted in the following sections:

1. Buoyancy Effects and Anchorage

The code must be able to model a buoyant structure floating in the sea. There are a couple of ways in which this could potentially be achieved.

a) Ignore any physical presence of the water and imitate the buoyancy effects by applying appropriate forces on the structure. The advantages of this are that they are easy to apply and are useful for the most simple of problems. However the dynamic nature of the loading will be harder to represent in

this way as some prior knowledge of the float movement would be required. Water-structure interaction effects could possibly be modelled using springs and damper systems perhaps, similar to techniques used for soil structure interaction modelling for buildings.

However, the dynamic nature of the moving elements at the interface of very stiff (Lagrangian) concrete and the smooth (zero shear resistance) water elements is difficult to simulate. Furthermore, updating the stiffness of these springs accordingly and representing the sliding nature of the contact at the interface both are a difficult task. Numerical error may be provoked by adding a very stiff spring, either within the FE model or as part of the boundary 'Ill-conditioning' situation where the solution is totally dominant by such very stiff element(s), Cook [79]. The 'pseudo' effects of the water forces on the structure could be modelled, however some of the important features of the water material such as dissipation of the pressure forces would be difficult to simulate.

b) The 'ALE' (Arbitrary Lagrangian Eulerian) feature available in LS-DYNA3D has been used for many fluid-structure interaction problems, mainly for transient impact analyses where severe mesh deformation of the Lagrangian material presents a problem. To date though there appears to be little information specifically on modelling buoyancy effects and subsequent dynamics. Although we are not expecting the mesh to deform in this case, it could provide the appropriate buoyancy and sought fluid material effects. This could however be at the expense of increased elements and solution runtime, so model complexity will need to be monitored carefully.

Typically, if using 'ALE', the turbine will have to float in a fluid 'half-space' of a size which will best represent the effects of the pseudo-infinite sea. The boundaries will need careful consideration, and perhaps employ non-reflecting (energy absorbing) representation. It is this representation which will be employed in this work and a study of buoyancy conducted for verification purposes.

c) **Floating turbines are typically anchored to the seabed using thick polypropylene mooring cables. This anchorage is best modelled using tension only spar elements which are pinned to the model. In reality the cables are attached to the concrete turbine base through slip-rings attached some distance from the top of the hull in a moment free arrangement near the top of the hull. This effect should be easy to model if required using the various nodal constraints available.**

2. The Turbine Model

a) **Given the mass and rigidity of the foam filled concrete hull, this can either be modelled as a rigid material or assigned concrete material properties as appropriate. The foam core just serves to lower the mass centre of float and can be modelled with the appropriate material and density.**

b) **The steel truss which resides above the hull is assumed to comprise of rolled hollow sections, and may be modelled using simple beam elements.**

c) **The nacelle with associated internal parts will present a fairly complex set of items to model depending on how relevant their real behaviour is to the response of the structure. Bearings and revolute gear can all be modelled using the appropriate constraint conditions.**

d) **The blades will require modelling and can either be represented using beam or shell elements. These will serve to capture the aerodynamic loading which is imparted to the rest of the structure. They can be made to rotate along the local rotor axis if appropriate.**

3. Loading

There are many load effects to consider, and the way in which they are applied may have significant influence on the model behaviour.

a) **Gravity will act upon the structure and will govern where the turbine floats in relation to the water. This will be counteracted by hydrostatic forces. For simple force equilibrium representation, the gravity forces are**

simply counteracted by an equilibrating pressure applied to the base of the structure. For the ALE representation an equation of state needs to be specified which initiates the pressure within the fluid. This demands that a position of equilibrium be reached after some period of time once these initial loads have been applied (ramped on over a short time interval), i.e. bobbing of the structure will be witnessed.

b) **Hydrodynamic forces from wave action may be present. These may be applied as static loads/pressures to the side of the turbine hull or possibly time varying loads if required. The use of the coupling between ALE grid and the lagrangian mesh tends to account for creation of these contact pressures.**

c) **Aerodynamic loads can be applied as nodal force to the blades. A variety of wind speed scenarios exist which cause a non-uniform pressure distribution along the length of the blade governed by the Blade Element Method and Momentum Method theories equation. This can be accurately represented or perhaps applied uniformly if the non-uniform distribution is found not to be significant through validation studies. Again time varying load curves can be employed to investigate the dynamics and subsequent loading through the structure.**

Finally it should be mentioned that typically each load action is normally applied at different times on the structure to confirm that its action is properly represented. For example wind loading will be applied some significant time after gravity and water pressure have had time to stabilise.

In summary, it is evident that there are a significant amount of parameters to be considered in order to achieve a comprehensive model of the floating turbine. As all of these parameters are addressed, this invariably results in an increase in model size with regard to the numbers of elements used and computer run-time. All of these parameters may affect the results obtained to a degree, hence verification and validation work is essential to confirm the behaviour of each aspect of the model against well known theory. Therefore simpler models will enable us to have confidence that our representations are

valid and can be taken forward into a more complex and comprehensive model if possible.

The sections that follow present aspects related to the validation work and procedures.

4.2 Lagrangian, Eulerian and ALE formulations:

In general the Lagrangian and Eulerian descriptions simply refer to the algorithm(s) of motion of material with respect to mesh of a quantum mechanics, while ALE (Arbitrary Lagrangian Eulerian) is developed to combine both descriptions arbitrarily in a fashion reducing their drawbacks and enhancing their advantages.

- **Lagrangian algorithms :**

In this case each individual node of the computational mesh follows the associated material particle during motion and is mainly used in structural and solid mechanics. It is allowing an easy tracking of free surfaces and interfaces between different materials and facilitates the treatment of materials with history dependant constitutive relations. Its weakness is its inability to follow large distortions of the computational domain without recourse to frequent re-meshing.

- **Eulerian Algorithms:**

Widely used for fluid dynamics modelling, the computational mesh is fixed and the quantum moves with respect to grid, in these descriptions, large distortions in the quantum motion can be handled with relative ease but at the expense of precise interface definition and the resolution of flow details.

- **(ALE) Description:**

In this description the nodes of the computational mesh may be moved with the quantum in a normal Lagrangian fashion, or hold fixed in Eulerian manner, or be moved in some arbitrarily specified way to a continuous rezoning capability. In ALE greater distortions due to the free domain in movement could be handled than would be allowed by a purely Lagrangian

method with more resolution than would be offered by a purely Eulerian approach. The ALE description is able to accommodate significant distortions of the computational mesh while preserving the clear delineation of interface typical of purely Lagrangian approach and conserving mass, energy and momentum. The ALE formulation basically works by re-meshing the material throughout the simulation so that the mesh stays relatively uniform, hence it will prevent local instabilities caused by highly distorted elements. Thus ALE is proposed to bypass the difficulties arising from large deformation computations which lead to numerical problems due to distortion of elements in classical Lagrangian formulation where mesh movement is attached to material movement. Buoyancy studies on simple model will illustrate and confirm how and whether the ALE is appropriate for use in this model.

4.3 Boundaries and Loads:

4.3.1 Non-reflecting boundaries:

LSDYNA uses this option in solid brick elements only to model the indefinite domain (limit the size of the model). Boundaries are defined as a collection of segments comprising the element faces. In half space, this option prevents artificial stress wave reflections generated at the model boundaries from re-entering the model and contaminating the results. Internally the code computes an impedance matching function for all non-reflecting boundary segments based on an assumption of linear material behaviour. Thus the finite element mesh should be constructed so that all significant non-linear behaviour is contained within the discrete analysis model. In this algorithm the infinite domain such as soil or seawater is truncated via an artificial boundary, thus spurious wave reflection effects are minimized.

Outside bounding nodes of the water 'ALE' part are locked against translation to prohibit material from escaping thus reducing the pressure within it. While the non-reflecting boundary action is achieved by creating a segment set containing of the outer faces of all the bounding solid elements and the function 'non-reflecting boundary' is evoked via this segment set.

4.3.2 Loads

Practically, the designer would consider that environmental loading experienced by typical structures comes from extreme values of all individual environmental parameters (wave, wind, current, etc.) that are usually encountered. In reality the likelihood that the maximum values of all environmental loads happening simultaneously is very remote. Therefore, since maximum values of environmental parameters do not occur at the same time, the application of joint probability of occurrence should be incorporated in determining the maximum loading exerted on the structure.

When considering the combination of wind and wave loads, the short-term wind climate is usually represented by the 10 minute mean wind speed 'U_{10}', and the short-term wave climate is usually represented by the significant wave height 'H_s', the two values usually interpreted as intensities of the corresponding wind speed and sea elevation process, respectively. The wind and waves, at a particular location usually have a common cause such as low pressure. Waves are driven by wind and generated locally, at the same time; roughness implied by wave-affected sea surface influences the wind. Therefore the two are the cause and effect of each other. Yet it is not reasonable to expect that the maximum wind speed will happen coincidently with the maximum wave height.

For design, it is reasonable to consider some relatively rare combination of wave and wind climate as the characteristic climate and then to find the maximum load response that occurs for this climate over its duration. In practice, usually the wave climate for the significant wave height with a 50 year reoccurrence period in combination with a wind climate conditioned on this wave e.g. the expected value of U_{10} conditioned on the 50 year significant wave height or some higher value of U_{10}. This methodology is suggested by Det Norske [88] and the UK Department of Energy [50] through [57]. The 100 year maximum occurrence period may be used instead, the two approaches are widely recommended throughout the literature Det Norske [88] and British Standards [96] through [100], in general the 50 year return period tends to be British practice, while the 100 year return period is used in American and Norwegian practices.

For linear load combinations, Torstar's rule plays a central role, Det Norske [88]. The rule states that the maximum value of the sum of two independent random processes occur when one of them has its maximum value. Application of this rule to the combination of two load processes, e.g. wave load and wind load implies that the combined load will be at its maximum either when the wave load is at its maximum or when the wind load is at its maximum.

Explicit finite element codes use time integration processes, therefore loads are defined with time as load curves. For the purpose of this verification, gravity loads are applied confirming buoyancy behaviour. The buoyancy is very much dependant on geometry and mass loads as will be discussed later in this Chapter. Due to the small inertia involved and to reduce run time in the 2-D model, the gravity load is applied ramped over a short time and the impact effect is assumed to be absorbed by the ALE damping action. Because of the size and mass of the 2-D model rendering it close to the neutral stable buoyancy case (to be discussed later in this Chapter), no side loads were therefore applied to it. In the 3-D small models as the inertia increases, the gravity is applied ramped over a relatively longer period. A small characteristic nodal horizontal load of 1 KN (arbitrary chosen) is applied ramped on a set of nodes representing the supporting hull side opposing wave and current direction to simulate hydrodynamic action.

Surrounding hydrostatic water pressure on the submerged part is readily evoked via constraining the outer nodes and the application of the 'equation of state' and coupling contact namely 'constrained lagrange in solid' function.

Wind loads on blades in the characteristic model are simulated by constant '10 N' "arbitrarily chosen" nodal loads applied on the two blades at three node set intervals in the horizontal direction, simulating wind action. Detailed theoretical description for creating actual loads on a full scale floating wind turbine was mentioned in Chapter III of this thesis. Meanwhile quantification considerations of these actual environmental service loads experienced by the full scale floating wind turbine in the form of load curves is left to Chapter V of this thesis.

4.4 Materials Models:

LS-DYNA3D is equipped with a vast material library which is updated regularly by adding new material models, some of these models are still under verification and their use is largely left to the user, while some are defined for certain types of elements. While for the purpose of verification rigid material can perform well, material models are suggested according to the expected action of the parts to which they are assigned. Some parts ought to be rigid material such as the yaw mechanism, nacelle with internal parts, transmission and rigid wall for seabed modelling. These parts are straight forward to model and therefore, not listed herein while their material properties are listed in the relevant sections. Rigid body material model can be defined for all elements used for structural purposes, keyword cards defining rigid material are given in Chapter V and Appendix-A2 of this thesis. Description of the used materials models and reasoning for their choice are given in the following bullets:

- **modelling the water quanta:**

For the floating wind energy converter hosting sea water is an integral part of the analysis and it is a prime driver for loading and structural behaviour. To simulate this behaviour the ALE brick elements are assumed acting in the finite quanta around and supporting the hull and the cable parts up to the specified height. This formulation assumes separate movement between Eulerian mesh 'brick elements' and multi-materials in dealing with fluid dynamics.

Material 'type 9' (*MAT_NULL) is typically defined by the code for fluids and is used which require the definition of an 'equation of state' to activate pressure inside fluid solid ALE elements. Also hourglass control card for fluid parts need to be defined, therefore the used cards are:

***MAT_NULL**

***SECTION_SOLID_ALE**

***EOS_GRÜNEISEN**

The *Grüneisen* equation is a formula adopted by the code to initiate the pressure inside a compressed material. A MathCAD sheet adopting the use of

this equation for water parameters is presented in the Appendix-A4 of this thesis.

ALE 'multi-material formulation 11' is used for which the seawater part needs to be defined as a 'multi-material group', hence a minimum of two 'ALE' materials should exist. The finite quanta are modelled by applying a 'non-reflecting' boundary along the water cube sides. To initiate buoyancy pressure build up due to gradual gravity loading, the outer nodes bounding the water body are prohibited from translational movements to prevent the ALE material from "running away" thus reducing pressure within it. This is done by defining a node set that contains all nodes in the bounding walls of the 'ALE' body.

To apply the coupling, Lagrangian parts are slaved to 'ALE' parts which are the master in this contact type. Therefore, the float is in contact with the fluid 'multi-material group' (water and air parts). To achieve this coupling a keyword 'constrained Lagrange in solid' card is defined. To guarantee full contact between the water 'ALE' part and the top air 'ALE' part, common nodes at their interface are merged dictating that their common boundary needs to be coincident nodes.

An extremely useful option for 'multi-material group' is the capability of defining the initial volume occupied and thus updating the 'ALE' geometry keeping clear separation (material resolution) by updating the surface following the deformed shape of the multi-material mesh. Through re-meshing of the ALE deformed elements, this function is used to accommodate the hull part inside the fluid parts in a way which guarantees coupling action and saves tedious time consuming geometry creation which could be very difficult in some configurations.

Therefore, to accommodate the hull part inside the fluid parts the used function is:

*INITIAL_VOLUME_FRACTION_GEOMETRY, it is used in creating three empty geometrical shape(s) representing the supporting hull. The value of 1025 kg/m^3 is used for seawater density. The contact between the float part and the fluid 'ALE' group is done via the coupling algorithm of 'constrained Lagrange in solid' expanded in Chapter V and Appendix-A2 of this thesis.

Default element 'type 1' (one point integration solid element) is used suggesting the necessary hourglass control be employed.

- **modelling air quanta:**

The air part is an 'ALE multi-material' part and intended for modelling air bounding the top surface of the water body in the formulation. Similar to the water part this part is modelled using material 'type 9' and 'ALE' solid brick elements 'formulation 11'. This dictates that air is defined as 'ALE multi-material group', therefore, fulfilling the condition of two materials need to be available for material group definition prerequisite for many functions to be used. An equation of state is also necessary for this type of material and therefore defined it is the 'linear polynomial', a density value of 1.1845 kg/m^3 is assigned for air elements.

The 'linear polynomial' equation of state is used by the LS-DYNA3D code to initiate and govern the pressure in 'ALE' elements, typically for ideal gas.

In using this equation the parameter (E0) defined as initial internal energy per unit reference specific volume needs to be calculated based on a given or assumed pressure in 'ALE' air elements. In this case the 'E0' value is calculated assuming atmospheric pressure of (101,325 Pa) in air elements using the formula:

$P = C_0+C_1\mu+C_2\mu^2+C_3\mu^3+(C_4+C_5\mu+C_6\mu^2)$ which is the equation of state for linear polynomial, LSTC [45].

With $C_0=C_1=C_2=C_3=0$, $C_4=C_5=0.4$ and $\mu=1.8444e-05$, thus the parameter E0 is calculated:

101325 = (0.4+0.4x 1.8444e-05) x E0

Hence E0 = 253,307.8 Pa

The values of μ being air dynamic viscosity and other used coefficients are detailed in the Appendix-A2 of this thesis. Therefore, required keyword cards for modelling air quanta are:

***MAT_NULL or 'type 9'**

***SECTION_SOILID_ALE**

***EOS_LINEAR_POLYNOMIAL for equation of state,**

The constraints applied to this part are coupling with the water part which is done through merging the common coincident nodes at the interface and coupling with the slaved float part at their common interfaces. The coupling which accounts for contact between the float and 'ALE' group is done by keyword:

***CONSTRAINED_LAGRANGE_IN_SOLID. This unique algorithm for defining coupling (contact) in fluid-structure interaction is combined with the capability of calculating forces, and stresses in the 3 global axes of the structure as well as the average pressure on element or set of element(s) segment(s). These forces, stresses and average pressure are activated only if the coupling between Lagrangian mesh and 'ALE' grid is defined, they are exported to the ASCII file 'd3plot' to be accessed and read by the post-processor and values are plotted. Further expansion of this useful algorithm is left to Chapter V and Appendix-A2 of this thesis.**

- **modelling the float**

Typically in the verification or debugging stage all materials are modelled as rigid body except the material to be verified. Rigid material 'type 20' provides a convenient way of turning one or more parts of any elements class into a rigid body. The LS-DYNA3D manual states that approximating deformable body as rigid is a preferred modelling technique in many real world applications.

Rigid bodies are robust and versatile and very well developed in the algorithms involving their use in LS-DYNA3D such as contacts, constraints, imposed motions and displacements. The common nodes of both rigid body parts used in defining 'joint revolute' are coincident but not merged to capture the 'joint revolute' behaviour. Elements defined as rigid are bypassed in the element processing and no strains or stresses are calculated for them, consequently they are calculation cost (memory and time) efficient, hence they are preferred.

In rigid body material, all elements of the same material number are treated as rigid body, these elements are integrated to determine their common mass and centre of gravity and moment of inertia of the group, this group is dealt

with as a rigid body with 6 degrees of freedom (3 rotations and 3 translations) applied to their common centre of gravity. The position of all rigid bodies is updated in LS-DYNA3D by a time integrator which works together with the central difference method of time integration (explicit method).

The float was modelled as a rigid body to confirm it's buoyancy behaviour and then switched to elastic 'material type 1' with concrete properties since the real stresses are expected to be within the elastic range for the real supporting hull simulated by the float in this verification. The reason for switching to the elastic material model (model with finite stiffness) is the need to calculate the strains, stresses and forces for the elements involved. These are necessary physical values which are element based and not processed for rigid body elements. Employed material properties for concrete are expanded in Chapter V and Appendix-A2 of this thesis.

- **modelling the truss**

The material 'type 98' '*Material_simplified_Johnson_Cook' which is a simplified version of the material 'type 15' is used. This material model is defined for (beam) truss elements, and is primarily intended for structural analysis where thermal effects are insignificant. The hollow heavy steel sections and their connections intended for offshore structures are typically designed as plastic sections. This material model is cheaper to run, (although alternatively elastic material 'type 1' could be used instead). The material is not expected to exhibit plasticity, although it is included in the event that this could possibly occur, and 'beam section' for element property is used. Factors defined for steel in this material type as well as properties are mentioned promptly in the characteristic model to follow in this Chapter, and expanded in Chapter V and Appendix-A2 of this thesis.

Only three material models are available for the truss (beam) elements, i.e. elastic 'material type 1', elastic plastic kinematic 'material type 3', or material 'type 098' Simplified Johnson Cook, in addition to the rigid body material. The Simplified Johnson Cook material was primarily conceived for use in structural analysis where large strain rates may be experienced without the more advanced features of thermal or damage effects (50% faster solution

than the full Johnson Cook). It could be argued that the elastic model or simpler plastic kinematic model would be suitable for use, and this point is accepted. But without fore knowledge of the behaviour of the system the employment of the simplified Johnson Cook plasticity model was judged to be appropriate in the event that large strain plasticity might occur, and an acceptable 'trade-off' in terms of its effects on solution run-time.

- **modelling the cables:**

The only material model defined by the code for cables modelling is material 'type 71', (*Mat_Cable _Discrete_Beam) specifically defined to model cable action, the material assumes elastic behaviour for section properties. Traditionally steel rope mooring will be the choice but due to the advantages of polyester taut ropes they will be chosen herein. These advantages include:

a) **Polyester ropes weigh one-seventh less in-water than steel wire and reduce the weight of the mooring system by as much as 80 percent. This leads to less vertical loads on the hull hence less size and less cost.**
b) **The use of polyester in the 'taught-leg' configuration is more effective in storing and releasing energy associated with fall and rise of wave, and the elastic response of the rope provides the restoring force to the hull. The straighter line to seabed reduces the length of the mooring by as much as 70 percent directly lowering the cost of the mooring system and reducing seabed 'footprint'.**
c) **In taut-leg configuration, the angle at which the mooring line is connected to the hull is much larger (as measured from vertical). A larger component of the line tension therefore acts horizontally counteracting the wind, wave and current forces.**
d) **Polyester ropes are superior to steel wire in fatigue characteristics which is one of the critical aspects in vibrating structures.**

The primary function of the mooring cables is to keep the body in position under the drifting action of wind, current and waves.

The eight mooring line choice is based on offshore engineering past experience, so that the buoy is kept in place even if one of the lines is lost. The mooring choice is adaptable to water depths between 75m and 500m. The

catenaries are of taut wire synthetic fibre rope for the whole water depth with the section passing through guiding shoes made from steel cables. Due to the cost and difficulty in erecting and anchoring piles, more than one mooring cable share the same anchor pile in the multiunit wind farm. Keyword cards associated with this material include element property and beam section as follows:

***MAT_CABLE_DISCRETE_BEAM and**

***SECTION_BEAM**

The top and lower ends of these cables are restrained against translational movement but not rotation this is readily defined via the keyword 'constrained interpolation'. More than one neighbouring node from the hull and seabed parts to the cable termination node(s) is used in this constraint to avoid local stress concentrations. Cables are coupled to surrounding 'ALE' water elements through the algorithm 'constrained lagrange in solid' as already discussed in previous bullets. Cross section properties used in the verification are mentioned promptly later in the relevant part while further expansion is given in Chapter V and Appendix-A2 of this thesis.

- **modelling the blades**

The blades are represented by material 'type 3' material plastic kinematics and of glass reinforced plastic 'GRP' properties. GRP dominates the market because it provides the necessary properties at low cost. The important characteristics of GRP are good mechanical properties, good corrosion resistance, high temperature tolerance, ease of manufacture, and favourable cost. Typical values are (170Mpa, 100Mpa, 170Mpa and 12E+03Mpa) for tensile strength, compressive strength, bending strength and modulus of elasticity, Det Norske Veritas [88]. Blades are modelled with plate shell fully integrated elements formulation (16) to avoid 'hourglass' energy in the system. Material 'type 3' is selected due to the overstressed condition of the blades once in service at the extreme wind conditions especially at the blades roots where the fluctuating (negative and positive) stresses are expected to reach plastic capacity in this region. Rigid material could be used but will offset the

possibility of calculating the element stresses. Properties of GRP used is expanded in Chapter V and Appendix-A2 of this thesis.

4.5 Running The Solver:

- **negative volume termination errors**

There is no obvious answer to the chronic problem of error termination due to the difficulties in identifying certain reason behind it. The problem is more complicated when more than one reason is involved. However, there are certain precautions might help in debugging, if not preventing these errors. There is in general a deficiency of error reporting in most of the finite element codes. In LS-DYNA3D some errors are reported especially those related to rigid bodies or constraints and material requirements while some are not. The most common solutions for negative volume errors can be addressed as follows:

a- Use the most updated release of the code (LS-DYNA3D).
b- Stiffen up the stress-strain curve for the material involved.
c- Double check units and material properties for relevant parts.
d- Turn all damping off.
e- In foam 57 increase damping parameter to the max. 0.5
f- Use *control_interior for soft materials (foam)
g- Turn logic off in *control_contact and ERODE=1 in *control_timestep
h- Reduce time step scale factor in *control_timestep
i- Avoid fully-integrated solids (formulation 2 or 3), which tends to be less stable in large deformations, instead use default (type 1) element with type 5 or 6 hourglass control, or tetrahedral solid elements with element formulation 10 for soft foams.
j- Use *contact_automatic and reduce bucket sort factor.

- **using dynamic relaxation:**

It was discussed in Chapter III that LS-DYNA3D has limited capabilities in performing static analysis. For dynamic problems the dynamic relaxation feature is used to initialise equilibrium (initial) state. During such transient

analysis both mass and damping matrices loose their physical background and become fictitious quantities to control the iteration process. Physically this method amounts to the imaginary situation of immersing the structure in a viscous fluid which damps the strong geometric nonlinearities. To start with a few runs were carried out on both the verification models and the full scale model to assist the use of this algorithm, however, it's use was excluded to reduce run time and because the kinetic energy difference (the criteria for dynamic relaxation convergence tolerance) was found to be small enough from the first few cycles. This suggests that convergence was either attained in early stage. Dynamic relaxation will continue to run unless a time limit to terminate it is imposed and the analysis continues until the convergence is successful. When dynamic relaxation was excluded the models were seen to equilibrate satisfactorily using the normal dynamic formulations, and a decision was made to use loads applied in the normal transient phase only.

- **hourglass control:**

Hourglass energy is noisy and erroneous and results in mathematical conditions that have no physical meaning and therefore need to be controlled. LS-DYNA3D assumes a default value type 4 unless modified via the hourglass control card. Due to high deformations inherited with the ALE, hourglass control is necessary for default 'type 1' one point integration elements, hence this is defined as type 4 with an hourglass factor of HQ = 0.0005 to guard against instability (defined and called in the part definition). Further discussion given in Chapter III aims at prevention of these modes, while more expansion is left to Chapter V and Appendix-A2 of this thesis.

- **damping**

Energy dissipation is damping, it causes the amplitude of free vibration to decay with time, and limiting the amplitude of vibration produced by a loading whose frequency coincides with a natural frequency (resonance). Damping can be inherited (material) or algorithm added (artificial), in structural dynamics response damping can be:

- **Viscous damping exerts forces proportional to velocity which appears as the damping matrix in the dynamics equation. Viscous damping is supplied by surrounding fluids or be added to the structure.**
- **Inherited damping is a material effect resulting from small plastic effects while the material is still within the elastic range. Other forms are friction or contact damping typically termed as Coulomb damping.**
- **Radiation damping refers to energy loses due to practically unbounded quanta such as soil and seawater like (infinite medium).**

In LS-DYNA3D damping is introduced as a default value that can be changed where it is needed. In some material models such as foam and in all contacts damping is mandatory. Fluid/structure interaction coupling (contact) also has the effect of dissipating energy, as it is adopts the penalty type of contact which uses artificial spring stiffness for penalty force calculation. The radiation damping effect is also present via the non-reflecting boundary algorithm intended to simulate the infinite where energy is dissipated or absorbed thus prohibited from re-entering the system. The algorithm (artificial) damping choice is also available in the code via the readily defined dynamic relaxation function. In LS-DYNA3D, system damping can be applied at any time during the solution either globally via damping keyword card(s), control card, or on the defined material keyword card. The calculation of factors involved in the damping calculation, by no means is an easy task, for over damping will result in prolonged analysis with all burdens of computer time and memory, while under-damping results in numerical noise (erroneous). In this verification the control damping card is activated to allow default damping values.

- **run time and time step**

The time step is crucial for the stability, convergence and accuracy of explicit analysis. LS-DYNA3D automatically chose the critical time step for the system based on the maximum frequency of the smallest element and uses this step throughout the analysis. This is what is known as conditional stability, i.e. time integration is stable if the time step decreases.

The time step is limited by stability and it usually falls during the analysis due to the elements being distorted, (it could also rise as well). It is not possible to use a time step larger than the critical time step but it is possible to use a lower time step which will increase the run time (but has been shown not to improve the results).

The time step is reduced by reducing the default 'SCFT' value (0.9) on '*control_timestep' keyword card, or by specifying a time step versus time load curve on the same card. Instability shown by rapid rising energy and a float over flow error will occur if the period of any mode of deformation in the model is less than π times the time step.

Roughly speaking, the time step Δt = 0.9 L/C for any element, L being the smallest distance between any two nodes and C being the sound speed in the material (the beam cross-section and shell thickness are not considered when calculating time step). If the time step does not conform to this criterion, computed displacements and velocities grow without limit, thus causing instability and error termination. In most of the problems the time step selected by the code is good enough for accurate analysis. The code uses different formulas for different types of elements employed based on element geometry properties, Young's modulus, Poisson's ratio and material density, then the smallest time step is used for analysis.

For lengthy simulations where the number of time steps goes above half a million or so, double precision executable version of the code must be used to minimize the numerical round off errors.

The time step calculated by the code were used in the verification models while using other possibilities of reducing the time step is advisable for the full model where the saving in time can be useful due to the number of DOF involved. The LS-DYNA3D code adapts two possibilities for improving the run time by adjusting the critical time step calculated by the code using one of the following two approaches:

i. Mass scaling technique:

In this approach the same time step (larger than the code calculated) is used for all elements by adjusting the density of elements. This is activated by positive 'DT2MS' on '*control_timestep', or adjustment applied to elements

with time step less than a specified value and activated by giving 'DT2MS' on the same keyword card negative value. Mass-scaling carries a burden of having to confirm that the addition of non-physical mass does not significantly affect the results (the same is said for time scaling).

ii. Sub-cycling:

In this technique elements are grouped and stored based on their time step (mixed time integration). This will speed up the analysis run time and allow local mesh refinement which is efficient when the element size in the mesh varies significantly. This approach is a mixed time step process where the time step is used for each group thus avoiding the use of the smallest one and improves the run time. Further important issues in running the solver are:

- ✓ **One point integration element reduces the amount of effort required to compute the strain matrix by 25 times over the 8 point integration element, while in the element strains and the nodal forces calculations the number of multipliers is reduced to 16 times for the one point integration element over the 8-point integration one.**
- ✓ **In the solution of the plasticity problems and problems where Poisson's ratio is close to 0.5, fully integrated elements can experience constant volume bending modes.**
- ✓ **Time integration is intended for finding numerical solutions for the nonlinear differential equations representing the equations of equilibrium for the nonlinear finite element system. This numerical solution is cheaper and easier to attain than an analytical solution.**
- ✓ **The time step need to be small enough to assure that the stress wave does not propagate across more than one element per time step.**
- ✓ **When imposing loads, load curves are gradually ramped up from zero to avoid the excitation of high frequency response caused by abrupt impact effects. This practice is observed throughout the process of creating load curves.**

- **mesh size:**

Finite element analysis is the simulation of a physical approximation of the real system. Using simple, interrelated building blocks called elements; a real system with infinite number of unknowns is approximated with a finite number of unknowns, since the FEA model is the mathematical idealization of the real system.

In the real world, no analysis is typical, as there are usually facets that cause it to differ from others.

The art of using the FEM lies in choosing the correct mesh density required to solve a problem. If the mesh is too coarse, then the element will not allow a correct solution to be obtained. Alternatively, if the mesh is too fine, the cost of the analysis in computing time can be out of proportion to the results obtained. In order to define a relevant mesh, some idea of the parameter distributions (stress, pressure, etc) within the component is required. If the answer is known, then a good mesh can be defined. A fine mesh is required where there are high parameter gradients and strain whereas a coarse mesh is sufficient in areas that have stress resultant contours of reasonably constant slope.

A good or appropriate mesh is one that enables accurate resolution of the underlying physical phenomena, yet is coarse enough to allow a fast solution time.

Element aspect ratio is the ratio between the longest and the shortest element dimension. Acceptable ranges for aspect ratio are element and problem dependant, but users are normally given limits such as 3:1 for stresses and 1:10 for displacements. There is no hard and fast rule, the limit to aspect ratio can be affected by the order of the element, displacement function, numerical integration used and the material behaviour.

The two mesh factors that affect accuracy are element quality and mesh density. Not all the features in a model will need the same level of accuracy and so a variation in mesh density through the model is usually appropriate; striking a balance between required accuracy and effort required in adjusting the mesh and time to run it.

LS-DYNA3D has the option of re-meshing and adaptivity that could be invoked via the control cards or some material cards. The manual however, elaborates that these options are still under development and testing, therefore their use was excluded. In the verification models following in this Chapter and in the full scale model presented in Chapter V of this thesis the above guidelines of aspect ratio, ease of defining coupling (contact), as well as time, pressure and stress criterion were observed in mesh construction. Also, one to one correspondence of the nodal elements at the contact interface was achieved thus guaranteeing full contact. Pressure and stress values showed good agreement giving confidence in the mesh size and the value of 0.01 default (FEMB 28) element size is used in the 2-D model. This meshing was arrived at after a few trials and therefore judged to be sufficient. In the full model and due to the size and number of elements involved fine meshes were observed at critical locations only while smooth transfer in mesh size is satisfied.

4.6 Validation of Buoyancy using ALE

To confirm the ability of ALE to model the effects of buoyancy correctly, a simple two-dimensional representation of a cuboid float was examined by simple hand calculation and also using LS-DYNA3D. The dimensions of the float examined are shown in the following Figure (4.1).

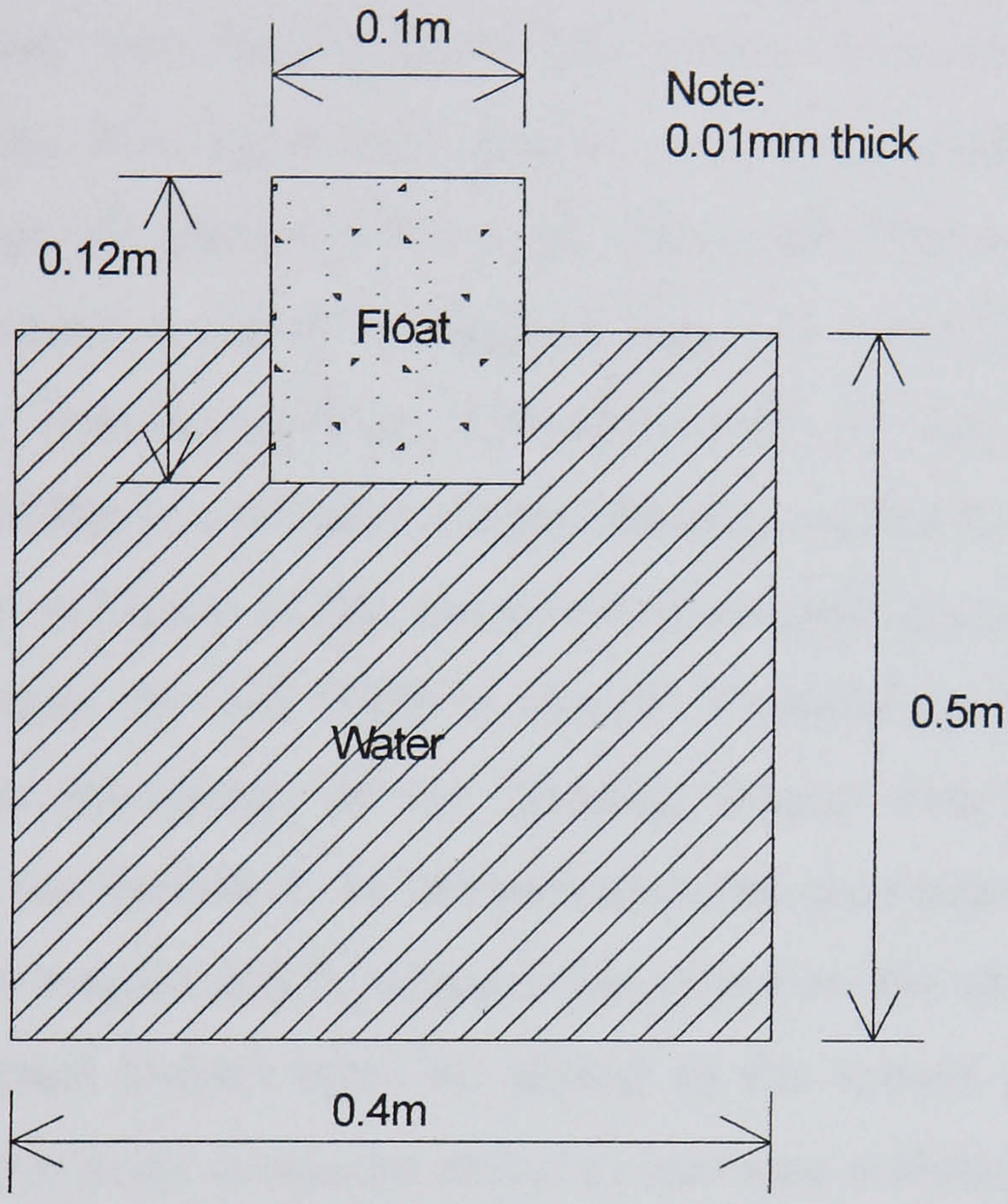

Figure (4.1) Two-dimensional representation of float model

There are a number of parameters which can be studied in terms of geometry and material properties, but for this exercise, only the influence of float density was studied. A number of different cases were chosen to illustrate different cases of floating stability and the angles of list expected to be taken up by the float. Firstly a discussion regarding the theory of buoyancy is presented.

4.6.1 Buoyancy and Stability of Floating Objects:

One of the most important problems involving buoyancy is the determination of the stability of a floating object. The analysis may be illustrated by considering a body shown in a cross section in an upright position Figure (4.2a). Point B is the centroid of the displaced volume and is known as the

centre of buoyancy. The resultant of the forces exerted on the body by the water pressure is the force F_B. Force F_B passes through B and is equal and opposite to body weight W.

If the body is caused to list through an angle $\Delta\theta$, Figure (4.2b) the shape of the displaced volume changes and the centre of buoyancy will shift to some new position such as B'. The point of intersection of the vertical line through B' with the centreline of the unlisted body is called the metacenter M and the distance measuring how far M from the centre of mass G is known as metacentric height. For most hull shapes the metacentric height remains practically constant for angles of list up to about 20^o. When M is above G, as in Figure (4.2b), there is clearly a righting moment which tends to bring the body back to its original position. The magnitude of this moment for any particular angle of list is a measure of the stability of the body. If M is below G, as for the body of Figure (4.2c), the moment accompanying any list is in the direction to increase the list. This is clearly a condition of instability and strictly avoided in the design of any floating object. This methodology has been observed in the models to be presented in the next headings. For a wind turbine where the weight and horizontal forces act so far above the centre of buoyancy, significant ballast must be added to the lowest possible location, thus the centre of gravity is moved down to increase stability. The larger the metacentric height 'GM' the greater is the restoring (righting) moment.

A floating body is stable if, when it is displaced, it returns to equilibrium.

A floating body is unstable if, when it is displaced, it moves to a new equilibrium.

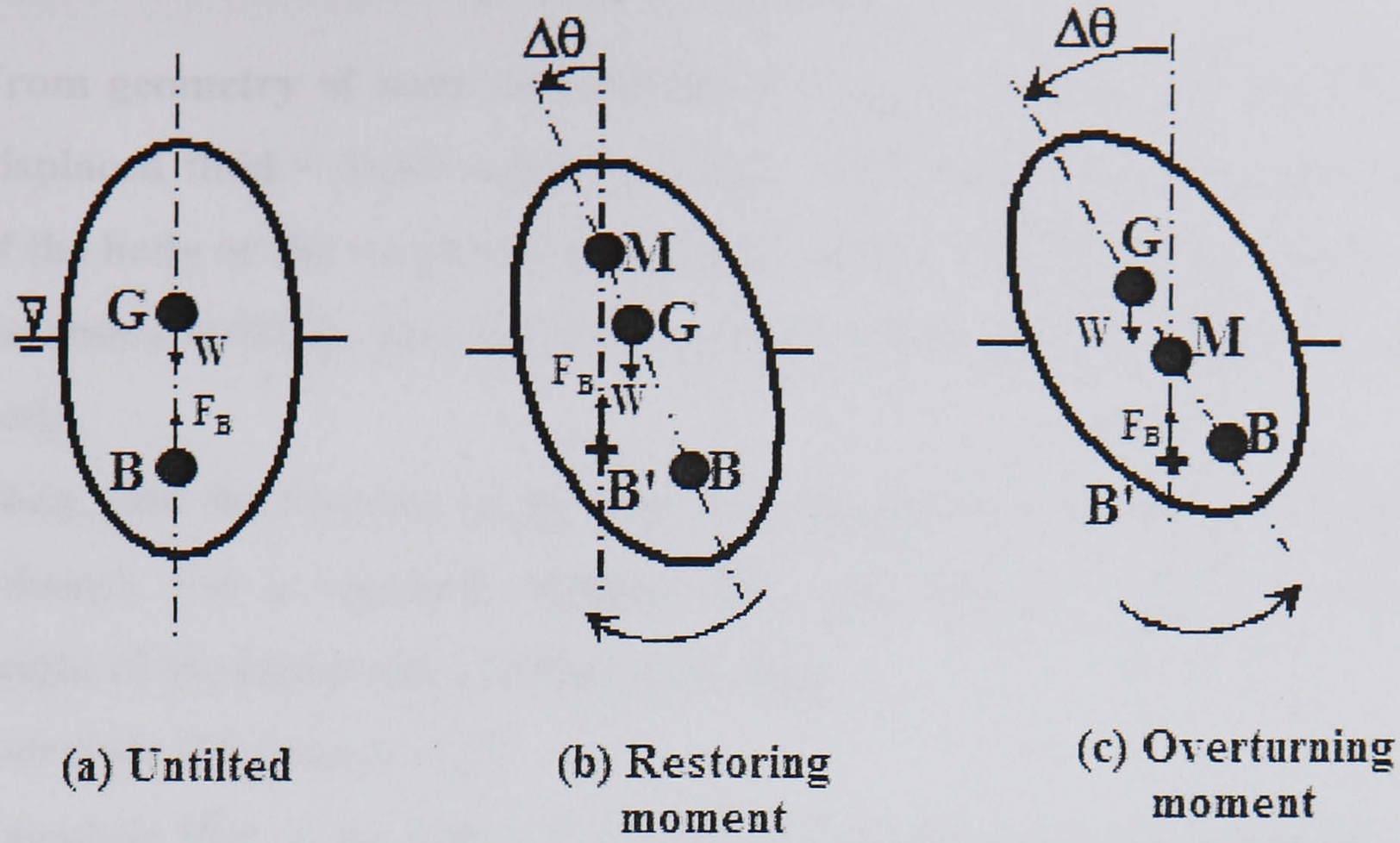

(a) Untilted (b) Restoring moment (c) Overturning moment

Figure (4.2) Stability of floating bodies

In the shown illustration, stability is attained if the metacentric height, MG, is positive ($MG = z_M - z_G > 0$). If the metacentre, M, lies below the centre of gravity, G, then the body is unstable. In other words the metacentric height, MG, is negative ($MG < 0$).

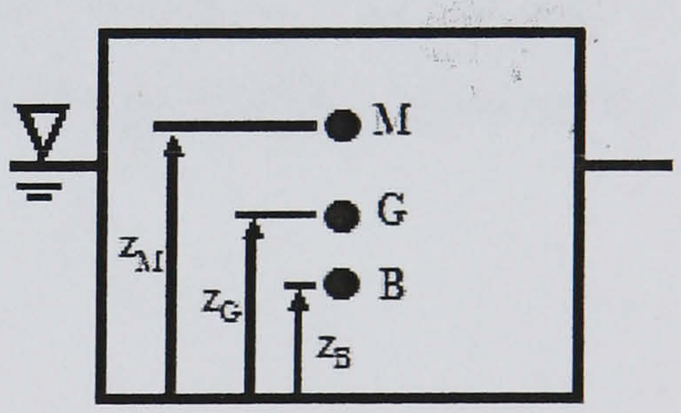

Where metacentric height, MG, is given by:

$$MG = MB - GB \quad \text{or} \quad MG = \frac{I}{V_S} - GB$$

I is the 2nd moment of area (moment of inertia) of the plan section of the body where it cuts the waterline. In other words, if someone were to cut horizontally through the body at the water surface and look at the area of the body exposed by the cut, I is the 2nd moment of area of that body about the *longest* axis. While V_S is the submerged volume (i.e. volume of fluid displaced) and GB is the distance between the centre of gravity and the centre of buoyancy ($= z_G - z_B$) found from the geometry.

To conclude steps for solving buoyancy problems are:

(1) From geometry of body and density of fluid and body equate; Weight of displaced fluid = Total weight of body. This gives the depth of immersion of the body or the weight (density) of the body, whichever is unknown.

(2) To assess stability, first find the location of the centre of gravity G of the body.

(3) Then, find the location of the centre of buoyancy B (centroid of displaced volume). For a regularly shaped body (cuboid) this will be at half the height of the immersed portion of the body.

(4) Calculate the distance GB.

(5) Calculate MB, using $MB = I / V_S$, ($I = \pi D^4/64$ for a circular section body and $bd^3/12$ for a rectangular section body, D is diameter, b and d are the sides of the rectangle).

(6) Calculate metacentric height, ($MG = z_M - z_G$), from $MG = MB - GB$. If $MG > 0$ then body is stable. If $MG < 0$ then body is unstable while $MG = 0$ is neutral stability.

In the proceeding MathCAD templates, the theoretical behaviour of the buoyancy action of the above mentioned 2-D model of varying float density is illustrated. The buoyancy stability is achieved at different listing angles for the various densities. These sheets are as follows:

Buoyancy Stability Check - Case No 1

$kN := 1000 \cdot N$

Problem Data

Size of object — Breadth $B := 0.1 \cdot m$ — Depth $D := 0.12 \cdot m$

Thickness $T := 0.01 \cdot m$

Density of object $\rho_s := 87.98 \cdot kg \cdot m^{-3}$

Density of Water $\rho_w := 1025 \cdot kg \cdot m^{-3}$

Displaced height of water

$$h := \frac{\rho_s \cdot B \cdot D \cdot T}{\rho_w \cdot B \cdot T} \qquad h = 0.01 \ m$$

Geometry of Part Submerged Bouyant Object

$$d_1(\theta) := \frac{2 \cdot \frac{\rho_s \cdot D}{\rho_w} - B \cdot \tan(\theta)}{2} \qquad d_2(\theta) := B \cdot \tan(\theta) + d_1(\theta)$$

Position of centroid

$$x_{bar}(\theta) := \frac{\left(d_1(\theta) \cdot B \cdot \frac{B}{2}\right) + \frac{B \cdot (d_2(\theta) - d_1(\theta))}{3} \cdot B}{\left(d_1(\theta) \cdot B\right) + \frac{B \cdot (d_2(\theta) - d_1(\theta))}{2}}$$

$$y_{bar}(\theta) := \frac{B \cdot \frac{d_1(\theta)^2}{2} + B \cdot \frac{d_2(\theta) - d_1(\theta)}{2} \cdot \left(d_1(\theta) + \frac{d_2(\theta) - d_1(\theta)}{3}\right)}{\left(d_1(\theta) \cdot B\right) + \frac{B \cdot (d_2(\theta) - d_1(\theta))}{2}}$$

Metacentre height above Centre of gravity (represented on subsequent graph plot)

$$m_h(\theta) := \frac{x_{bar}(\theta) - \frac{B}{2}}{\tan(\theta)} - \left(\frac{D}{2} - y_{bar}(\theta)\right)$$

$i := 1 \cdot deg, 2 \cdot deg .. 37 \cdot deg$

$m_h(0.01 \cdot deg) = 26.055 \ mm$

$STABILITY := if(m_h(0.01 \cdot deg) > 0, "STABLE", "UNSTABLE")$ STABILITY = "STABLE"

Angle of List

THETA = 0 degrees

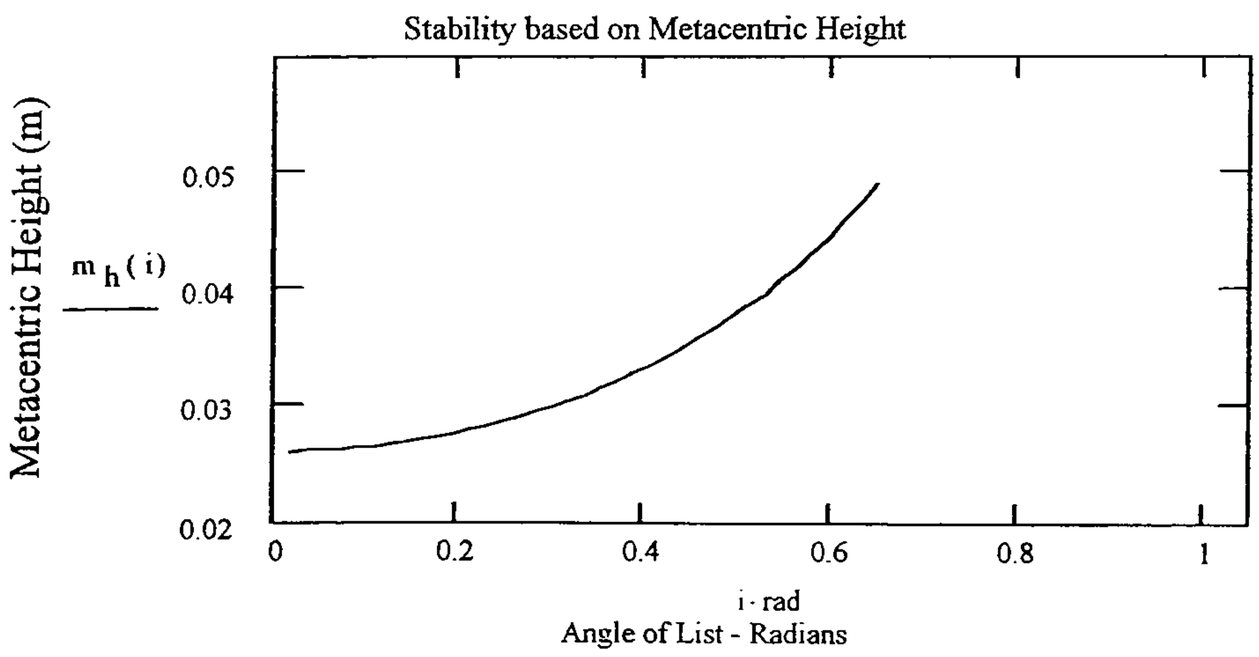

Buoyancy Stability Check - Case No 2

$kN := 1000 N$

Problem Data

Size of object — Breadth $B := 0.1 \cdot m$ — Depth $D := 0.12 \cdot m$

Thickness $T := 0.01 \cdot m$

Density of object $\rho_s := 113.6 kg \cdot m^{-3}$

Density of Water $\rho_w := 1025 kg \cdot m^{-3}$

Displaced height of water

$$h := \frac{\rho_s \cdot B \cdot D \cdot T}{\rho_w \cdot B \cdot T} \qquad h = 0.013m$$

Geometry of Part Submerged Bouyant Object

$$d_1(\theta) := \frac{2 \cdot \frac{\rho_s \cdot D}{\rho_w} - B \cdot \tan(\theta)}{2} \qquad d_2(\theta) := B \cdot \tan(\theta) + d_1(\theta)$$

Position of centroid

$$x_{bar}(\theta) := \frac{\left(d_1(\theta) \cdot B \cdot \frac{B}{2}\right) + \frac{B \cdot (d_2(\theta) - d_1(\theta))}{3} \cdot B}{(d_1(\theta) \cdot B) + \frac{B \cdot (d_2(\theta) - d_1(\theta))}{2}}$$

$$y_{bar}(\theta) := \frac{B \cdot \frac{d_1(\theta)^2}{2} + B \cdot \frac{d_2(\theta) - d_1(\theta)}{2} \cdot \left(d_1(\theta) + \frac{d_2(\theta) - d_1(\theta)}{3}\right)}{(d_1(\theta) \cdot B) + \frac{B \cdot (d_2(\theta) - d_1(\theta))}{2}}$$

Metacentre height above Centre of gravity (represented on subsequent graph plot)

$$m_h(\theta) := \frac{x_{bar}(\theta) - \frac{B}{2}}{\tan(\theta)} - \left(\frac{D}{2} - y_{bar}(\theta)\right)$$

$i := 1 \cdot deg, 2 \cdot deg .. 37 \cdot deg$

$m_h(0.01 \cdot deg) = 9.309mm$

$STABILITY := if(m_h(0.01 \cdot deg) > 0, "STABLE", "UNSTABLE")$ STABILITY = "STABLE"

Angle of List

THETA = 0 degrees

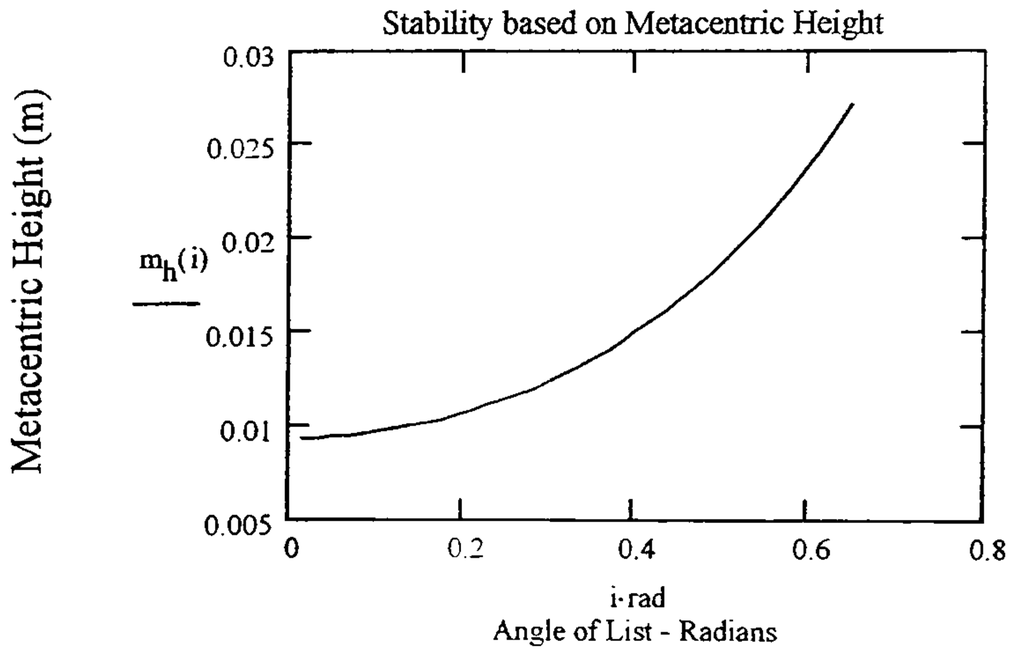

Buoyancy Stability Check - Case No 3

$kN := 1000 \cdot N$

Problem Data

Size of object — Breadth $B := 0.1 \cdot m$ — Depth $D := 0.12 \cdot m$

Thickness $T := 0.01 \cdot m$

Density of object $\rho_s := 136.9 \cdot kg \cdot m^{-3}$

Density of Water $\rho_w := 1025 \cdot kg \cdot m^{-3}$

Displaced height of water

$$h := \frac{\rho_s \cdot B \cdot D \cdot T}{\rho_w \cdot B \cdot T} \qquad h = 0.016 \ m$$

Geometry of Part Submerged Bouyant Object

$$d_1(\theta) := \frac{2 \cdot \frac{\rho_s \cdot D}{\rho_w} - B \cdot \tan(\theta)}{2} \qquad d_2(\theta) := B \cdot \tan(\theta) + d_1(\theta)$$

Position of centroid

$$x_{bar}(\theta) := \frac{\left(d_1(\theta) \cdot B \cdot \frac{B}{2}\right) + \frac{B \cdot (d_2(\theta) - d_1(\theta))}{3} \cdot B}{(d_1(\theta) \cdot B) + \frac{B \cdot (d_2(\theta) - d_1(\theta))}{2}}$$

$$y_{bar}(\theta) := \frac{B \cdot \frac{d_1(\theta)^2}{2} + B \cdot \frac{d_2(\theta) - d_1(\theta)}{2} \cdot \left(d_1(\theta) + \frac{d_2(\theta) - d_1(\theta)}{3}\right)}{(d_1(\theta) \cdot B) + \frac{B \cdot (d_2(\theta) - d_1(\theta))}{2}}$$

Metacentre height above Centre of gravity (represented on subsequent graph plot)

$$m_h(\theta) := \frac{x_{bar}(\theta) - \frac{B}{2}}{\tan(\theta)} - \left(\frac{D}{2} - y_{bar}(\theta)\right)$$

$i := 1 \cdot deg, 2 \cdot deg .. 37 \cdot deg$

$m_h(0.01 \cdot deg) = 0.008 \ mm$

STABILITY := if($m_h(0.01 \cdot deg) > 0$, "STABLE", "UNSTABLE") STABILITY = "STABLE"

Angle of List

THETA = 0 degrees

AT CHANGEOVER FROM
VERTICAL TO LISTING STABILITY

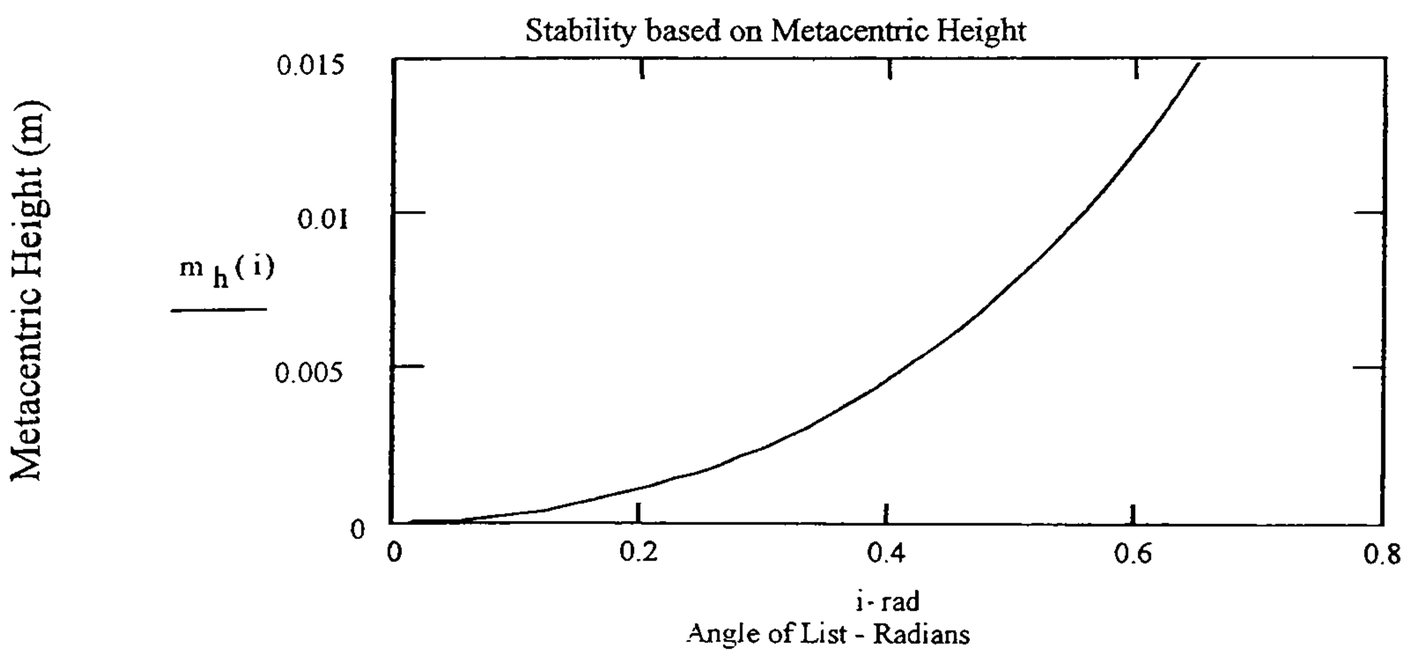

Buoyancy Stability Check - Case No 4

$kN := 1000 \cdot N$

Problem Data

Size of object — Breadth $B := 0.1 \cdot m$ — Depth $D := 0.12 \cdot m$

Thickness $T := 0.01 \cdot m$

Density of object $\rho_s := 228.07 \cdot kg \cdot m^{-3}$

Density of Water $\rho_w := 1025 \cdot kg \cdot m^{-3}$

Displaced height of water

$$h := \frac{\rho_s \cdot B \cdot D \cdot T}{\rho_w \cdot B \cdot T} \qquad h = 0.027 \ m$$

Geometry of Part Submerged Bouyant Object

$$d_1(\theta) := \frac{2 \cdot \frac{\rho_s \cdot D}{\rho_w} - B \cdot \tan(\theta)}{2} \qquad d_2(\theta) := B \cdot \tan(\theta) + d_1(\theta)$$

Position of centroid

$$x_{bar}(\theta) := \frac{\left(d_1(\theta) \cdot B \cdot \frac{B}{2}\right) + \frac{B \cdot (d_2(\theta) - d_1(\theta))}{3} \cdot B}{(d_1(\theta) \cdot B) + \frac{B \cdot (d_2(\theta) - d_1(\theta))}{2}}$$

$$y_{bar}(\theta) := \frac{B \cdot \frac{d_1(\theta)^2}{2} + B \cdot \frac{d_2(\theta) - d_1(\theta)}{2} \cdot \left(d_1(\theta) + \frac{d_2(\theta) - d_1(\theta)}{3}\right)}{(d_1(\theta) \cdot B) + \frac{B \cdot (d_2(\theta) - d_1(\theta))}{2}}$$

Metacentre height above Centre of gravity (represented on subsequent graph plot)

$$m_h(\theta) := \frac{x_{bar}(\theta) - \frac{B}{2}}{\tan(\theta)} - \left(\frac{D}{2} - y_{bar}(\theta)\right)$$

$i := 1 \cdot deg, 2 \cdot deg .. 50 \cdot deg$

$m_h(0.01 \cdot deg) = -15.44 \ mm$

$STABILITY := if(m_h(0.01 \cdot deg) > 0, "STABLE", "UNSTABLE")$ $STABILITY = "UNSTABLE"$

Angle of List

Stability achieved at 45 deg $m_h(44.9 \cdot deg) = 0.057 \ mm$

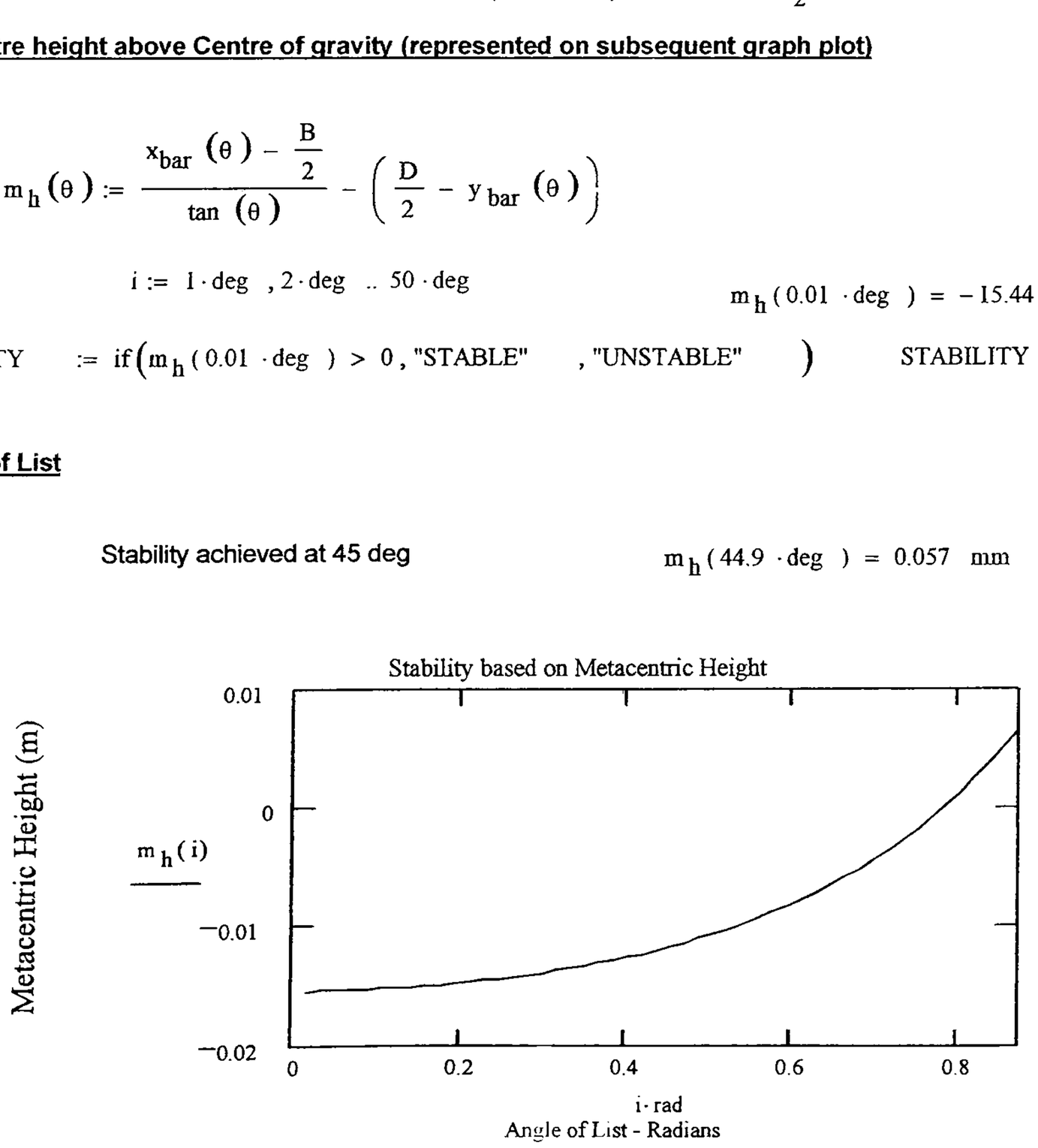

Buoyancy Stability Check - Case No 5

$kN := 1000 \cdot N$

Problem Data

Size of object — Breadth $B := 0.1 \cdot m$ — Depth $D := 0.12 \cdot m$

Thickness $T := 0.01 \cdot m$

Density of object $\rho_s := 341.67 \cdot kg \cdot m^{-3}$

Density of Water $\rho_w := 1025 \cdot kg \cdot m^{-3}$

Displaced height of water

$$h := \frac{\rho_s \cdot B \cdot D \cdot T}{\rho_w \cdot B \cdot T} \qquad h = 0.04 \ m$$

Geometry of Part Submerged Bouyant Object

$$d_1(\theta) := \frac{2 \cdot \frac{\rho_s \cdot D}{\rho_w} - B \cdot \tan(\theta)}{2} \qquad d_2(\theta) := B \cdot \tan(\theta) + d_1(\theta)$$

Position of centroid

$$x_{bar}(\theta) := \frac{\left(d_1(\theta) \cdot B \cdot \frac{B}{2}\right) + \frac{B \cdot (d_2(\theta) - d_1(\theta))}{3} \cdot B}{(d_1(\theta) \cdot B) + \frac{B \cdot (d_2(\theta) - d_1(\theta))}{2}}$$

$$y_{bar}(\theta) := \frac{B \cdot \frac{d_1(\theta)^2}{2} + B \cdot \frac{d_2(\theta) - d_1(\theta)}{2} \cdot \left(d_1(\theta) + \frac{d_2(\theta) - d_1(\theta)}{3}\right)}{(d_1(\theta) \cdot B) + \frac{B \cdot (d_2(\theta) - d_1(\theta))}{2}}$$

Metacentre height above Centre of gravity (represented on subsequent graph plot)

$$m_h(\theta) := \frac{x_{bar}(\theta) - \frac{B}{2}}{\tan(\theta)} - \left(\frac{D}{2} - y_{bar}(\theta)\right)$$

$i := 1 \cdot deg, 2 \cdot deg .. 60 \cdot deg$

$m_h(0.01 \cdot deg) = -19.167 \ mm$

STABILITY := if($m_h(0.01 \cdot deg) > 0$, "STABLE", "UNSTABLE") STABILITY = "UNSTABLE"

Angle of List

Stability achieved at 54 deg $m_h(53.7 \cdot deg) = 0.138 \ mm$

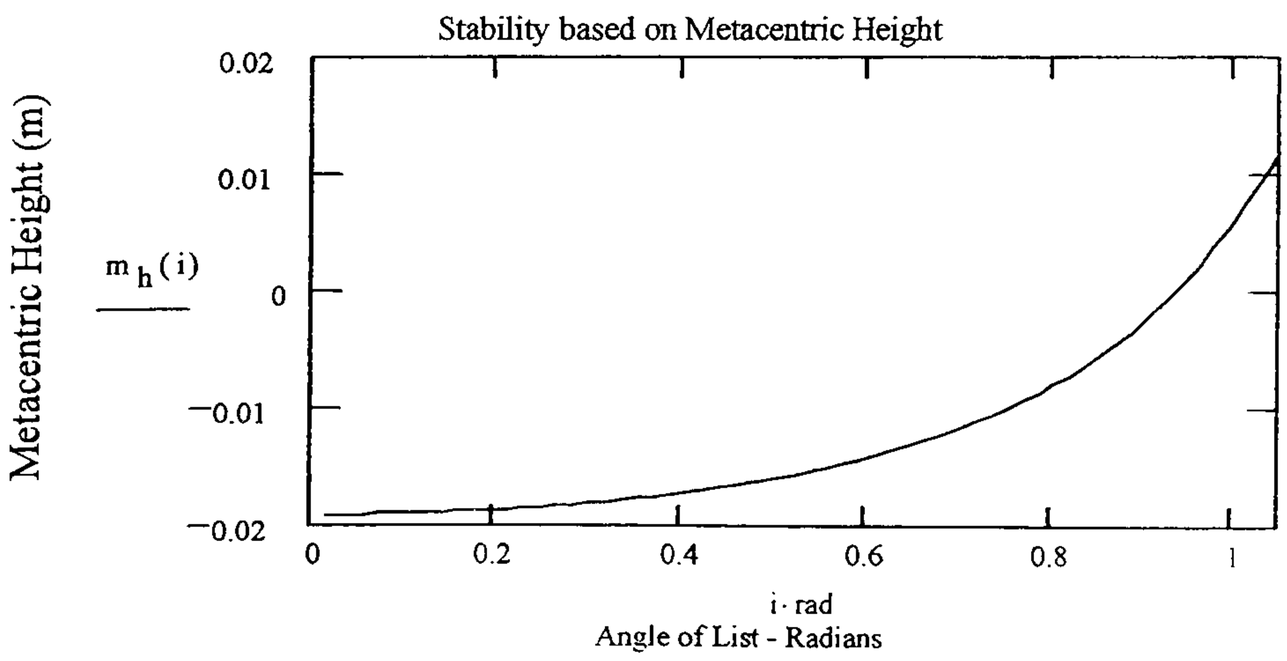

Buoyancy Stability Check - Case No 6

$kN := 1000 \cdot N$

Problem Data

Size of object — Breadth $B := 0.1 \cdot m$ — Depth $D := 0.12 \cdot m$

Thickness $T := 0.01 \cdot m$

Density of object $\rho_s := 455.271 \cdot kg \cdot m^{-3}$

Density of Water $\rho_w := 1025 \cdot kg \cdot m^{-3}$

Displaced height of water

$$h := \frac{\rho_s \cdot B \cdot D \cdot T}{\rho_w \cdot B \cdot T} \qquad h = 0.053 \ m$$

Geometry of Part Submerged Bouyant Object

$$d_1(\theta) := \frac{2 \cdot \frac{\rho_s \cdot D}{\rho_w} - B \cdot \tan(\theta)}{2} \qquad d_2(\theta) := B \cdot \tan(\theta) + d_1(\theta)$$

Position of centroid

$$x_{bar}(\theta) := \frac{\left(d_1(\theta) \cdot B \cdot \frac{B}{2}\right) + \frac{B \cdot (d_2(\theta) - d_1(\theta))}{3} \cdot B}{(d_1(\theta) \cdot B) + \frac{B \cdot (d_2(\theta) - d_1(\theta))}{2}}$$

$$y_{bar}(\theta) := \frac{B \cdot \frac{d_1(\theta)^2}{2} + B \cdot \frac{d_2(\theta) - d_1(\theta)}{2} \cdot \left(d_1(\theta) + \frac{d_2(\theta) - d_1(\theta)}{3}\right)}{(d_1(\theta) \cdot B) + \frac{B \cdot (d_2(\theta) - d_1(\theta))}{2}}$$

Metacentre height above Centre of gravity (represented on subsequent graph plot)

$$m_h(\theta) := \frac{x_{bar}(\theta) - \frac{B}{2}}{\tan(\theta)} - \left(\frac{D}{2} - y_{bar}(\theta)\right)$$

$i := 1 \cdot deg, 2 \cdot deg .. 60 \cdot deg$

$m_h(0.01 \cdot deg) = -17.715 \ mm$

STABILITY := if($m_h(0.01 \cdot deg) > 0$, "STABLE", "UNSTABLE") STABILITY = "UNSTABLE"

Angle of List

Stability achieved at 56.5 deg $m_h(56.5 \cdot deg) = 0.129 \ mm$

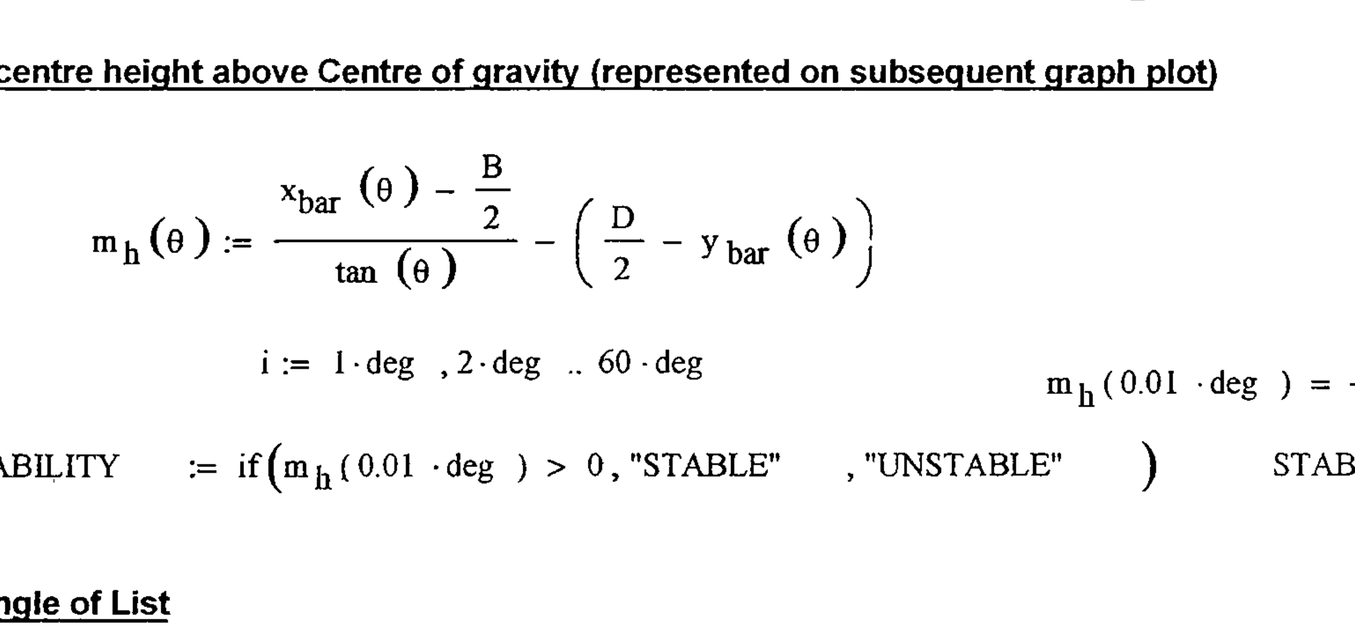

Buoyancy Stability Check - Case No 7

$kN := 1000 \cdot N$

Problem Data

Size of object — Breadth $B := 0.1 \cdot m$ — Depth $D := 0.12 \cdot m$

Thickness $T := 0.01 \cdot m$

Density of object $\rho_s := 569.729 \cdot kg \cdot m^{-3}$

Density of Water $\rho_w := 1025 \cdot kg \cdot m^{-3}$

Displaced height of water

$$h := \frac{\rho_s \cdot B \cdot D \cdot T}{\rho_w \cdot B \cdot T} \qquad h = 0.067 \ m$$

Geometry of Part Submerged Bouyant Object

$$d_1(\theta) := \frac{2 \cdot \frac{\rho_s \cdot D}{\rho_w} - B \cdot \tan(\theta)}{2} \qquad d_2(\theta) := B \cdot \tan(\theta) + d_1(\theta)$$

Position of centroid

$$x_{bar}(\theta) := \frac{\left(d_1(\theta) \cdot B \cdot \frac{B}{2}\right) + \frac{B \cdot (d_2(\theta) - d_1(\theta))}{3} \cdot B}{(d_1(\theta) \cdot B) + \frac{B \cdot (d_2(\theta) - d_1(\theta))}{2}}$$

$$y_{bar}(\theta) := \frac{B \cdot \frac{d_1(\theta)^2}{2} + B \cdot \frac{d_2(\theta) - d_1(\theta)}{2} \cdot \left(d_1(\theta) + \frac{d_2(\theta) - d_1(\theta)}{3}\right)}{(d_1(\theta) \cdot B) + \frac{B \cdot (d_2(\theta) - d_1(\theta))}{2}}$$

Metacentre height above Centre of gravity (represented on subsequent graph plot)

$$m_h(\theta) := \frac{x_{bar}(\theta) - \frac{B}{2}}{\tan(\theta)} - \left(\frac{D}{2} - y_{bar}(\theta)\right)$$

$i := 1 \cdot deg, 2 \cdot deg .. 60 \cdot deg$

$m_h(0.01 \cdot deg) = -14.156 \ mm$

$STABILITY := if(m_h(0.01 \cdot deg) > 0, "STABLE", "UNSTABLE")$ $STABILITY = "UNSTABLE"$

Angle of List

Stability achieved at 56.5 deg $m_h(56.5 \cdot deg) = 0.103 \ mm$

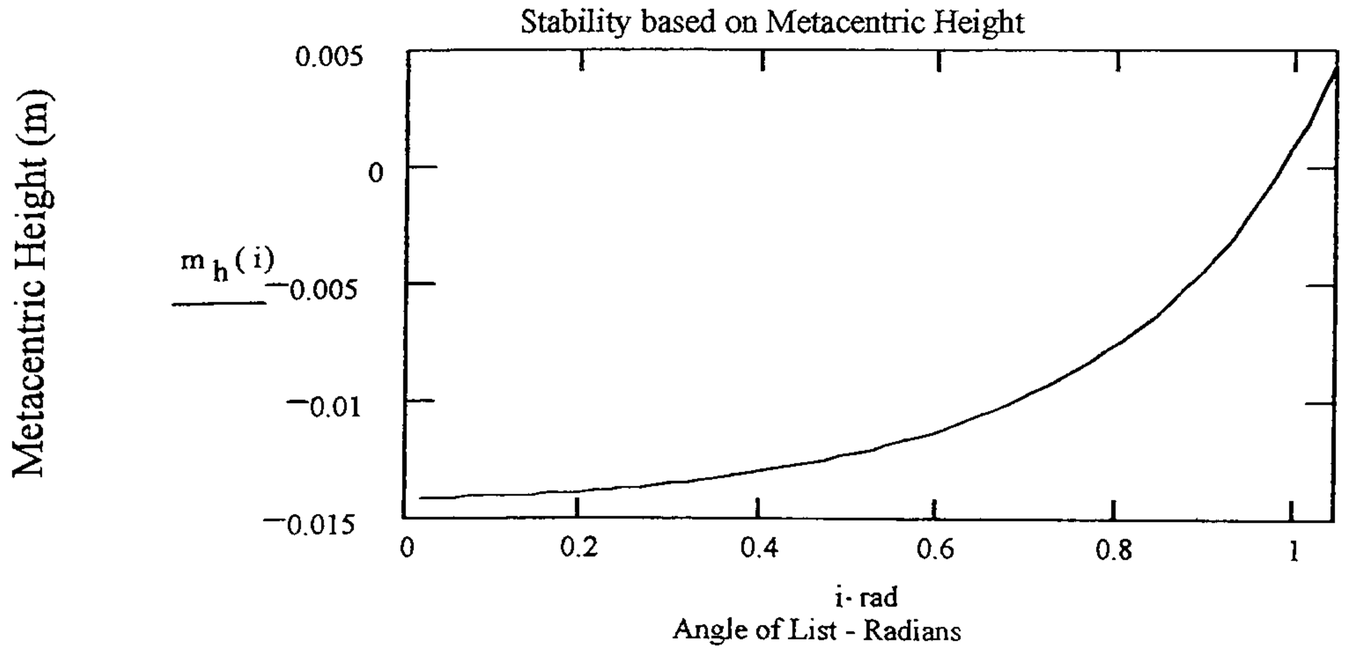

Buoyancy Stability Check - Case No 8

$kN := 1000 \cdot N$

Problem Data

Size of object — Breadth $B := 0.1 \cdot m$ — Depth $D := 0.12 \cdot m$

Thickness $T := 0.01 \cdot m$

Density of object $\rho_s := 683.333 \cdot kg \cdot m^{-3}$

Density of Water $\rho_w := 1025 \cdot kg \cdot m^{-3}$

Displaced height of water

$$h := \frac{\rho_s \cdot B \cdot D \cdot T}{\rho_w \cdot B \cdot T} \qquad h = 0.08 \ m$$

Geometry of Part Submerged Bouyant Object

$$d_1(\theta) := \frac{2 \cdot \frac{\rho_s \cdot D}{\rho_w} - B \cdot \tan(\theta)}{2} \qquad d_2(\theta) := B \cdot \tan(\theta) + d_1(\theta)$$

Position of centroid

$$x_{bar}(\theta) := \frac{\left(d_1(\theta) \cdot B \cdot \frac{B}{2}\right) + \frac{B \cdot (d_2(\theta) - d_1(\theta))}{3} \cdot B}{(d_1(\theta) \cdot B) + \frac{B \cdot (d_2(\theta) - d_1(\theta))}{2}}$$

$$y_{bar}(\theta) := \frac{B \cdot \frac{d_1(\theta)^2}{2} + B \cdot \frac{d_2(\theta) - d_1(\theta)}{2} \cdot \left(d_1(\theta) + \frac{d_2(\theta) - d_1(\theta)}{3}\right)}{(d_1(\theta) \cdot B) + \frac{B \cdot (d_2(\theta) - d_1(\theta))}{2}}$$

Metacentre height above Centre of gravity (represented on subsequent graph plot)

$$m_h(\theta) := \frac{x_{bar}(\theta) - \frac{B}{2}}{\tan(\theta)} - \left(\frac{D}{2} - y_{bar}(\theta)\right)$$

$i := 1 \cdot deg, 2 \cdot deg .. 60 \cdot deg$

$m_h(0.01 \cdot deg) = -9.583 \ mm$

STABILITY := if($m_h(0.01 \cdot deg) > 0$, "STABLE", "UNSTABLE") STABILITY = "UNSTABLE"

Angle of List

Stability achieved at 53.7 deg $m_h(53.7 \cdot deg) = 0.069 \ mm$

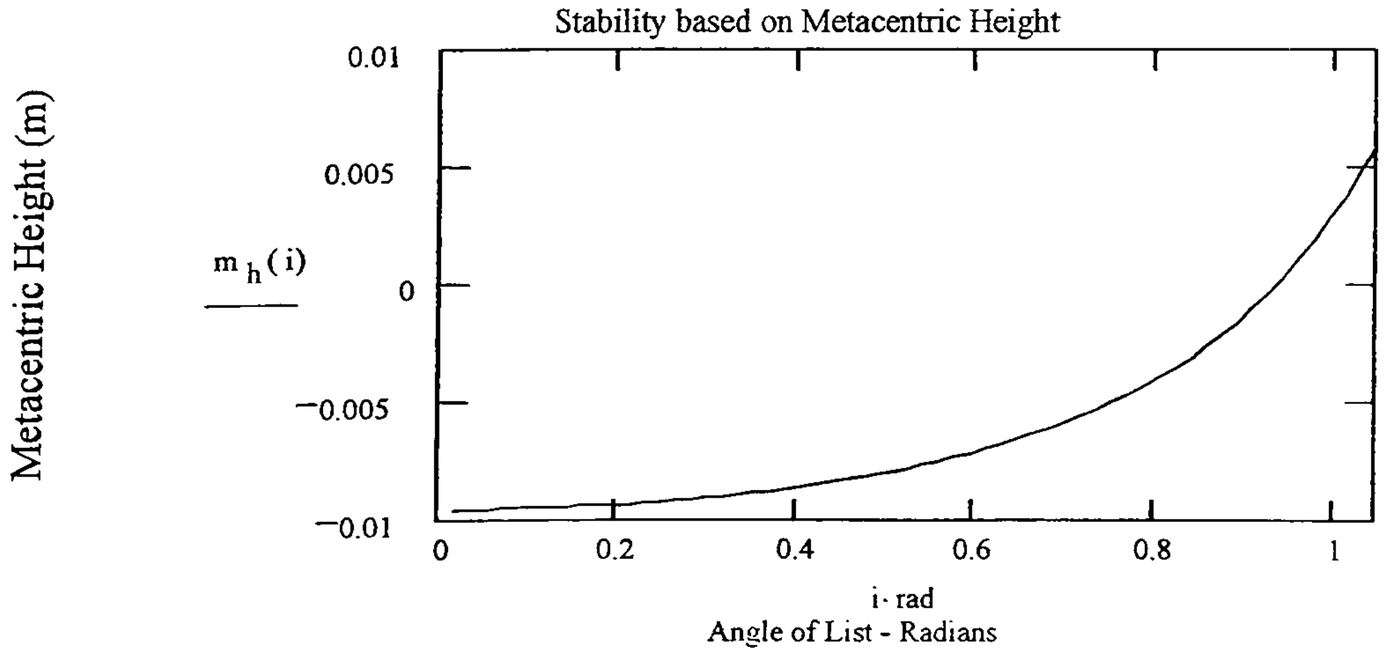

Buoyancy Stability Check - Case No 9

$kN := 1000 \cdot N$

Problem Data

Size of object — Breadth $B := 0.1 \cdot m$ — Depth $D := 0.12 \cdot m$

Thickness $T := 0.01 \cdot m$

Density of object $\rho_s := 796.938 \cdot kg \cdot m^{-3}$

Density of Water $\rho_w := 1025 \cdot kg \cdot m^{-3}$

Displaced height of water

$$h := \frac{\rho_s \cdot B \cdot D \cdot T}{\rho_w \cdot B \cdot T} \qquad h = 0.093 \ m$$

Geometry of Part Submerged Bouyant Object

$$d_1(\theta) := \frac{2 \cdot \frac{\rho_s \cdot D}{\rho_w} - B \cdot \tan(\theta)}{2} \qquad d_2(\theta) := B \cdot \tan(\theta) + d_1(\theta)$$

Position of centroid

$$x_{bar}(\theta) := \frac{\left(d_1(\theta) \cdot B \cdot \frac{B}{2}\right) + \frac{B \cdot (d_2(\theta) - d_1(\theta))}{3} \cdot B}{(d_1(\theta) \cdot B) + \frac{B \cdot (d_2(\theta) - d_1(\theta))}{2}}$$

$$y_{bar}(\theta) := \frac{B \cdot \frac{d_1(\theta)^2}{2} + B \cdot \frac{d_2(\theta) - d_1(\theta)}{2} \cdot \left(d_1(\theta) + \frac{d_2(\theta) - d_1(\theta)}{3}\right)}{(d_1(\theta) \cdot B) + \frac{B \cdot (d_2(\theta) - d_1(\theta))}{2}}$$

Metacentre height above Centre of gravity (represented on subsequent graph plot)

$$m_h(\theta) := \frac{x_{bar}(\theta) - \frac{B}{2}}{\tan(\theta)} - \left(\frac{D}{2} - y_{bar}(\theta)\right)$$

$i := 1 \cdot deg, 2 \cdot deg .. 60 \cdot deg$

$m_h(0.01 \cdot deg) = -4.418 \ mm$

$STABILITY := if(m_h(0.01 \cdot deg) > 0, "STABLE", "UNSTABLE")$ STABILITY = "UNSTABLE"

Angle of List

Stability achieved at 44.9 deg $m_h(44.9 \cdot deg) = 0.017 \ mm$

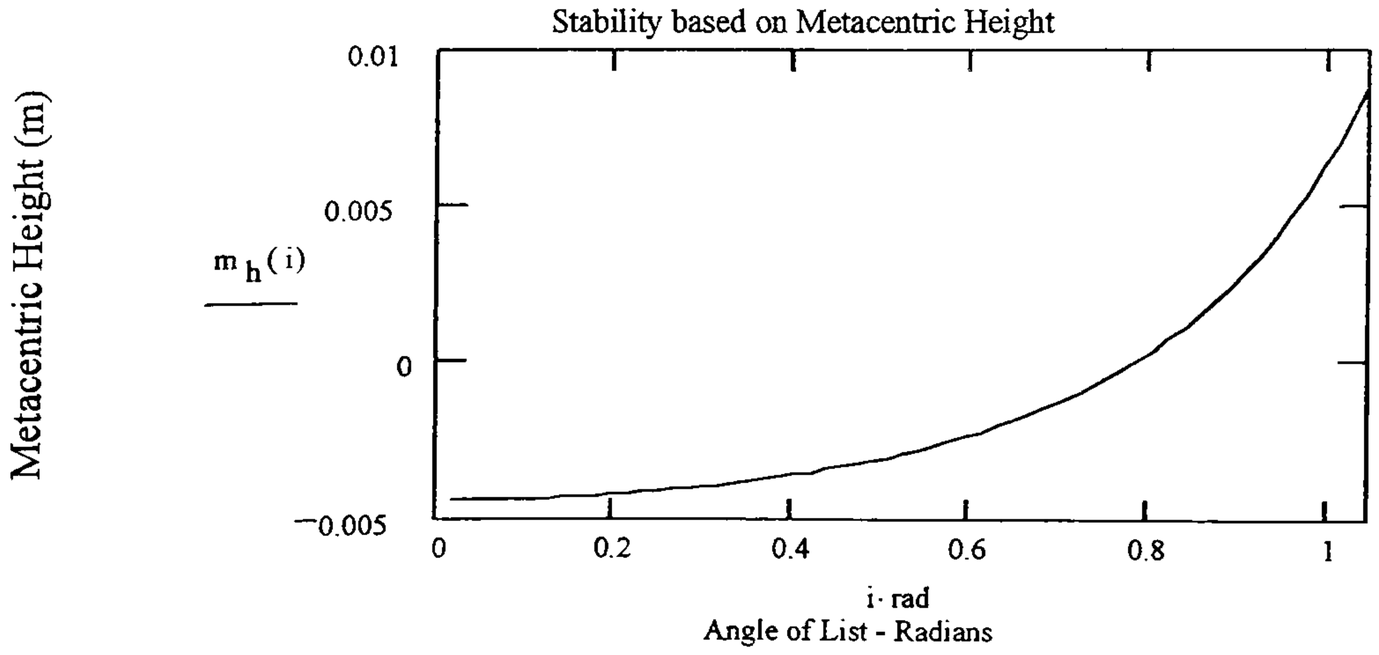

Buoyancy Stability Check - Case No 10

$kN := 1000 \cdot N$

Problem Data

Size of object — Breadth $B := 0.1 \cdot m$ — Depth $D := 0.12 \cdot m$

Thickness $T := 0.01 \cdot m$

Density of object $\rho_s := 854.17 \cdot kg \cdot m^{-3}$

Density of Water $\rho_w := 1025 \cdot kg \cdot m^{-3}$

Displaced height of water

$$h := \frac{\rho_s \cdot B \cdot D \cdot T}{\rho_w \cdot B \cdot T} \qquad h = 0.1\ m$$

Geometry of Part Submerged Bouyant Object

$$d_1(\theta) := \frac{2 \cdot \frac{\rho_s \cdot D}{\rho_w} - B \cdot \tan(\theta)}{2} \qquad d_2(\theta) := B \cdot \tan(\theta) + d_1(\theta)$$

Position of centroid

$$x_{bar}(\theta) := \frac{\left(d_1(\theta) \cdot B \cdot \frac{B}{2}\right) + \frac{B \cdot (d_2(\theta) - d_1(\theta))}{3} \cdot B}{(d_1(\theta) \cdot B) + \frac{B \cdot (d_2(\theta) - d_1(\theta))}{2}}$$

$$y_{bar}(\theta) := \frac{B \cdot \frac{d_1(\theta)^2}{2} + B \cdot \frac{d_2(\theta) - d_1(\theta)}{2} \cdot \left(d_1(\theta) + \frac{d_2(\theta) - d_1(\theta)}{3}\right)}{(d_1(\theta) \cdot B) + \frac{B \cdot (d_2(\theta) - d_1(\theta))}{2}}$$

Metacentre height above Centre of gravity (represented on subsequent graph plot)

$$m_h(\theta) := \frac{x_{bar}(\theta) - \frac{B}{2}}{\tan(\theta)} - \left(\frac{D}{2} - y_{bar}(\theta)\right)$$

$i := 1 \cdot deg, 2 \cdot deg .. 60 \cdot deg$

$m_h(0.01 \cdot deg) = -1.667\ mm$

$STABILITY := if(m_h(0.01 \cdot deg) > 0, "STABLE", "UNSTABLE")$ $STABILITY = "UNSTABLE"$

Angle of List

Stability achieved at 32.4 deg $m_h(32.4 \cdot deg) = 0.012\ mm$

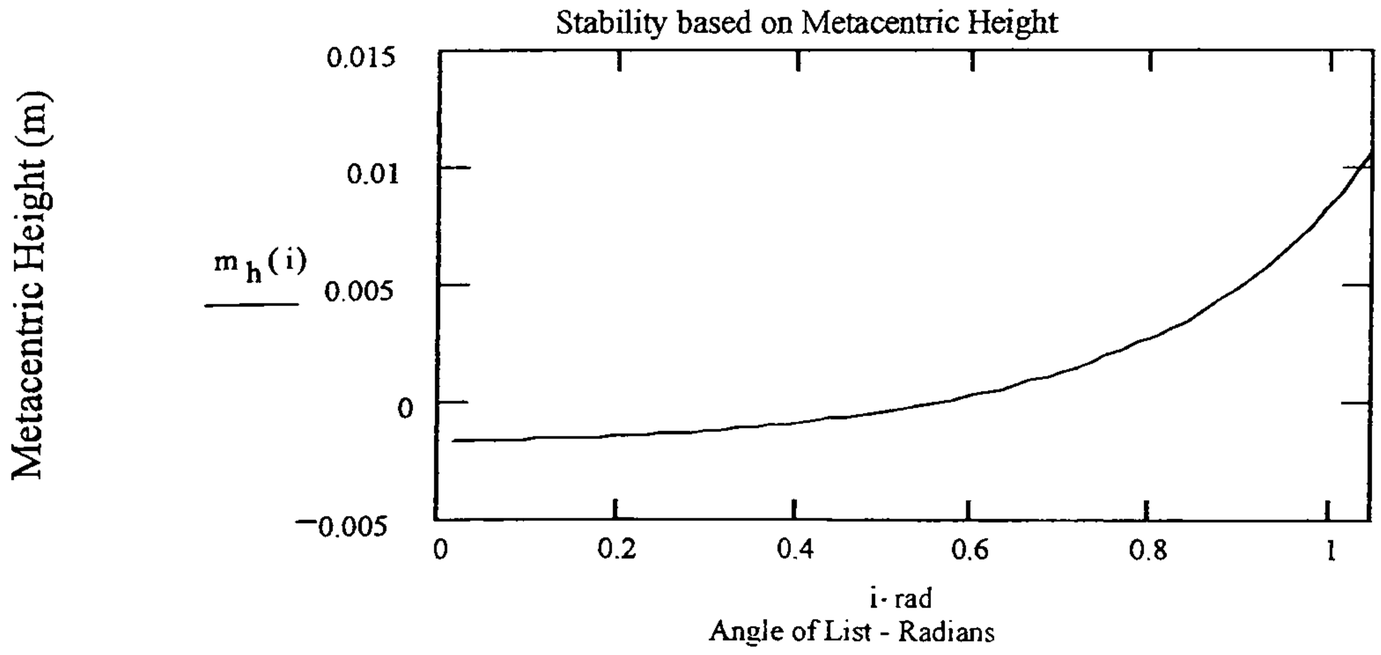

Buoyancy Stability Check - Case No 11

$kN := 1000 \cdot N$

Problem Data

Size of object — Breadth $B := 0.1 \cdot m$ — Depth $D := 0.12 \cdot m$

Thickness $T := 0.01 \cdot m$

Density of object $\rho_s := 888.1 \cdot kg \cdot m^{-3}$

Density of Water $\rho_w := 1025 \cdot kg \cdot m^{-3}$

Displaced height of water

$$h := \frac{\rho_s \cdot B \cdot D \cdot T}{\rho_w \cdot B \cdot T} \qquad h = 0.104 \ m$$

Geometry of Part Submerged Bouyant Object

$$d_1(\theta) := \frac{2 \cdot \frac{\rho_s \cdot D}{\rho_w} - B \cdot \tan(\theta)}{2} \qquad d_2(\theta) := B \cdot \tan(\theta) + d_1(\theta)$$

Position of centroid

$$x_{bar}(\theta) := \frac{\left(d_1(\theta) \cdot B \cdot \frac{B}{2}\right) + \frac{B \cdot (d_2(\theta) - d_1(\theta))}{3} \cdot B}{(d_1(\theta) \cdot B) + \frac{B \cdot (d_2(\theta) - d_1(\theta))}{2}}$$

$$y_{bar}(\theta) := \frac{B \cdot \frac{d_1(\theta)^2}{2} + B \cdot \frac{d_2(\theta) - d_1(\theta)}{2} \cdot \left(d_1(\theta) + \frac{d_2(\theta) - d_1(\theta)}{3}\right)}{(d_1(\theta) \cdot B) + \frac{B \cdot (d_2(\theta) - d_1(\theta))}{2}}$$

Metacentre height above Centre of gravity (represented on subsequent graph plot)

$$m_h(\theta) := \frac{x_{bar}(\theta) - \frac{B}{2}}{\tan(\theta)} - \left(\frac{D}{2} - y_{bar}(\theta)\right)$$

$i := 1 \cdot deg, 2 \cdot deg .. 60 \cdot deg$

$m_h(0.01 \cdot deg) = 0.001 \ mm$

$STABILITY := if(m_h(0.01 \cdot deg) > 0, "STABLE", "UNSTABLE")$ $STABILITY = "STABLE"$

Angle of List

THETA = 0 degrees — AT CHANGEOVER FROM LISTING TO VERTICAL STABILITY

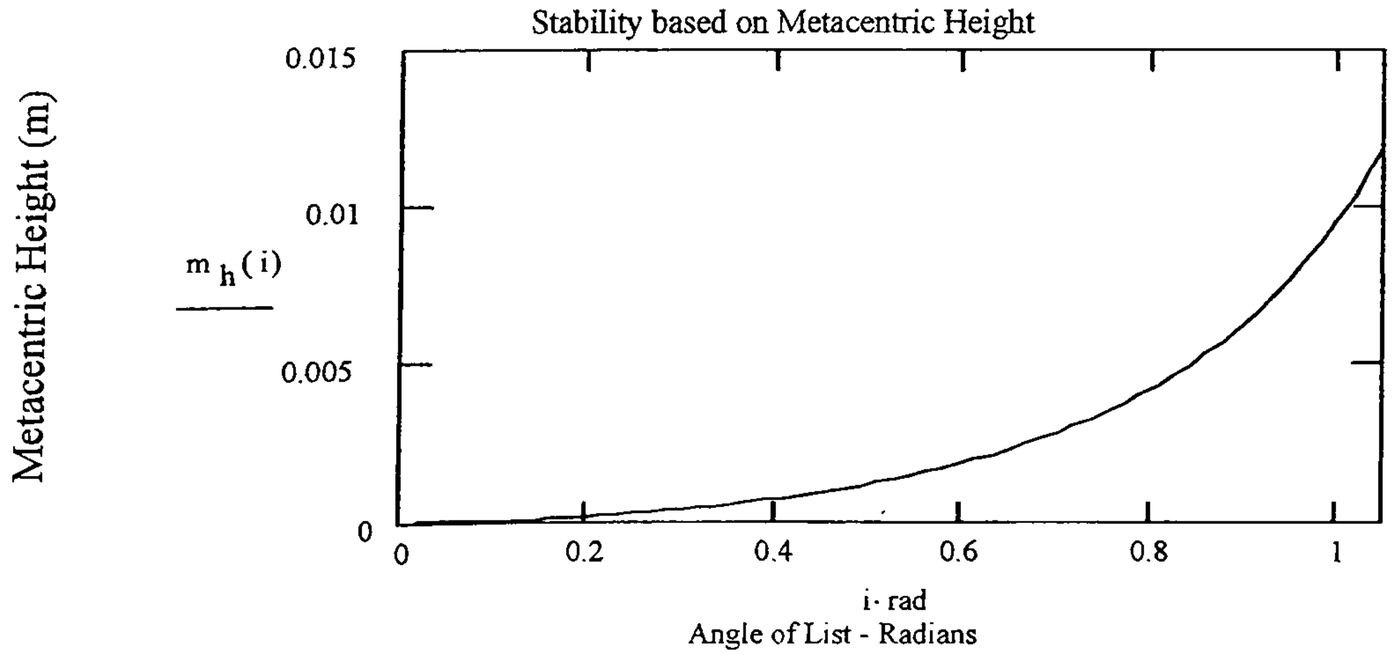

Buoyancy Stability Check - Case No 12

$kN := 1000 \cdot N$

Problem Data

Size of object — Breadth $B := 0.1 \cdot m$ — Depth $D := 0.12 \cdot m$

Thickness $T := 0.01 \cdot m$

Density of object $\rho_s := 900 \cdot kg \cdot m^{-3}$

Density of Water $\rho_w := 1025 \cdot kg \cdot m^{-3}$

Displaced height of water

$$h := \frac{\rho_s \cdot B \cdot D \cdot T}{\rho_w \cdot B \cdot T} \qquad h = 0.105 \quad m$$

Geometry of Part Submerged Bouyant Object

$$d_1(\theta) := \frac{2 \cdot \frac{\rho_s \cdot D}{\rho_w} - B \cdot \tan(\theta)}{2} \qquad d_2(\theta) := B \cdot \tan(\theta) + d_1(\theta)$$

Position of centroid

$$x_{bar}(\theta) := \frac{\left(d_1(\theta) \cdot B \cdot \frac{B}{2}\right) + \frac{B \cdot (d_2(\theta) - d_1(\theta))}{3} \cdot B}{(d_1(\theta) \cdot B) + \frac{B \cdot (d_2(\theta) - d_1(\theta))}{2}}$$

$$y_{bar}(\theta) := \frac{B \cdot \frac{d_1(\theta)^2}{2} + B \cdot \frac{d_2(\theta) - d_1(\theta)}{2} \cdot \left(d_1(\theta) + \frac{d_2(\theta) - d_1(\theta)}{3}\right)}{(d_1(\theta) \cdot B) + \frac{B \cdot (d_2(\theta) - d_1(\theta))}{2}}$$

Metacentre height above Centre of gravity (represented on subsequent graph plot)

$$m_h(\theta) := \frac{x_{bar}(\theta) - \frac{B}{2}}{\tan(\theta)} - \left(\frac{D}{2} - y_{bar}(\theta)\right)$$

$i := 1 \cdot deg, 2 \cdot deg .. 60 \cdot deg$

$m_h(0.01 \cdot deg) = 0.592 \quad mm$

$STABILITY := if(m_h(0.01 \cdot deg) > 0, "STABLE", "UNSTABLE")$ $STABILITY = "STABLE"$

Angle of List

THETA = 0 degrees

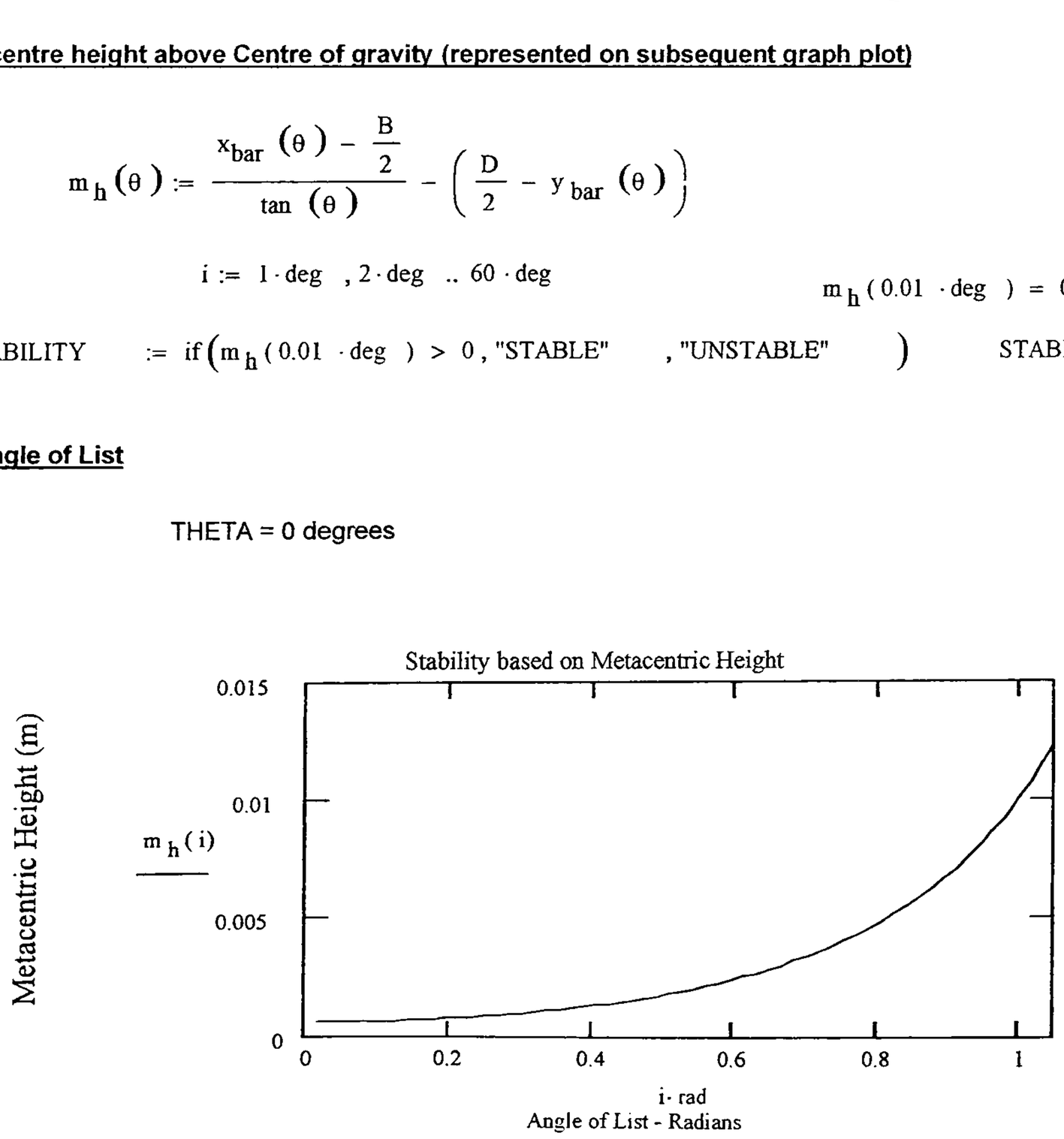

The preceding calculations address the theoretical mechanics of stability of floating objects in water. The object in question Figure (4.1) is (0.1x0.12x0.01m) in x, y and z directions and at very low densities will remain with its long axis vertical. At some density (137kg/m^3), the float is no longer in stable equilibrium with its long axis vertical, and will list in the water at some angle theta, at which it will then be stable. This angle has been calculated for increasing densities of the object, and the relationship between stable angle and density is plotted below:

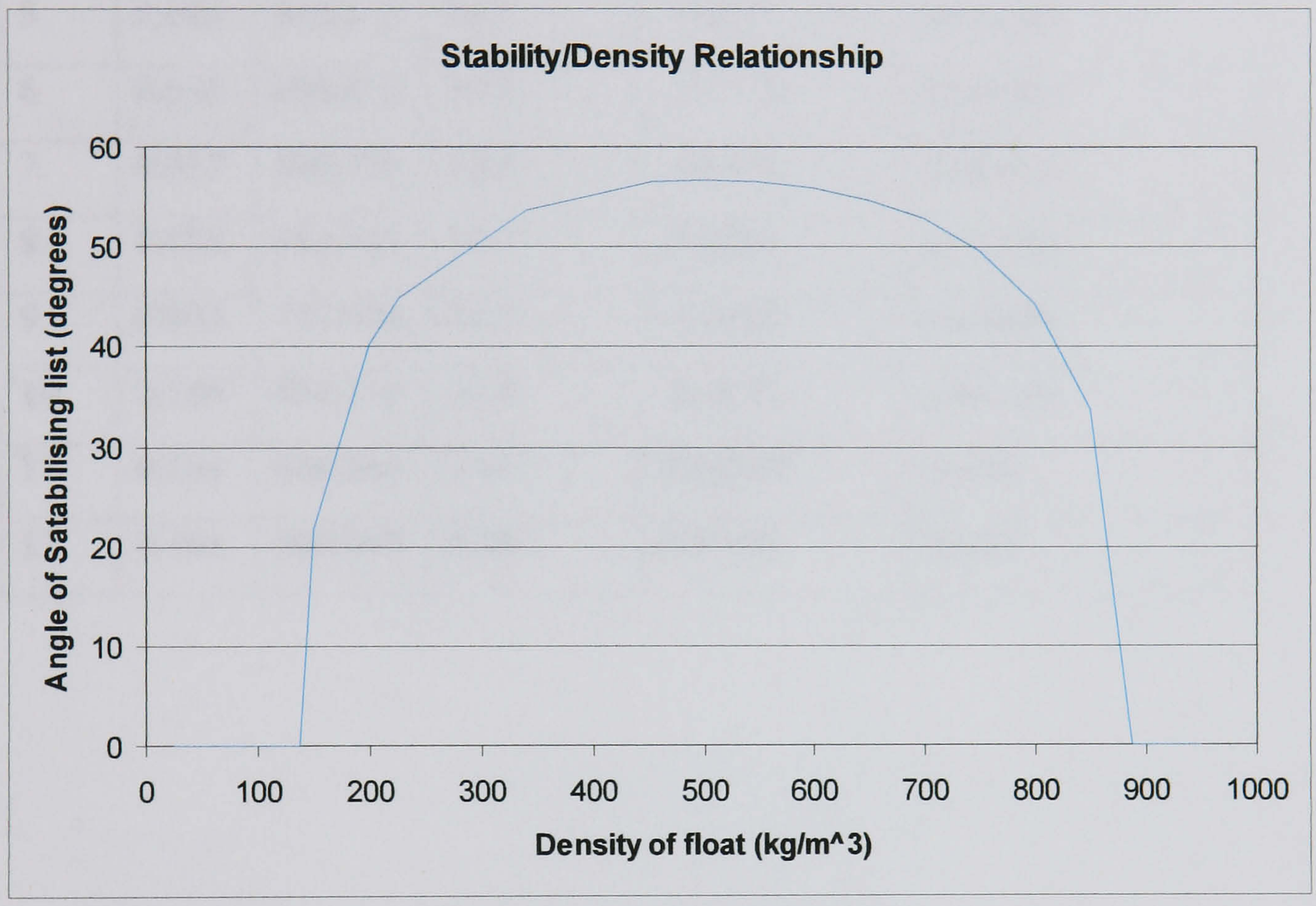

Stability position of floating box

The graph shows that at extremes of density the angle returns to zero, whereas for intermediate values of density, the angle of stability increases to a maximum of 57 degrees when the density of the float is half that of the water.

Note: this particular problem is related purely to geometry of the structure. The above mentioned buoyancy positions based on static buoyancy behaviour of the twelve cases are summarized in Table 4-1

Table 4-1 Stability positions for buoyant small 2-D box

Case	h m	γ kg/m^3	$\Theta_{theoritical}$ degree	metacentric height mm	stability condition
1	0.010	087.980	0.00	26.055	stable
2	0.013	113.600	0.00	9.3090	stable
3	0.016	136.900	0.00	0.0080	stable
4	0.027	228.070	44.9	-15.440	unstable
5	0.040	341.670	53.7	-19.167	unstable
6	0.053	455.271	56.5	-17.715	unstable
7	0.067	569.729	56.5	-14.156	unstable
8	0.080	683.333	53.7	-9.5830	unstable
9	0.093	796.938	44.9	-4.4180	unstable
10	0.100	854.170	32.4	-1.6670	unstable
11	0.104	888.100	0.00	0.00100	stable
12	0.105	900.000	0.00	0.59100	stable

4.6.2 Two-dimensional verification model for buoyancy:

The first of the models is shown in Figure (4.3) and consists of a floating two dimensional box Figure (4.4), of one solid element thickness floating under its own body force and buoyancy force exerted by water shown in Figure (4.5). Above this is the air part shown in Figure (4.6).

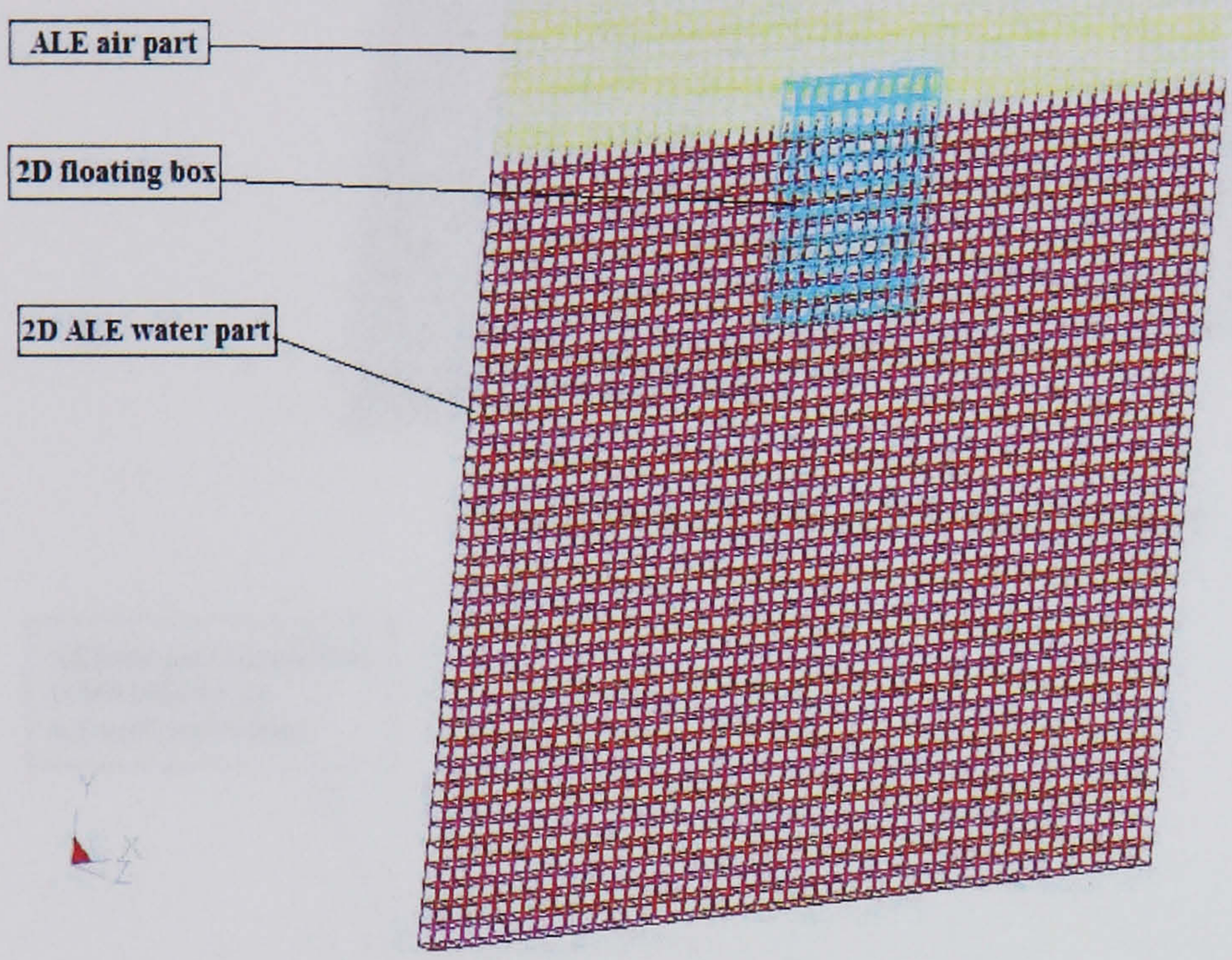

Figure (4.3) The 2D model, all parts

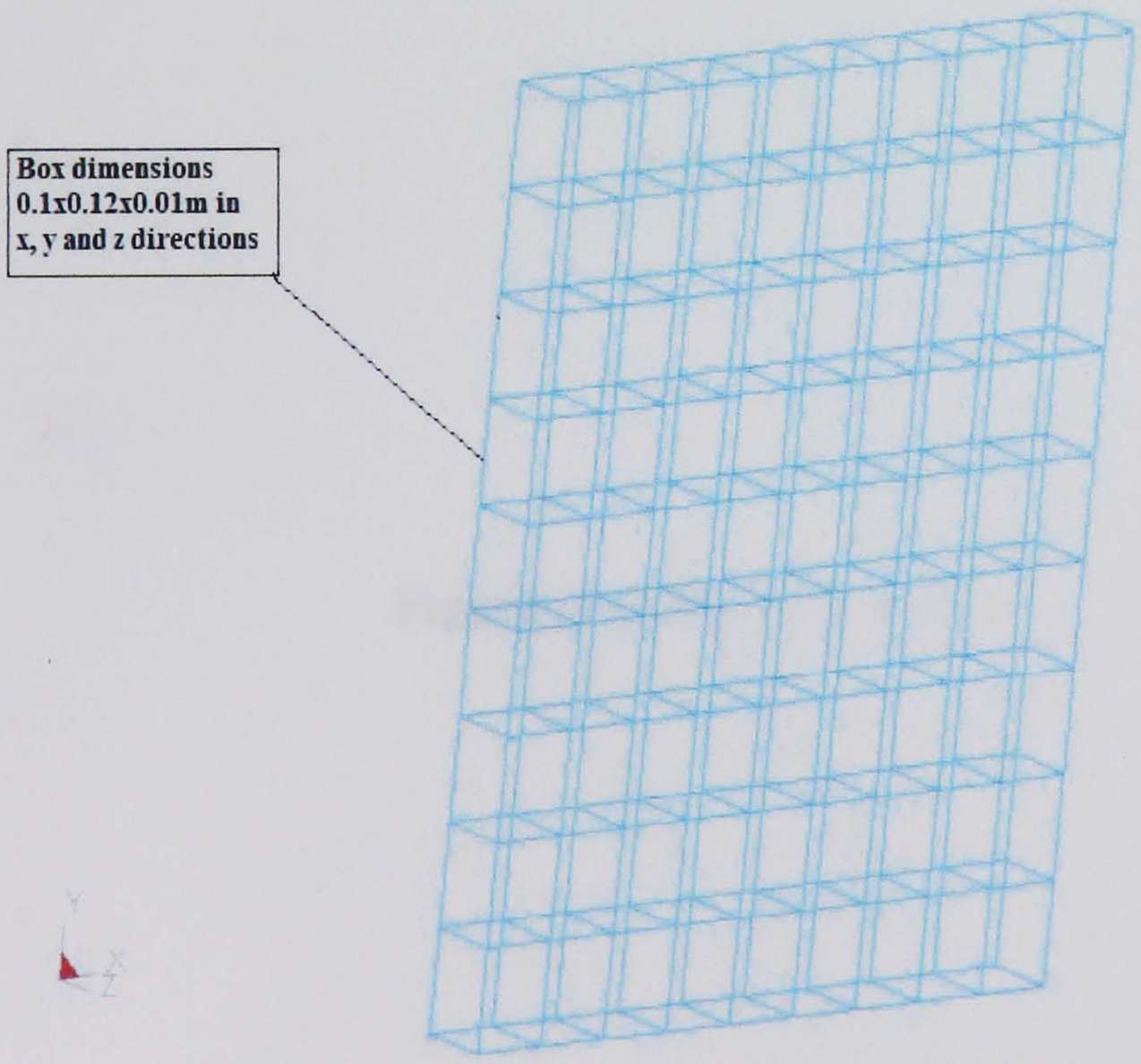

Figure (4.4) 2D-floating box

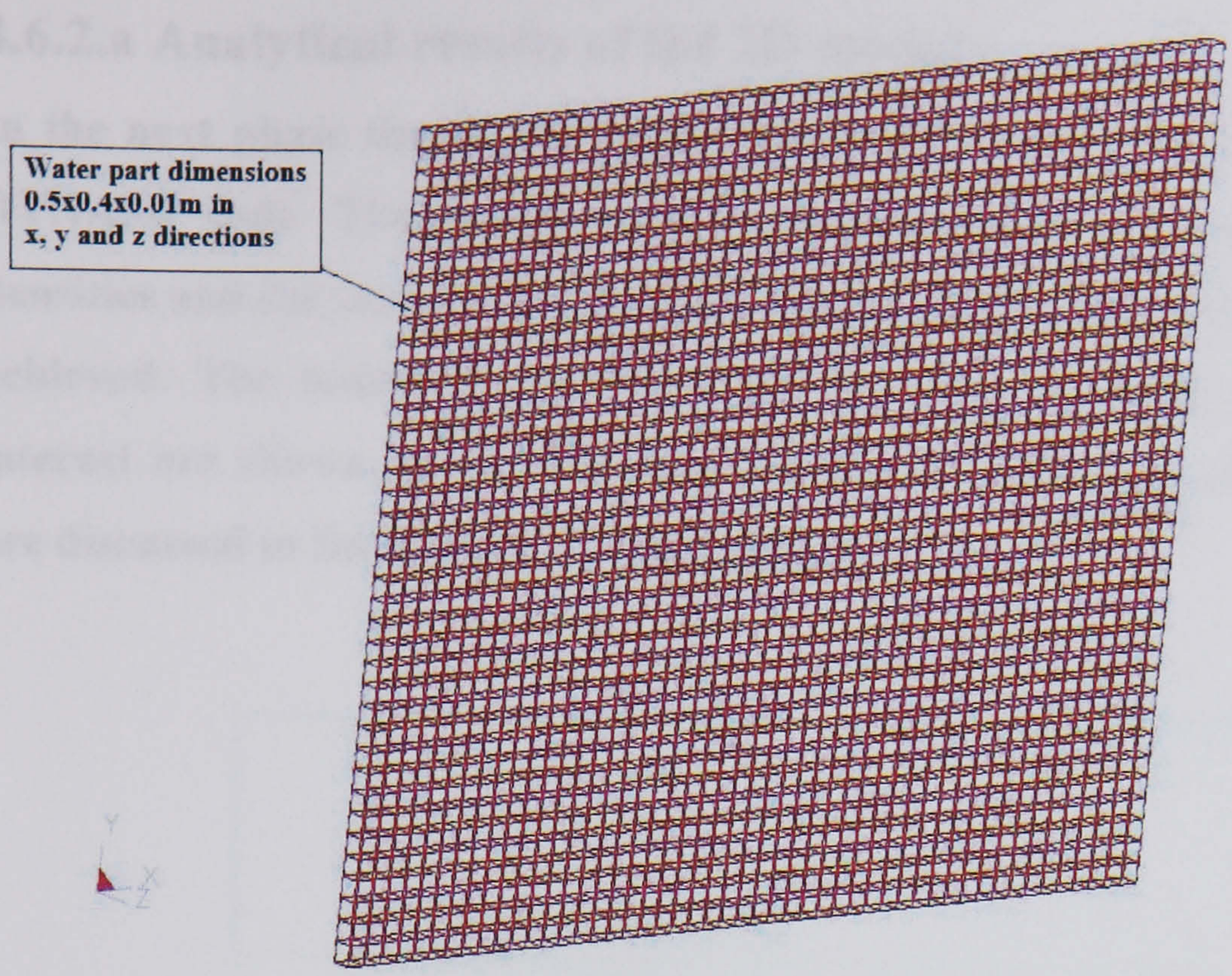

Figure (4.5) 2D-ALE water part

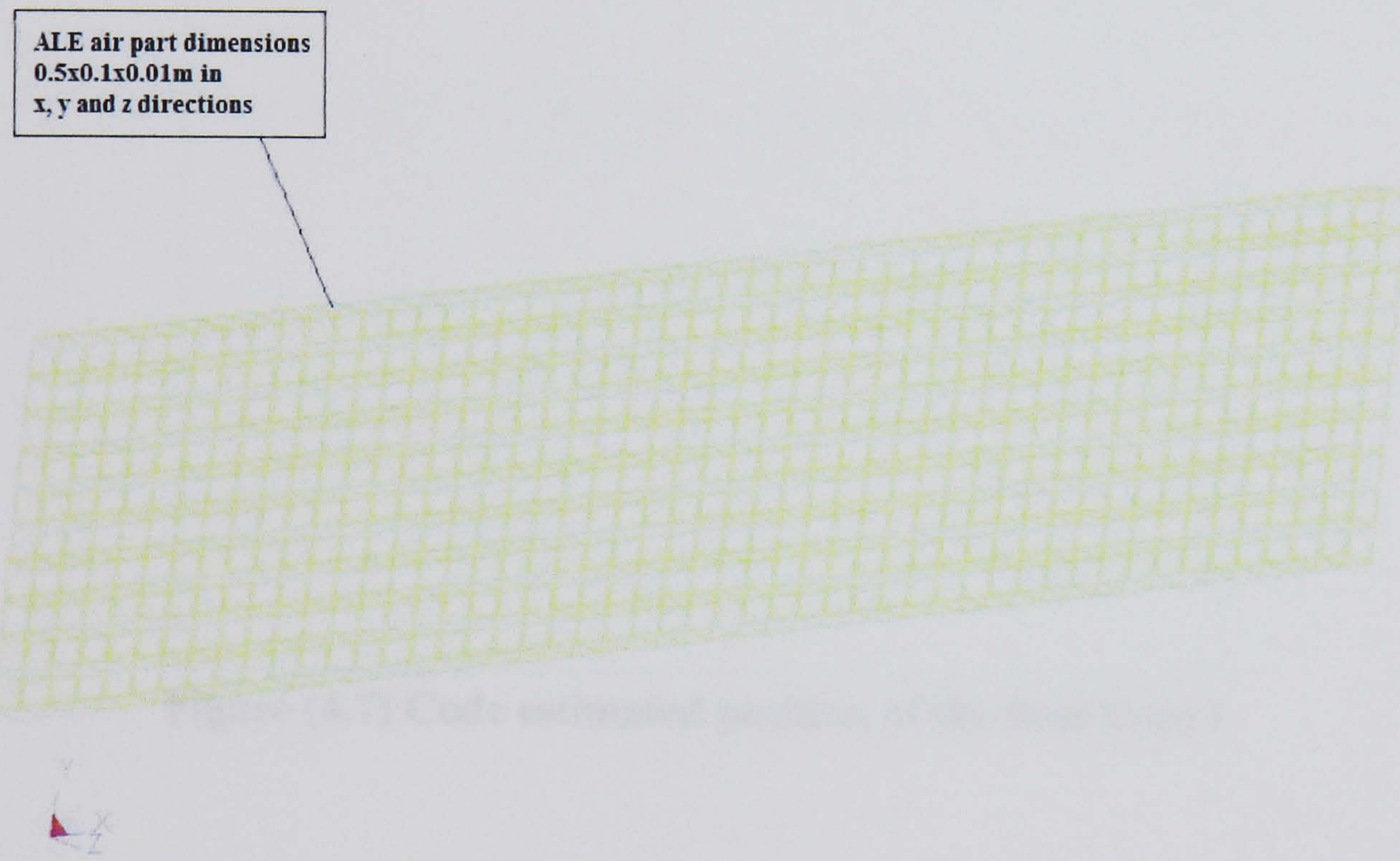

Figure (4.6) 2D-ALE air part

4.6.2.a Analytical results of the 2D model:

In the next phase the twelve cases reported in Table 4-1 were run using LS-DYNA3D code. The different buoyancy positions were based on different densities and the model were allowed to float till sufficient submerged height is achieved. The assumed position(s) of this float in eight configurations of interest are shown in the following Figures (4.7) through (4.14). The results are discussed in Section 4.7.1 of this chapter.

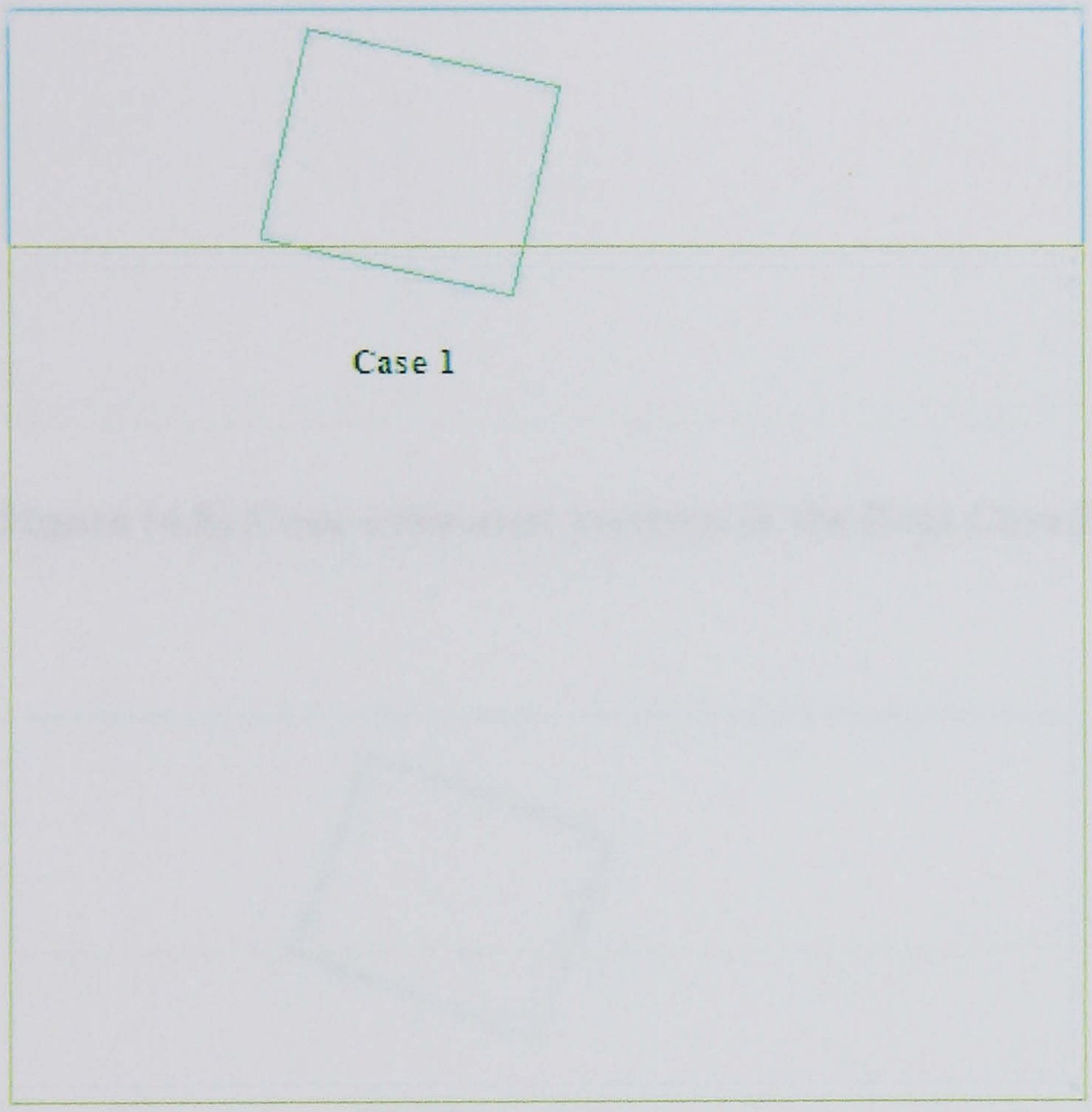

Figure (4.7) Code estimated position of the float Case 1

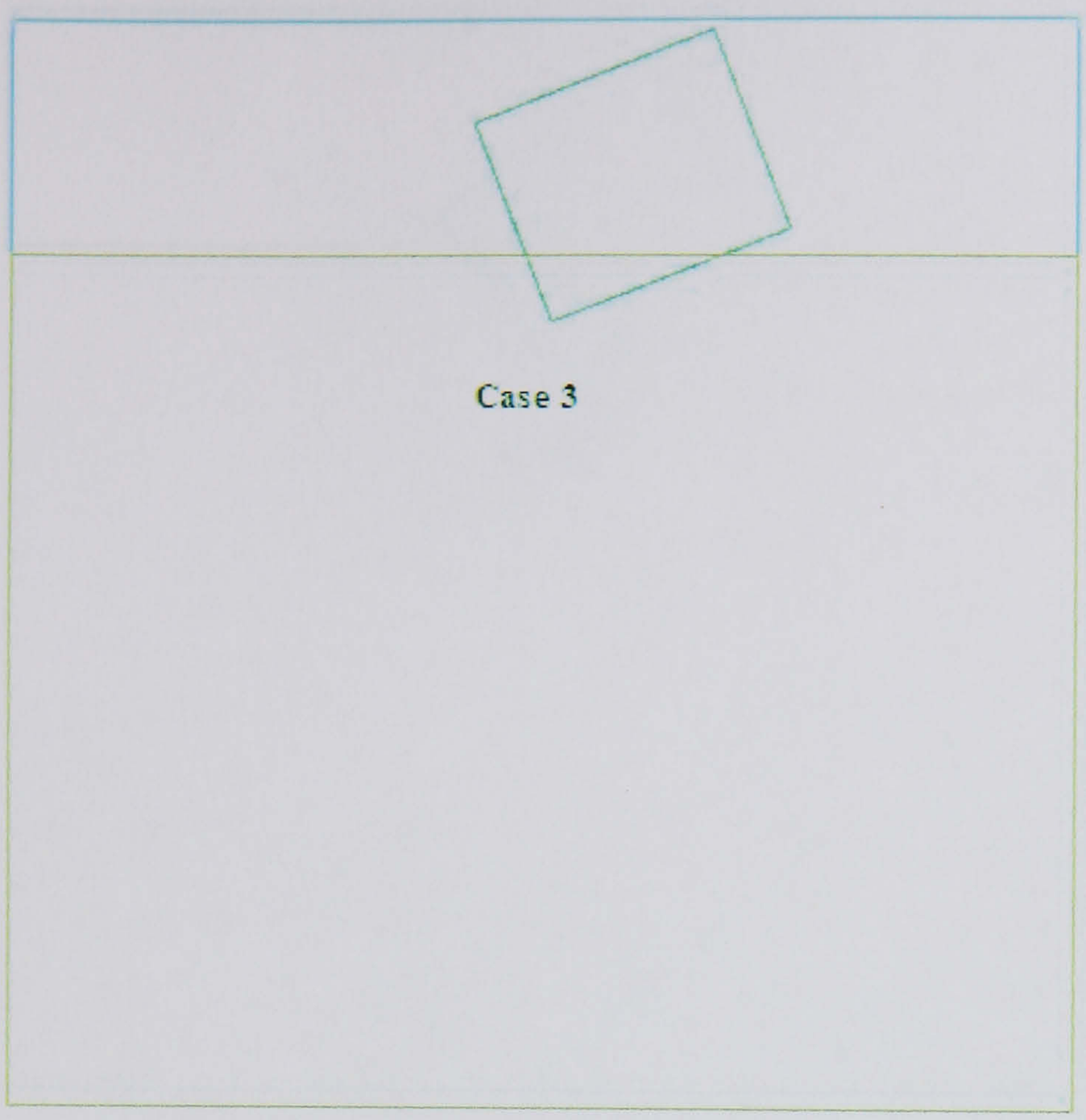

Figure (4.8) Code estimated position of the float Case 3

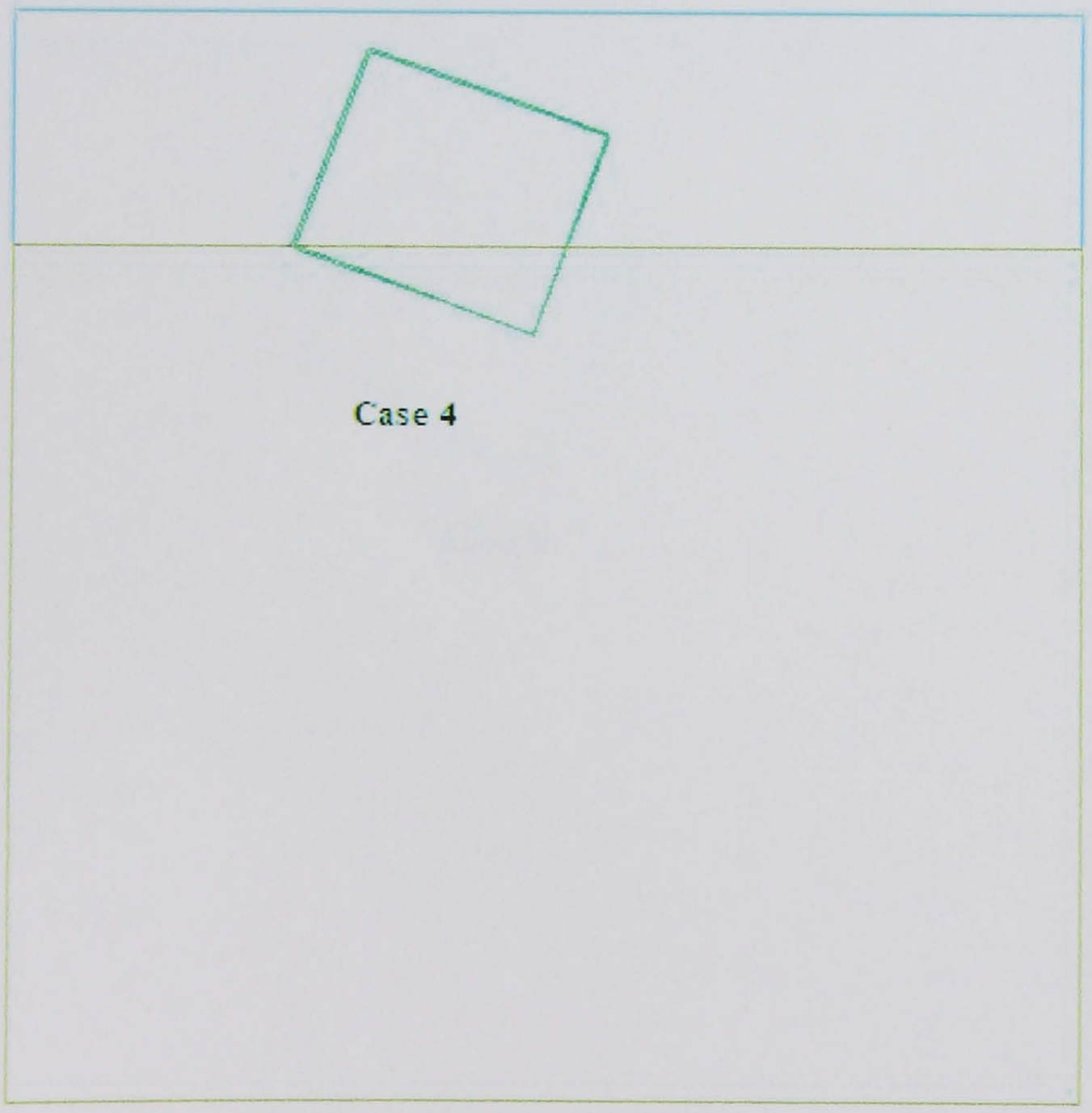

Figure (4.9) Code estimated position of the float Case 4

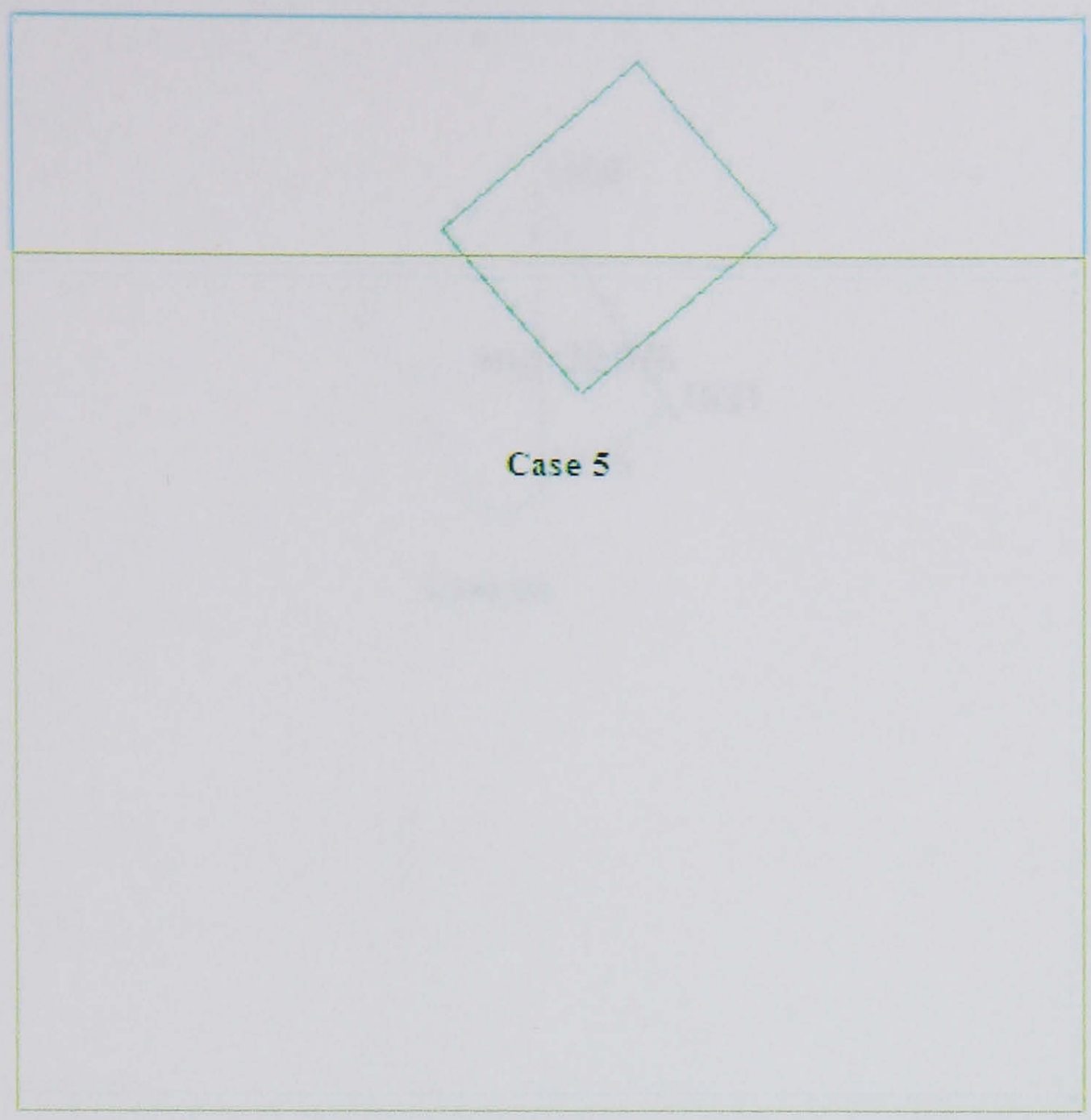

Figure (4.10) Code estimated position of the float Case 5

Figure (4.11) Code estimated position of the float Case 8

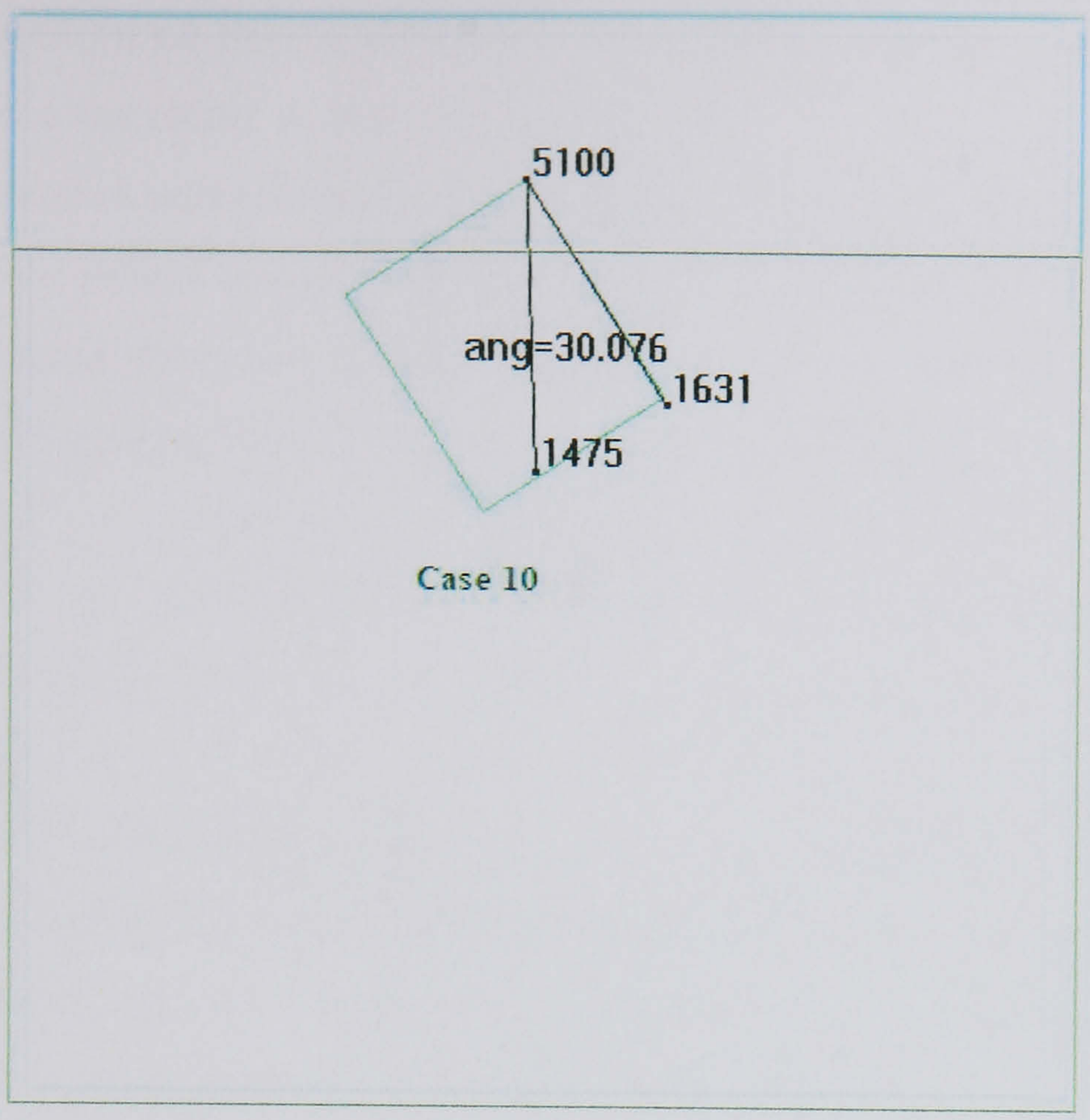

Case 10

Figure (4.12) Code estimated position of the float Case 10

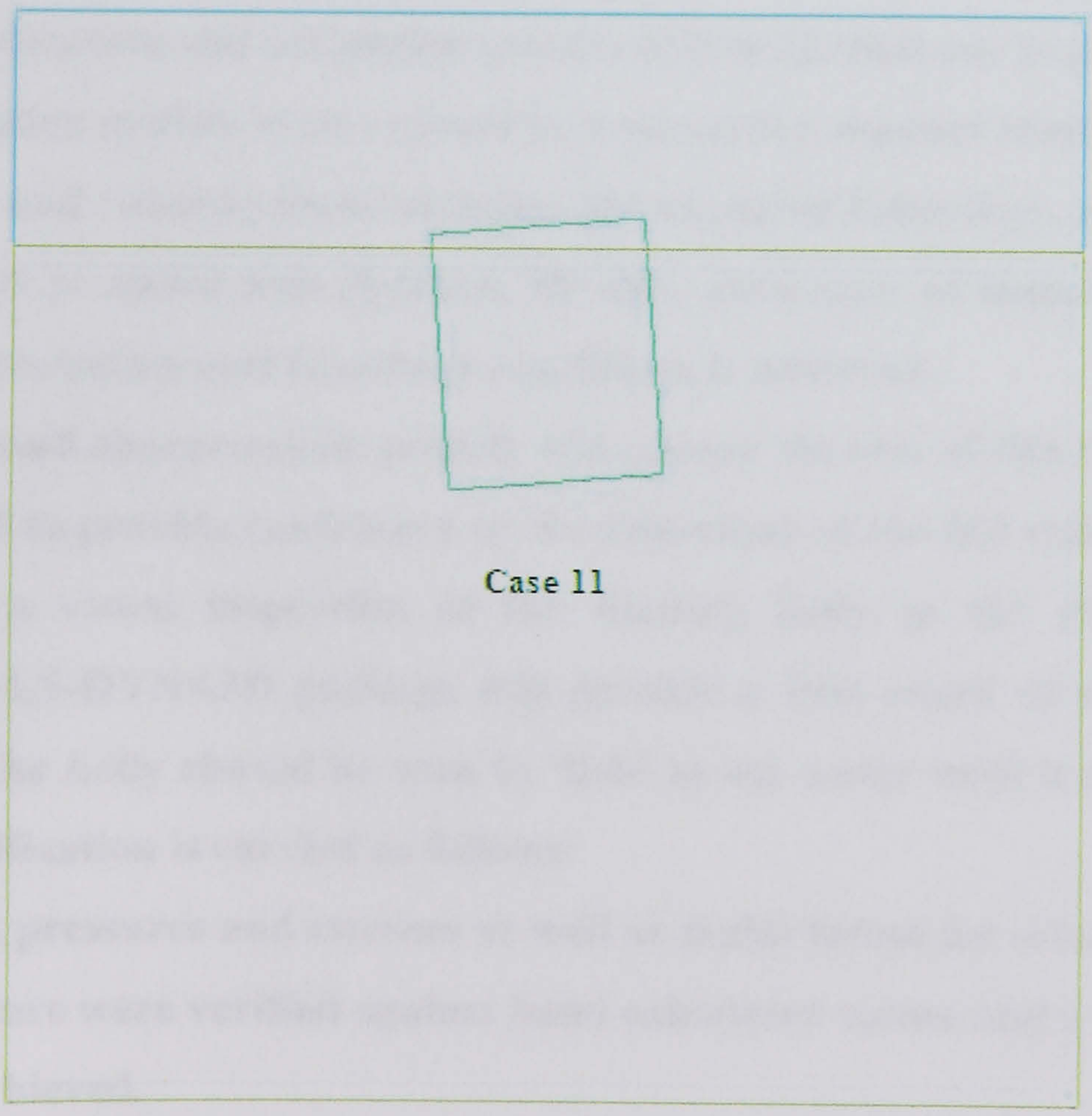

Case 11

Figure (4.13) Code estimated position of the float Case 11

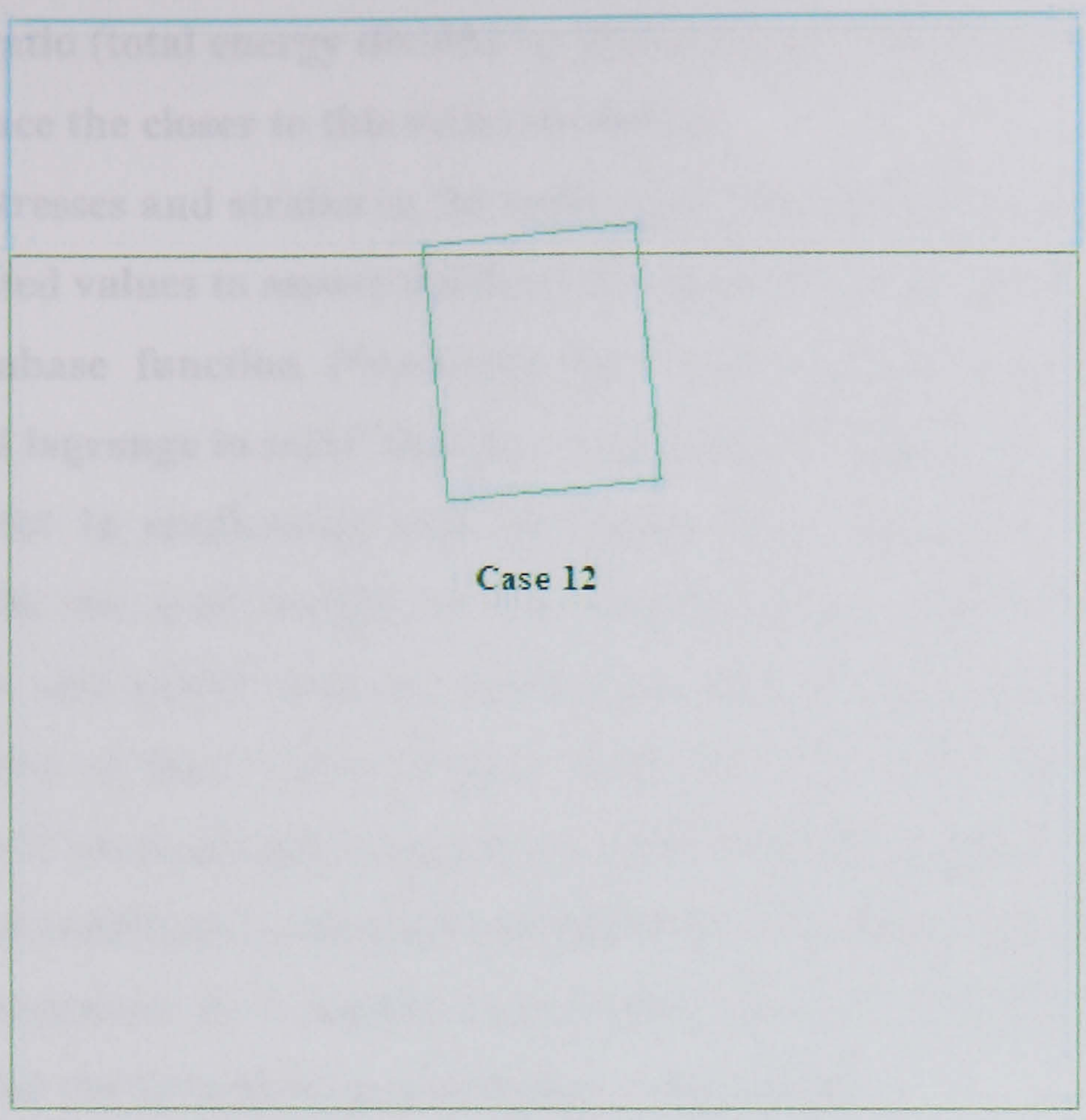

Figure (4.14) Code estimated position of the float Case 12

4.7 Further Verification and Validation

Further verification and validation process will be carried out as follows;

The verification models were created in a successive manner starting with the lower parts and running them to insure the expected behaviour, once assured the next part is added and checked. By this, assurance of materials, section properties, restraints and boundary conditions is achieved.

The three small characteristic models will occupy the rest of this Chapter and are intended to provide confidence in the behaviour of the full scale model. To start with, a visual inspection of the floating body in the postprocessor attached to LS-DYNA3D package will provide a first check of the required behaviour, the body should be seen to 'bob' in the water until it equilibrates. Further verification is carried as follows:

a) Element pressures and stresses as well as nodal forces for selected regions of the structure were verified against hand calculated values and a good match should be achieved.

b) The kinetic energy should die out which is indication of attaining the system stability.

c) Energy ratio (total energy divided by initial energy) should ideally be equal to unity, hence the closer to this value the better.

d) Linear stresses and strains in the cable elements are studied and compared to the expected values to assure the desired behaviour of the cables.

e) The database function (*database_fsi) to be used in conjunction with 'constrained lagrange in solid' function is created as "ASCII" file in 'd3plot' it is very useful in confirming that the uplift force calculated by the code matches with the total weight of the floating body. Stresses and average pressure are also useful tools for verification, the existence of these files and the correlation of their values is good indication that the coupling (contact) between 'ALE' elements and Lagrangian solid elements is achieved properly. Based on the verification and assured reliability of results, such results will be screened, presented in a useful format and can be used for constructive judgement for the structural performance of the model.

Analytical verification is done using the time history values of the analysis as follows:

The density of the floating box is chosen according to the buoyancy principle.

Total weight of the box = weight of the displaced water by the submerged volume of this box 'Case 12' in Table 4-1.

$$= (0.1 \times 0.105 \times 0.01) \times 1025 = 0.1076 \text{ kg.}$$

Total buoyancy upward lift force = 0.1076 x 9.81 = 1.056 N this will produce stress on the lower face of the box as follows:

$$\sigma_{yy} = \frac{1.056}{0.1 \times 0.01} = 1055.8 \text{ Pa}$$

These values are in conformance with the uplift y-force and bottom stress at the box lower face shown in Figure (4.15) and Figure (4.16) respectively.

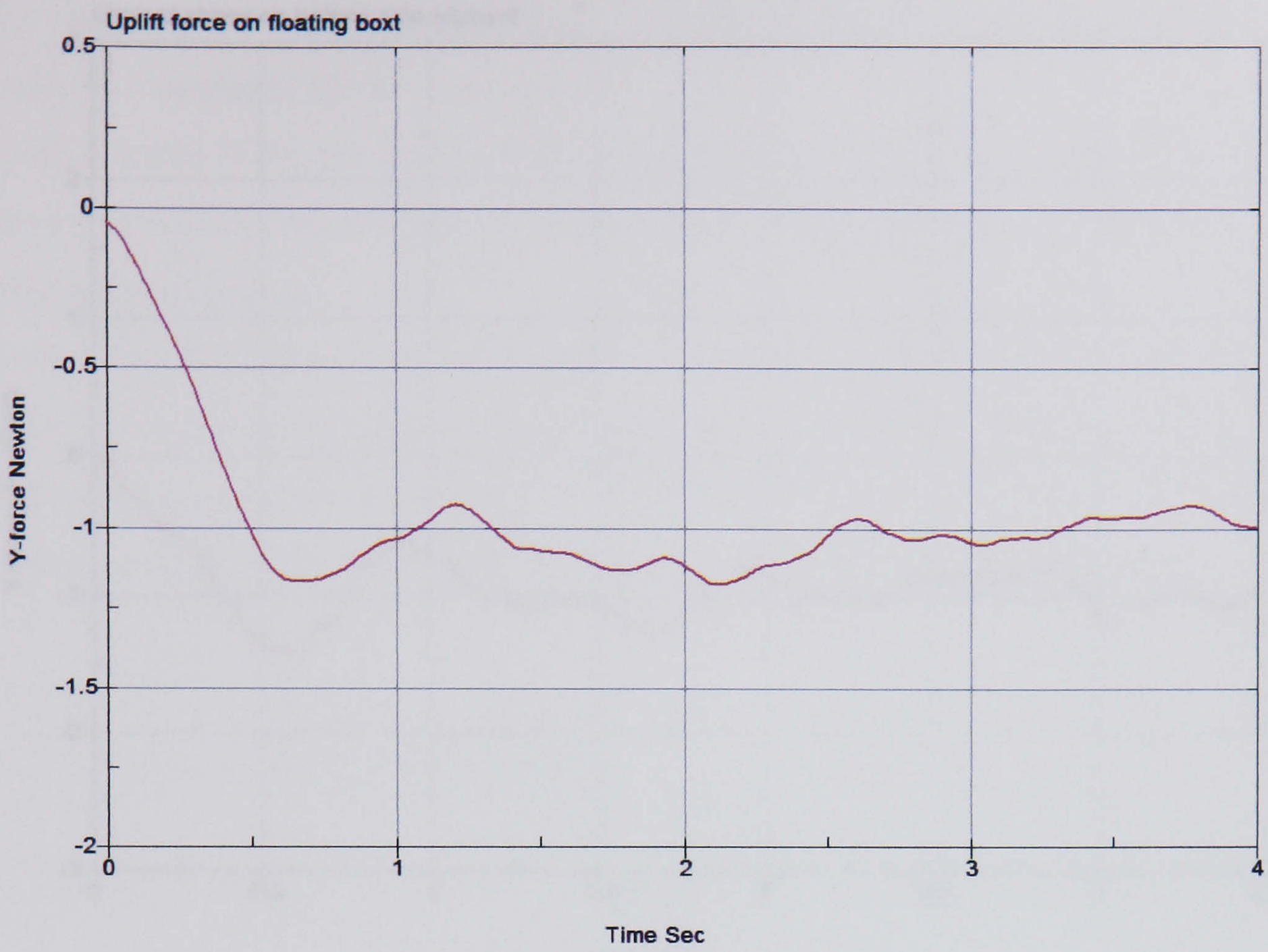

Figure (4.15) Uplift force under floating box

Choosing bottom side element in the z-side of the floating box with the centre of this element at depth of 0.0984m from free water surface giving a hydrostatic side pressure of:

P_{water}= 0.0984 x 1025 x 9.81 = 989 Pa, this value is conforming to the mean value of the code calculated pressure for the same element shown in Figure (4.17).

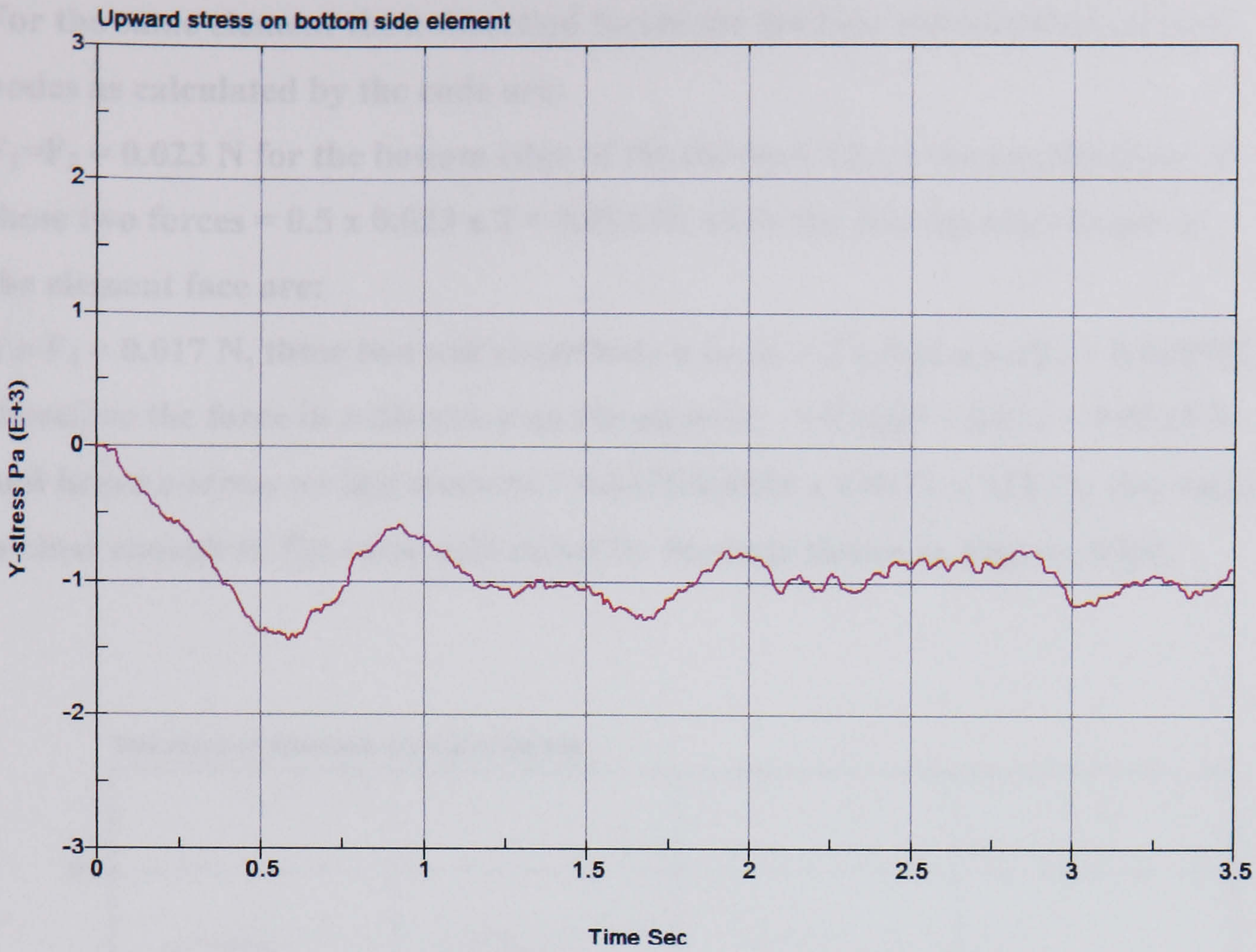

Figure (4.16) Bottom stress under lower side element of the box

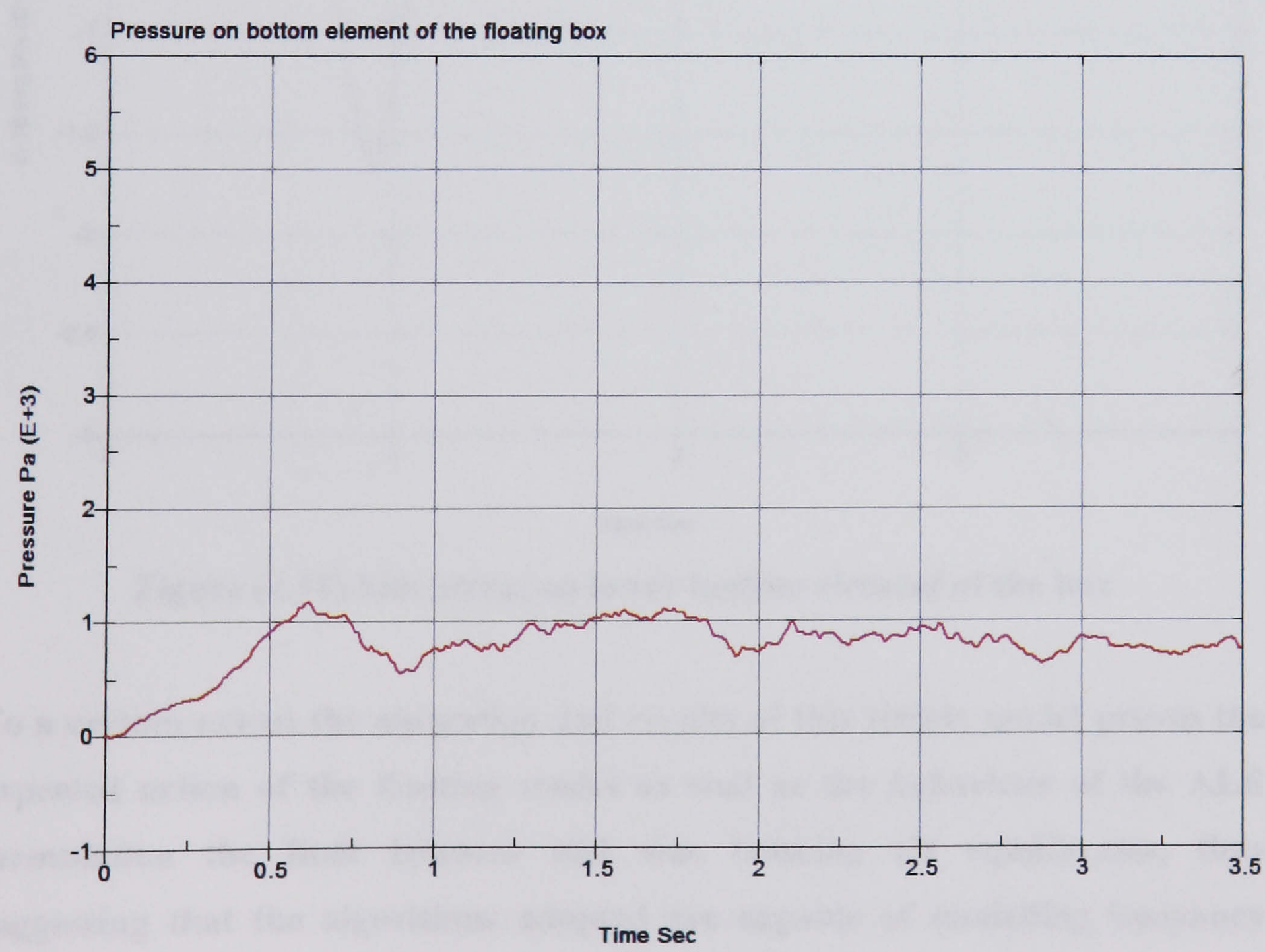

Figure (4.17) Pressure on lower bottom element of the box

For the same element the z-direction forces for the four surrounding element nodes as calculated by the code are:

F_1=F_2 = 0.023 N for the bottom edge of the element where the contribution of these two forces = 0.5 x 0.023 x 2 = 0.023 N, while the two top edge forces of the element face are:

F_3=F_4 = 0.017 N, these two will contribute a force = 2 x 0.25 x 0.017 = 0.0085 N, therefore the force in z-direction on the element = 0.0085 + 0.023 = 0.0315 N and hence z-stress on this element = 0.0315/0.0133 x 0.0111 = 213 Pa, this value is close enough to the value calculated by the code shown in Figure (4.18).

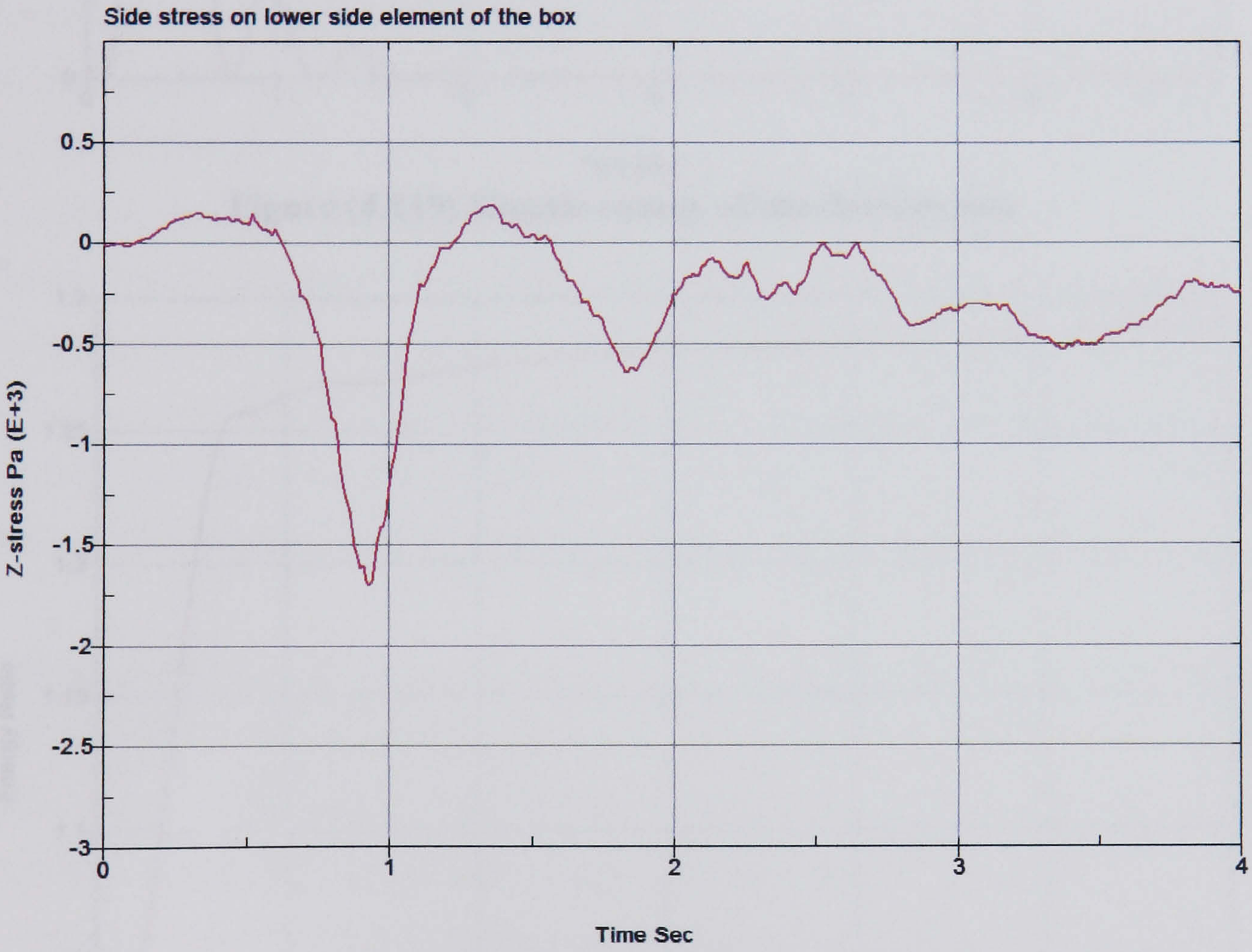

Figure (4.18) Side stress on lower bottom element of the box

To a certain extent the animation and results of this simple model proves the expected action of the floating model as well as the behaviour of the ALE formulation the float bounces and was bobbing till equilibrates, thus suggesting that the algorithms adopted are capable of modelling buoyancy action.

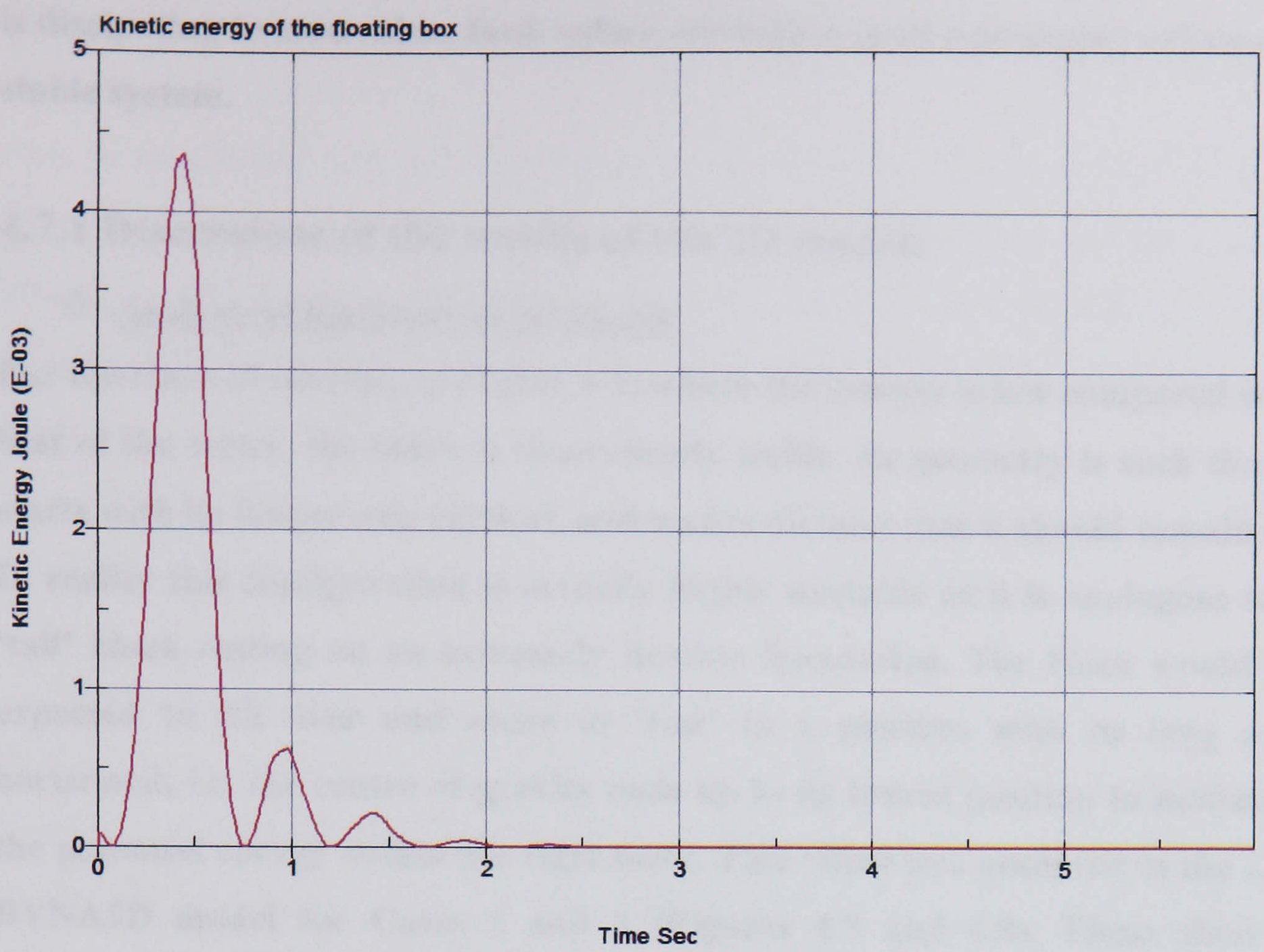

Figure (4.119) Kinetic energy of the floating box

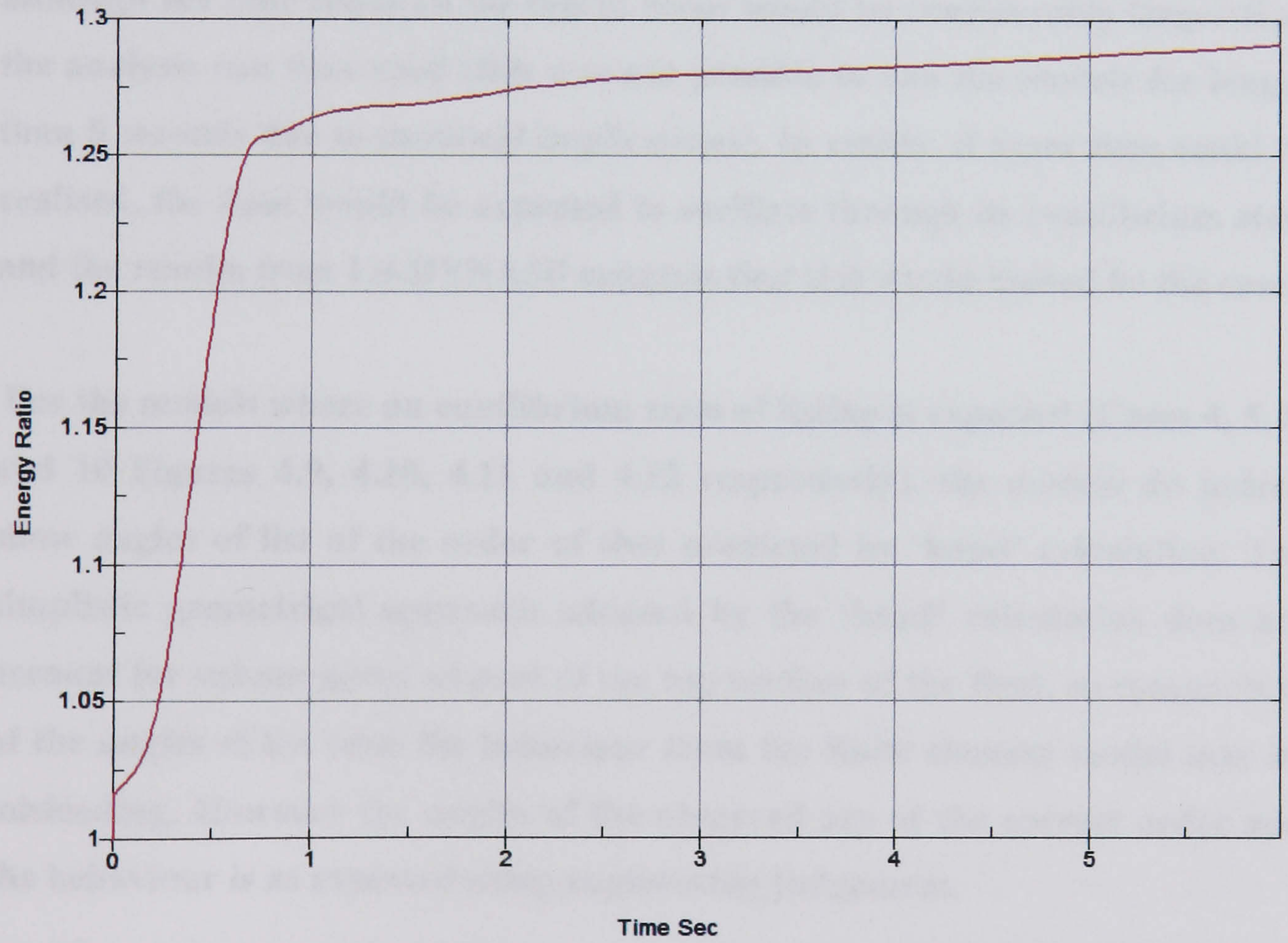

Figure (4.20) Energy ratio for the floating box

Looking to the kinetic energy, Figure (4.19) and energy ratio, Figure (4.20) of this system, the energy ratio is close to the unity value while the kinetic energy

is dissipating to zero value. Both values are within good converging values of a stable system.

4.7.1 Discussions of the results of the 2D model:

❖ **Analysis of Buoyancy of 2D Model**

For the cases of stability of (Table 4-1) where the density is low compared with that of the water, the block is theoretically stable. Its geometry is such that it starts with its longer axis vertical, and statics dictates that it should remain so. In reality this configuration is actually highly unstable as it is analogous to a 'tall' block resting on an extremely flexible foundation. The block would be expected to tilt over and come to 'rest' in a position with its long axis horizontal, i.e. the centre of gravity ends up in its lowest position to minimise the potential energy within the rigid body. This effect was observed in the LS-DYNA3D model for Cases 1 and 3 (Figures 4.7 and 4.8). These show a 'snapshot' in time where the body would be approaching its equilibrium state, although the time required for this to occur would be considerably larger than the analysis run time used (this was not possible to run the models for longer than 5 seconds due to practical implications). In reality, if more time could be realised, the float would be expected to oscillate through its equilibrium state and the results from LS-DYNA3D suggests that this would indeed be the case.

For the models where an equilibrium state of listing is expected (Cases 4, 5, 8, and 10 Figures 4.9, 4.10, 4.11 and 4.12 respectively), the models do indeed show angles of list of the order of that predicted by 'hand' calculation. The simplistic geometrical approach adopted by the 'hand' calculation does not account for submergence of part of the top surface of the float, so comparison of the angles of list with the behaviour from the finite element model may be misleading. However the angles of list observed are of the correct order and the behaviour is as expected using engineering judgement.

For the cases where the float has a large density compared with that of the water, the float will theoretically sit low and vertical in the water. Cases 11 and 12 shown in Figure 4.13 and 4.14 respectively demonstrate that this is

indeed the case, with only a small angle of list evident from the LS-DYNA3D modelling.

This investigation has also highlighted the differences between the pseudo-static hand calculation approach and the dynamic behaviour demonstrated by LS-DYNA3D. It is likely that behaviour is captured more realistically under dynamic action than the static calculation can predict without adopting a more complex calculation approach.

These results give confidence that the effects of buoyancy are being modelled sufficiently correct for the purposes of transient load events.

- **Presence of High Frequency 'Noise'**

With a large number of stress/time history plots, it was evident that higher frequency components/oscillations are corrupting the results. The average 'form' of most of the plots conforms to that expected from theoretical hand calculation and expected behaviour. Within LS-DYNA3D, the filtering functions were used in all cases to remove this high frequency component and effectively smooth the data. Filtering frequencies above 1000Hz was adequate in most cases to produce smoothed data plots.

The immediate concern was to investigate the source of the noise and to whether its effects could be influencing the global behaviour of the floating body. There are two likely sources for the high frequency noise which need to be considered:

1. **Internal reflection of waves from the boundaries of the structure.**
2. **High frequency oscillations generated by the fluid/structure coupling.**

The most likely culprit for the spurious oscillations is the fluid/structure coupling. The effects of each of these causes is considered in turn

(i) Boundary Reflections

The external boundaries of the model are represented with non-reflecting (energy absorbing) boundaries therefore it is hoped that these should minimise reflection of generated waves. However there are internal boundaries within the float model and these are ideal for causing reflection of waves. For example, if we consider the speed of sound in the air/water/solid mediums, the frequency at which waves are returned to their source can be easily calculated from the model geometry.

Invariably these frequencies are in excess of 1000Hz (generally 2000Hz to 4000Hz) and are not expected to cause any unwanted effects on the global behaviour.

(ii) Fluid/Structure Coupling

High frequency contact oscillations for penalty coupling are well documented. Contact 'chatter' often occurs as the contacting boundaries adjust themselves relative to each other once penetration initiates. In LS-DYNA3D this problem has been witnessed in many contact models and methods for its mitigation are also well documented, N.Aquelet et al [67]. To mitigate these effects the data may simply be filtered using the built in functions of the coupling keyword. Alternatively damping across the penalty force may be specified to smooth the response and aid convergence. LS-DYNA3D command 'CTYPE=4' was specified for the models in hand, which sets the contact algorithm to penalty coupling without erosion. However the optimum value of this damping may be the subject of parametric studies as this may effect the global behaviour of the model if the wrong values are used as already discussed under the damping bullet earlier in this Chapter. So the value chosen for the float model was the program default option, which is possibly (conservatively) low.

To investigate this further, spectral analysis was carried out using the Fast Fourier Transform (FFT) approach on data from a particular stress/time history plot extracted from the 2D float model. The frequency analysis of results was carried out on data before and after filtering was carried out in the post-processing program.

It should be noted that the sampling rate of the numerical data dumped from LS-DYNA3D during its runs was 0.001 second. Hence this sampling rate can only capture frequencies up to 1000Hz when the time history trace is analysed. Runs were repeated with a higher frequency of data dumps to enable a smaller sampling rate of data, but unfortunately this caused premature termination due to machine specific criteria. Hence the FFT frequency analysis is only valid up to 1000Hz:

The plots in the following MathCAD templates shown afterward illustrate that before filtering there is noise at around 50Hz and 150Hz. Reflection is unlikely to have caused this noise as it will be found at higher frequencies if present. However multiple reflections may manifest at lower frequencies so this cannot be ruled out entirely. The frequency of contact 'chatter' is harder to ascertain, and may well be causing noise at these frequency levels. Hence the frequency analysis is inconclusive as to the source of the high frequency noise. In terms of the global behaviour, the filtered data oscillates at a significantly lower frequency about the expected values of stress, and the high frequency content is successfully removed. So in conclusion there is a high degree of confidence that the source of the noise will not significantly affect the results and that the filtering process of the post-processor is adequate for smoothing and presenting the data.

Original unfiltered data from Figure (4.16)

Frequency Analysis using Fast Fourier Transform

TEST := READPRN ("c:\FFT\noise.txt")

Number of records on file $i := 0 .. 1001$

Amplitude of data $x_i := TEST_{i,1}$

$\Delta t := 0.001 \cdot sec$ $\max\left(\overrightarrow{|x|}\right) = 1.53 \times 10^3$

Waveform in Time

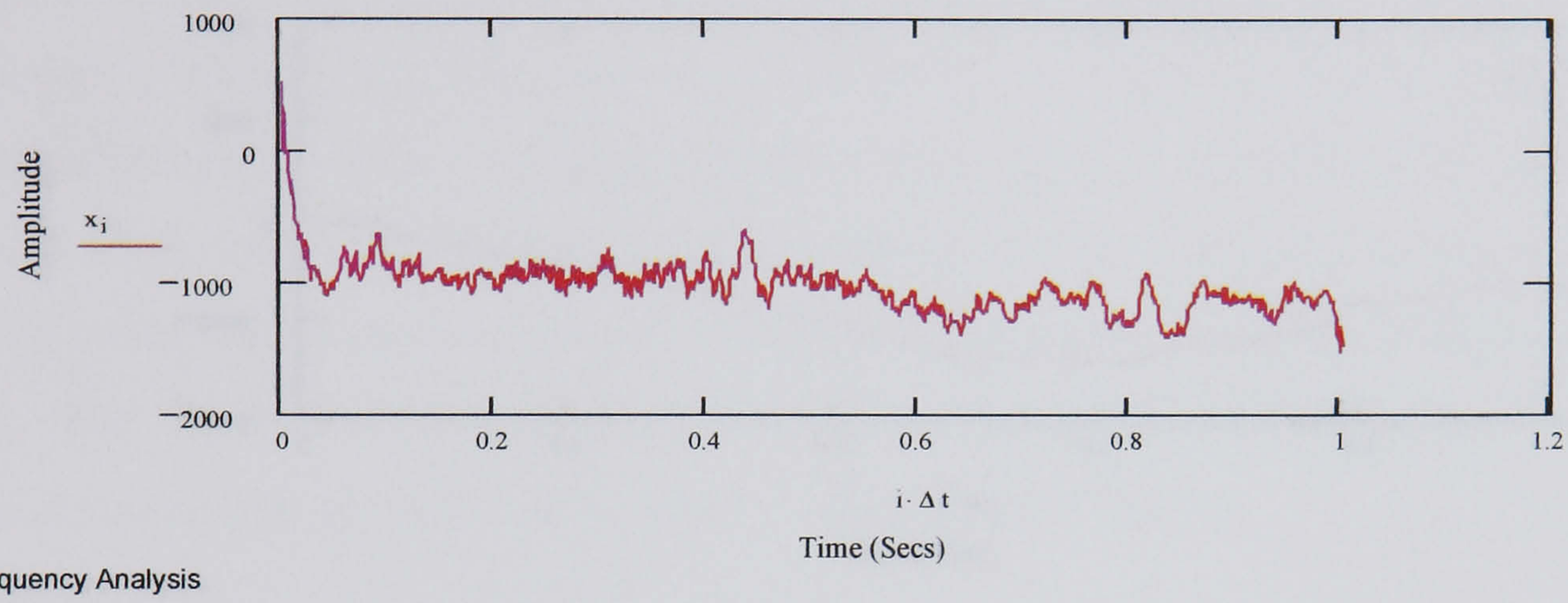

Frequency Analysis

Number of Samples $N := 600$ $k := 0 .. N - 1$

Sample Rate: $T := 0.001$ Frequencies $f_s := \frac{1}{T}$ $freq_k := \frac{k}{N} \cdot f_s$

$X := CFFT(x)$

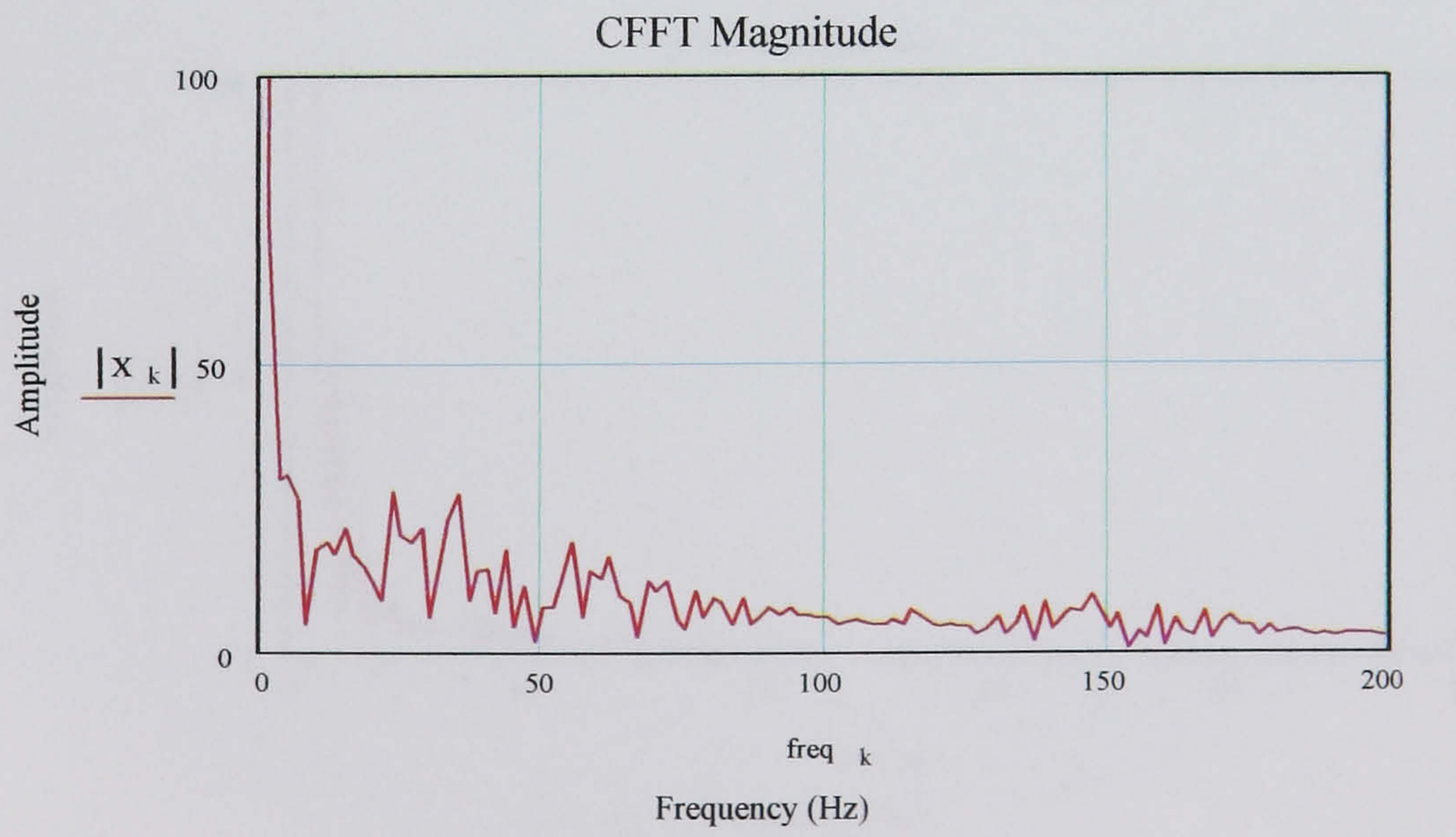

Same data from Figure (4.16) only filtered

Frequency Analysis using Fast Fourier Transform

TEST := READPRN ("c:\FFT\fig4-7.txt")

Number of records on file $i := 0 .. 600$

Amplitude of data $x_i := TEST_{i,1}$

$\Delta t := 0.01 \cdot sec$ $\max\left(\overrightarrow{|x|}\right) = 1.76 \times 10^3$

Waveform in Time

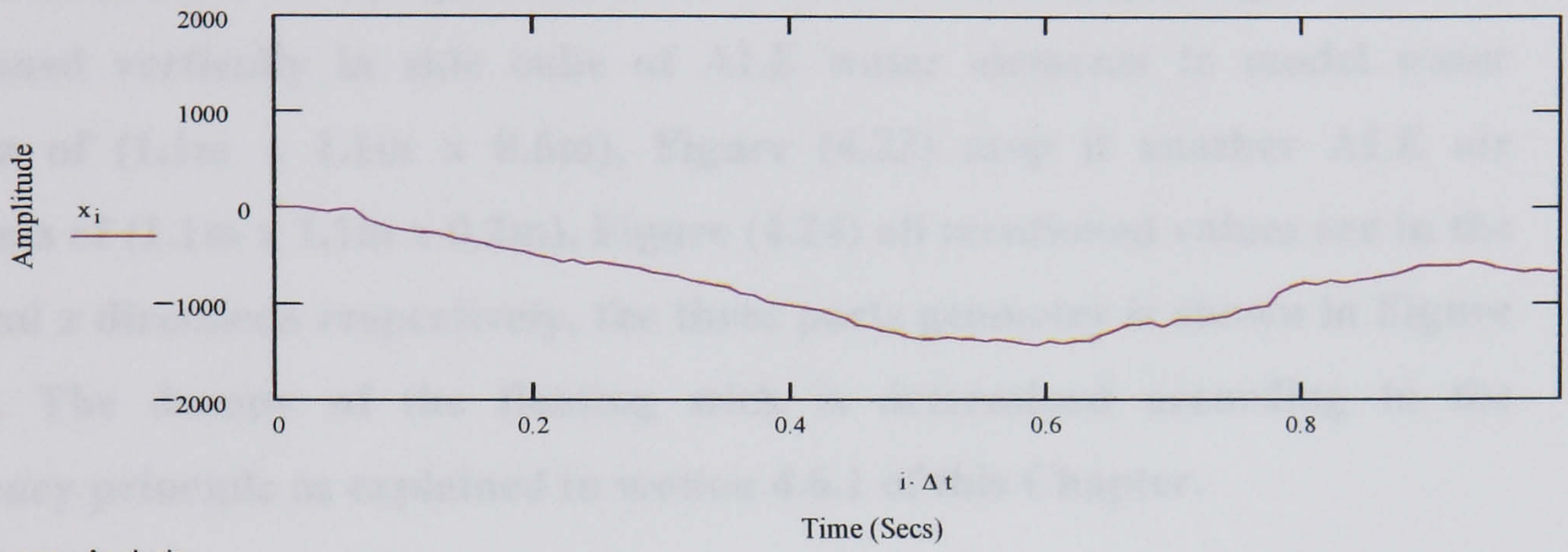

Frequency Analysis

Number of Samples $N := 600$ $k := 0 .. N - 1$

Sample Rate: $T := 0.01$ Frequencies $f_s := \frac{1}{T}$ $freq_k := \frac{k}{N} \cdot f_s$

$X := CFFT(x)$

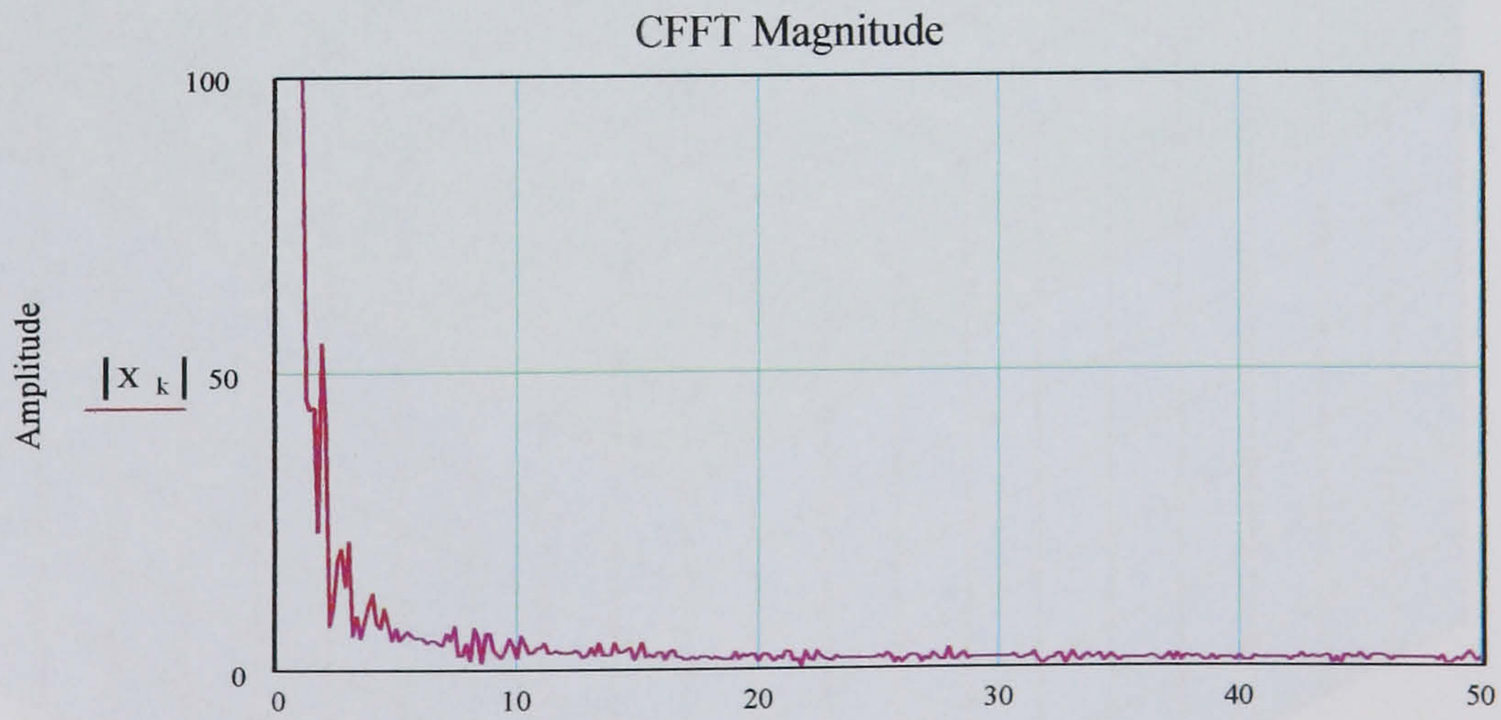

4.8 Three-dimensional verification model:

Following the methodology and formulations mentioned in the previous section, three dimensional model of a floating object is developed to further test the action in three dimensions and increase confidence in the aforementioned findings before to expand them to a prototype floating turbine to be discussed later.

4.8.1 Three-dimensional stick model:

A stick of (0.1m x 0.1m) square cross section and 0.4m height Figure (4.22) is positioned vertically in side cube of ALE water elements to model water quanta of (1.1m x 1.1m x 0.6m), Figure (4.23) atop it another ALE air elements of (1.1m x 1.1m x 0.2m), Figure (4.24) all mentioned values are in the x, y and z directions respectively, the three parts geometry is shown in Figure (4.21). The density of the floating stick is determined according to the buoyancy principle as explained in section 4.6.1 of this Chapter.

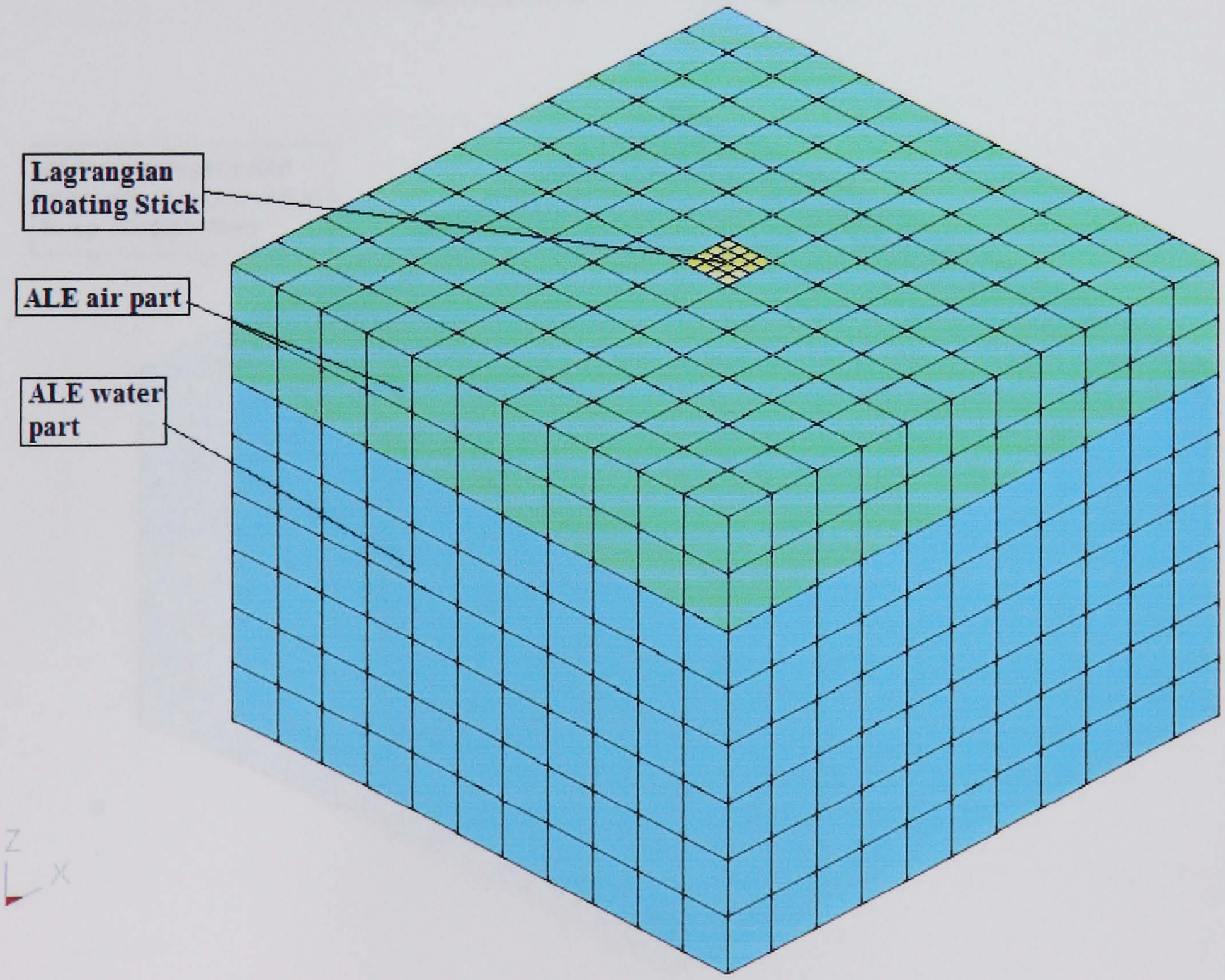

Figure (4.21) The 3-D Stick model

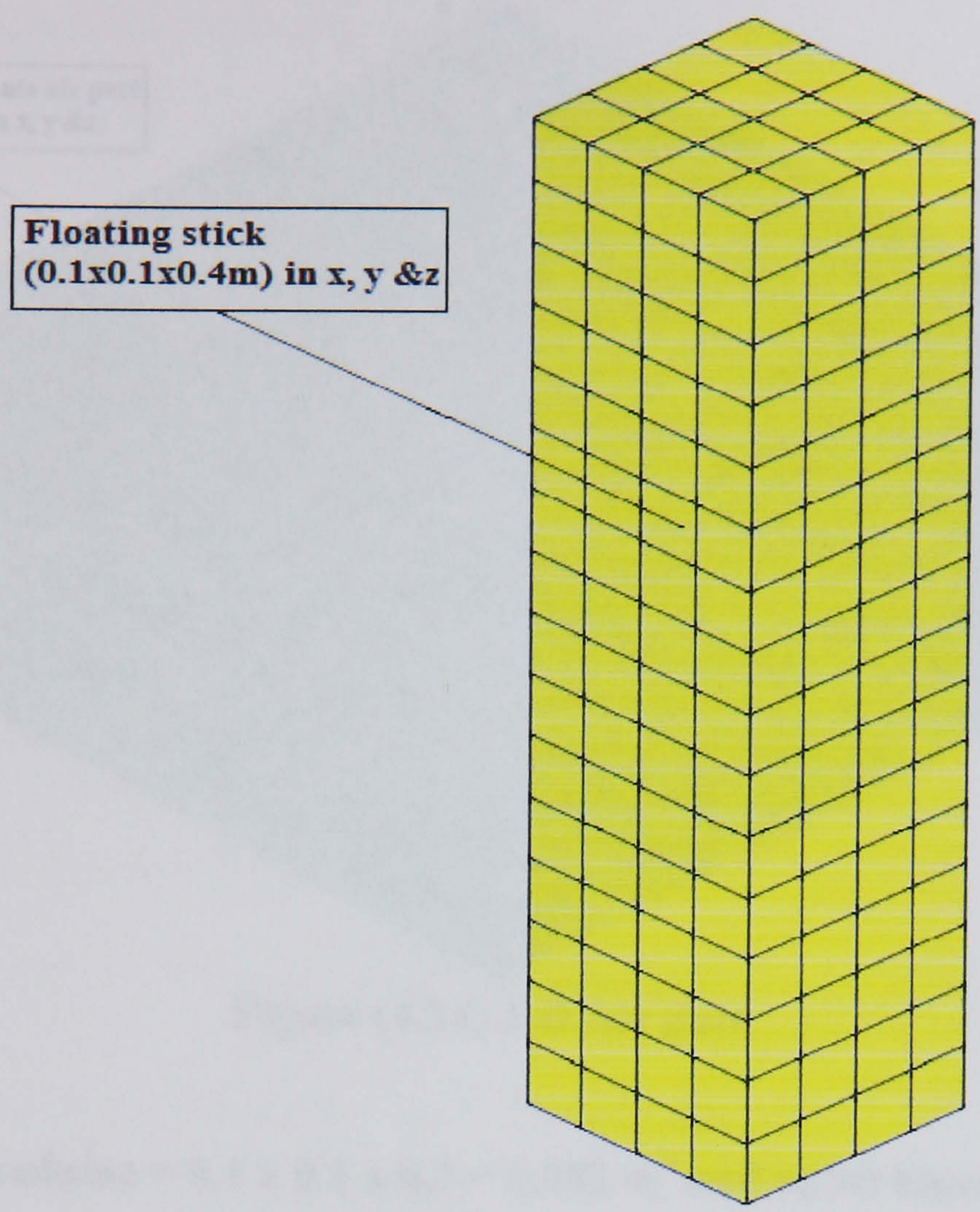

Figure (4.22) 3-D floating stick

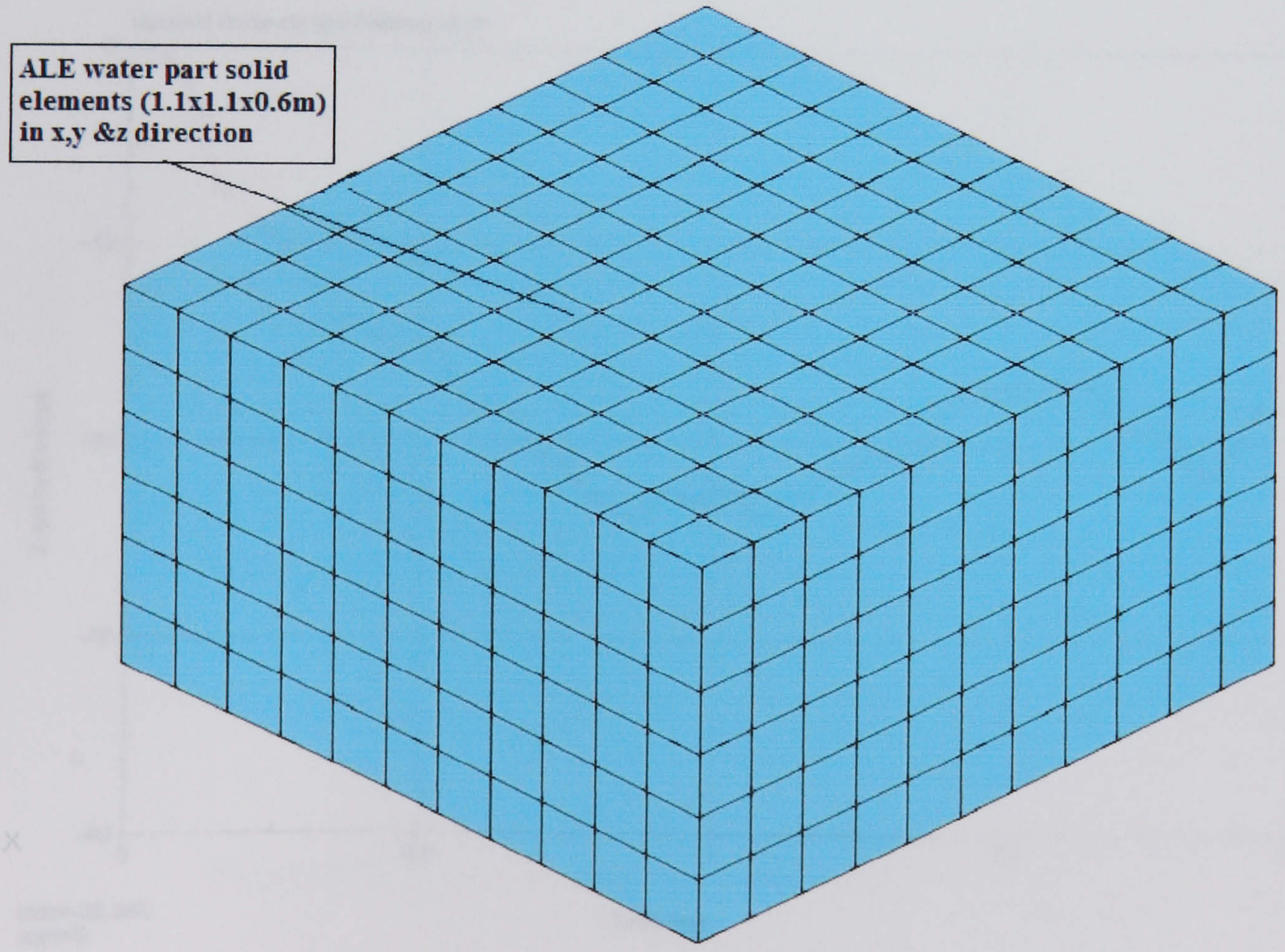

Figure (4.23) 3-D Water part

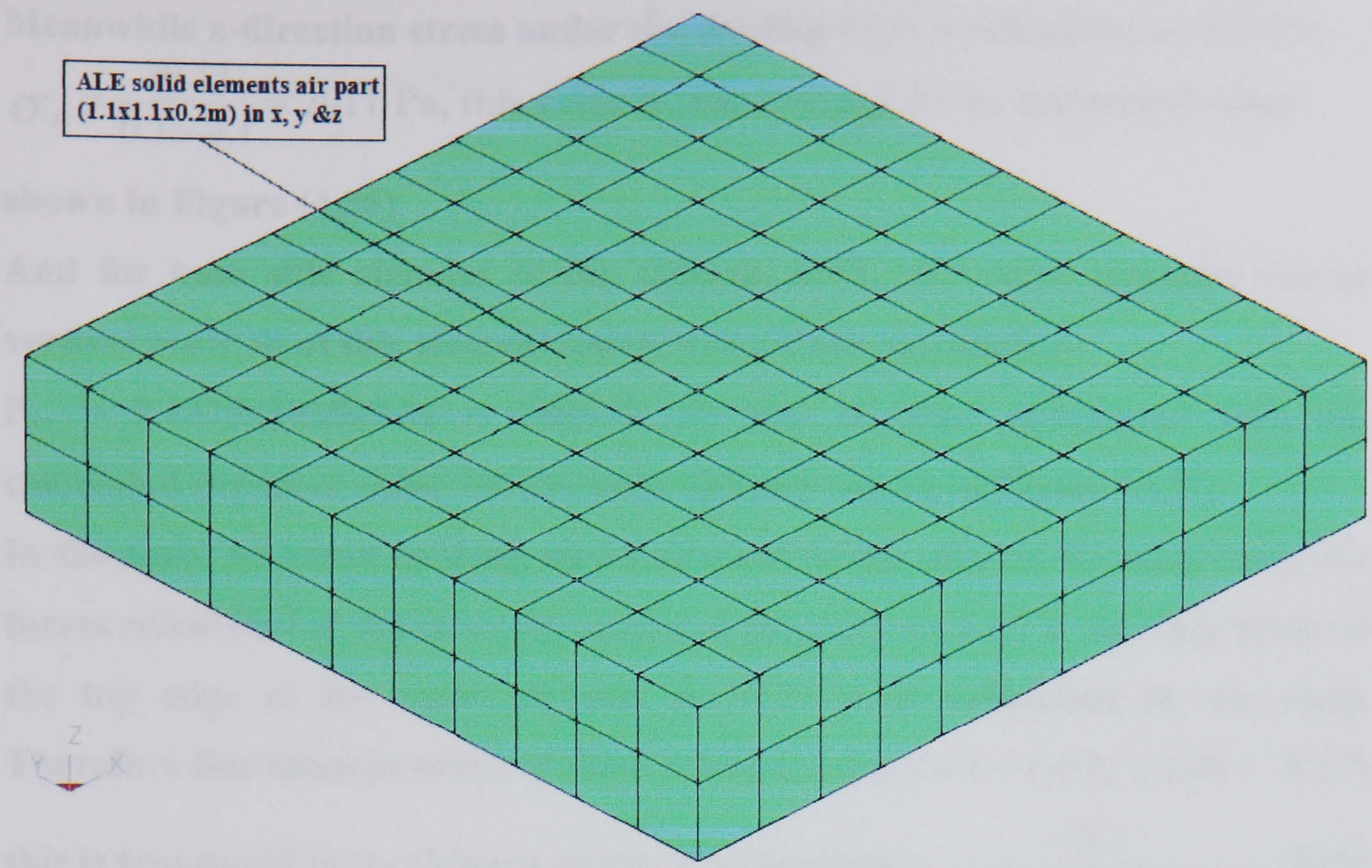

Figure (4.24) 3-D Air part

The displaced volume = 0.1 x 0.1 x 0.2 = 0.002 m^3 and uplift buoyancy force is $F_{buoyancy}$ = 0.002 x 1025 x 9.81 = 20.11 N, this is close enough to the z-force shown in Figure (4.25).

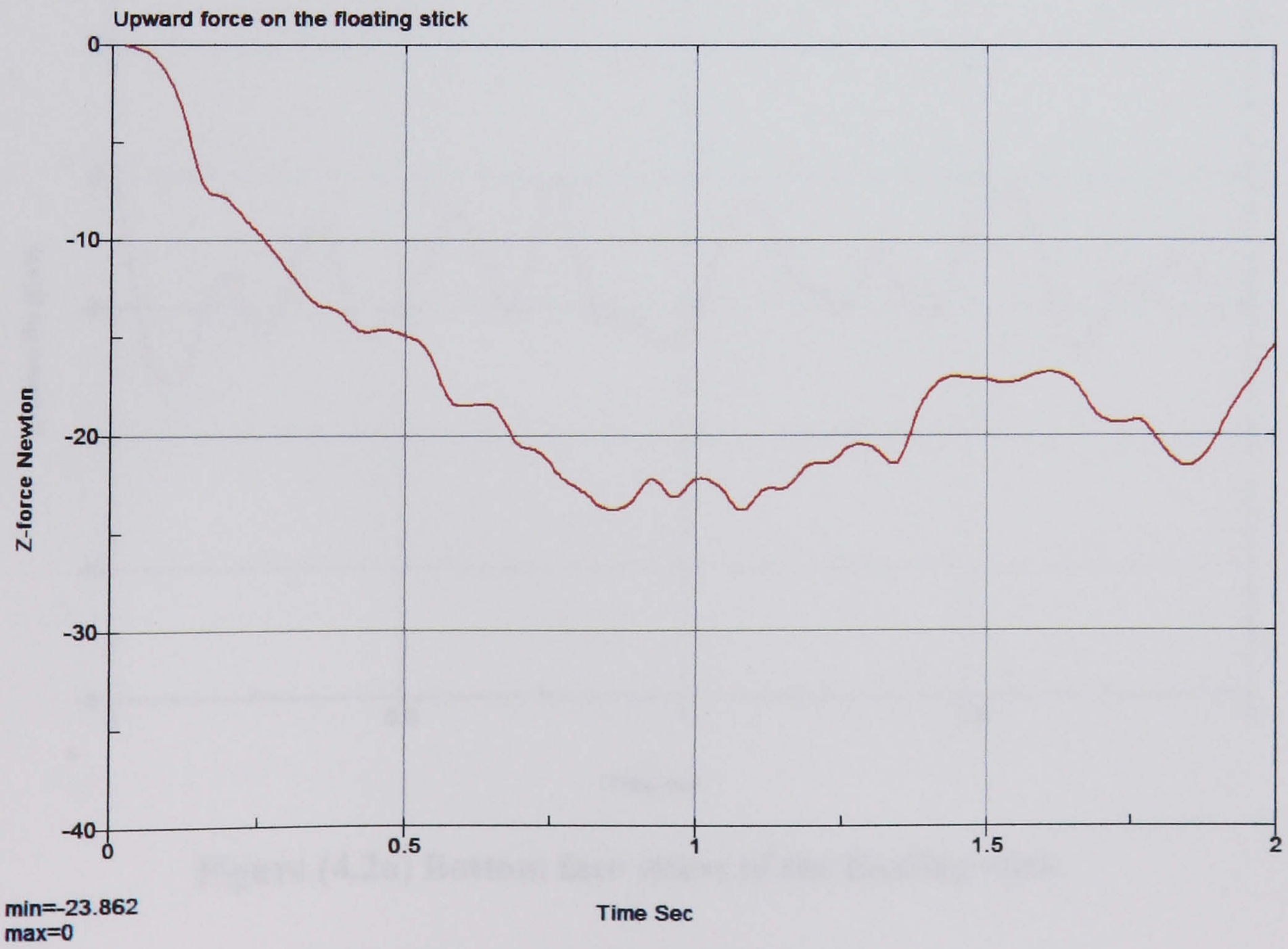

Figure (4.25) Uplift buoyancy force on the floating stick bottom

Meanwhile z-direction stress under the floating stick is calculated as follows:

$\sigma_{zz} = \frac{20.11}{0.1 \times 0.1} = 2011$ **Pa, this value is close enough to the calculated value shown in Figure (4.26).**

And for base side element of the floating stick, the water pressure due to vertical position of this element centre at 0.1875m elevation is:

P_{xx} = 0.1875x1025x9.81 = 1885.36 Pa this in close agreement with the calculated pressure value for the same element shown in Figure (4.27).

In the same sequence picking up an element at the edge of the stick base, the forces calculated at the two edge nodes of the element is (-1.6 N) while those at the top edge of the same element is (-3.2 N) as calculated by the code. Therefore this element share of these forces is (-2 x 1.6/2 + (-3.2) x 2/4) = -3.2 N

this is translated to an element stress in x-direction = $\frac{-3.2}{(0.025) \times (0.025)}$ **= -5120 Pa which is close to the value shown in Figure (4.28).**

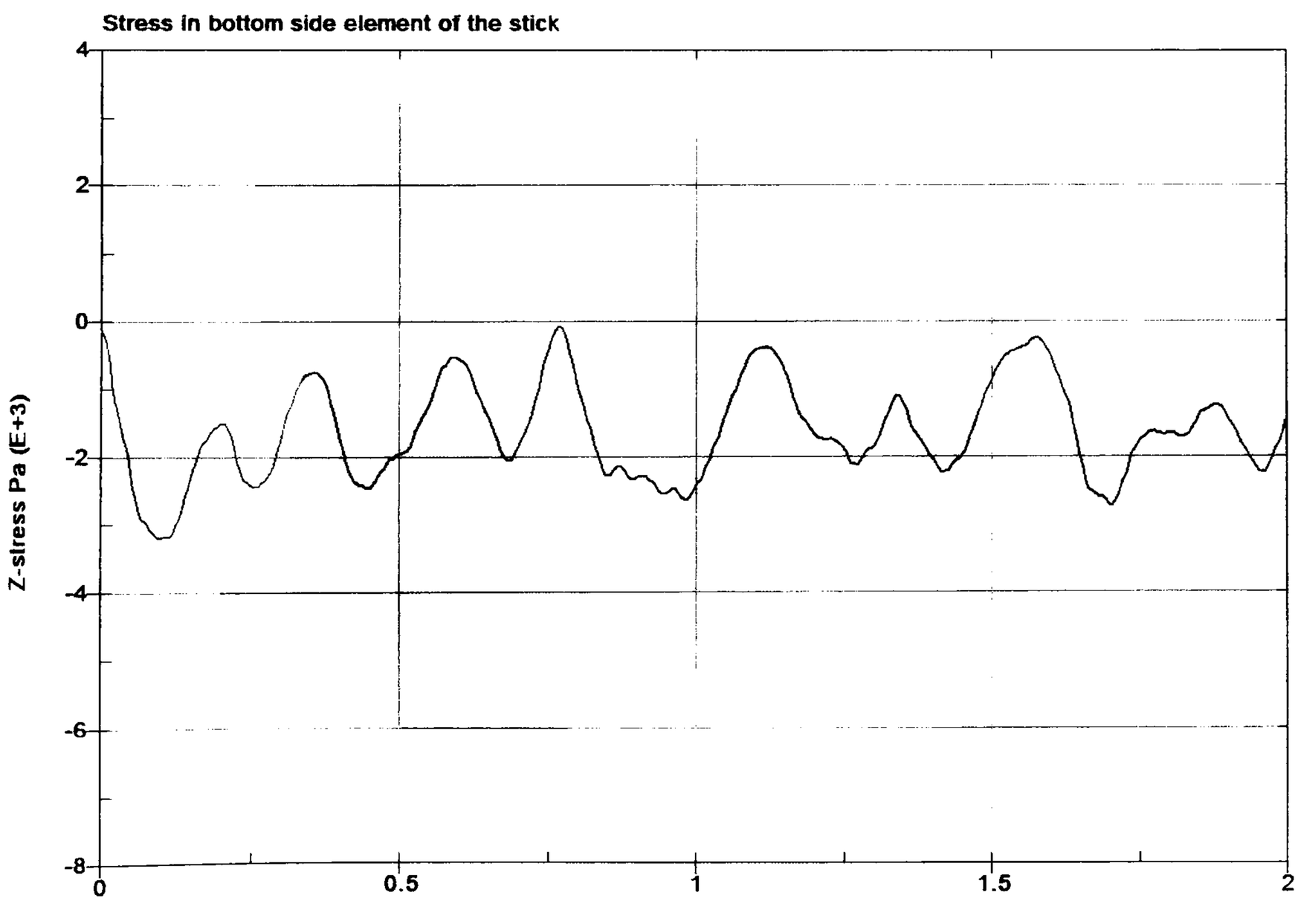

Figure (4.26) Bottom face stress of the floating stick

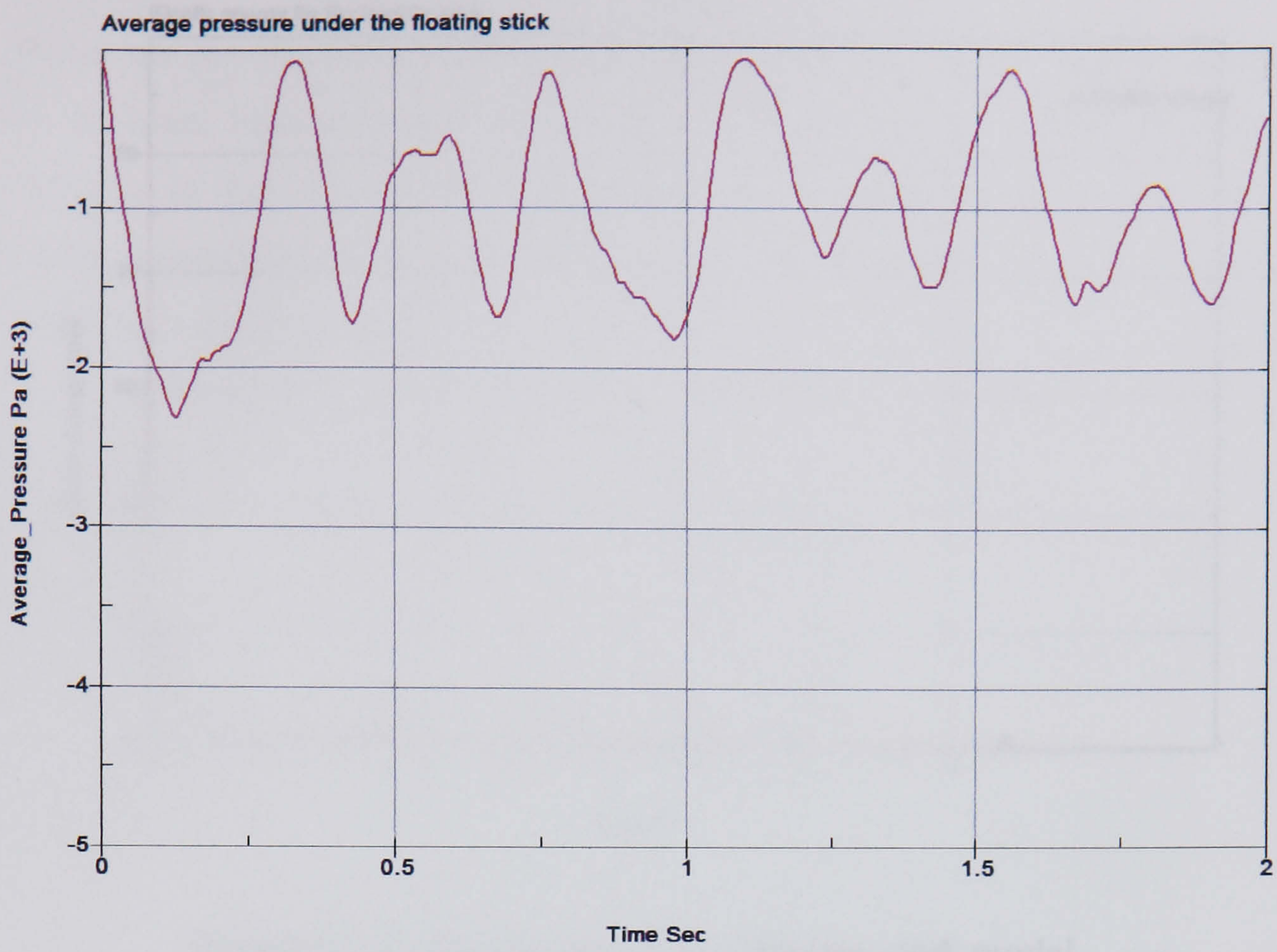

Figure (4.27) Bottom face pressure on the floating stick

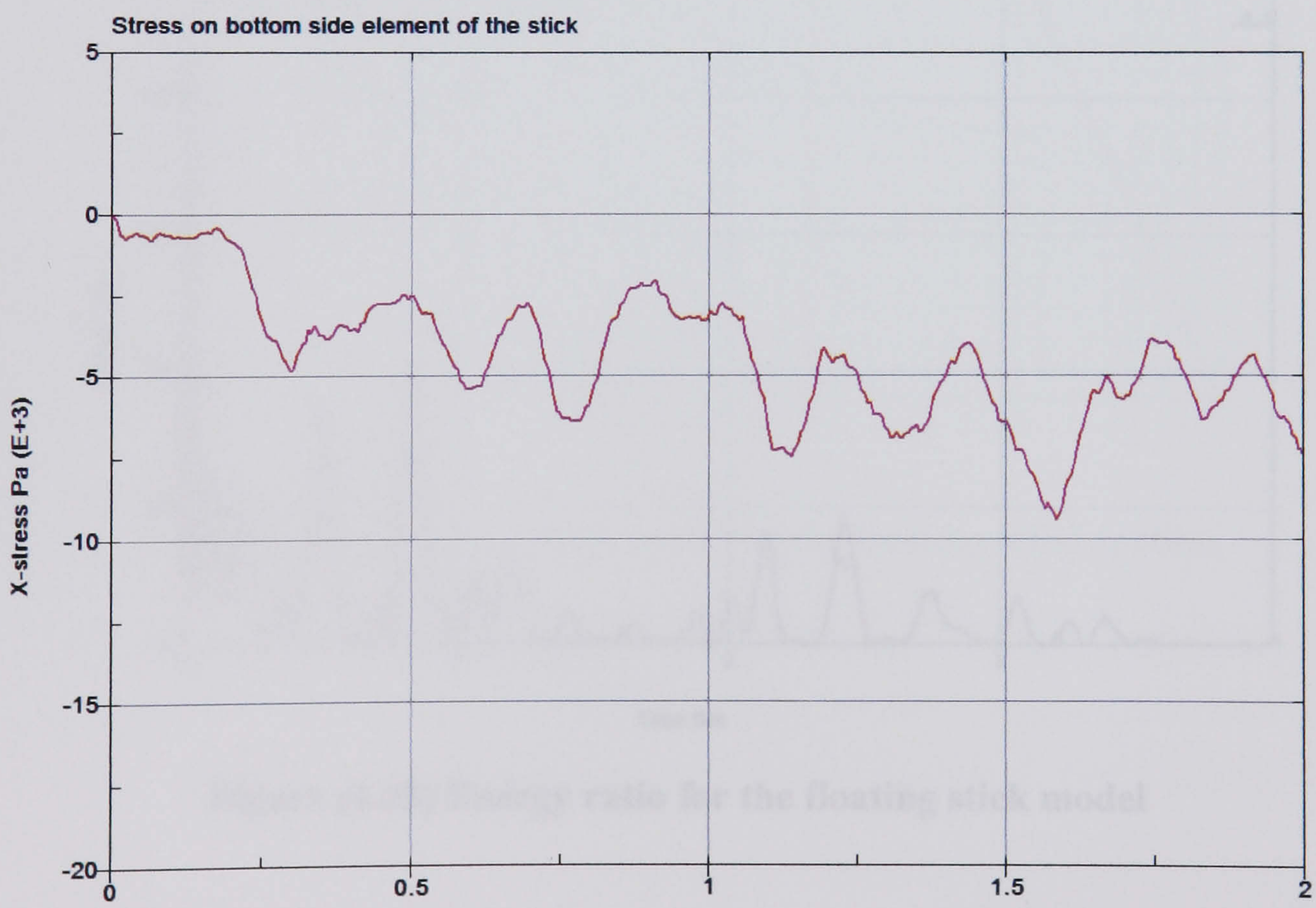

Figure (4.28) Stress in the base side element of the stick

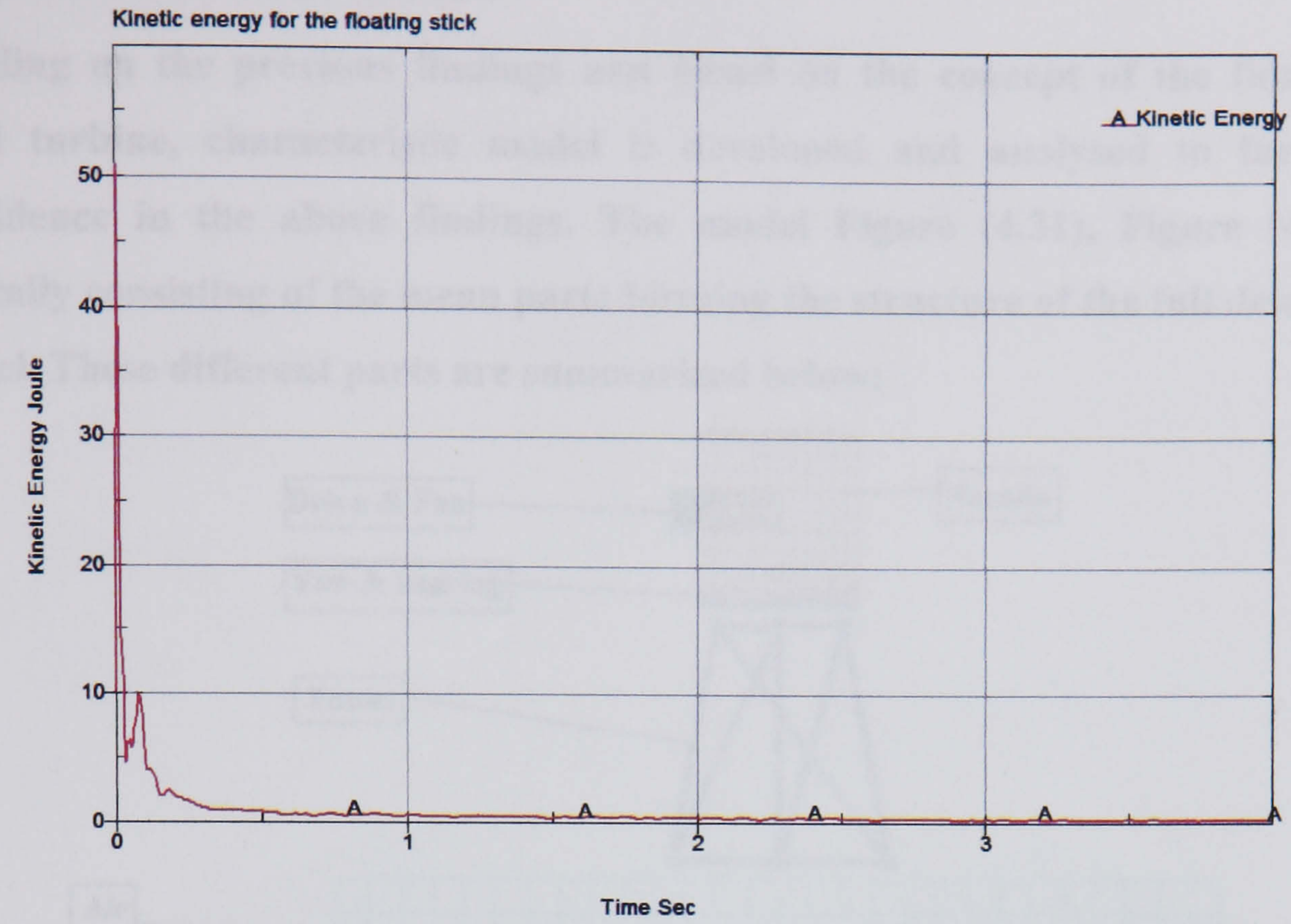

Figure (4.29) Kinetic energy for floating stick model

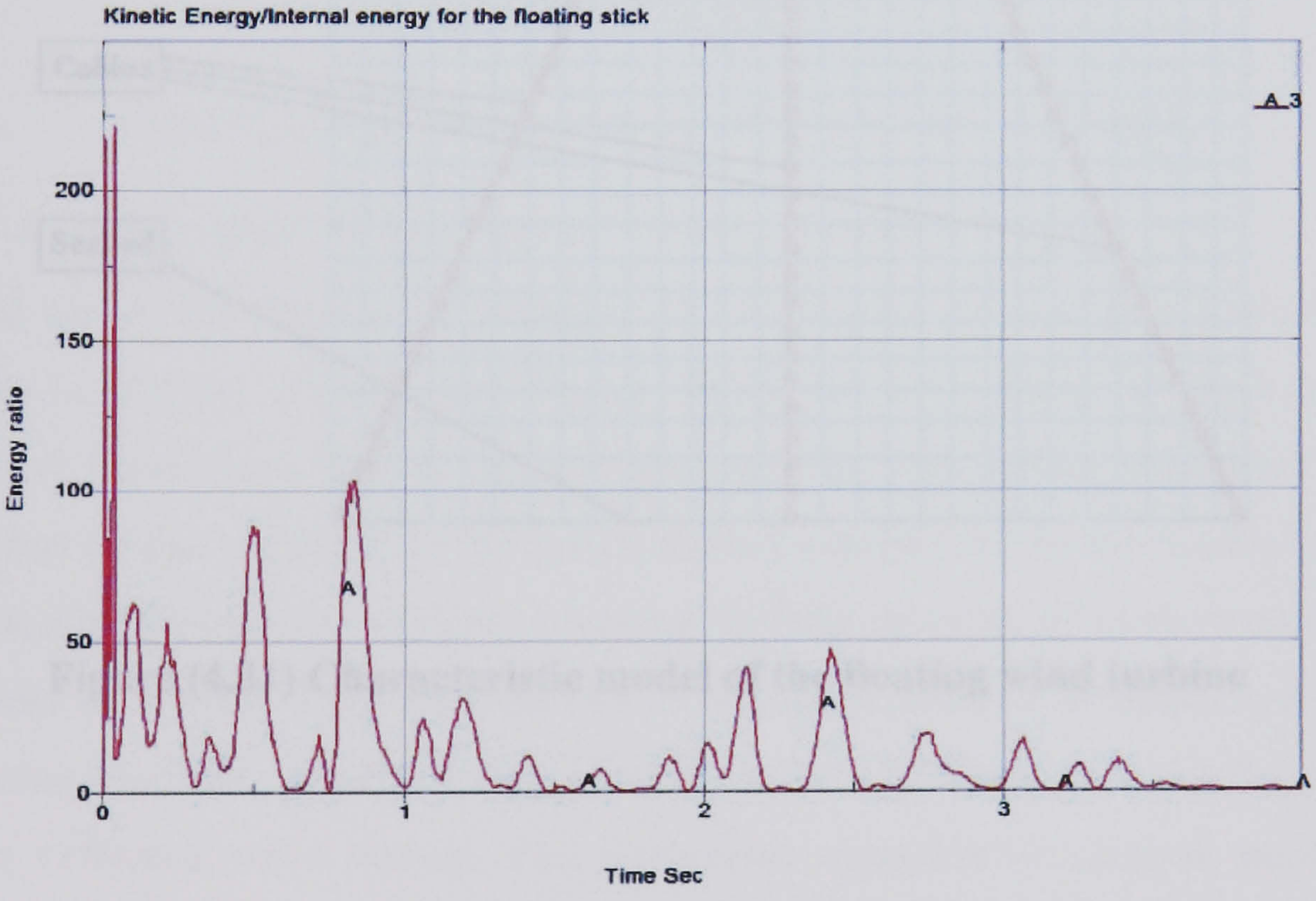

Figure (4.30) Energy ratio for the floating stick model

The system kinetic energy and energy ratio shown in Figure (4.29) and Figure (4.30) is shown to be well within the converged stable system with nearly unity for energy ratio and zero kinetic energy.

4.8.2 Characteristic model:

Building on the previous findings and based on the concept of the floating wind turbine, characteristic model is developed and analysed to further confidence in the above findings. The model Figure (4.31), Figure (4.32) typically consisting of the mean parts forming the structure of the full detailed model. These different parts are summarized below:

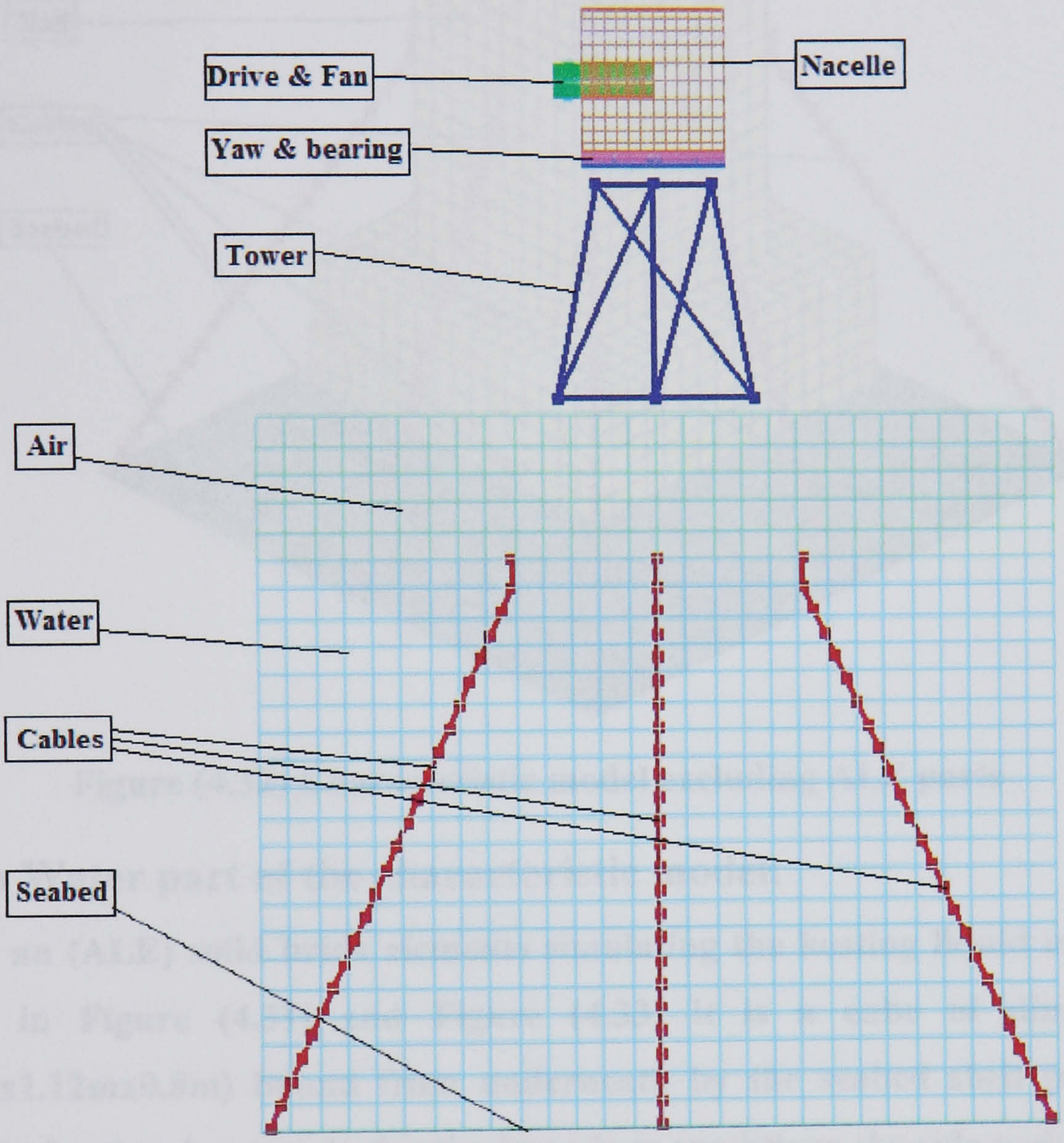

Figure (4.31) Characteristic model of the floating wind turbine

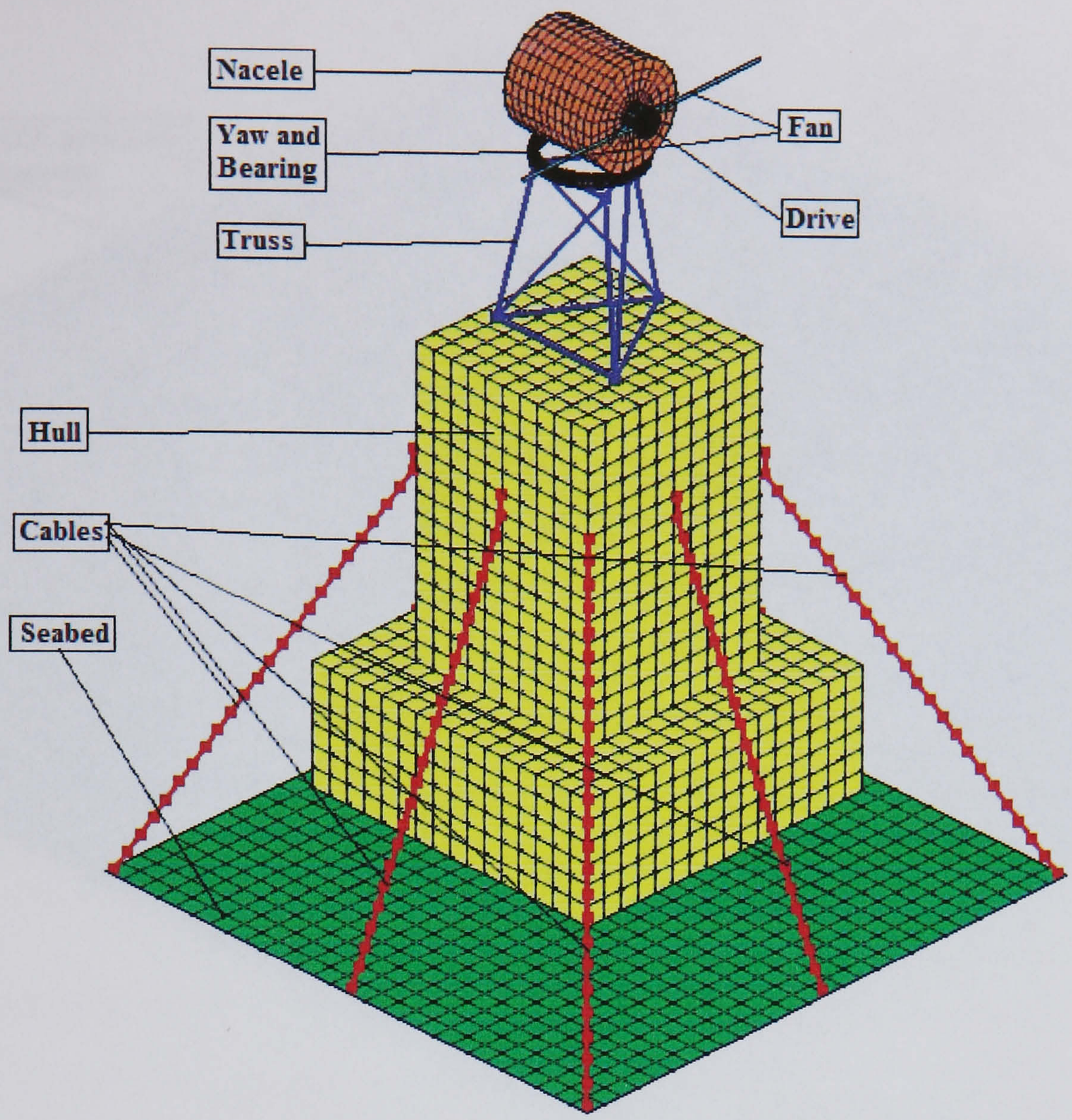

Figure (4.32) Characteristic model excluding ALE parts

4.8.2.a Water part of the characteristic model:

This is an (ALE) solid brick elements simulating the hosting liquid media as shown in Figure (4.31) and Figure (4.33) it is a cube of dimensions (1.12mx1.12mx0.8m) bound from underneath by the seabed shell part and from top by the air part. As for the boundary conditions the side nodes of the ALE mesh is restrained against movement to help building pressure within the elements body while the side segments of the outer elements is defined as non-reflecting boundary surface to simulate the infinite medium through the offset of the reflected wave action. The Grüneisen equation of state is used for pressure generation within this part as detailed earlier in this Chapter and Appendix-A4 of this thesis.

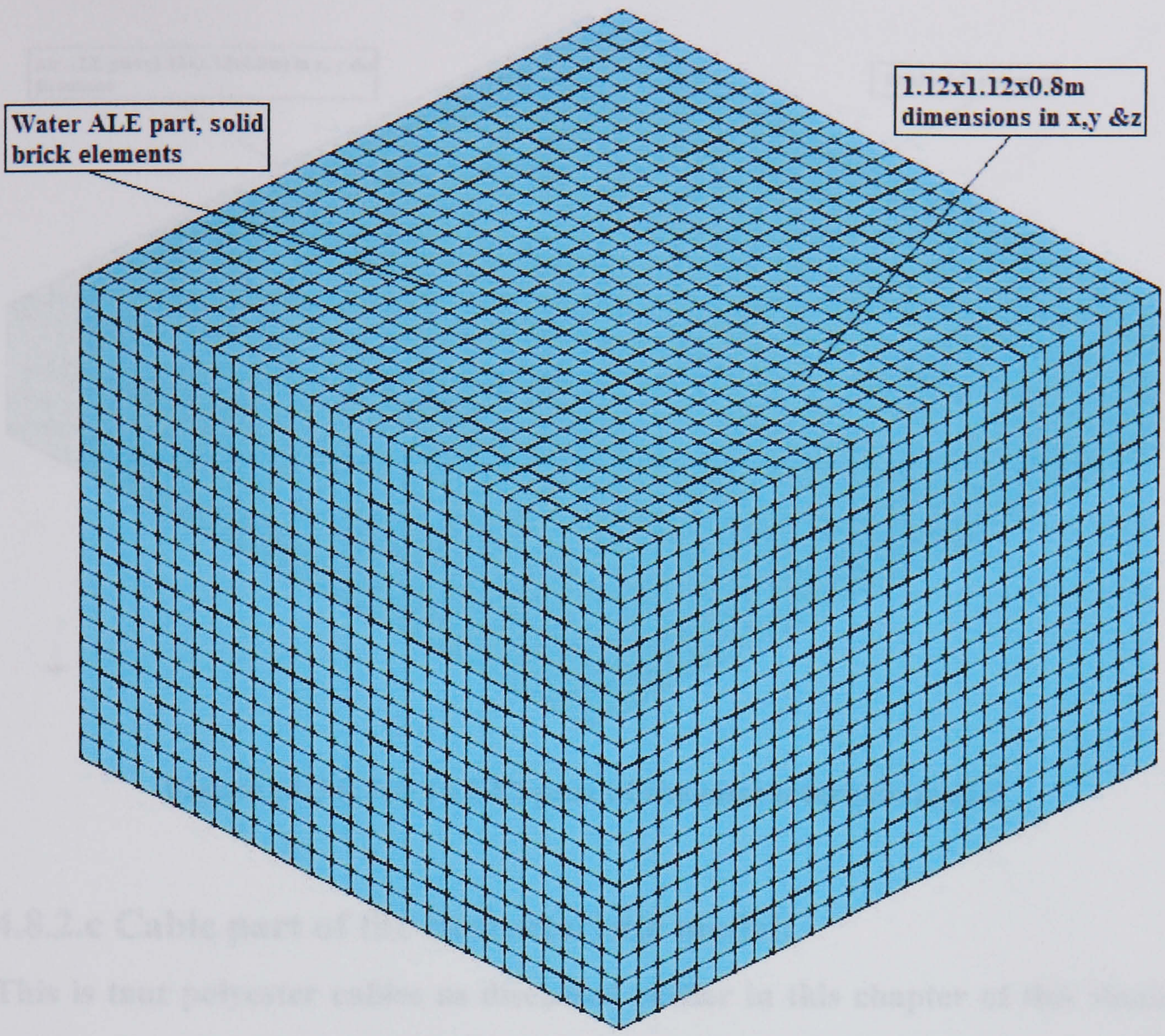

Figure (4.33) Water (ALE) part of the characteristic model

4.8.2.b Air part of the characteristic model:

This is the second ALE part simulating air fluid part atop the water part, shown in Figure (4.31) and Figure (4.34) it is consisting of solid brick elements of dimensions (1.12mx1.12mx0.2m). Pressure within air elements is initiated using polynomial equation of state and coincident nodes between ALE parts are merged simulating proper contact.

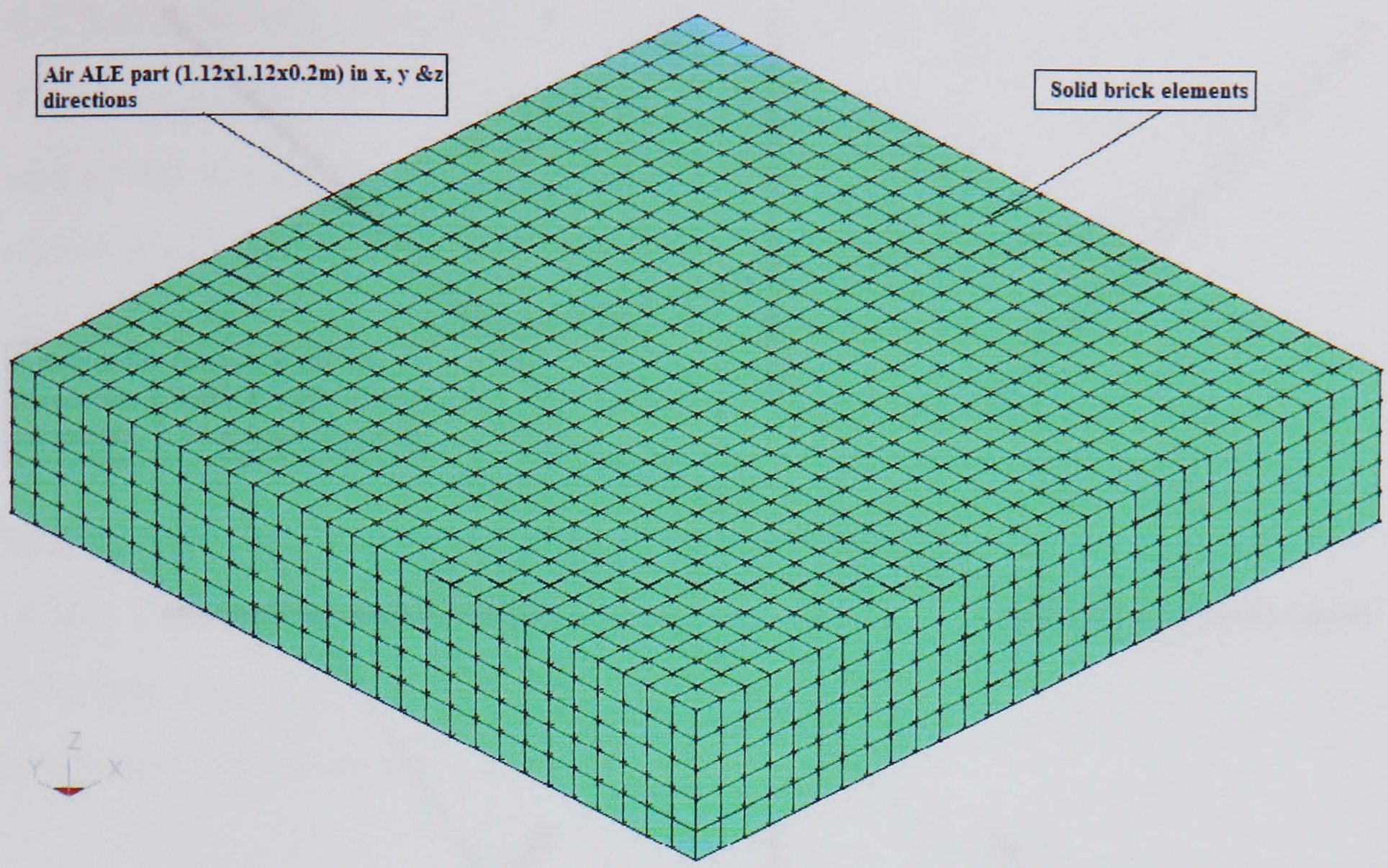

Figure (4.34) Air (ALE) part of the characteristic model

4.8.2.c Cable part of the characteristic model:

This is taut polyester cables as discussed earlier in this chapter of this thesis and as shown in Figure (4.31), Figure (4.32), Figure (4.35 a) and Figure (4.35 b) the 8 cables are of total length 7.24m pined at top ends to the floating support and at the bottom ends to the seabed part. More than one node of the meeting parts are constrained against translation to the cable end nodes, thus avoiding high stress concentration and forcing the failure (if any) to occur in cables. The LS-DYNA3D cable material (type 71) is used to model this part. Cables are coupled to water using constrained Lagrange in solid keyword.

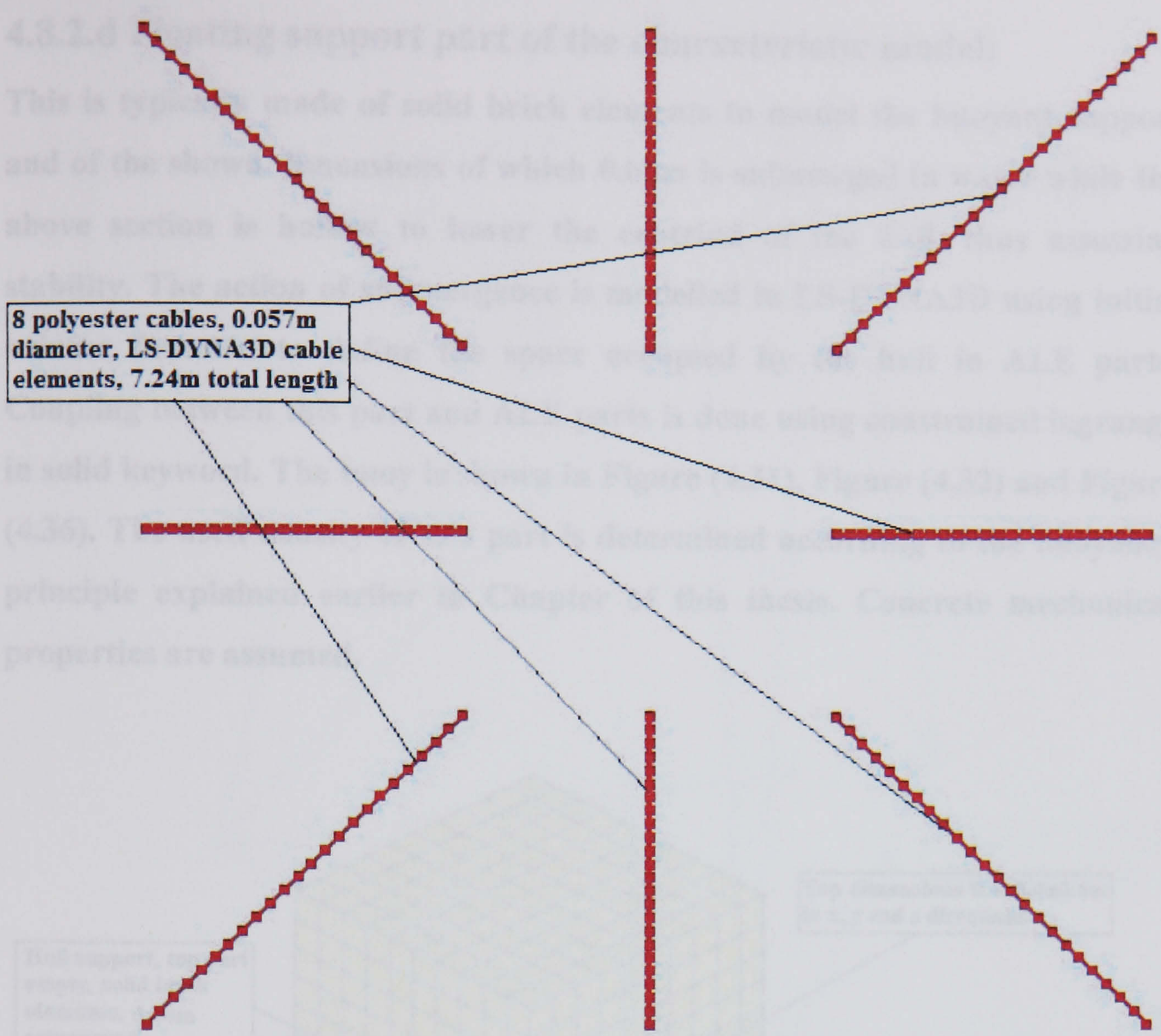

Figure (4.35 a) Cable part of the characteristic model (plan view)

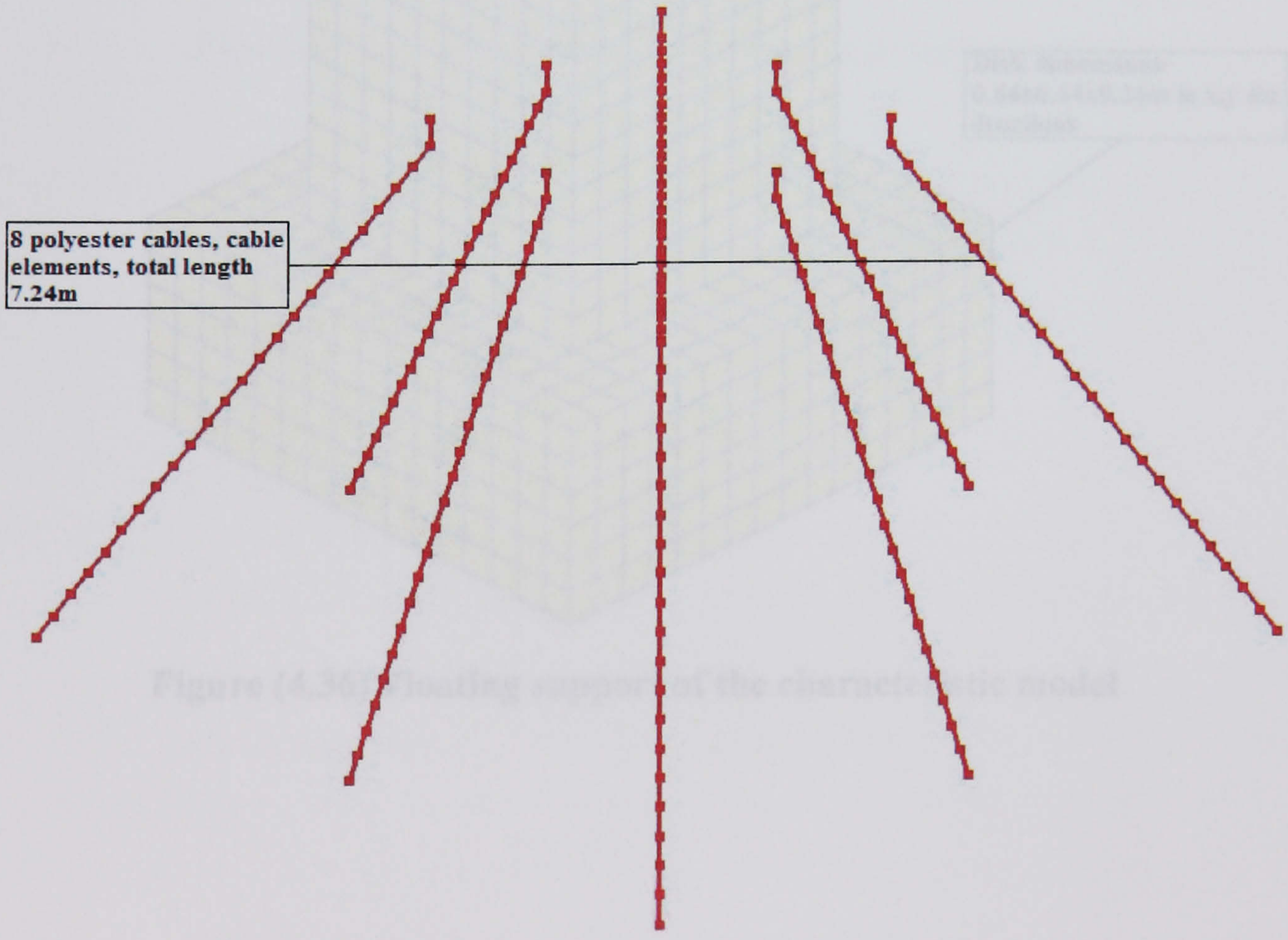

Figure (4.35 b) Cable part of the characteristic model (isometric view)

4.8.2.d Floating support part of the characteristic model:

This is typically made of solid brick elements to model the buoyant support and of the shown dimensions of which 0.60m is submerged in water while the above section is hollow to lower the centriod of the hull, thus assessing stability. The action of submergence is modelled in LS-DYNA3D using initial volume function to define the space occupied by the hull in ALE parts. Coupling between this part and ALE parts is done using constrained lagrange in solid keyword. The buoy is shown in Figure (4.31), Figure (4.32) and Figure (4.36). The used density of this part is determined according to the buoyancy principle explained earlier in Chapter of this thesis. Concrete mechanical properties are assumed.

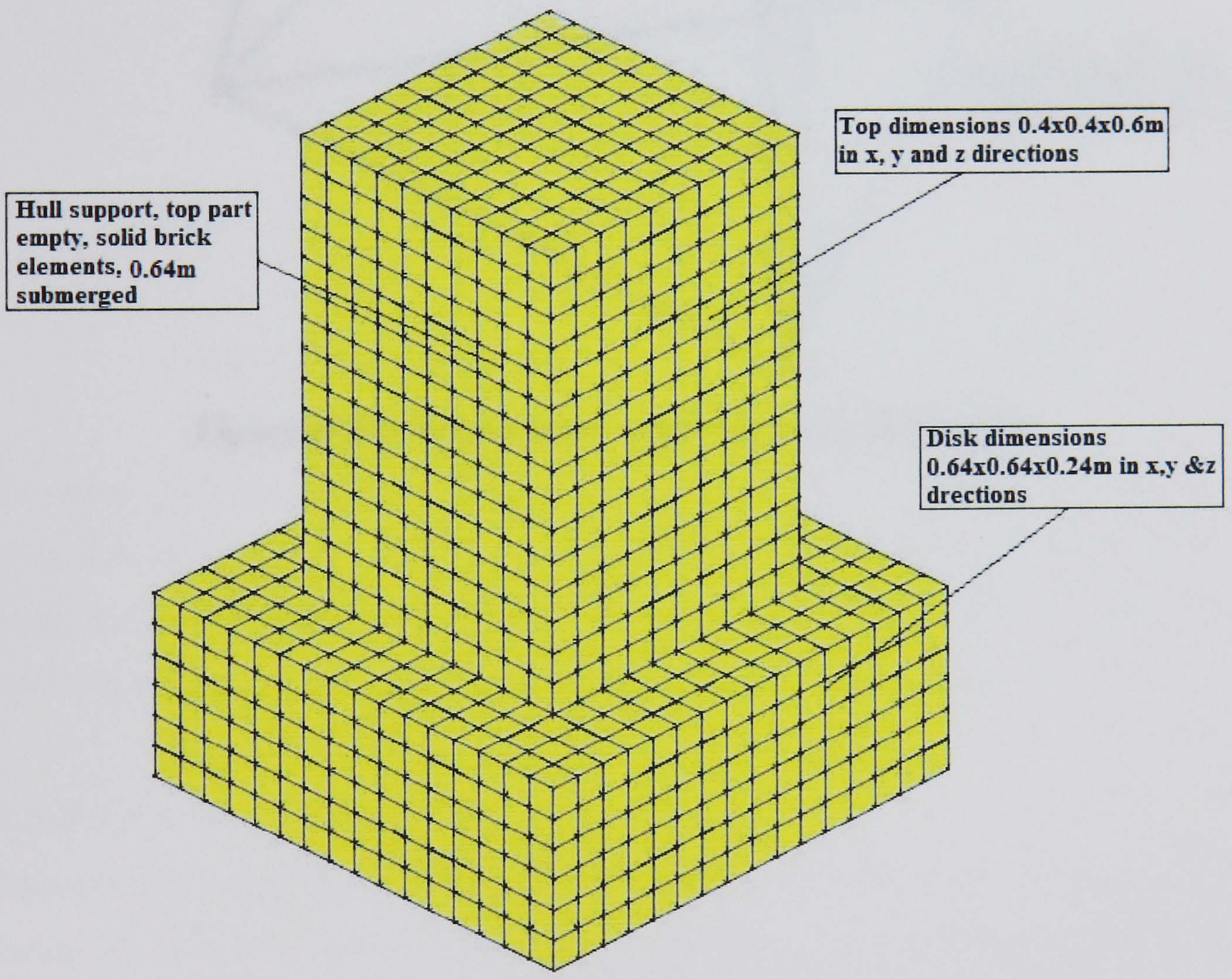

Figure (4.36) Floating support of the characteristic model

4.8.2.e Tripod truss part of the characteristic model:

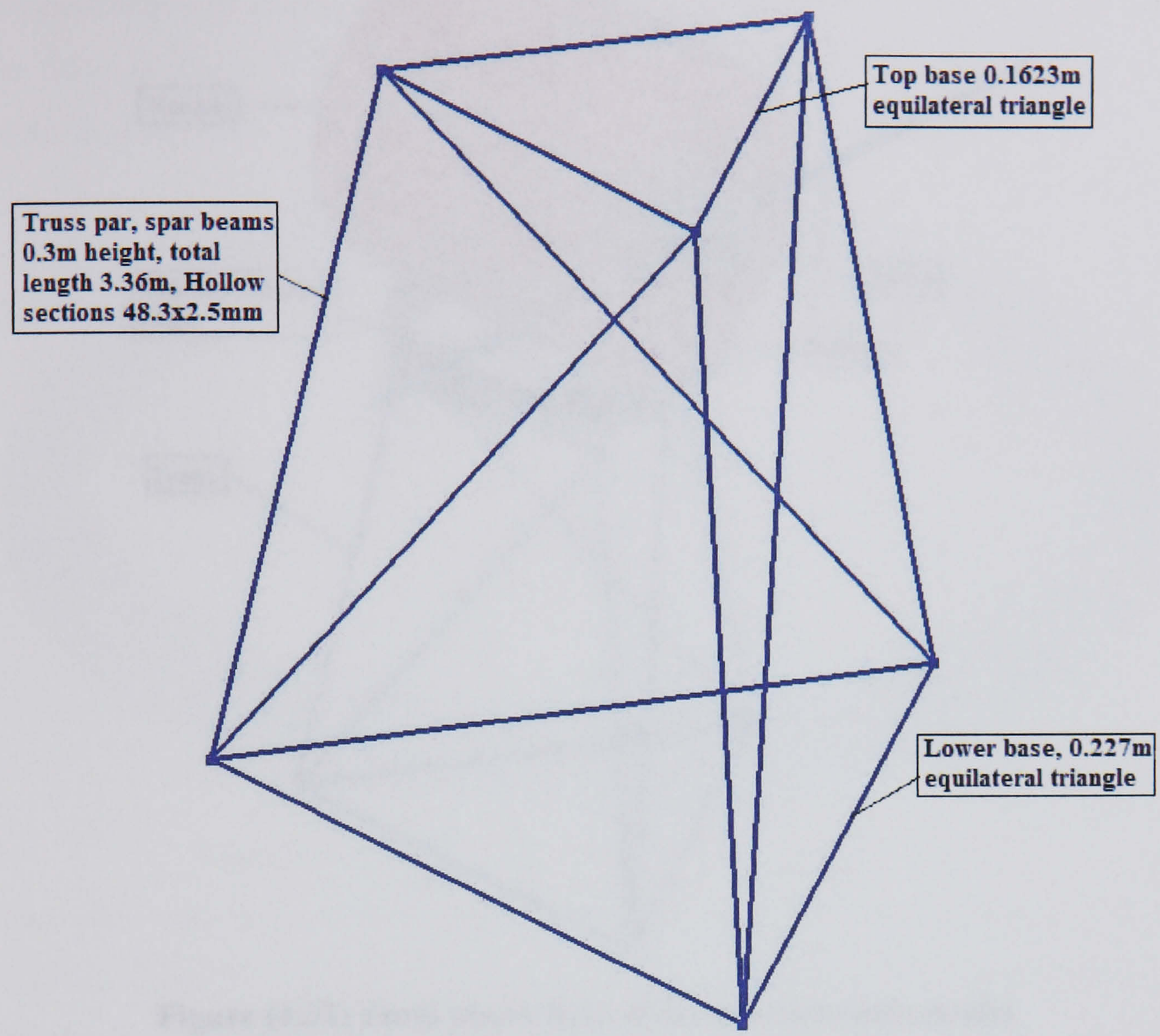

Figure (4.37) Tripod truss of the characteristic model

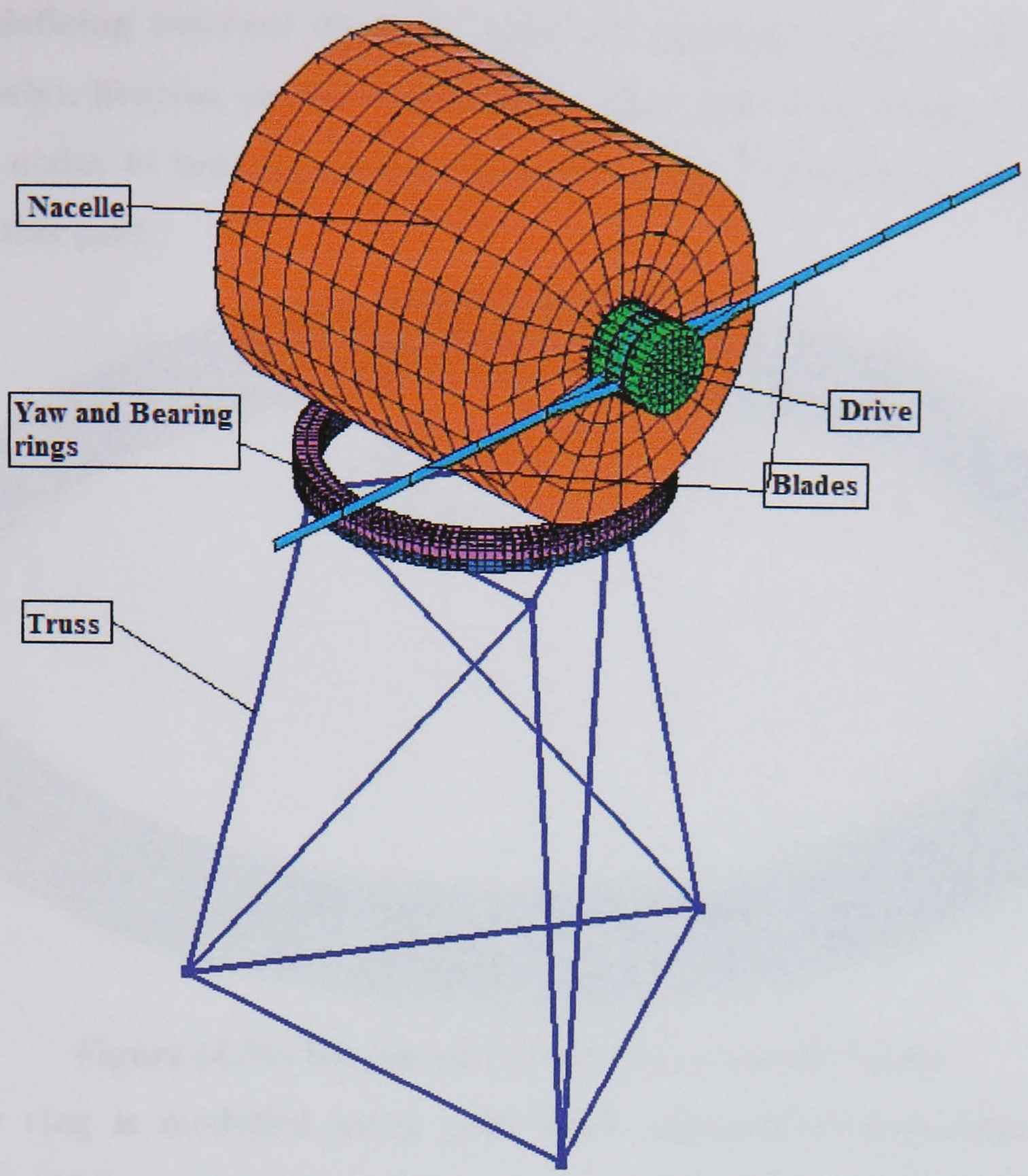

Figure (4.38) Parts above float of the characteristic model

As shown in Figure (4.31), Figure (4.32), Figure (4.37) and Figure (4.38), the tripod truss is made of hollow steel sections (48.3x2.5mm), having a total elements length of 3.9m, the truss is of 0.4m height and modelled using truss beam elements. Its function is to mount other parts to the required level.

4.8.2.f Bearing part of the characteristic model:

The bearing is the part offering the rotational movement of the yaw system firmly fixed to the tower top and fixed to the parts above it through rotational free 'joint revolute' in order to simulate this action the bearing part is split to two parts; namely the bearing part and the yaw part. Both parts are defined as rigid material giving enough confidence in their stiffness and paving the way for the use of the 'revolute joint' restraint as required by the code. Shown in Figure (4.31), Figure (4.32), Figure (4.38) and Figure (4.39) the bearing part is made of solid brick elements and of geometry (0.2m, 0.175m, 0.0125m and

0.006m defining external diameter, internal diameter, height and thickness respectively). Bearing part is connected to truss part by merging truss nodes as extra nodes to bearing part (rigid part). Steel mechanical properties are used for this part.

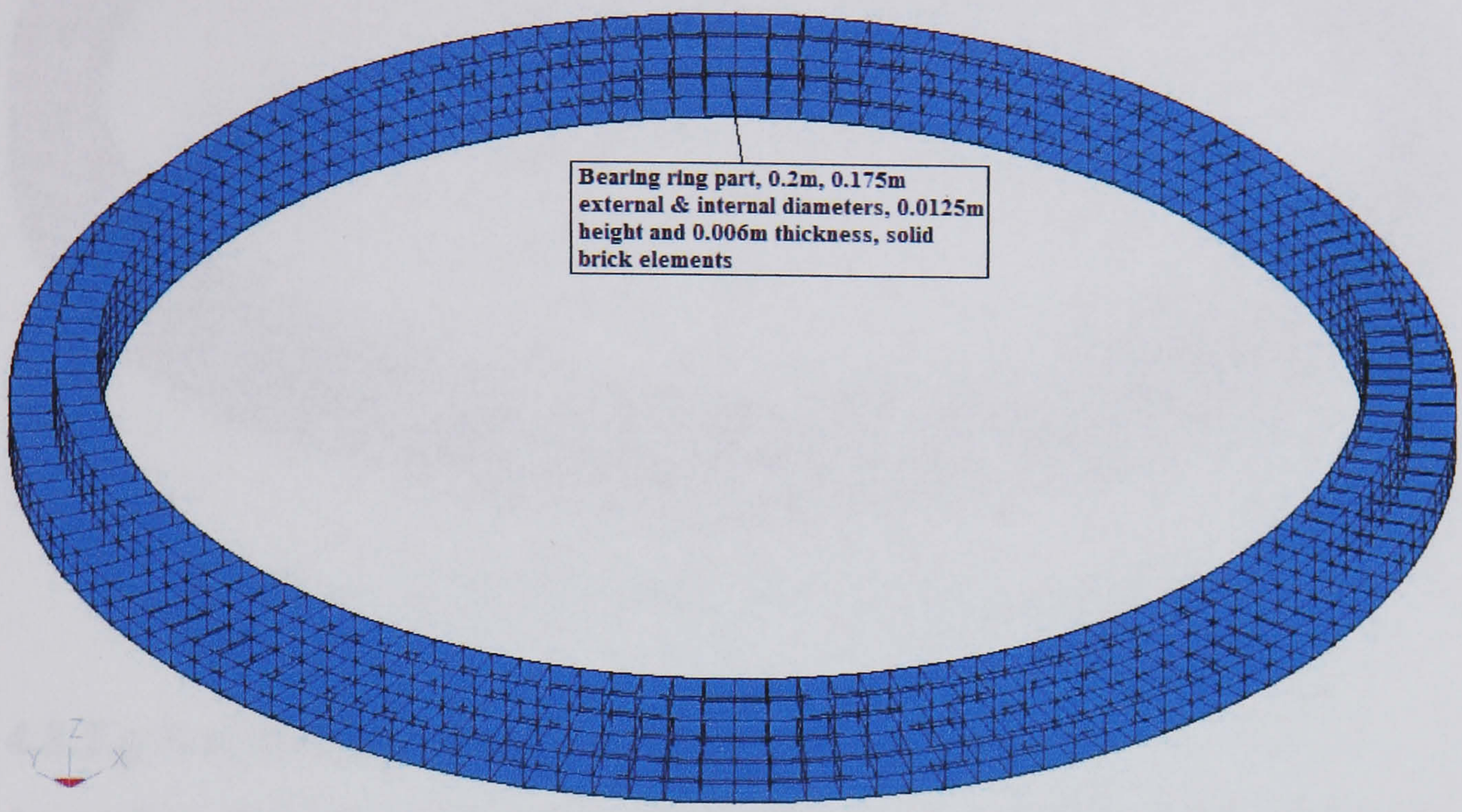

Figure (4.39) Bering part of the characteristic model

The yaw ring is modelled using solid brick elements of dimensions (0.2m, 0.175m, 0.0125m and 0.006m defining external diameter, internal diameter, height and thickness respectively). It is shown in Figure (4.31), Figure (4.32), Figure (4.38) and Figure (4.40). Yaw part is firmly connected to nacelle above it by merging the two rigid parts. Steel mechanical properties are used for this part.

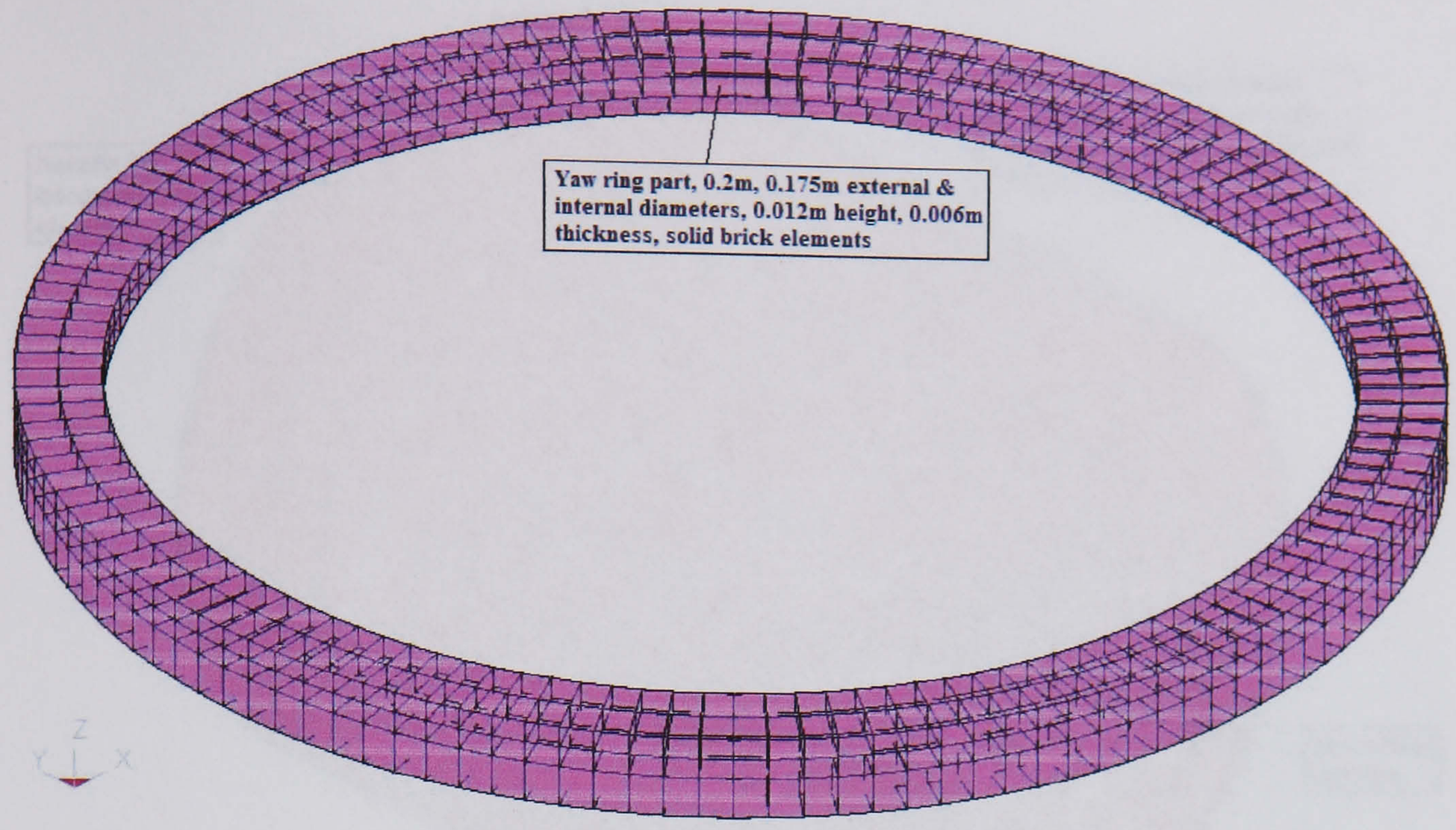

Figure (4.40) Yaw part of the characteristic model

4.8.2.g Nacelle part of the characteristic model:

As explained earlier in this chapter of this thesis, it is the housing space for electricity generation equipment, connected to both the yaw through rigid body merge and to the rotor parts via 'joint revolute' both connections intended to give rotational free but rigid connections thus requiring the nacelle to be defined as rigid material. Fully integrated shell elements (type 16) are used for this part to avoid hourglass energy effects, and structural steel mechanical properties are assumed. The nacelle geometry is 0.2m length and 0.2m diameter for external surface while for the internal cylinder it 0.1m length and 0.05m diameter. Nacelle geometry and arrangement in the assembly is shown in Figure (4.31), Figure (4.32), Figure (4.38) and Figure (4.41).

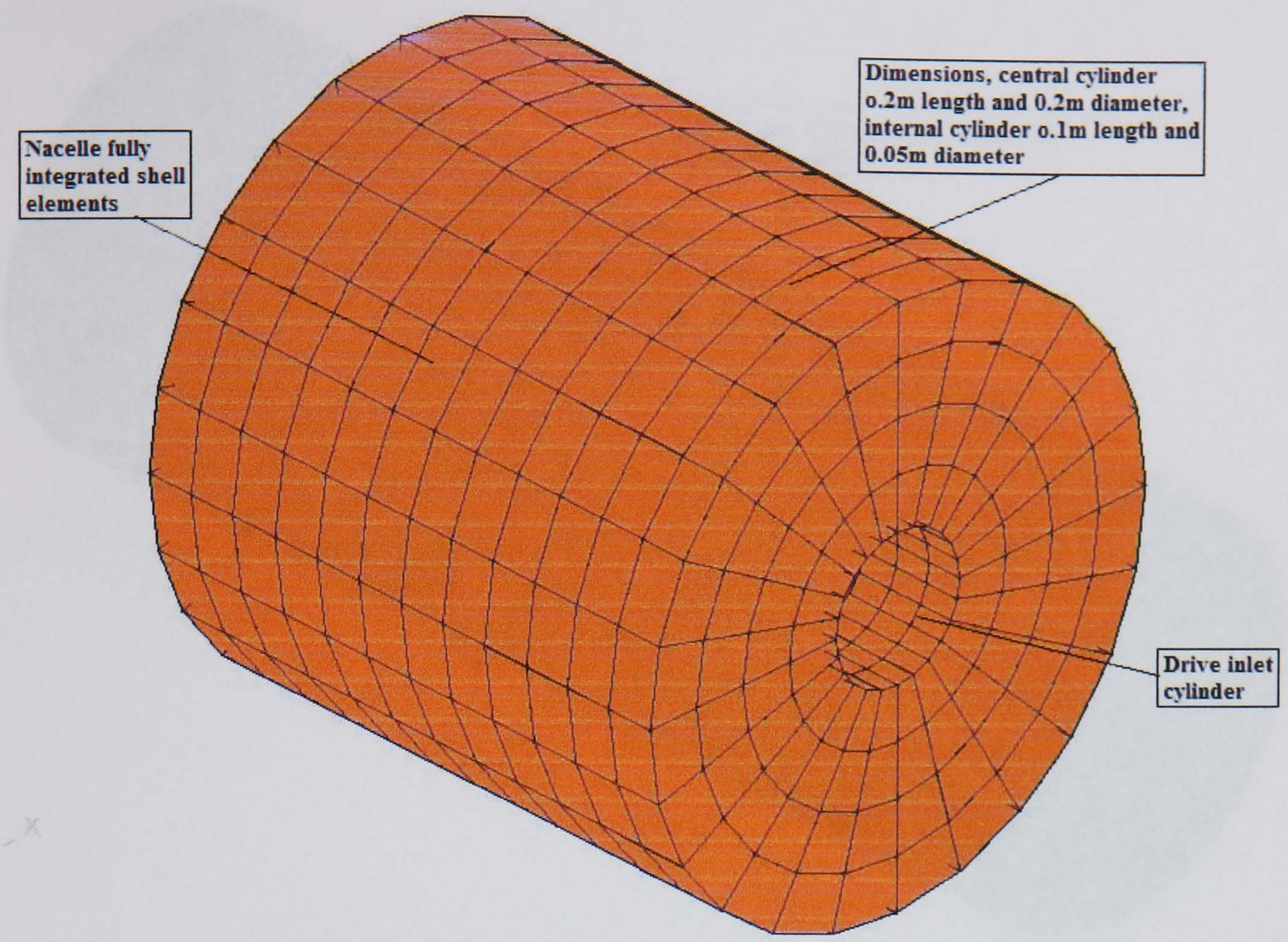

Figure (4.41) Nacelle part of the characteristic model

4.8.2.h Rotor parts of the characteristic model:

This is typically would have consisted of three parts as detailed in Chapter V of this thesis, here two parts only are used for the purpose of this verification. First the drive part: solid shaft of o.14m length and 0.05m diameter modelled with rigid material (joint requirement) and solid brick elements. Second the blades part: this is modelled in 2 blades of 0.6m diameter modelled by fully integrated shells assuming 'GRP' mechanical properties, all nodes of the blades are constrained to drive (rigid part) as extra nodes thus assuring full fixity and integral rotation. The drive part geometry and location in the assembly is shown in Figure (4.31), Figure (4.32), Figure (4.38) and Figure (4.42).While that of the blades part is shown in Figure (4.31), Figure (4.32), Figure (4.38) and Figure (4.43). Steel mechanical properties are defined for this part.

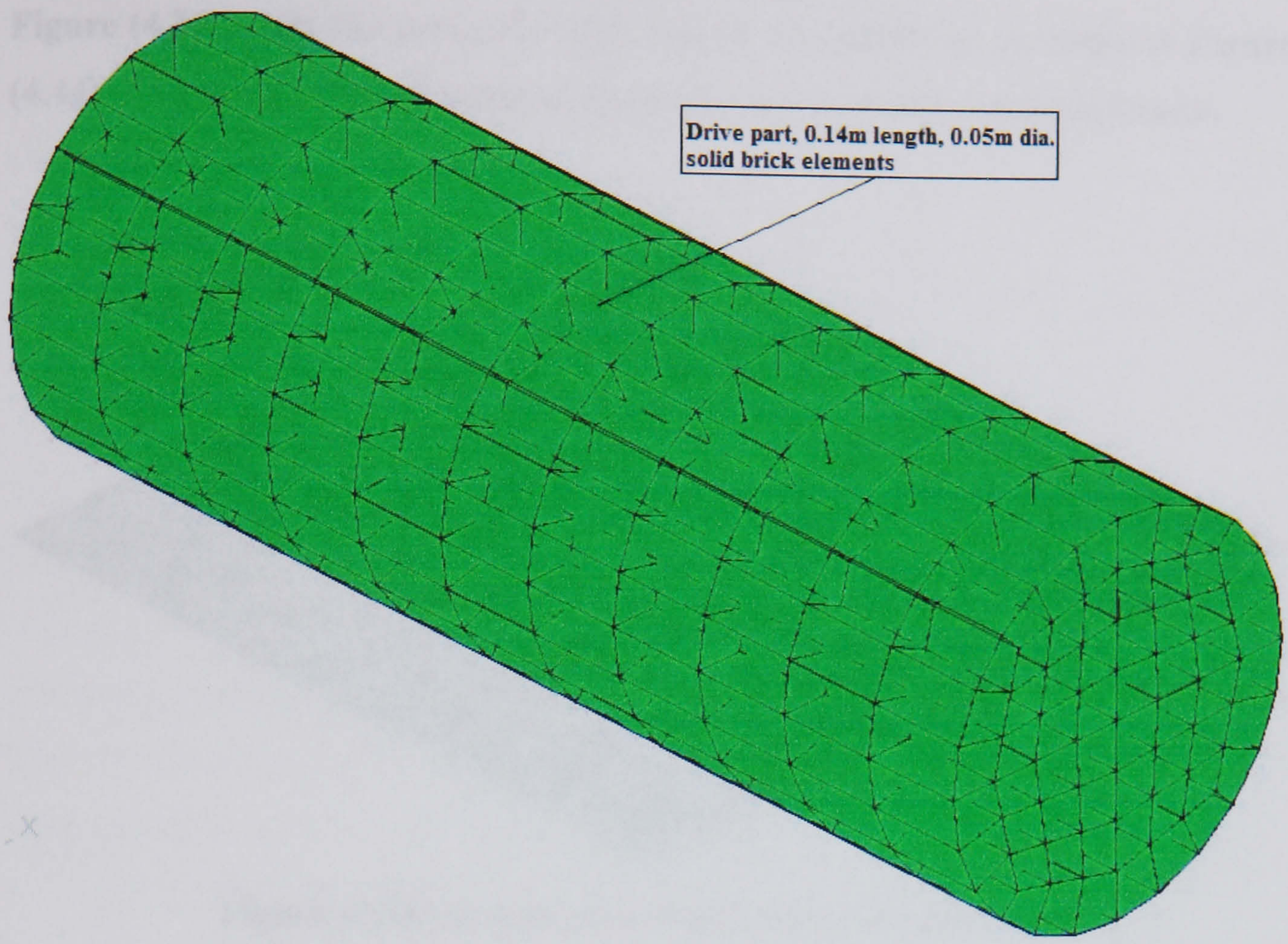

Figure (4.42) Drive part of the characteristic model

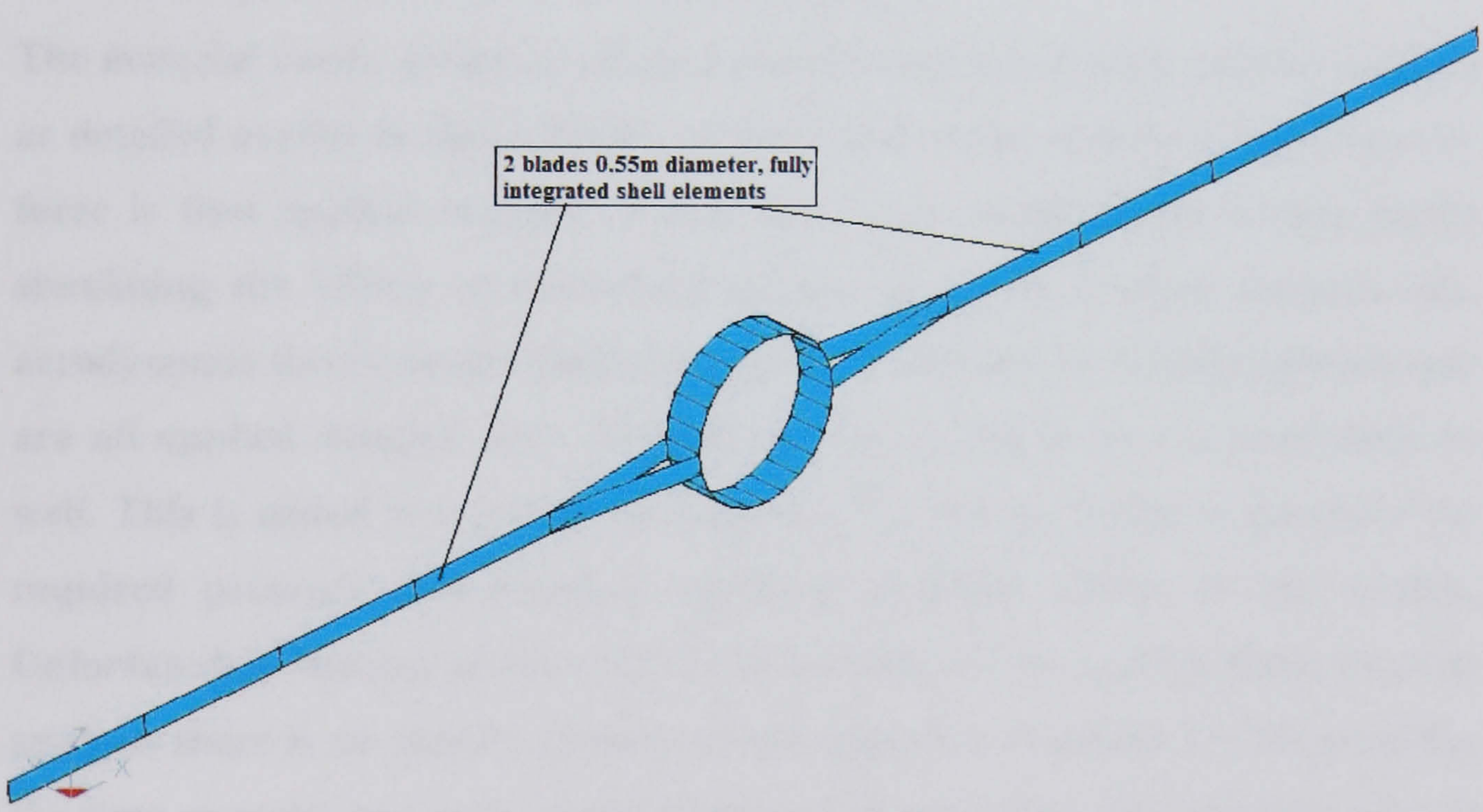

Figure (4.43) Blades part of the characteristic model

4.8.2.n Seabed part of the characteristic model:

Defined to simulate seabed it is modelled with fully integrated shells (type 16) and rigid material as required by the finite rigid wall contact condition is given to this part. The location of this part is shown in Figure (4.31) and

Figure (4.32) while the geometry of (1.12mx1.12mx0.002m) is shown in Figure (4.44). The assumed mechanical properties are those of the soil mechanics.

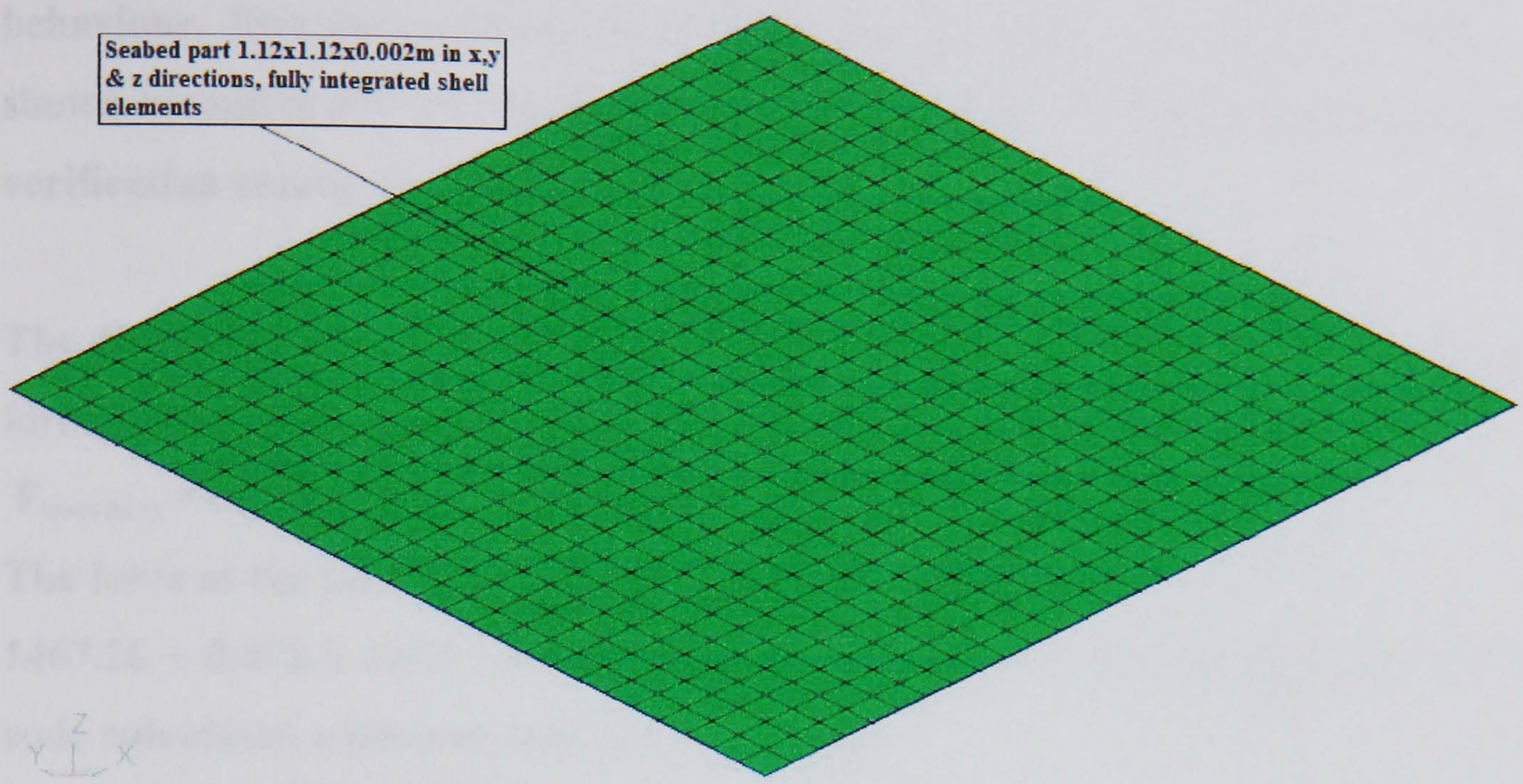

Figure (4.44) Seabed part of the characteristic model

4.8.3 Analysis of the characteristic model:

The material cards, property cards, control cards, constraints and boundaries as detailed earlier in this Chapter of this thesis were employed here. Gravity force is first applied ramped over a short time, while characteristic forces simulating the effects of hydrodynamic forces on the floating support side, aerodynamic forces on the blades and upwind pressure on nacelle upwind face are all applied ramped after full gravity was in action over a short time as well. This is aimed at allowing enough time for gravity forces to generate the required pressure and avoiding spurious dynamic effects in the system. Unfortunately because of the conditional stability of the explicit finite element analysis there is no 'quick' solution to the long time required for the analysis, the time step size has to be smaller than a critical value. This critical value is directly dependent on the largest frequency of the finite element discretization (smallest element). As a consequence, in larger scale problems the time step becomes extremely short (10^{-7} sec) in this case, with all negative effects on the computer run time and possibly memory as well. In order for the buoyancy pressure to build up in the (ALE) water elements longer time is needed for body load application to achieve this. Different parts of this model were

created in consecutive order starting with the rigid wall representing the seabed, the two ALE parts and the floating support. Then the model is run and the next top parts are added one at a time and run to assure the desired behaviour. Due to problems introduced by modelling the cable the results shown hereafter are for the float only with other parts excluded. These model verification results are as follows:

The displaced volume = $(0.4)^3 + (0.64)^2 \times 0.2 = 0.1459\ m^3$ and uplift buoyancy force is:

$F_{buoyancy} = 0.1459 \times 1025 \times 9.81 = 1467.26$ N,

The force at the bottom face of the hull is:

$1467.26 + 0.472 \times 1025 \times 9.81 \times (0.64)^2 = 3411.25$ N, this is conforming to the code calculated z-force shown in Figure (4.45).

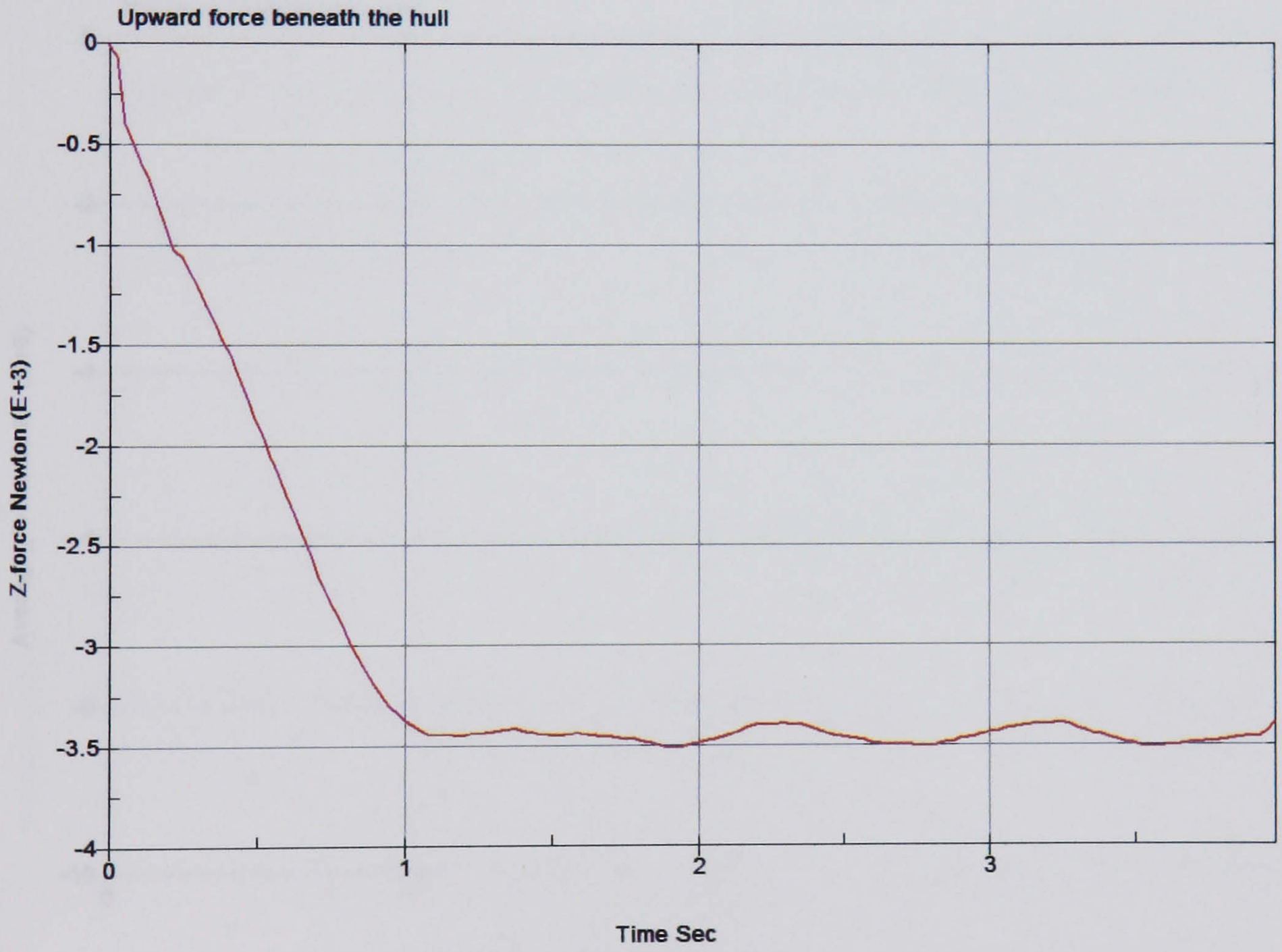

Figure (4.45) Uplift force on the floating support bottom

Meanwhile z-direction stress under the floating support is calculated as follows:

$$\sigma_{zz} = \frac{3411.25}{0.64 \times 0.64} =$$ **8328.25 Pa, this value is close enough to the code calculated value shown in Figure (4.46).**

And for base side element of the floating support, the water pressure due to vertical position of this element centre of 0.60m is:

P_{xx} =0.60 x 1025 x 9.81 = 6033 Pa this in close agreement with the calculated pressure value for the same element shown in Figure (4.47).

In the same sequence picking up an element at the edge of the floating support base, the forces calculated at the two edge nodes of the element is (-5.8 N) while those at the two top edge of the same element is (-6.6 N) as calculated by the LS-DYNA3D code. Therefore this element share of these forces is (-2 x 5.8 /2 + (-6.6) x 2/4) = - 9.1N this is translated to an element stress in x-direction =

$$\frac{9.1}{0.04 \times 0.04}$$ **= - 5688 Pa which is close to the value shown in Figure (4.48).**

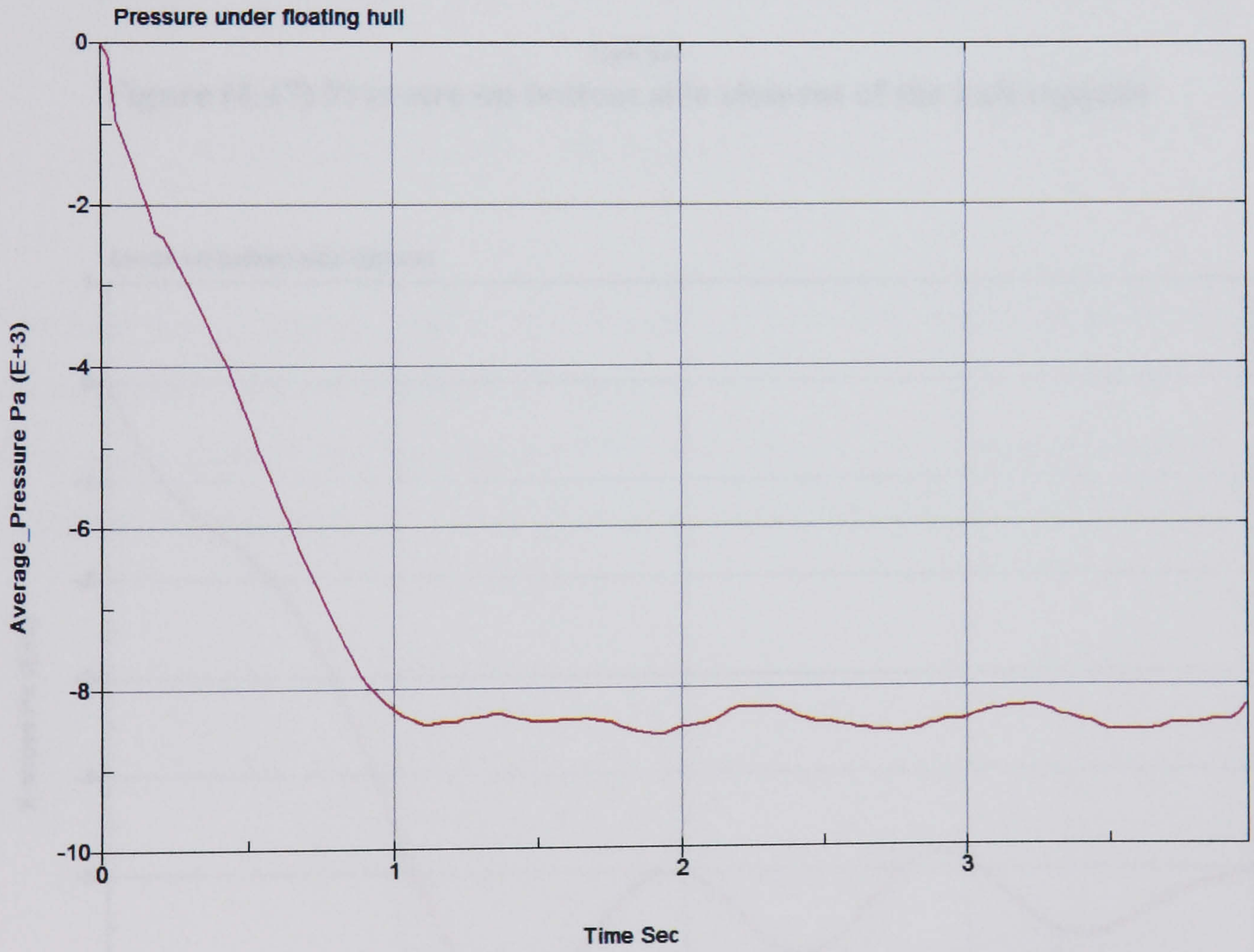

Figure (4.46) Pressure on the bottom face of the hull support

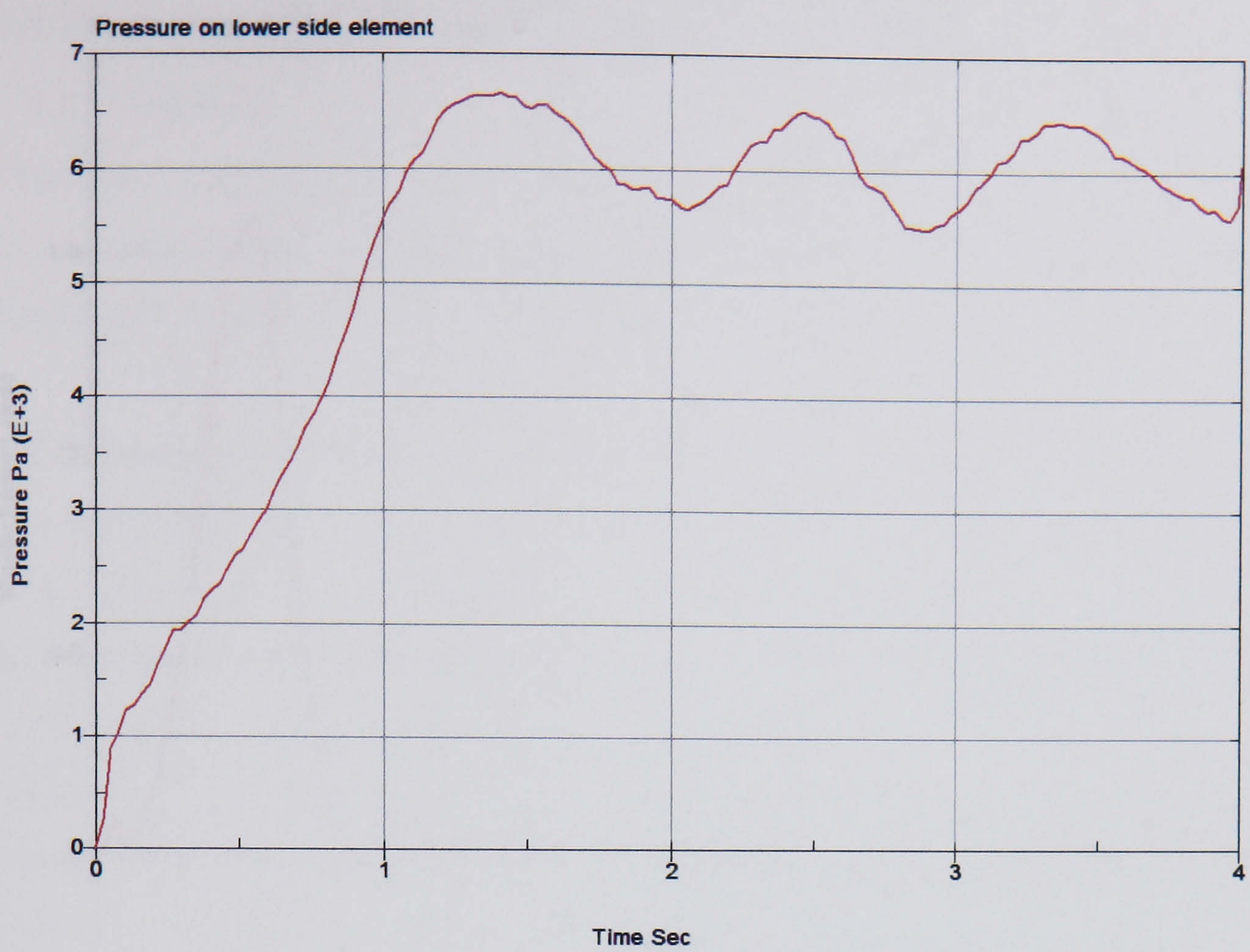

Figure (4.47) Pressure on bottom side element of the hull support

Figure (4.48) Stress on the base side element face of the support hull

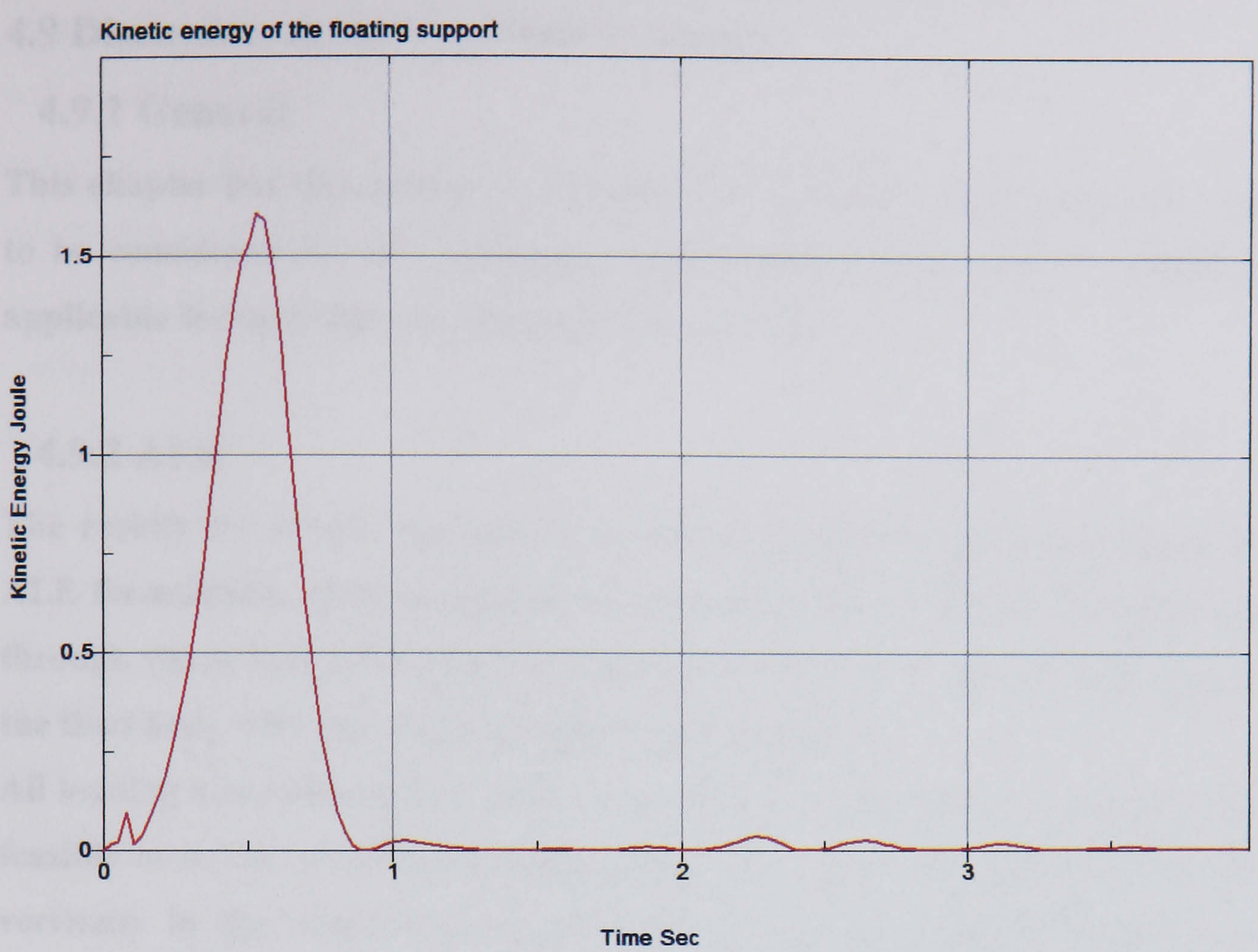

Figure (4.49) Kinetic energy for floating support hull

The hull kinetic energy as shown in Figure (4.49) is well within the converged stable system with dying kinetic energy.

It is worth noting that the smoothness of the above curves is attributed to a higher damping applied for the floating hull run of the characteristic model.

4.9 Discussion of the Verification Models

4.9.1 General

This chapter has demonstrated that there are a number of options and issues to be considered for the validation/verification of finite element techniques applicable for modelling an offshore wind turbine.

4.9.2 ALE

The results for simple two and three dimensional float models utilizing the ALE formulation yield believable results under normal gravity loading, both through visual inspection and comparison of buoyancy states and pressures on the float body with that derived from hand calculation.

All loading was ramped from zero over what was judged to be a suitable (and feasible in terms of analysis runtime) time scale. The float was seen to 'bob' vertically in the water with its amplitude of motion decreasing with time, therefore it was judged that any effects from the short ramping duration of loading to its full value causing a 'pseudo-impact' are negligible if the model is given enough time for the kinetic energy to dissipate. The two dimensional finite element modelling has studied buoyancy effects and it can be concluded that LS-DYNA3D models this correctly. Different states of stability and angles of list are comparable with hand calculation predictions and engineering judgement based on prior knowledge of rigid blocks on very flexible foundations gives confidence in the model behaviour.

The application of transverse loading caused the float to rotate and sink as expected, though no comparisons were made with hand calculations for this load case. Based on these observations it was judged that the ALE formulation would be suitable as modelled and applicable for incorporation in a detailed model.

4.9.3 Turbine model

The tower, turbine rotor blades, nacelle (with associated inside parts) and bearings are all relatively straight forward parts to model in terms of achieving the appropriate coupling and desired behaviour. The rotor blades are seen to turn and the nacelle rotates in plan under appropriate load

regimes, and there is therefore a high degree of confidence that these parts will perform as expected. Further details of the boundary conditions and coupling applied at the top and submersed sections of the structure are presented in Chapter V of this thesis.

4.9.4 Mooring cables

In reality the polyester cables are anchored to the seabed and pass through a slip-ring mounted on the side of the concrete hull and the cable is ultimately fixed near the top of the hull. Hence the cable can effectively slide through the slip-ring. As a simplified logical representation, ordinary beam elements with tension only formulation were employed. Again, logically these beam elements were coupled to the body of the water so that they could interact with the water as they would do in reality.

Many problems were faced in modelling the cables due to contact and coupling problems with the ALE. Different approaches were adopted such as replacing the tension only 'cable' elements with 'seatbelt' representations, and applying pre-tension to the cables. However the results all showed problems of sinking or breakdown of the cable representation at the air/water interface. Some of the problems faced have since been alleviated, but the solution run times involved have meant that there are no meaningful results currently available in terms of cable anchorage forces.

There are a number of issues surrounding the modelling of cable and membrane structures which theoretically carry only tensile forces. Cook et al [79] highlights some of these issues which relate to the absence of flexural stiffness and subsequent large deflections. In some instances these problems may lead to convergence difficulties which may be overcome by adding some small flexural stiffness, i.e. produce along very flexible beam element.

4.9.5 Boundary conditions

Aside from the coupling and constraints for the nacelle, bearing, and rotor blades, the other important boundary is that which surrounds the water. A

suitable size for the body of the water was selected appropriately to model the semi-infinite space. Guidelines exist on modelling 'half-spaces' in finite element models when dealing with soil in soil-structure interaction problems, but for now the size of the water was modelled as a conservatively large enough body to capture interaction effects. To dissipate the energy of the wave and water motion from the model, energy-absorbing (non-reflecting) boundaries were employed.

Some of the time-history stress plots initially showed some 'noise' before filtering was applied. Analysis using the fast fourier transform approach was inconclusive, though two areas of which may be sourcing the noise were identified. Internal reflection from boundaries cannot be ruled out, and the more likely cause is that of chattering of the fluid-structure coupling. In either case, filtering appears to remove the noise and the results appear to be as expected when compared with hand calculated values, therefore it can be concluded that the noise has little effect on the action of the model.

4.9.6 Overall

As a general conclusion, there is a high degree of confidence that the majority of the modelling techniques investigated in this validation and verification section can be employed in a detailed structure. The main area for concern is that for the cables as these provide the all important anchoring forces which will affect the forces generated in the float structure.

CHAPTER V

The Detailed Finite Element Model

At the outset, the final aim of the study was to produce a detailed finite element model of a floating offshore wind turbine. Version 970 of the LS-DYNA3D explicit dynamic finite element analysis code is used to develop and verify the model. Detailed listing of the model creation is presented herein. The pre-processor FEMB 28 (attached to LS-DYNA3D package) was used for the geometry creation as well as preparation of the input file readily exported to the LS-DYNA3D solver.

5.1 Float Model Developed in This Study

The produced wind turbine is based upon the float model principle explained in Chapter II and typical sizing is from Tong [10], Sore [58], Rehfeldt [59], Hogler [121]. The turbine comprises a 3-bladed 60m rotor diameter rated at 1.4MW power, as shown in Figure (5.1) and Figure (5.2).

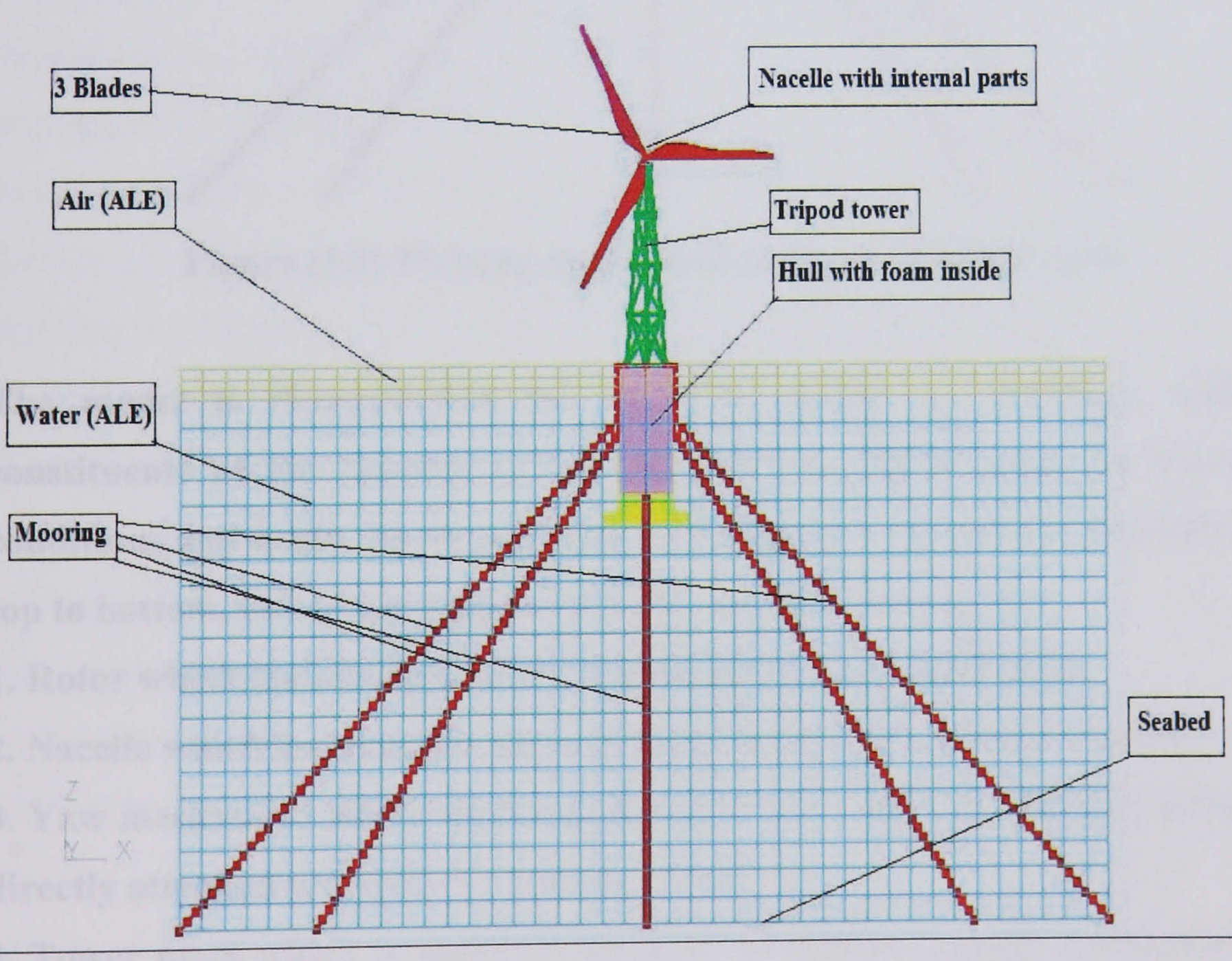

Figure (5.1) Developed floating turbine model all parts

The rotor and nacelle are mounted on a tripod lattice steel tower, at 45.6m above sea water level. This design represents a compromise between conflicting requirements: minimizing size (cost), maximizing stability, and minimizing dynamic motion response. Stability is the main driver of the design parameters; therefore the weight of the top part of the structure is kept to a minimum possible value. This will result in driving the centre of gravity down as discussed in Chapter IV of this thesis, which will reduce the size of the concrete buoy, hence improves economy.

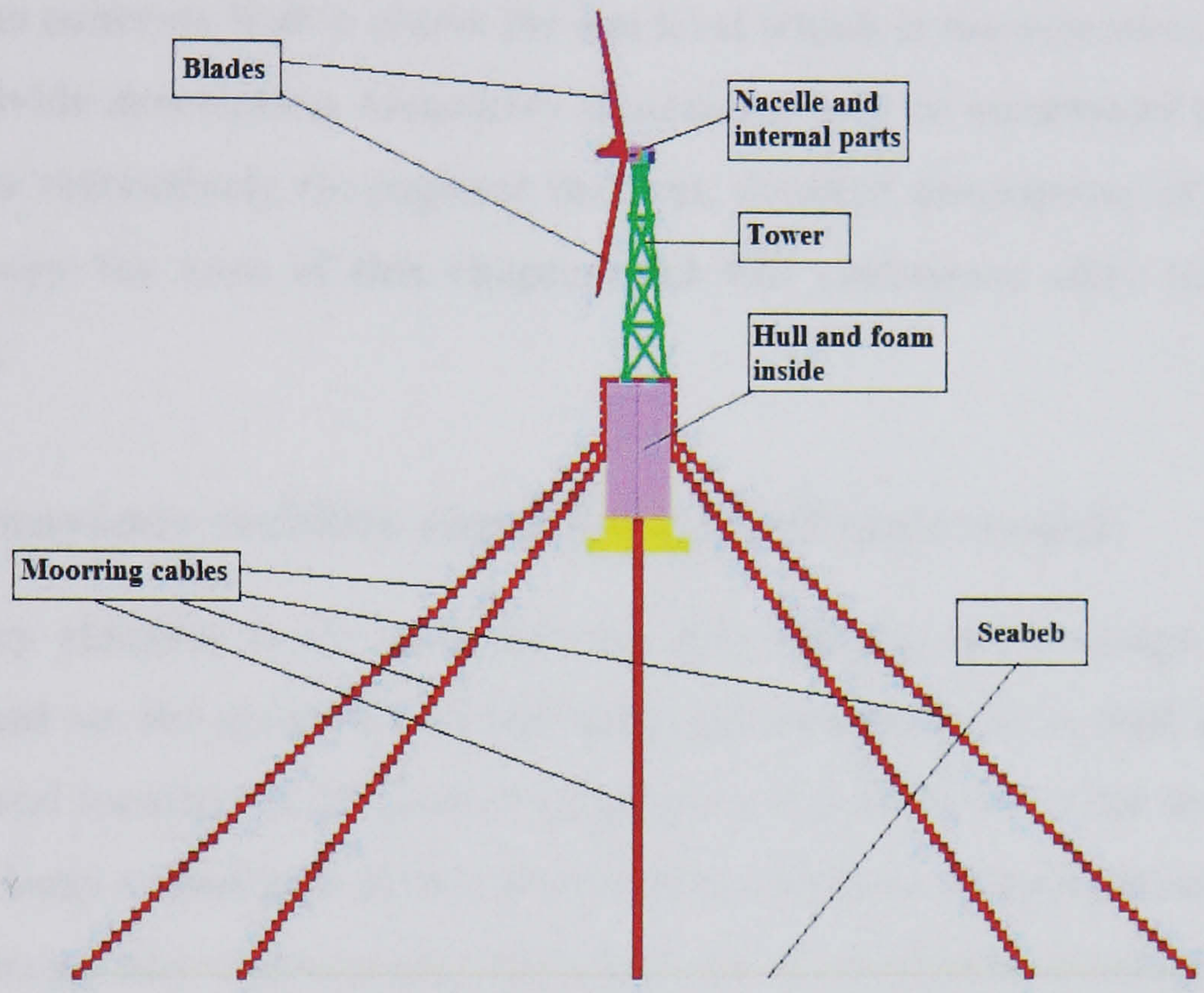

Figure (5.2) Floating model excluding ALE (fluid) parts

The model is characterised by 16 parts, chosen to represent different constituents of the floating turbine, as well as ease of applying boundary conditions and loads. These parts are arbitrary mentioned here in order from top to bottom, and are grouped according to their function as:

1. Rotor which includes the parts (blades, hub and transmission).

2. Nacelle which includes the parts (nacelle, gear, drive, and generator).

3. Yaw mechanism which includes the parts (yaw ring and bearing) these are directly attached to nacelle bottom and tower top.

4. Tower upon which is mounted the yaw mechanism, nacelle and rotor part up to the desired level.

5. Concrete hull where tower and all above parts are firmly resting upon it.

6. Mooring cables are 8 polyester taut ropes firmly attached to the floating hull outside the top circular circumference passing through fairleaders 10m below the attachment points and the ropes are terminated at seabed anchors.

7. Seabed surface which is modelled by rigid wall fully integrated shell elements.

8. Fluid parts are water and air, the water part divide the whole structure into two main groups, submerged parts and floating parts. Fluid parts are modelled by ALE (Arbitrary Lagrangian Eulerian) solid brick elements with 6m of the concrete hull is above the sea level which is the reference level in the above divide description. Geometry dimensions will be mentioned in x, y and z direction respectively throughout the text, detailed description of these parts will occupy the core of this chapter and will commence after the following heading.

5.1.1 Buoyancy stability check for the full scale model:

Buoyancy stability is the base line for any floating body design it is much dependant on the geometry of the deck plan dimensions as well as the body weight and location of the centre of gravity. It is therefore vital to design any floating body to conform to this criterion and to have enough righting moment to counteract any overturning effect with sufficient factor of safety during the service life of the body. Following the discussion presented in Chapter IV of this thesis and referring to Figure (5.3) the buoyancy stability of the full scale model is checked as follows:

With the aid of the pre-processor (FEMB 28) attached to the LS-DYNA3D code, the centre of gravity 'G' is located, while point 'B' is the centre of gravity of the displaced water. Using point 'O' as a reference point, the metacentric height 'GM' is calculated herein:

$$\mathbf{GB = GO - BO = 8.68 - 11.94 = -\ 3.26m}$$

$$\mathbf{MB} = I/V_{displaced} = \frac{\pi 12.5^4/64}{3470} = \mathbf{0.345m,\ where}$$

I = moment of inertia of the hull deck about its diameter axis and

$V_{displaced}$ = the volume of the displaced water

GM = MB – GB = 0.345 – (-3.26) = 3.6m 〉 (greater than) zero, hence it is stable, to further enhance this stability the point 'G' ought to be pushed further down by reducing the upper loads or placing ballast loads furthest down as discussed in Chapter IV of this thesis, otherwise geometry changes are required.

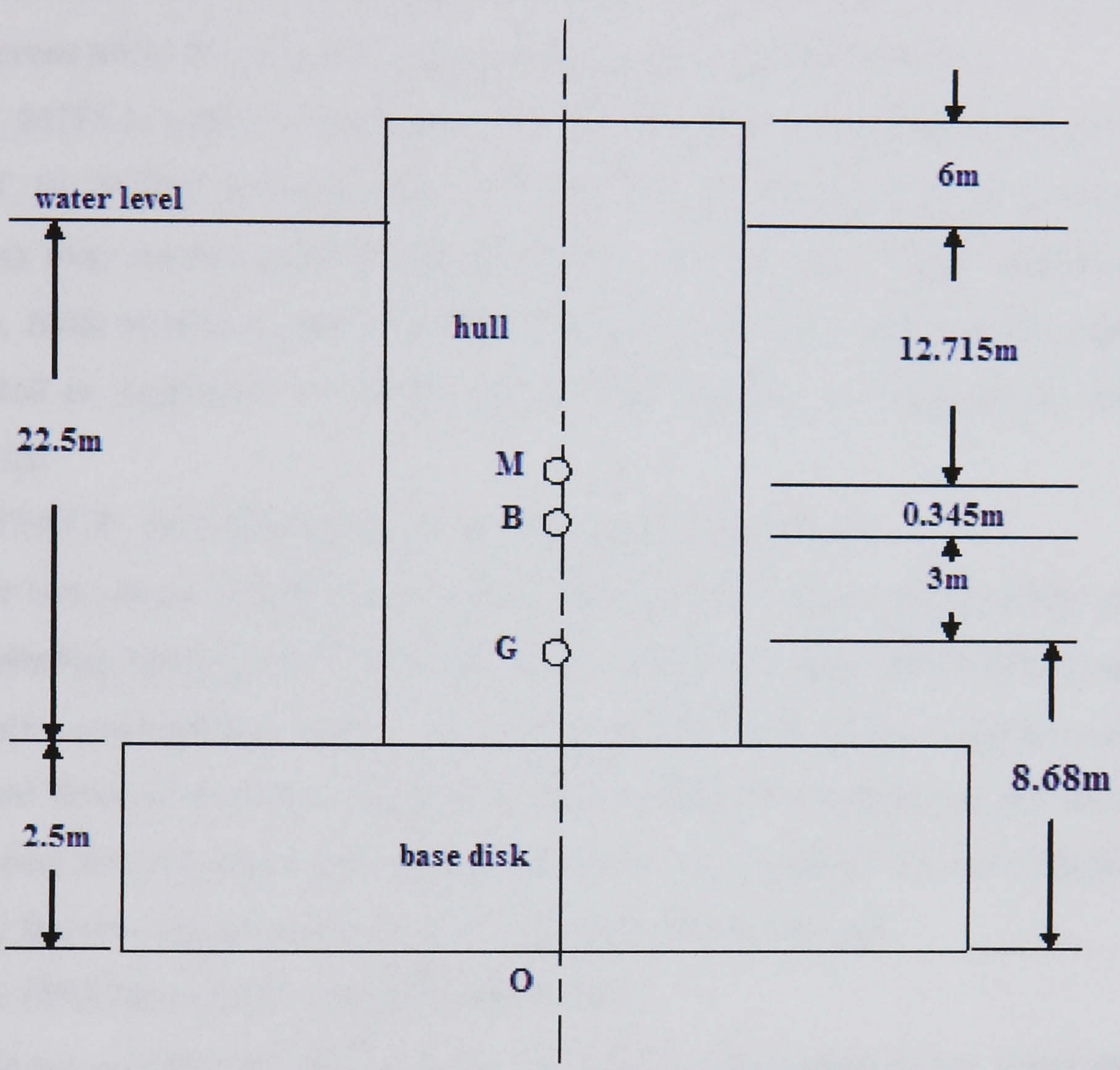

Figure (5.3) Buoyancy stability check of the full scale model

As it will be presented later in Section 5.2 of this Chapter the total weight of the floating loads W = 3,556,750.00 kg, assuming that the maximum angle of list is limited to a typical 'small value' of maximum 20 degrees, the resisting (righting) moment available by the buoyancy action that helps in restoring the floating wind turbine to the floating upright position is calculated herein:

The maximum restoring moment = (3,556,750.0) (9.81) (10^{-3}) (3.6) (20)

= 2,512,204.00 KN. M

5.1.2 Rotor:

5.1.2. a Blades part:

The blades are an integral part of the rotor and it is the means by which moving air kinetic energy is captured and transformed to mechanical energy. Shown in Figure (5.4) and Figure (5.5) the 3 blades are made of glass reinforced plastic epoxy (GRP). Blades are rotating to spin a swept area of 60m diameter and are as pointed before in downwind side of the tower coned 10 degrees away from tower. Element property keyword card of:

***SEC_SHELL which is shell type 16, while material 'type 3' keyword card**

***MAT_PLASTIC_KINEMATIC is used to model blades (in the event that the stresses may exceed yield at the interface with the hub under extreme load cases). Both material and element property keyword cards for this part are reported in Appendix-A2 of this thesis. The blades are contacted to the hub part via:**

***CONTACT_AUTOMATIC_SURFACE_TO_SURFACE**

Where two segment set(s) are used to define this contact keyword the master representing blades roots while the slave represents hub inside tubes, special geometry precautions where taken to properly define this contact such as segment normal direction as well as the number of segments at the interface point and leaving the proper gap in between the surfaces. In turn blades are rigidly fixed to the transmission part through the keyword:

***BC_CONSTRAINED_EXTRA_NODESET.**

A node set comprising the '3 blades' nodes is constrained to the transmission part (rigid body) in this keyword.

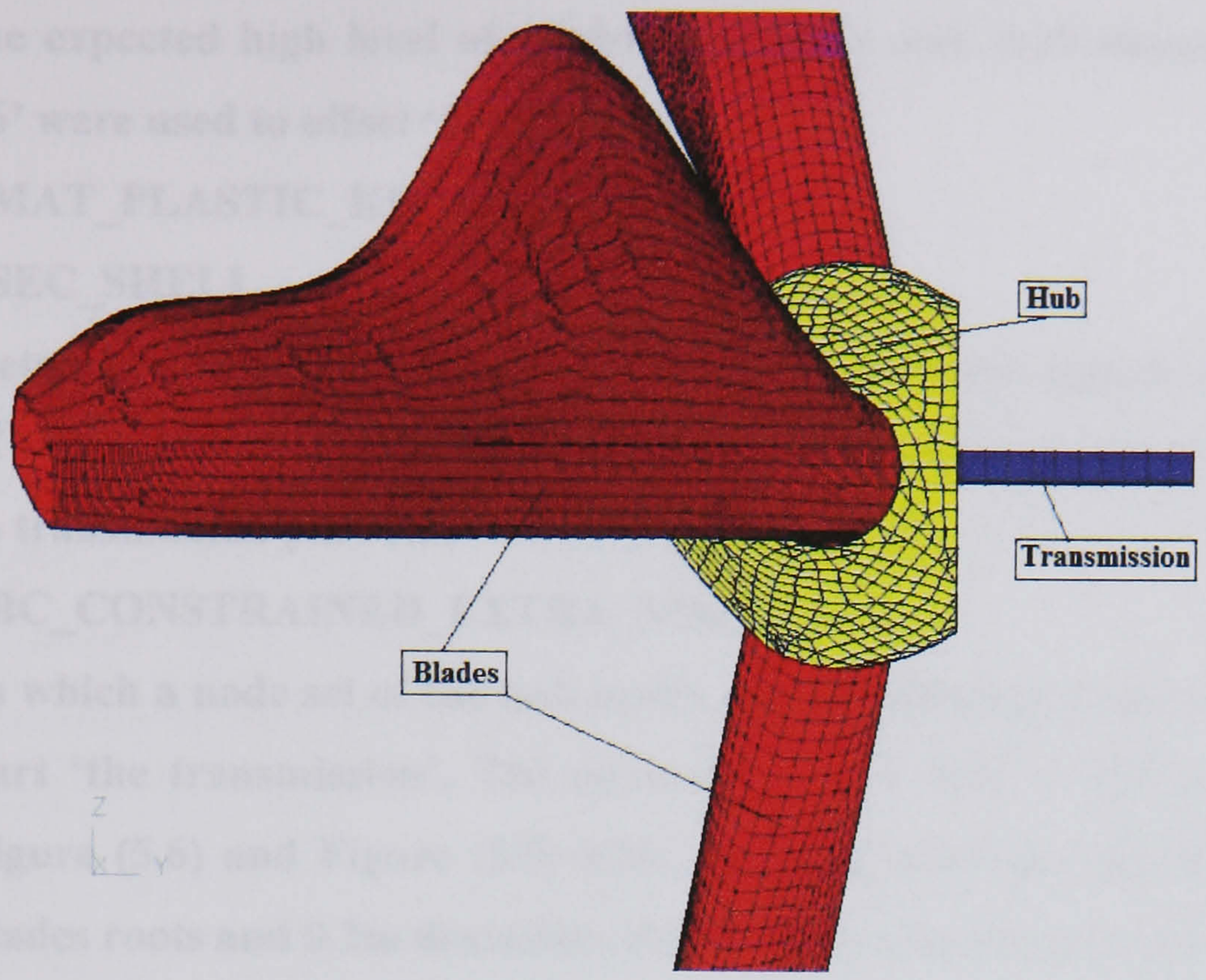

Figure (5.4) Rotor parts

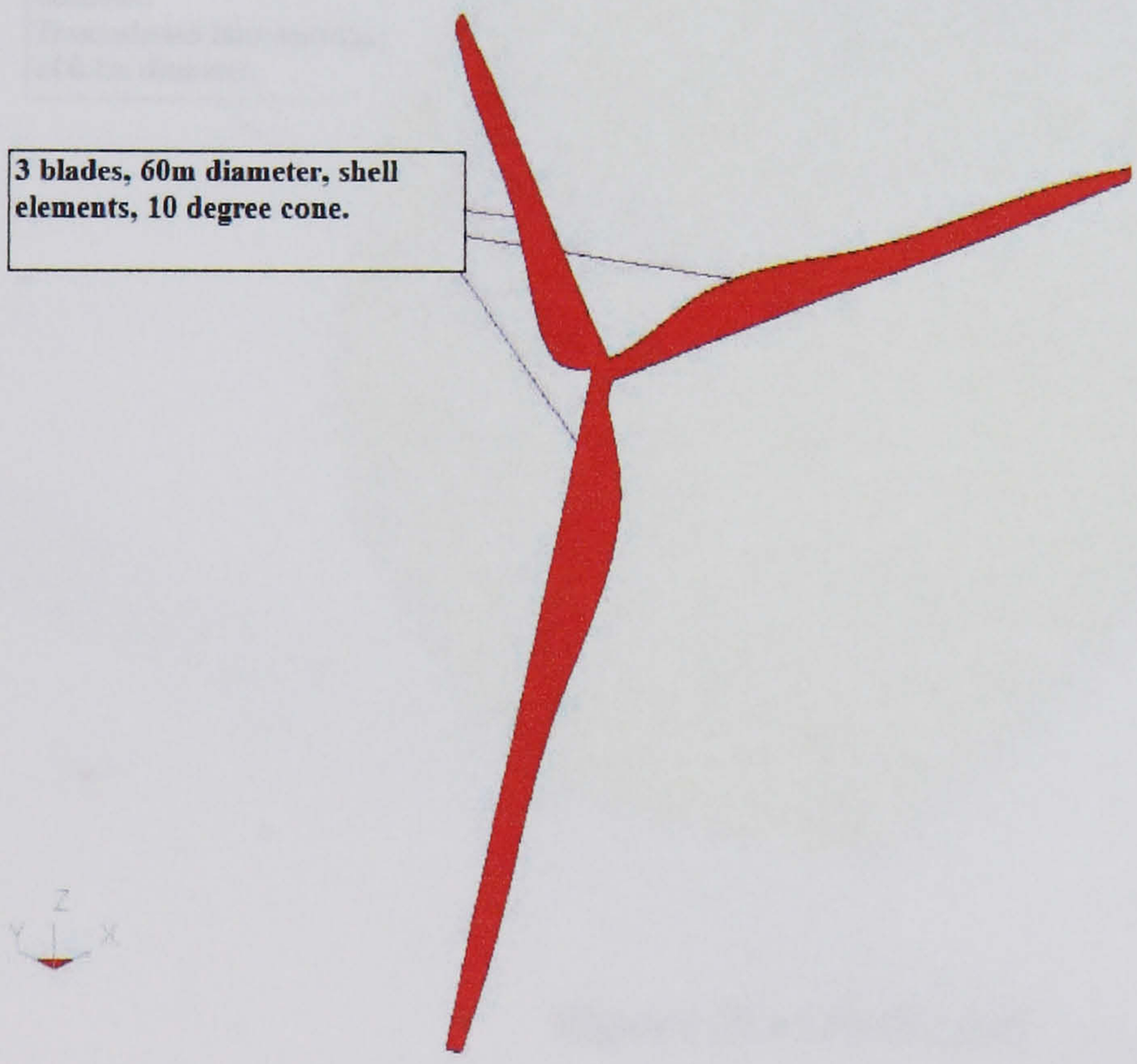

Figure (5.5) Blades part

5.1.2.b Hub part:

The hub is the second part in the rotor, intended to house and provide the necessary continuity and connection mechanism that will allow integral rotation of the three parts. This part is modelled by material 'type 3' due to

the expected high level of vibrating stresses and shell elements 'formulation 16' were used to offset 'hourglass':

***MAT_PLASTIC_KINEMATIC**

***SEC_SHELL**

Detailed input values used in these two keywords are reported in Appendix-A2 of this thesis. Hub is contacting blades as mentioned in previous heading and to transmission part via:

***BC_CONSTRAINED_EXTRA_NODESET**

In which a node set of the hub nodes is constrained as extra nodes to the rigid part 'the transmission'. The geometry of the hub is shown in Figure (5.4), Figure (5.6) and Figure (5.9) with three 1m diameter openings to house the blades roots and 0.2m diameter opening to let the transmission in.

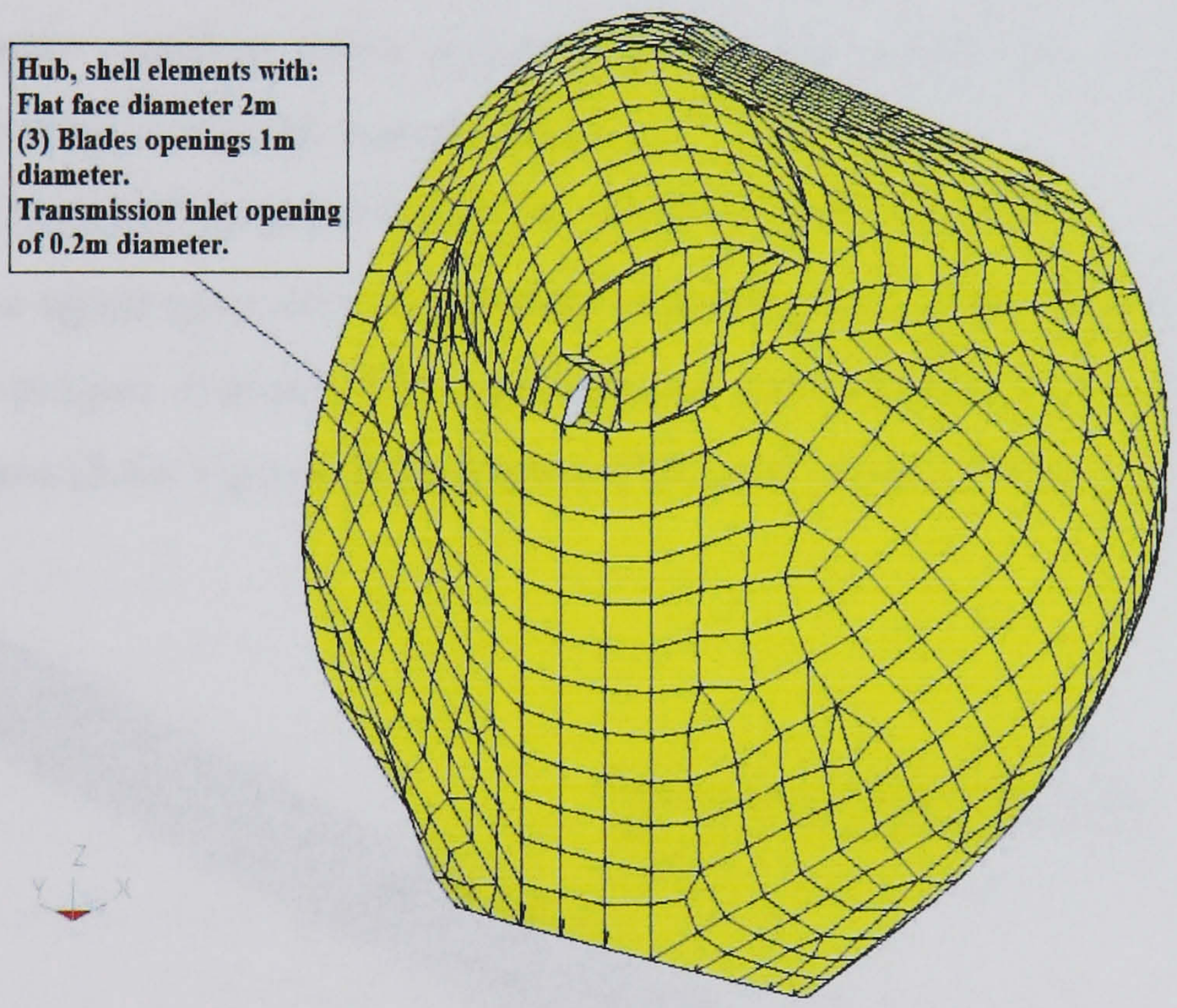

Figure (5.6) Hub part

The flat face of the hub part (2m in diameter) is slaved to the opposing flat face of the nacelle part in the contact keyword:

***CONTACT_AUTOMATIC_SURFACE_TO_SURFACE**

Segment sets representing the two surfaces are used in this contact definition necessitating that segment normal being pointing at each other for good

contact action, numerical presentation of this keyword is also reported in Appendix-A2 of this thesis.

5.1.2.c Transmission part:

Transmission is 4.36m in length and 0.2m diameter and is the means by which the mechanical rotational energy resulted from the blades air contact is transformed to the gear part inside the nacelle, therefore transmission is modelled using brick solid elements and material 'type 20' (rigid) it is necessary for constraining this part using 'joint revolute' to model rotation:

***SEC_SOLID and**

***MAT_RIGID**

As already detailed in the last two subheadings, the transmission is rigidly connected to both hub and blades parts in a fashion guaranteeing combined angular rotation when applied. To accommodate this rotating transmission part is linked to the nacelle part via:

***ELEMENT_CONSTRAINED_JOINT_REVOLUTE.**

Once again geometry is carefully chosen to house this relative rotational action and proper contact. The transmission part location and geometry is shown in Figure (5.4), Figure (5.7), Figure (5.9) and Figure (5.12).

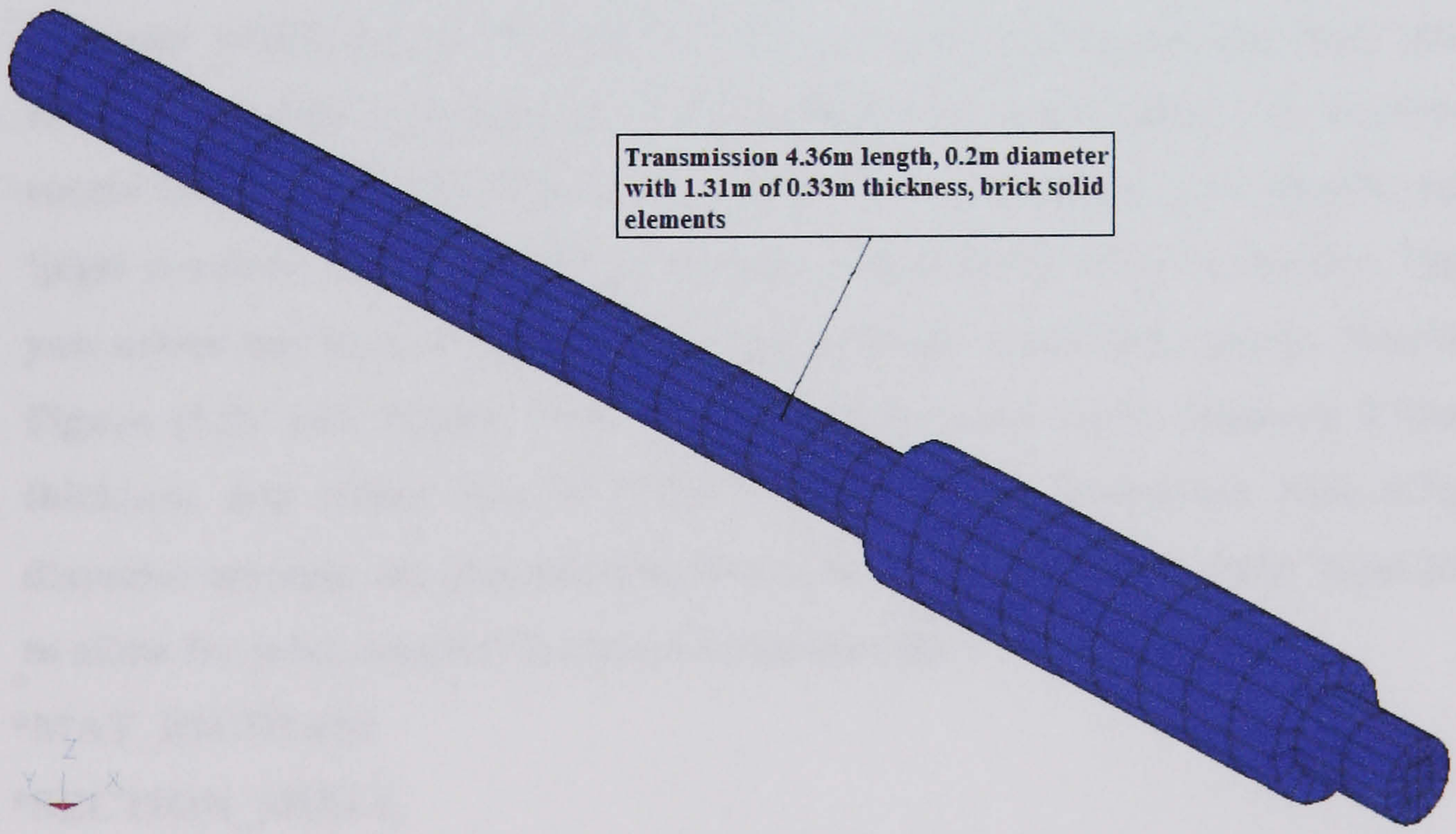

Figure (5.7) Transmission part

The weight of the rotor constituents is:

- **Blades 11,666 kg**
- **Hub 3,592 kg**
- **Transmission 1459 kg**

Therefore total rotor weight is 16,717 kg

These are compliant with those reported by, Sore Krohn [58], Rehfeldt Knud Dr and Matthias S Dr. [59] and Hans Christian Soerensen [90], Group [91] and geometry have been modelled specifically to generate the correct mass in LS-DYNA3D.

All three constituents are rigidly attached to each other and are prevented from all relative movements except common rotation about the rotor horizontal local (y-axis) to model the actual movement. The rotational movement initiation and relevant load curve will be mentioned under the loading subheading of this chapter, also, the blades are operating on downwind concept, at 10 degrees coning angle to offset yaw control negative effects, as well as providing adequate clearance of the blades from the tower.

5.1.3 Nacelle part:

A small boat in French, it is the housing for the electricity generation equipments, providing stiff support, weather protection, and coupled with free yaw rotational mechanism for the parts above the bearing ring. The rotor is attached to nacelle in a mechanism that would allow the rotor to rotate about its local horizontal (y-axis) by constraining it to nacelle via 'joint revolute' while allowing it to yaw with nacelle when necessary. The yaw action has to be done through bearing rings at interface points. Nacelle Figure (5.8) and Figure (5.9) is modelled by plate shell elements 0.03m thickness and empty box of (2.5m x 5m x 2.5m) dimensions with 0.2m diameter opening for transmission let in, the used material is rigid 'type 20' to allow for joint creation keyword cards therefore are:

***MAT_RIGID and**

***SECTION_SHELL**

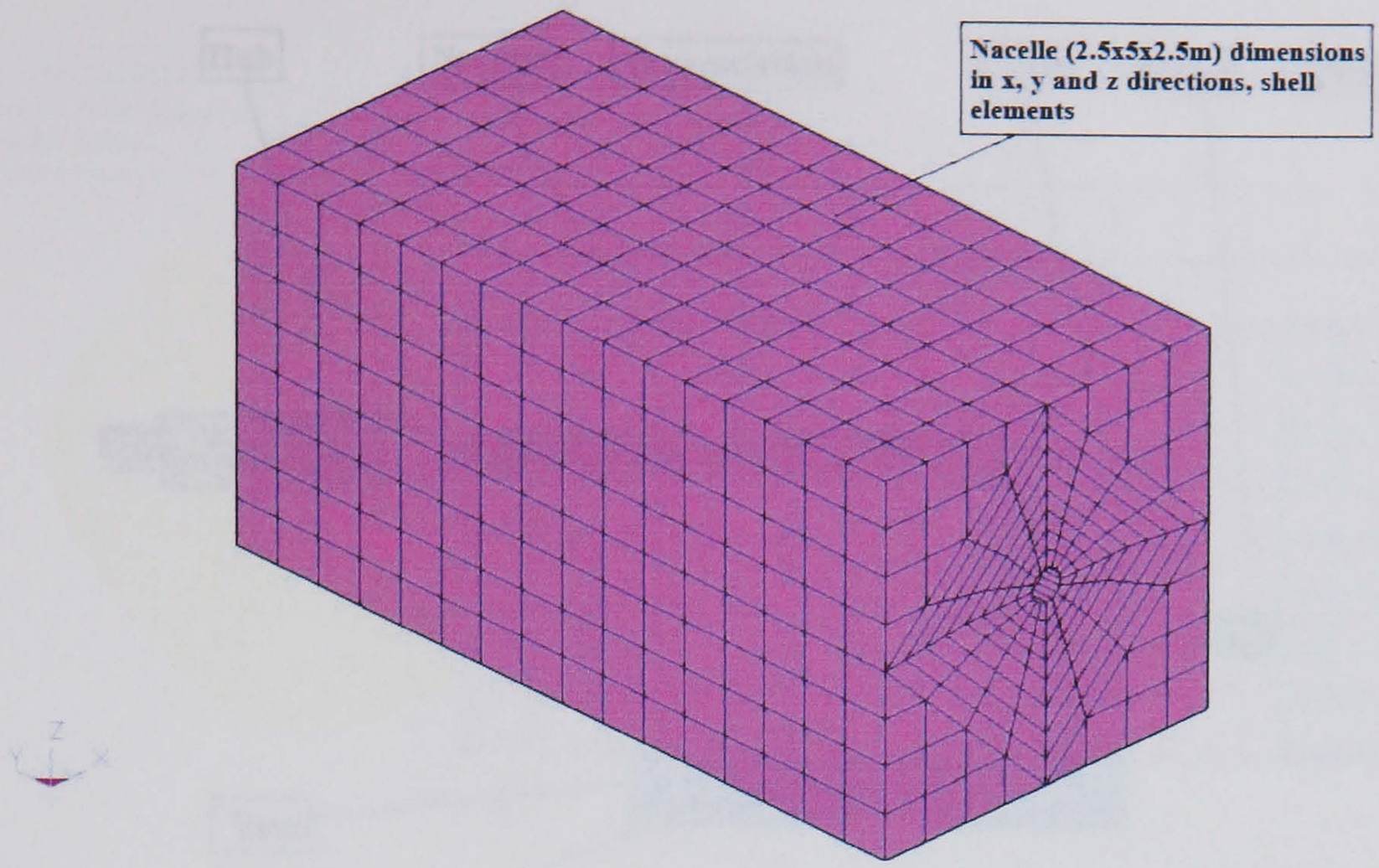

Figure (5.8) Nacelle part

Both of the above keywords numerical inputs are listed in Appendix-A2 of this thesis, to guarantee fixity between nacelle and its internal constituents (to be detailed) all these parts were created as rigid parts making it easy therefore to couple their action via the function:

***CONSTRAINED_RIGID_BODIES**

The parts: gear, generator, and yaw ring are all merged to the nacelle part acting as a common slave part to all of them. As already mentioned the nacelle is jointed to the transmission part to allow for rotor rotation and connected to the hub part as mentioned above. The internal parts of the nacelle are:

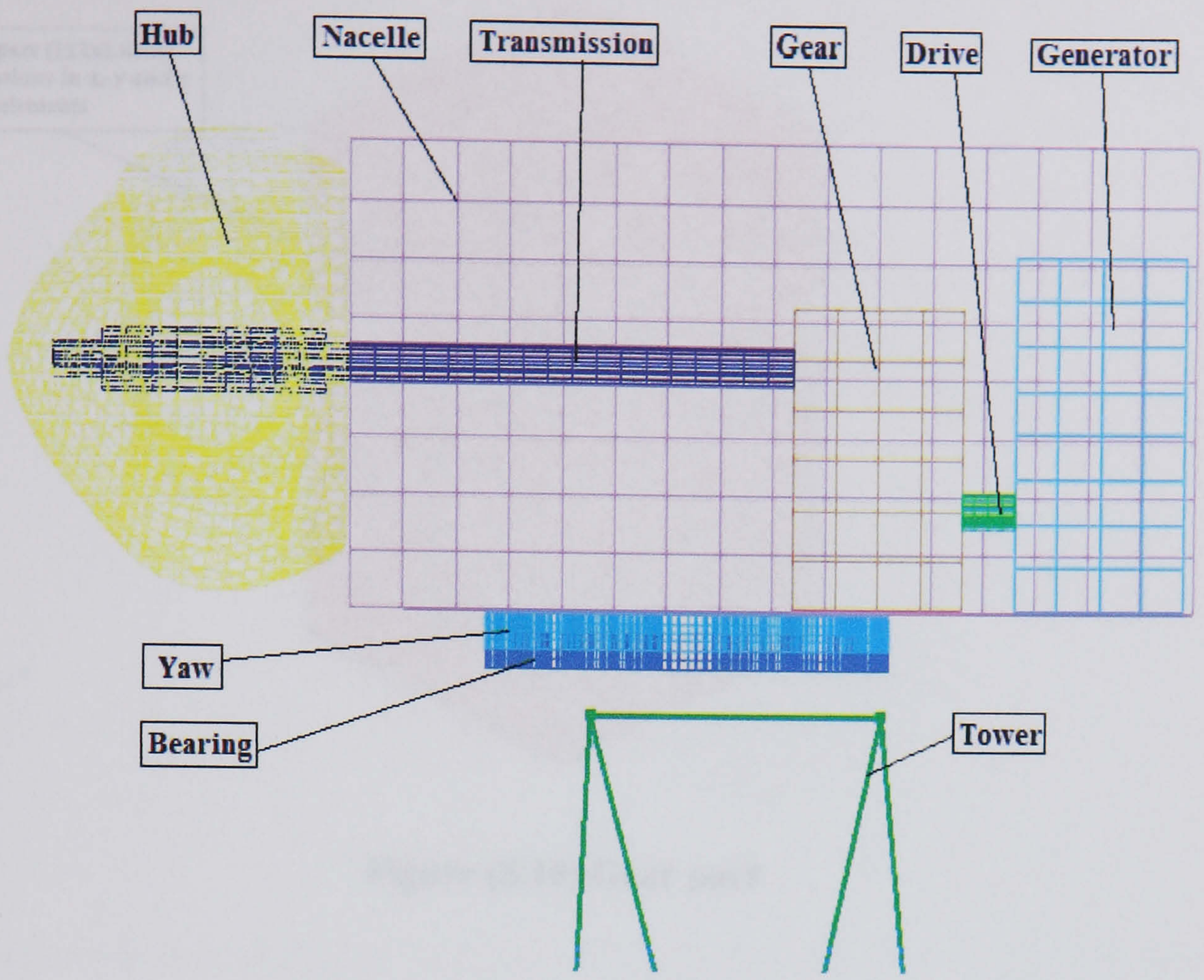

Figure (5.9) Nacelle and parts connected to it

5.1.3.1 Gear part:

A two or three stage epicyclical gearbox, with the relevant rotational characteristics is implemented in the finite element representation. The material and section properties are 8-noded solid elements of steel material properties, rigid material 'type 20' as said before are employed, quantities reflecting these formulations are reported in Appendix-A2 of this thesis, the gear part is of cube size with dimensions (1m x 1m x 1.62m) to reflect the required mass as shown in Figure (5.9), Figure (5.10) and Figure (5.12). The restraints applied are its rigid body merge to the nacelle part as stated earlier and 'joint revolute' connection to the drive part.

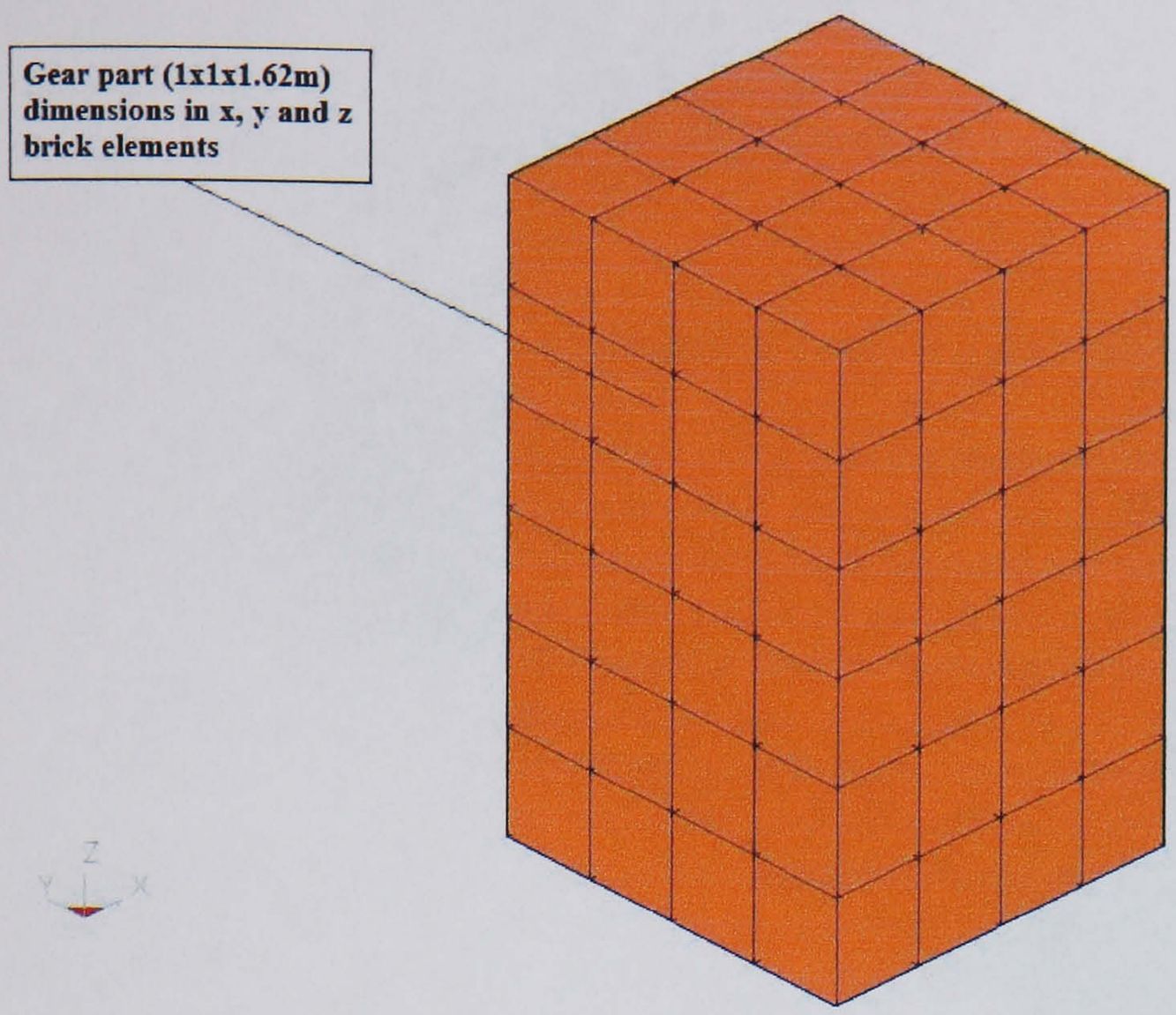

Figure (5.10) Gear part

5.1.3.2 Drive part:

As shown in Figure (5.9), Figure (5.11) and Figure (5.12) it is a solid shaft modelled by brick solid elements, providing a means of transforming the rotational rotor movement, after being upgraded by the gear to match generator specification of high-speed movement. The geometry is reflecting the expected mass of the part. To accommodate the rotational action, the drive is linked to the gear part via:

***ELEMENT_CONTRAINT_JOINT_REVOLUTE**

Therefore, the geometry was modelled carefully to insure this constraint action and rotational angular speed is applied. The load curve and function used will be discussed later. The geometry of 0.31m length and 0.2m diameter is used.

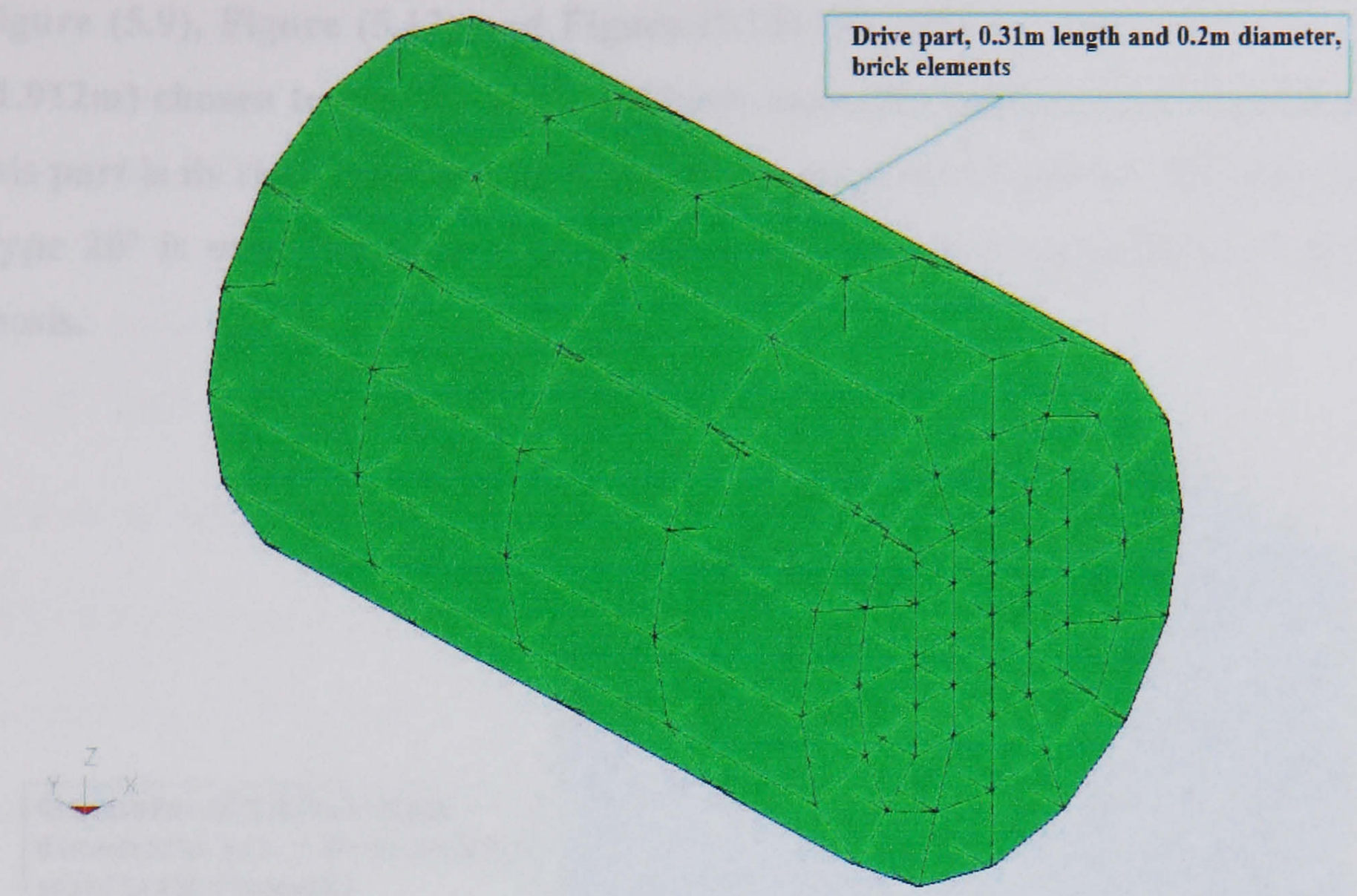

Figure (5.11) Drive part

The numerical quantification of material and section properties used for drive part will be reported in Appendix-A2 of this thesis.

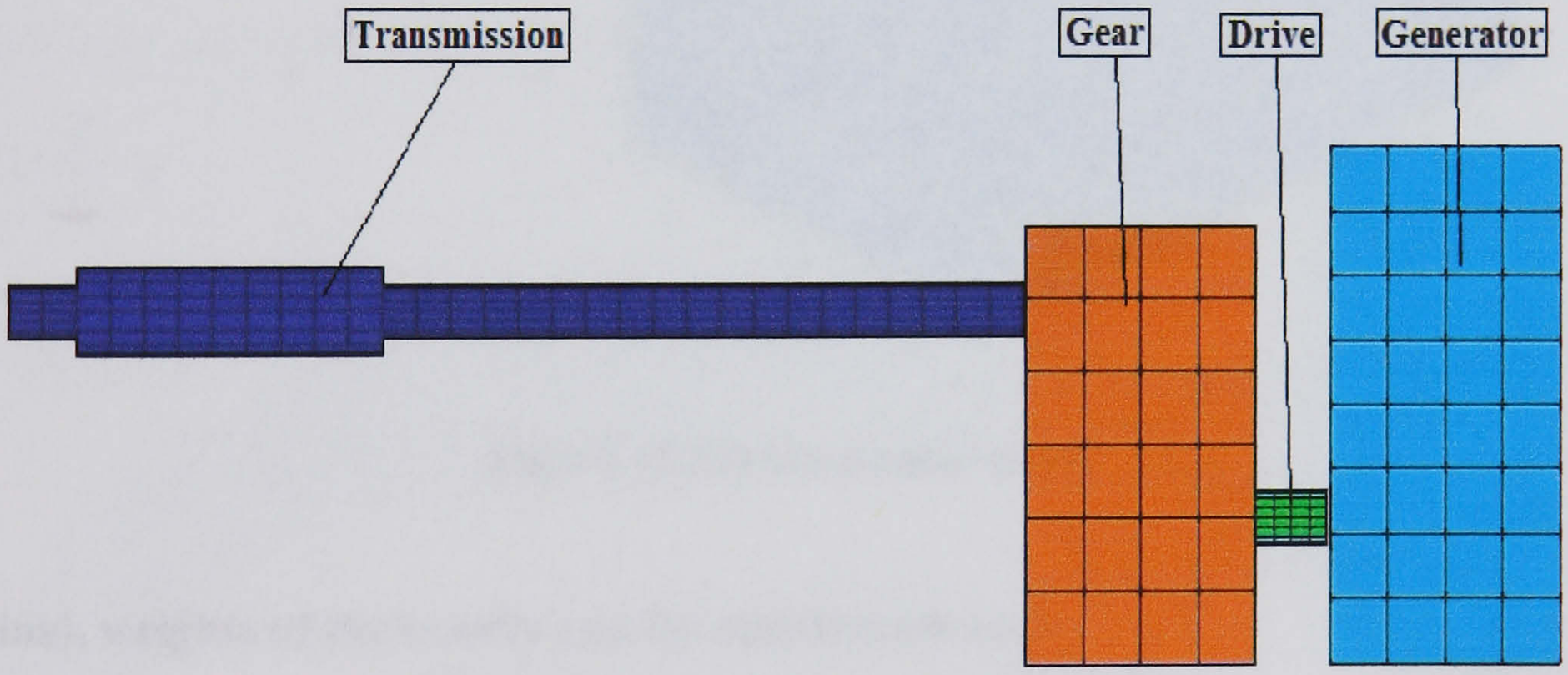

Figure (5.12) Transmission and parts inside nacelle

5.1.3.3 Generator part:

It is the heaviest part in the nacelle, and probably in the whole super structure, modelled by 8-noded solid elements of copper (dominant material) properties. Its dimensions reflect the expected mass of this part. Shown in

Figure (5.9), Figure (5.12) and Figure (5.13) the cube geometry is (1.4mx 1m x1.912m) chosen to give the required body mass, the only constraint applied to this part is its rigid body merge to nacelle as been stated earlier. Material rigid 'type 20' is used the numerical values are reported in Appendix-A2 of this thesis.

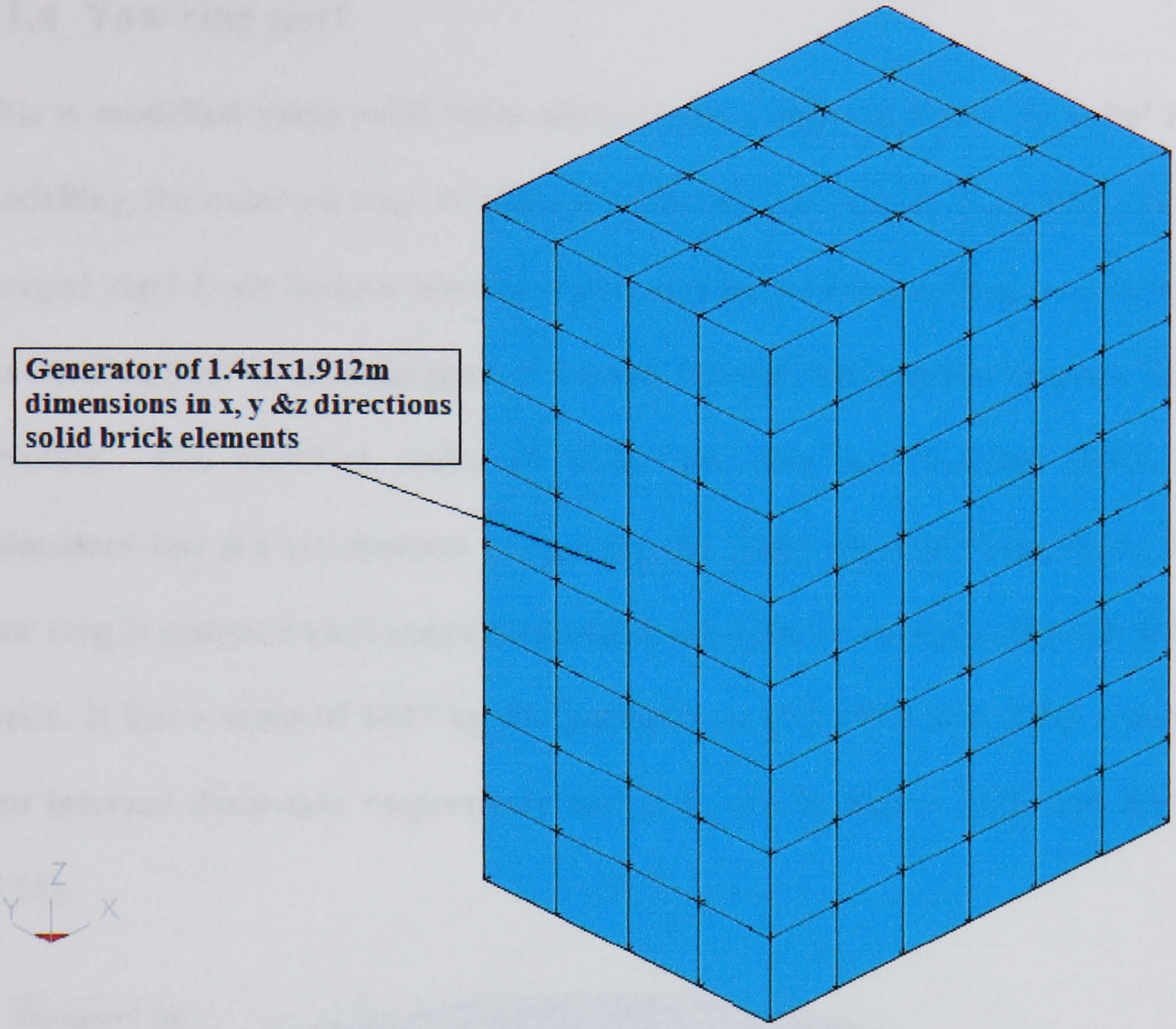

Figure (5.13) Generator part

Final, weights of the nacelle and its constituents are:

- **Nacelle shell** **10,088 kg**
- **Gear** **12,717 kg**
- **Drive** **75 kg**
- **Generator** **23,819 kg**

Total mass of nacelle is **46,699 kg**

These are in conformance with reported guidelines, Sore Krohn [58], Rehfeldt Knud Dr and Matthias S Dr [59] and Hans Christian Soerensen [90], Group

[91], and have been modelled specifically to generate the correct mass in LS-DYNA3D.

Obviously these loads would include any cooling and lubricating fuels, connectors, any frame local stiffening, or any necessary supporting equipment for the employed parts.

5.1.4 Yaw ring part

This is modelled using solid brick elements and rigid material 'type 20' it is modelling the external ring. It is fixed to the nacelle bottom deck face via the merged rigid body feature already mentioned in nacelle heading, and fixed to the bearing part or internal part of the yaw bearing mechanism through 'joint revolute'. The common nodes of both yaw ring and bearing parts are coincident but are not merged to capture the 'joint revolute' behaviour. The yaw ring is assigned steel properties which are detailed in Appendix-A2 of this thesis. It has a mass of 1647 kg the geometry is of 2.397m and 2.0m external and internal diameters respectively and is shown in Figure (5.9) and Figure (5.14).

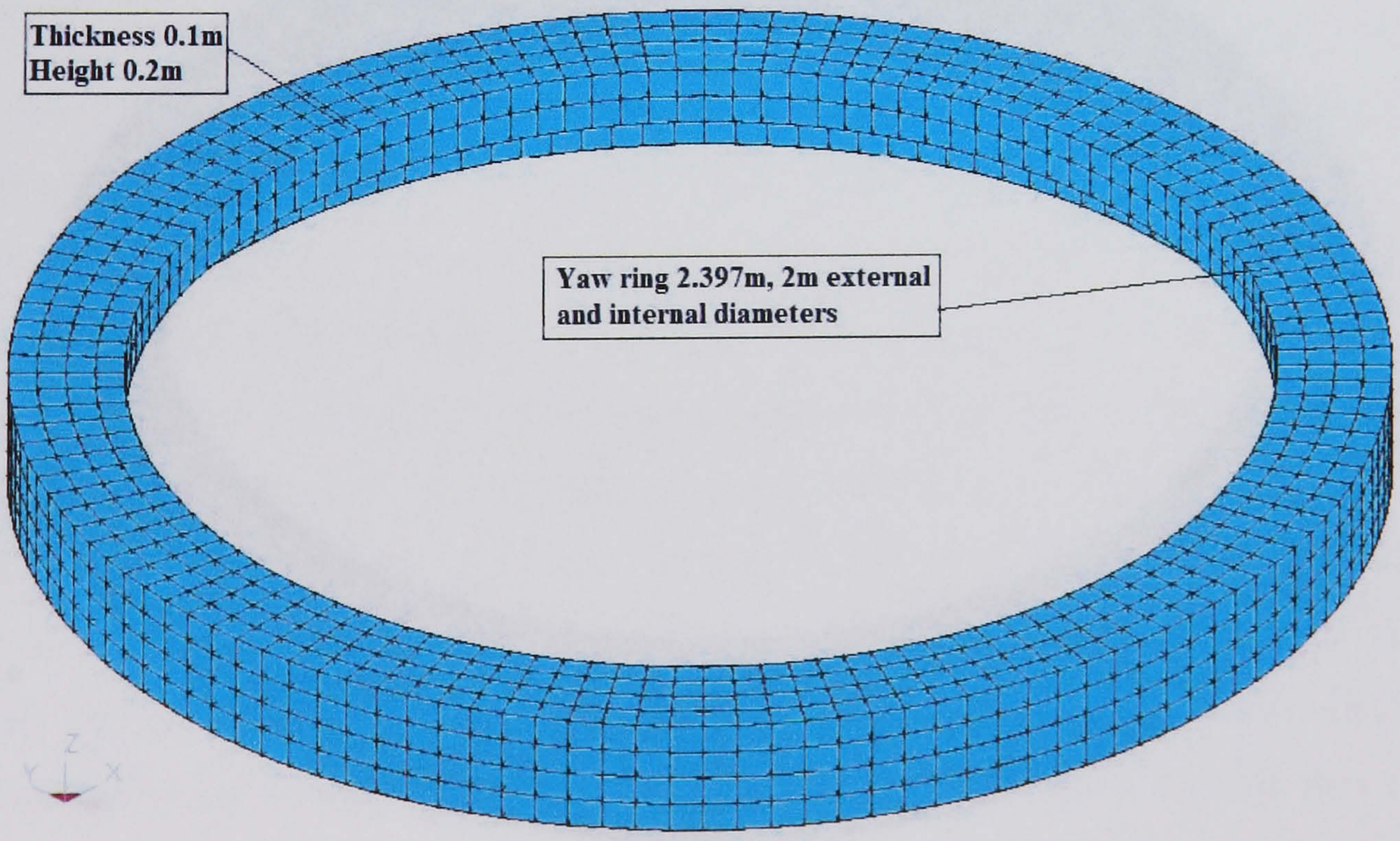

Figure (5.14) Yaw ring part

5.1.5 Bearing part:

The bearing forms the internal part of the yaw-bearing mechanism, made of steel properties, brick solid elements and rigid material 'type 20' to allow for joint definition, quantification of these parameters is reported in Appendix-A2 of this thesis. Bearing is firmly connected to the tower top via:

***CONSTRAINED_EXTRA_NODESET**

Where a node set consists of all tower nodes is constrained as extra nodes to the bearing part 'rigid body' and connected to the yaw ring part through: *ELEMENT_CONSTRAINED_JOINT_REVOLUTE as already explained. The mass of this part is 1600 kg, with the geometry of 2.4m and 2.0m outside and inside diameters respectively as shown in Figure (5.9) and Figure (5.15). Actually both bearing and yaw rings would be one body (bearing) and modelled here in two parts to simulate the rotation provided by the 'joint revolute'. The fact that they are both rigid bodies as required to define the joint would assume that they are strong enough to carry and transfer applied forces which is of main concern here.

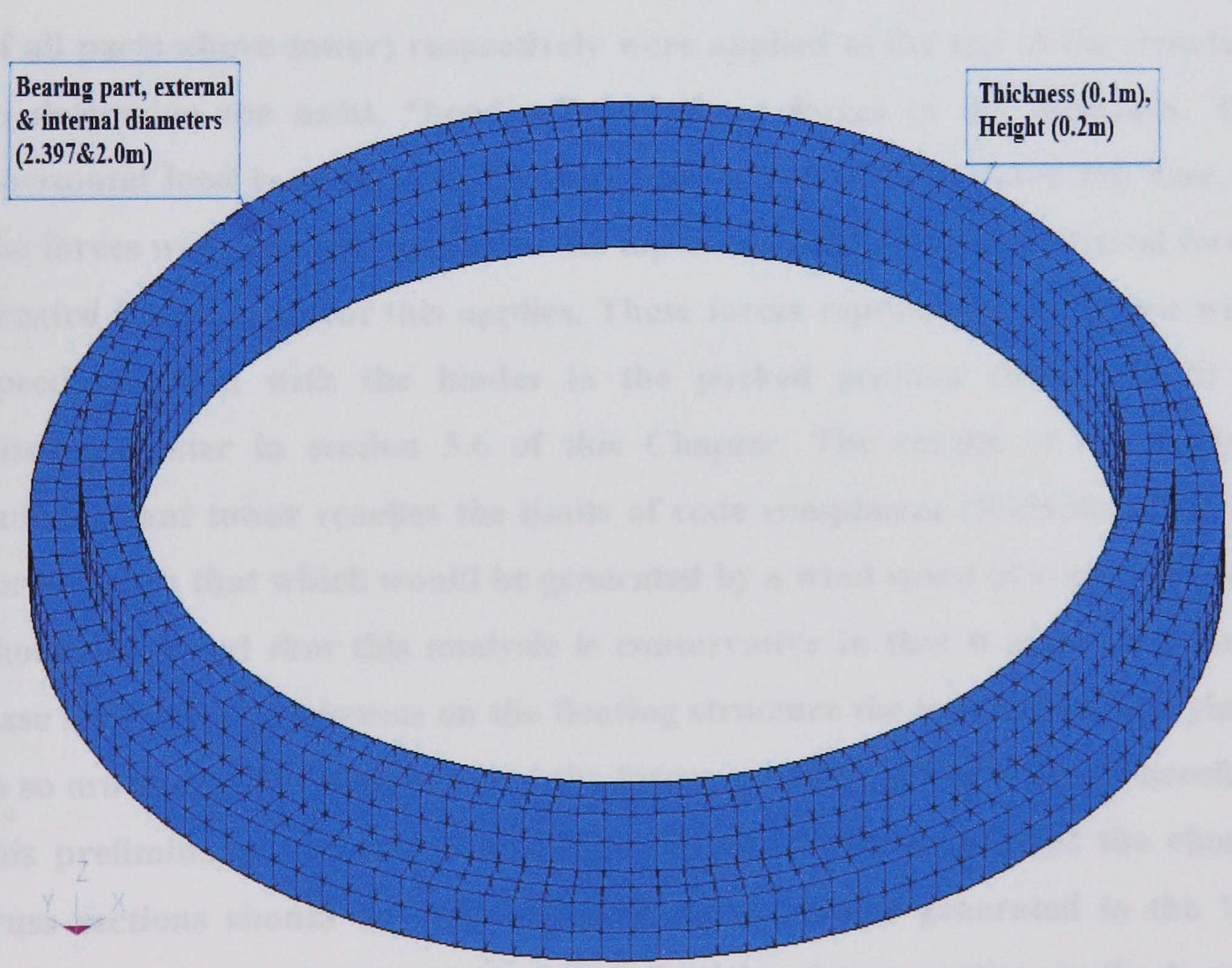

Figure (5.15) Bearing part

5.1.6 Tower part:

The critical design of the tower is to avoid resonance at multiples of the turbine frequency, and minimum weight which is a cost reduction. Tripod lattice steel tower is constructed from 355N/mm^2 yield stress steel tubular sections. The geometry of the tower at the base is governed by the supporting hull deck diameter therefore it is modelled as an equilateral triangle of 8.8m side, while the tower top is equilateral triangle of 2m side compatible with the yaw bearing dimensions. The tower height of 38m is governed by the 45.6m hub elevation above mean sea level. Truss elements are used to model this part, with one bar per length between nodes. The total length of tower truss members is 365.5m. A standard CHS (S355) of 508 x 20 size hot or cold rolled section was chosen using BS5950 [49], with a mass per unit length of 241 kg/m, worked out a total mass of 88,086 kg. Choice is verified in a preliminary approximate analysis performed using the ANSYS 7.1 finite element code. Only the truss was modelled with a fixed base, and typical horizontal and vertical design loads of 2551 KN (the sum of the wind load on nacelle upwind face and rotor blades at 40.5m/sec survival wind speed), and 654 KN (weight of all parts above tower) respectively were applied to the top of the structure to determine the axial, "bending" and shear forces in the members. The horizontal load is applied at 1.89m eccentricity above the tower top base, so the forces were applied directly to the top nodes with additional vertical forces created by the moment this applies. These forces represent the extreme wind speed situation with the blades in the parked position (load case 5) as discussed later in section 5.6 of this Chapter. The results of the analysis indicate that tower reaches the limits of code compliance (BS5950) when the forces reach that which would be generated by a wind speed of about 35m/s. It should be noted that this analysis is conservative in that it assumed a fixed base for the truss, whereas on the floating structure the foundation can 'yield' in so much that it is buoyant, and the forces are expected to be less. Therefore this preliminary analysis gives a high degree of confidence that the chosen truss sections should be able to withstand the forces generated in the LS-DYNA3D model. (It should be noted that the chosen section is the largest standard available, but was done so to enable a conservative design solution to

withstand comfortably the forces generated by the highest wind speeds). A typical plot of the truss showing a displacement of 0.37m under the forces generated for a wind speed of 40.5m/s is shown in Figure (5.16).

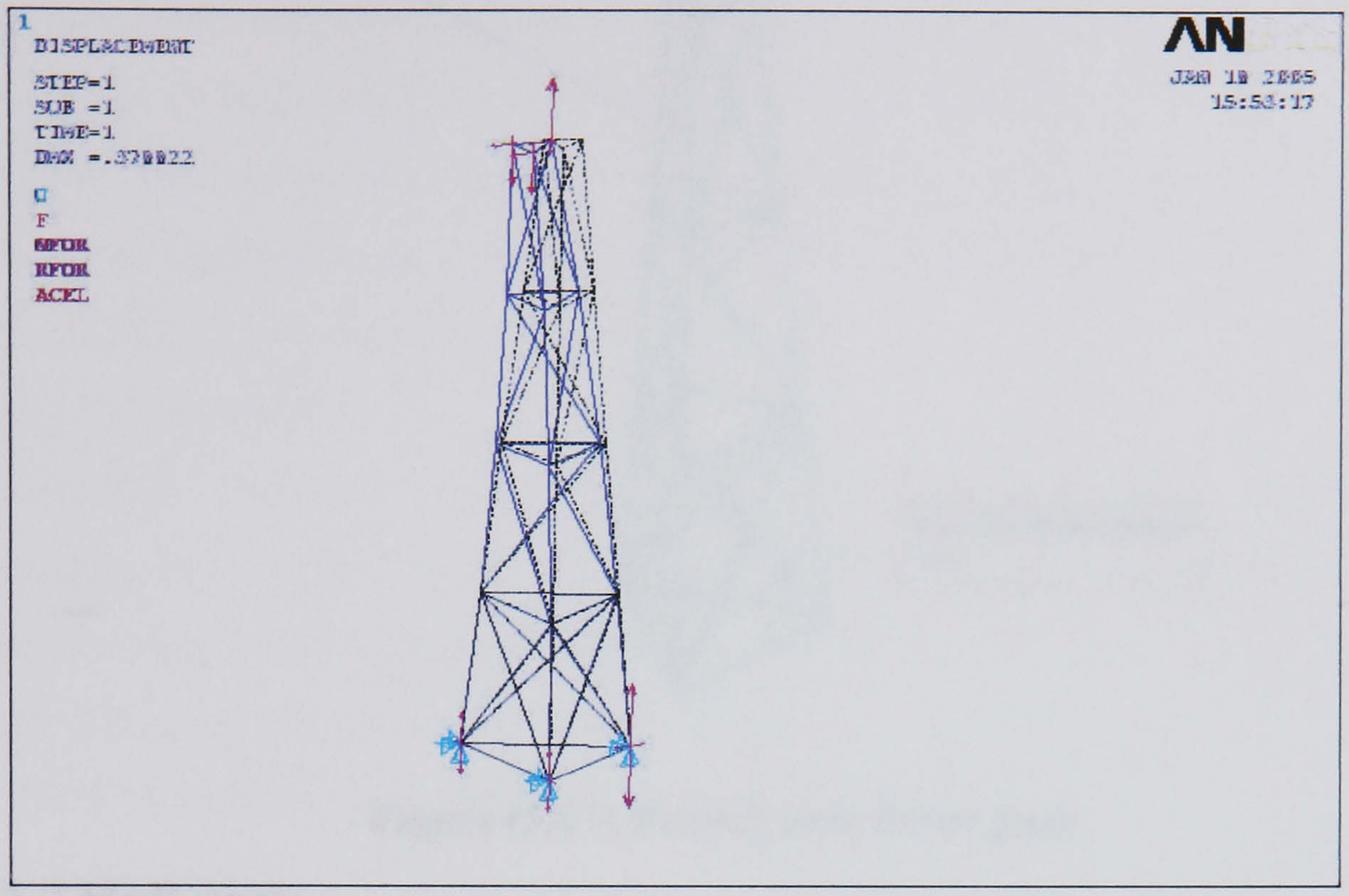

Figure (5.16) Truss displacement under extreme wind speed

The material 'type 98' is used it is defined for truss elements which is primarily intended for structural analysis and it is cheaper to run and can adopt any plastic action in case it occur, while beam section for element property is used. These are:

*MAT_SIMPLIFIED_JOHNSON_COOK and

*SECTION_BEAM

Both keyword card values are reported in Appendix-A2 of this thesis. The tower shown in Figure (5.9) and Figure (5.17), a node set comprising the whole tower, hull and foam nodes is constrained to bearing part 'rigid part' as an extra node set to model firm connection between these parts.

While drawing, a gap of 0.254m (half the tube radius) is left below and above the tower part to accommodate proper contact for the beam elements.

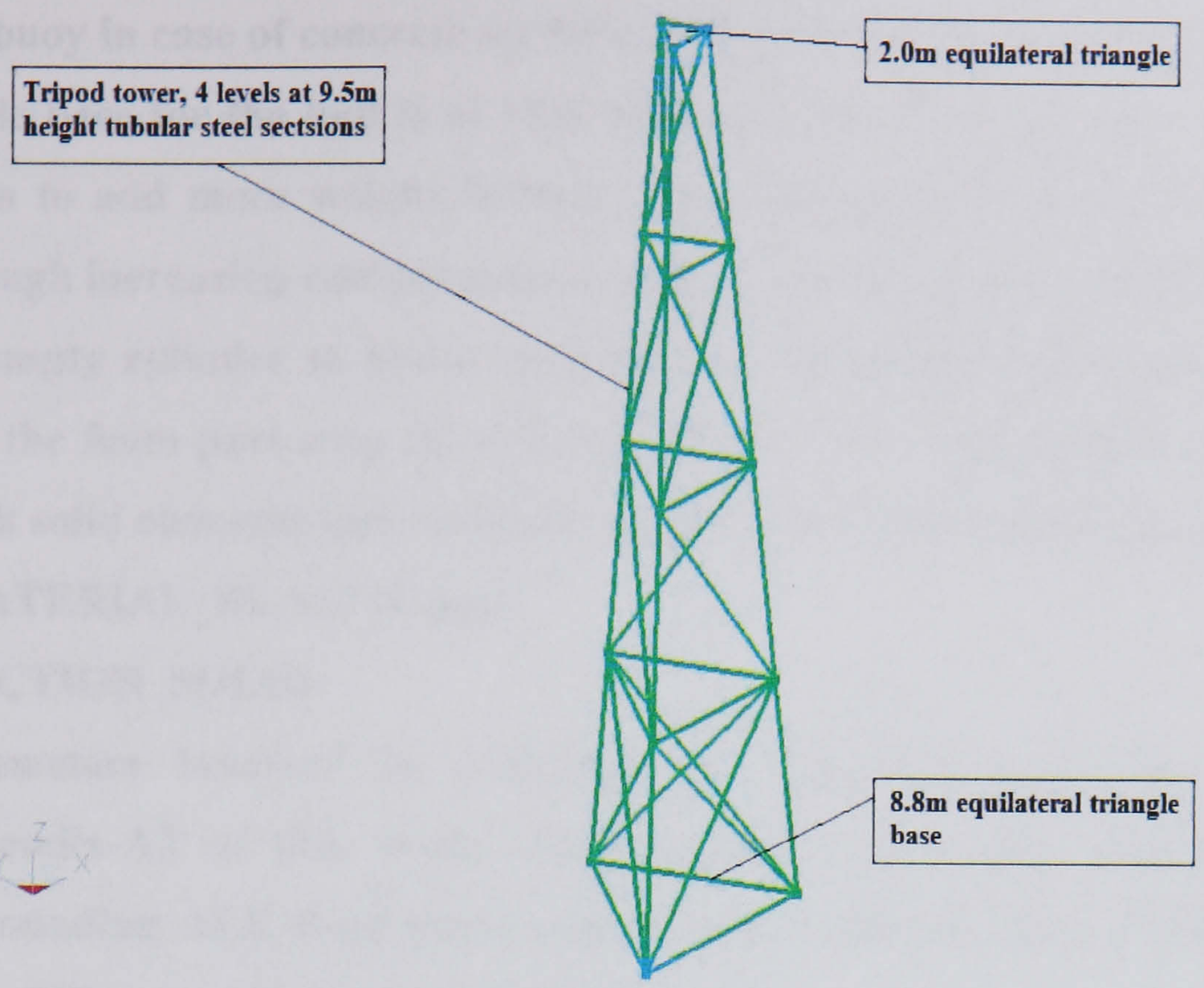

Figure (5.17) Tripod steel tower part

5.1.7 Hull part:

The hull buoy is a reinforced concrete pre-cast cylinder, firmly resting on reinforced pre-cast concrete disk and monolithically linked to it. The floating hull is serving as a foundation for the tripod steel tower; the hull is modelled in brick solid elements, of 12m internal diameter, 0.25m wall thickness, 0.40m deck thickness, and 4m base thickness. The total height of the buoy cylinder is 28.5m, with 6m of this height above sea level. The Hull deck is thickened at the points of fixing of the three lower ends of the tower to house anchor bolts. The outer perimeter of the hull deck is holding the 8 mooring cable grippers, meanwhile at 10m below these grippers are the bent shoe fairleaders serving as a guide for the mooring cables attached to gripping points. These bent shoes are fixed in the outer perimeter of the hull buoy 4m below mean sea level.

In addition to the buoy weight an extra mass of (664,374 kg) ballast is added inside the hull, as an option (544,374 kg) of this extra mass provided as plain concrete filling produced as an integral part of the hull distributed evenly on its base and (120,000 kg) of low-density foam to be mentioned later. This extra mass will balance the upward buoyancy forces and increase structural stability by lowering the centre of mass downwards as discussed in Chapter IV of this thesis. These fillings are also necessary to prevent water leakage inside

the buoy in case of concrete serviceability failure. The concrete disk serving as stable base for the hull is of 19m diameter and 2.5m in height. The disk also helps to add more weight further down and reduce upward water pressure through increasing contact area as well as providing more stability. The hull is an empty cylinder to house the concrete fill (monolithically connected to it) and the foam part atop the concrete filling. The concrete part is modelled by brick solid elements and material 'type 1' (elastic material) that is:

***MATERIAL_ELASTIC and**

***SECTION_SOLID**

Parameters involved in defining both keyword cards are reported in Appendix-A2 of this work. The concrete hull is also constrained to the surrounding ALE fluid parts namely water and air and in contact with the foam filling part inside these is done using:

***CONSTRAINED_LAGRANGE_IN_SOLID for ALE**

For foam part is:

***CONTACT_AUTOMATIC_SURFACE_TO_SURFACE**

The hull geometry is shown in Figure (5.18).

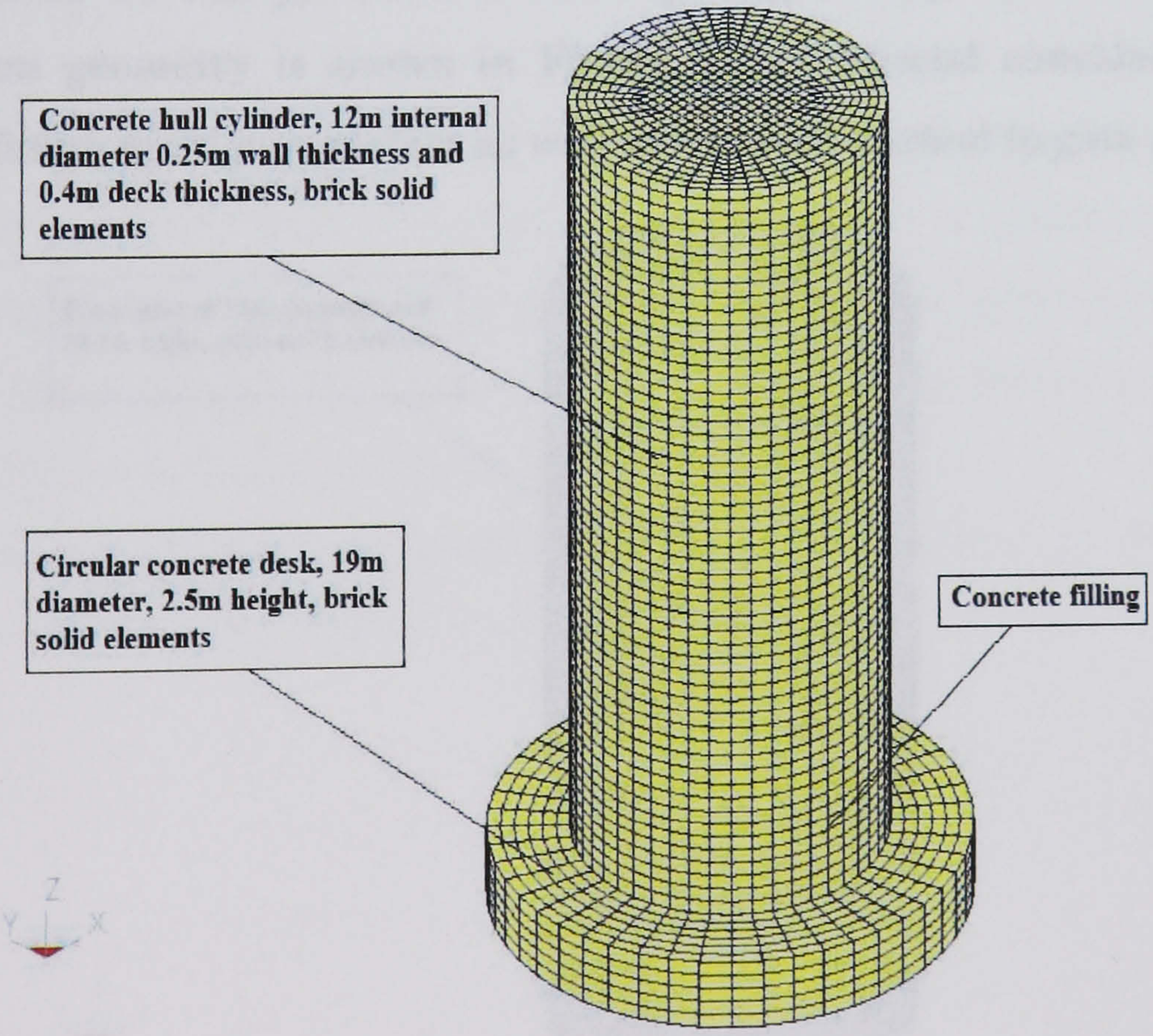

Figure (5.18) Concrete hull buoy part

5.1.8 Foam part:

As already mentioned, the low density synthetic foam, is used as an option for providing a filling for the 24.1m height inside the buoy cylinder above the concrete ballast filling. It is modelled using solid block 8 node elements and material 'type 57' specifically defined for low density foam. As already stated, the function of this foam filling is to provide more stabilising extra mass as well as preventing water from leaking inside in an event of concrete cracking.

The Foam part is in the form of a solid cylinder 12m in diameter and 24.1m in height occupying the gap between the concrete filling disk and hull deck lower surface. The foam part mass is 120,000kg. Material and element property cards as well as two contacts are defined for this part, they are:

***MAT_LOW_DENSITY_FOAM**

***SECTION_SOLID**

***CONTACT_INTERIOR to prevent negative volume occurrence and**

***CONTACT_AUTOMATIC_SURFACE_TO_SURFACE, between foam and hull parts through two segment sets representing both parts with the foam segments (the softer) being the slave. Material and property cards are presented in Appendix-A2. The hourglass control card also needs to be defined for this part, and is also reported in Appendix-A2 of this thesis. The foam geometry is shown in Figure (5.19). Special consideration is given to defining foam parameters as well as segment normal to gain good contact.**

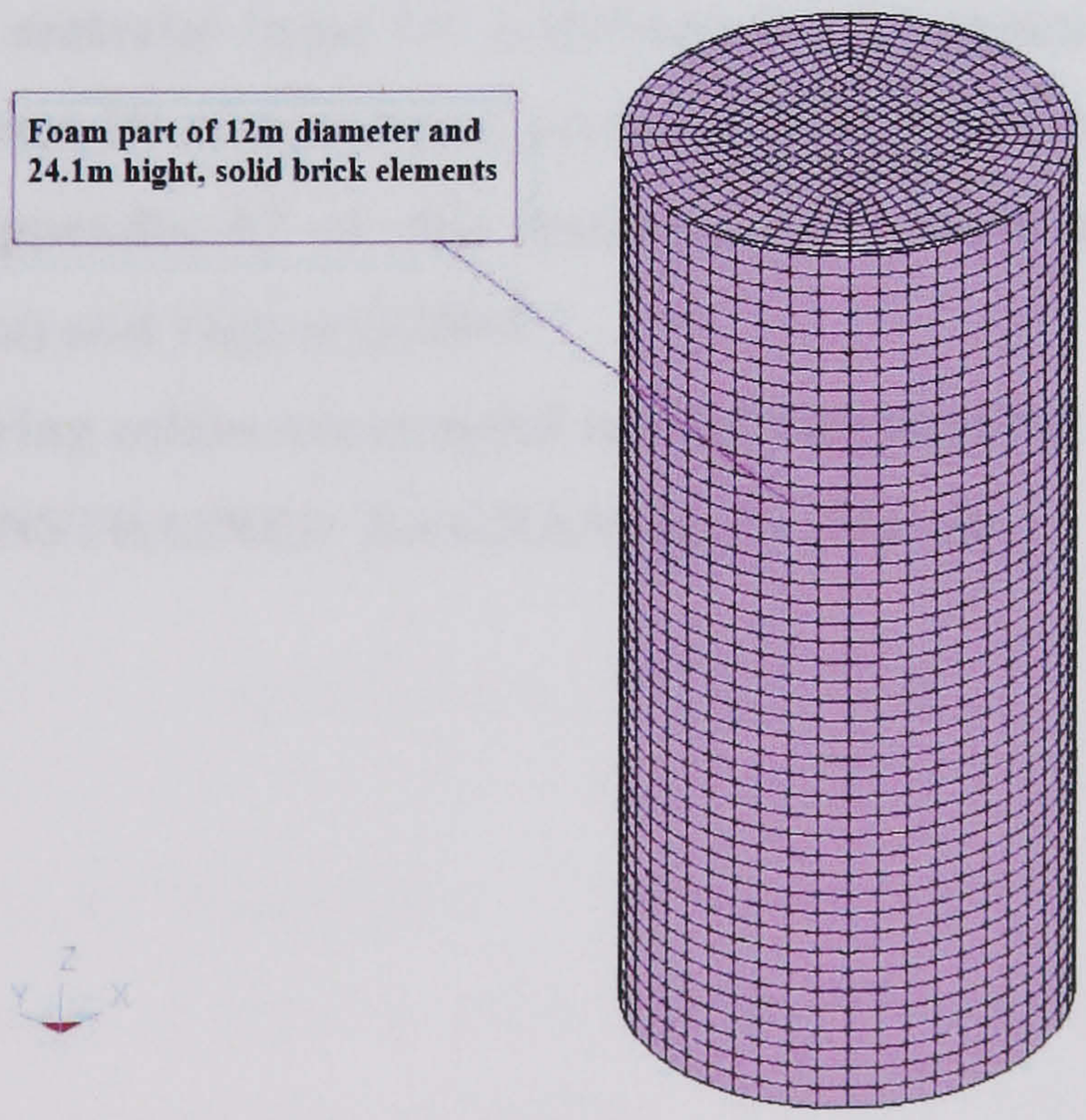

Figure (5.19) Foam part

5.1.9 Mooring part:

These are cable elements, attached at the hull deck outer top edge, passed through guide shoes to be finally pinned at the anchoring points at the seabed, eight mooring cables are provided. The length of the cable above the guiding shoes is 10m, while it is stretching 137.5m below this guide points to the seabed inclined at an angle of approximately 45 degrees. This length is dictated by the cable footprint assuming 100m depth, thus giving total length for all cables as 1,180.10m. A polyester rope of diameter 0.232m with 15MN breaking strength, 0.00125 elongation and 34.5 kg/m in air (7.8 kg/m in water) density is used here as taut mooring configuration giving a total submerged mass of the part as 9,205 kg., advantages of polyester ropes over their traditional steel rope substitute was discussed in Chapter IV of this thesis. Mooring cables are attached to concrete hull at grip nodes as well as at leading nodes below them and to the seabed part at termination nodes. This is done through the keyword:

***BC_CONSTRAINED_INTERPOLATION**

The material 'type 71' is defined for the cables as already been discussed in Chapter IV of this thesis, property and constraint keywords used are reported in Appendix-A2 of this thesis and the cable geometry is shown in Figure (5.20a) and Figure (5.20b).

Mooring cables are coupled to ALE surrounding elements through:

***CONSTRAINED_LAGRANGE_IN_SOLID**

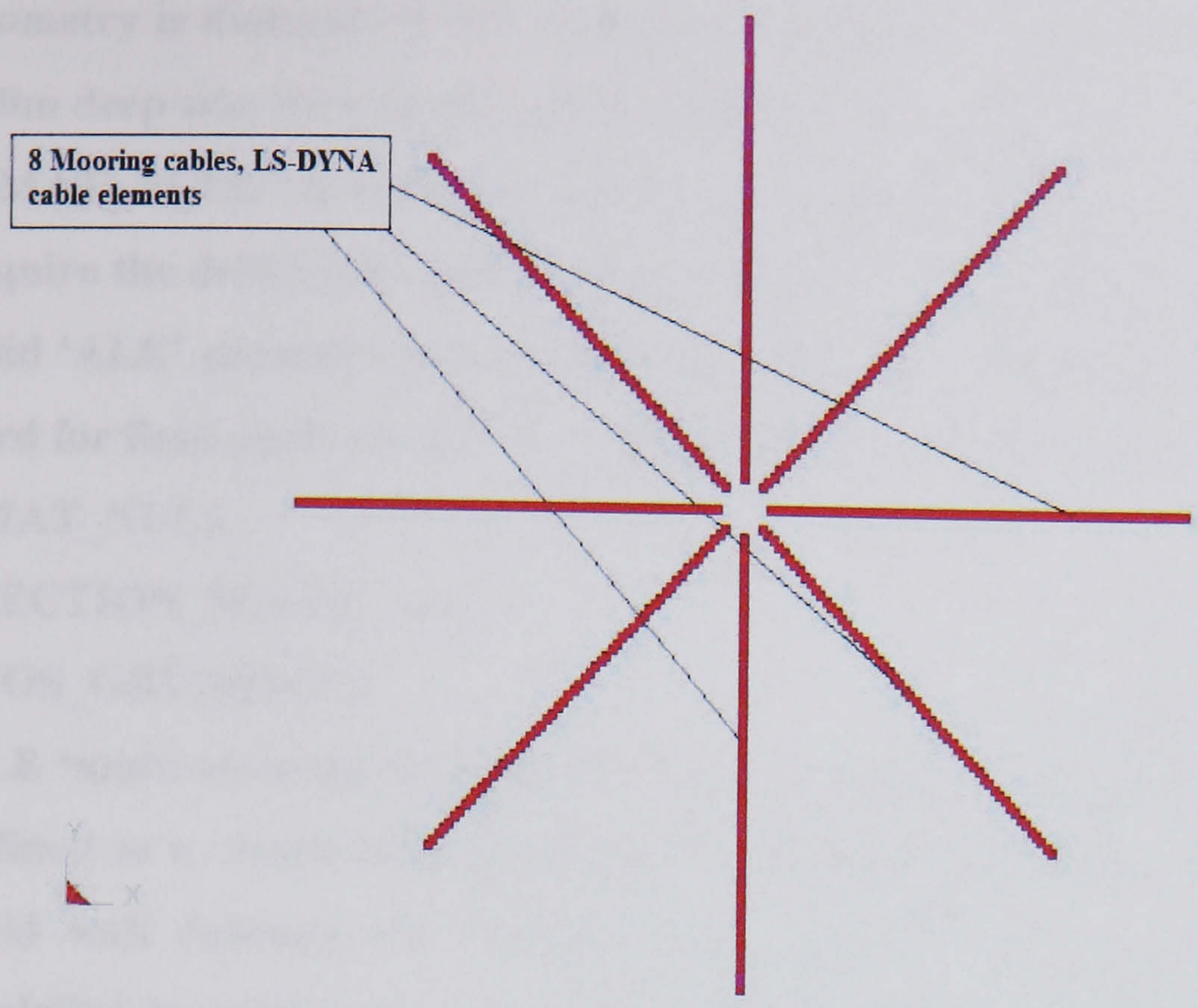

Figure (5.20a) Mooring cables part (plan view)

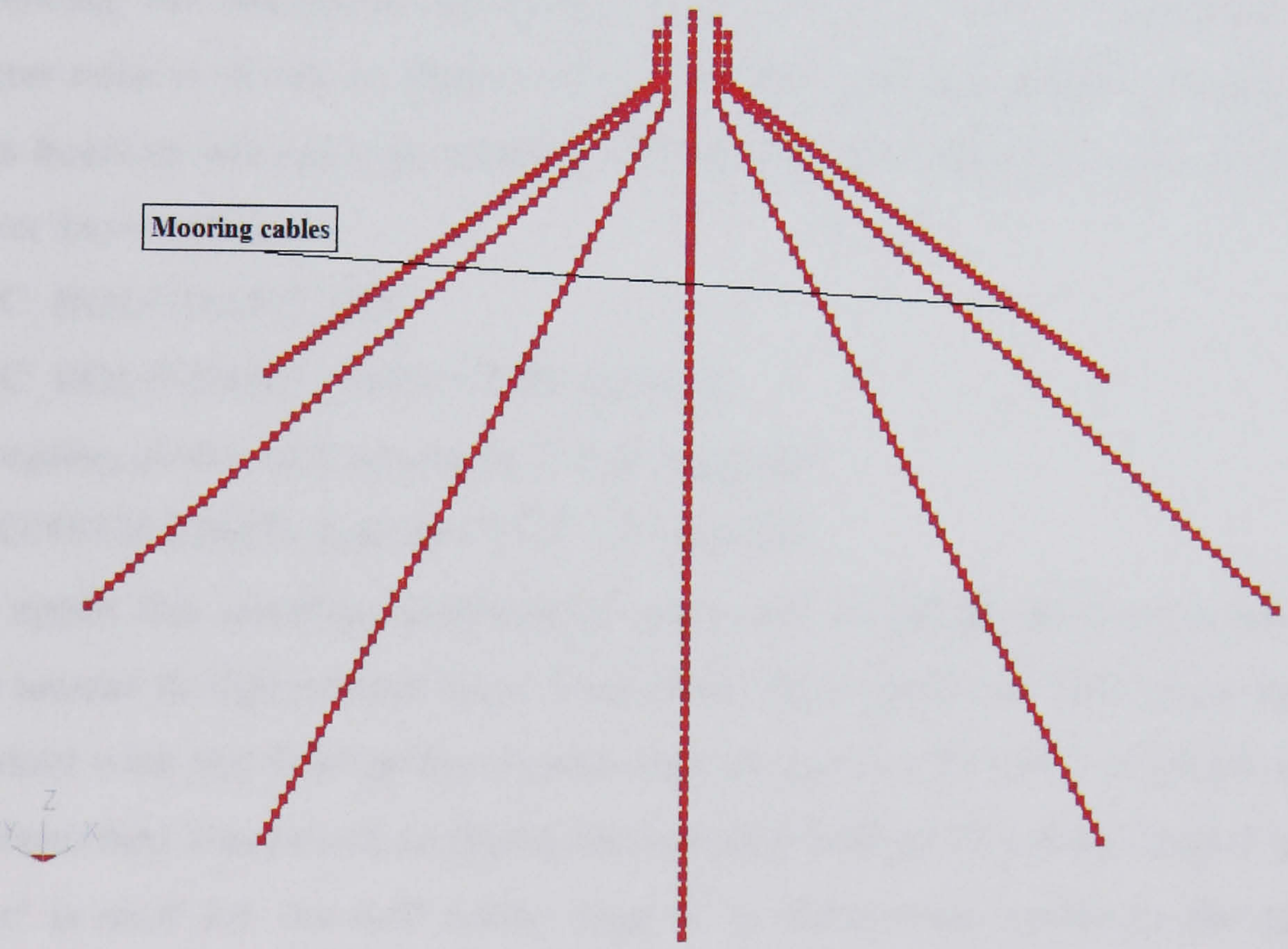

Figure (5.20b) Mooring cables part (isometric view)

5.1.10 Water part:

The cube of (210m x 210m x 100m) in x, y and z directions is defining the water around the supporting hull unit using brick solid elements, the

geometry is dictated by the 'footprint' of the anchored cables and suggesting 100m deep site. As was discussed in Chapter IV of this thesis, material 'type 9' "*MAT_NULL" is typically defined by the code for fluids and is used which require the definition of an 'equation of state' to activate pressure inside fluid solid 'ALE' elements (discussed in the same source), as well hourglass control card for fluid parts need to be defined, therefore used cards are:

***MAT_NULL**

***SECTION_SOLID_ALE**

***EOS_GRÜNEISEN**

ALE 'multi-material formulation 11' is used for which water part need to be defined as a 'multi-material group'. The water body cube is bounded by the rigid wall defining the seabed at the bottom while the finite quanta are modelled by applying a 'non-reflecting' boundary along the water cube sides as mentioned in Chapter IV of this thesis. This is readily done by defining a segment set containing all segments along the five sides (excluding top side) following the discussion presented in the previous source. Geometry of the water cube is shown in Figure (5.21) and the used keywords are mentioned in this heading but their parameters are detailed in Appendix-A2 of this thesis, these keywords are:

***BC_BOUNDARY_SPC**

***BC_BOUNDARY_NON_REFLECTING**

Coupling of the ALE elements is done through:

***CONSTRAINED_LAGRANGE_IN_SOLID**

To apply this coupling Lagrangian parts are slaved to ALE parts which are the master in this contact type. Therefore, the 2 parts hull and mooring are in contact with the fluid group (water and air parts) and water respectively, this dictates that 2 keyword coupling cards being defined. Coupling type 4 'penalty type' is used for the hull while 'type 2' is defined for cables in the previous coupling keywords. To achieve full contact between the water 'ALE' part and the top air 'ALE' part, common nodes at their interface are merged dictating that their common boundary needs to be coincident nodes.

***INITIAL_VOLUME_FRACTION_GEOMETRY is used in creating three empty cylinders representing the hull and its base disk both air and water parts. The keyword for this function is detailed in Appendix-A2 of this thesis.**

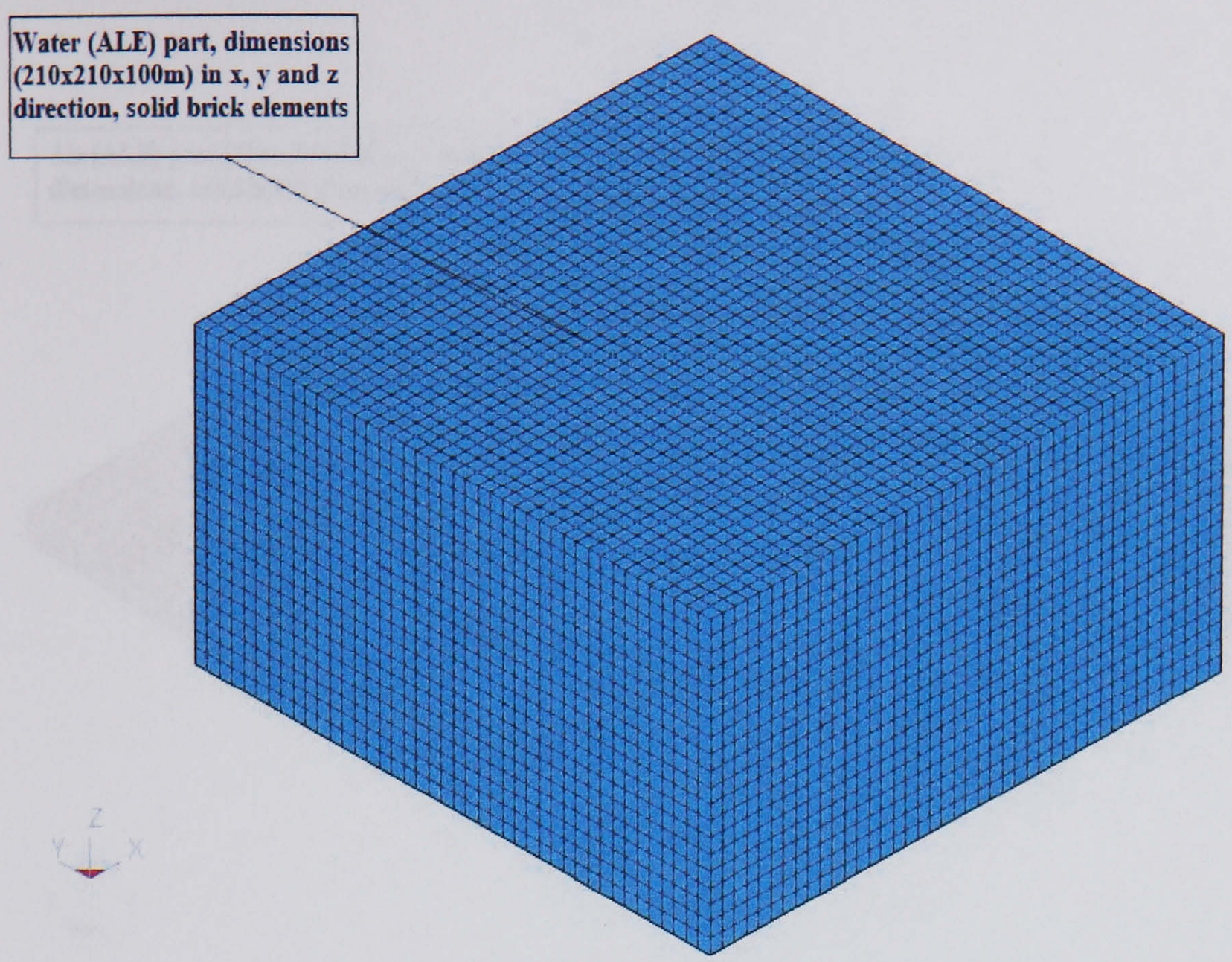

Figure (5.21) Water part

5.1.11 Air part:

The air part is an 'ALE' material part intended for modelling air bounding the top surface of the water body in the formulation. Similar to the water part this part is modelled using material 'type 9' and ALE solid brick elements 'formulation 11', hence air is defined as 'ALE multi-material group'. An equation of state is also necessary for this type of material and therefore defined and was discussed in Chapter IV of this thesis, the used keywords are:

***MAT_NULL or type 9**

***SECTION_SOILID_ALE**

***EOS_LINEAR_POLYNOMIAL**

The constraints applied to this part are coupling with water part which is done through merging the common coincident nodes at the interface and coupling with the slaved part modelling concrete hull at their common interfaces. The coupling is done by:

***CONSTRAINED_LAGRANGE_IN_SOLID**

Geometry of the air box is (210m x 210m x 6m) bounding the hull and water parts and is shown in Figure (5.22) while all keywords defined here including hourglass and coupling cards are detailed in Appendix-A2 of this thesis.

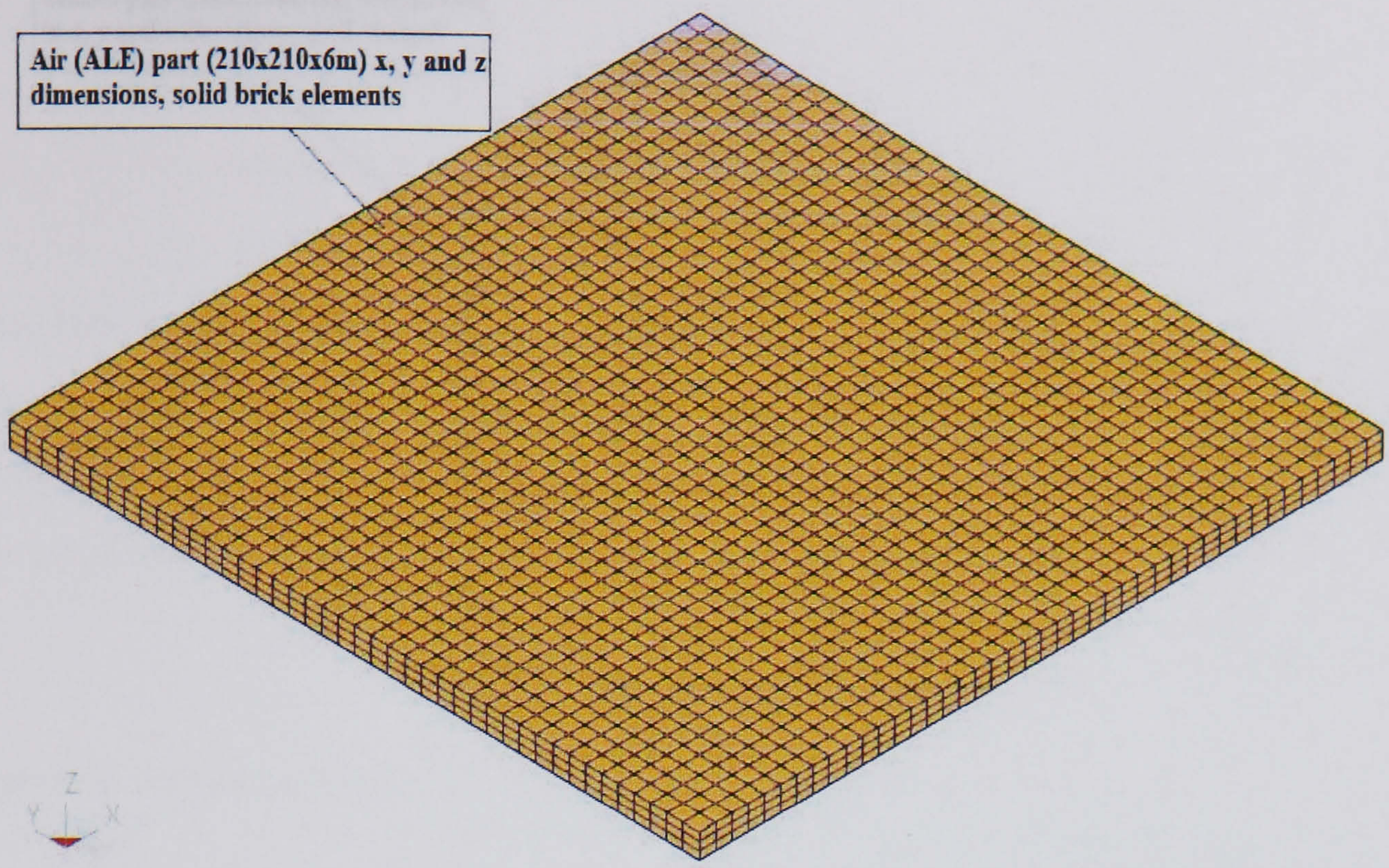

Figure (5.22) Air part (situated above the water block)

The hull deck is elevated to punch 6m above water level once in operation. This elevation is believed to be enough for most wave heights and to give reserve displaced volume if the structure suffers extra weight e.g. during construction. Submergence of the hull by an extra 1m will lead to 125,786 kg (1,234 KN) of upward buoyancy lifting force. If the buoy goes down, mooring cables will sag, loosing tension, thus decreasing the translational constraints (causing less wind capture, hence less energy output). Equally important, is the maintenance of the gap of 6m height of the hull deck leading to the blades being dry and hence less corroded.

5.1.12 Seabed part:

It is modelled with rigid body material 'type 20' compulsory for rigid wall definition and fully integrated shell elements, the geometry of (210m x 210m x 0.5m) as required by cable foot print and shown in Figure (5.23). This part represents the finite seabed bounding the water part from beneath. Contacts are represented by defining this part as a finite rigid wall with all parts slaved to it using the card:

***RIGIDWALL_PLANAR_FINITE**

Details of the two cards are presented in Appendix-A2 of this thesis.

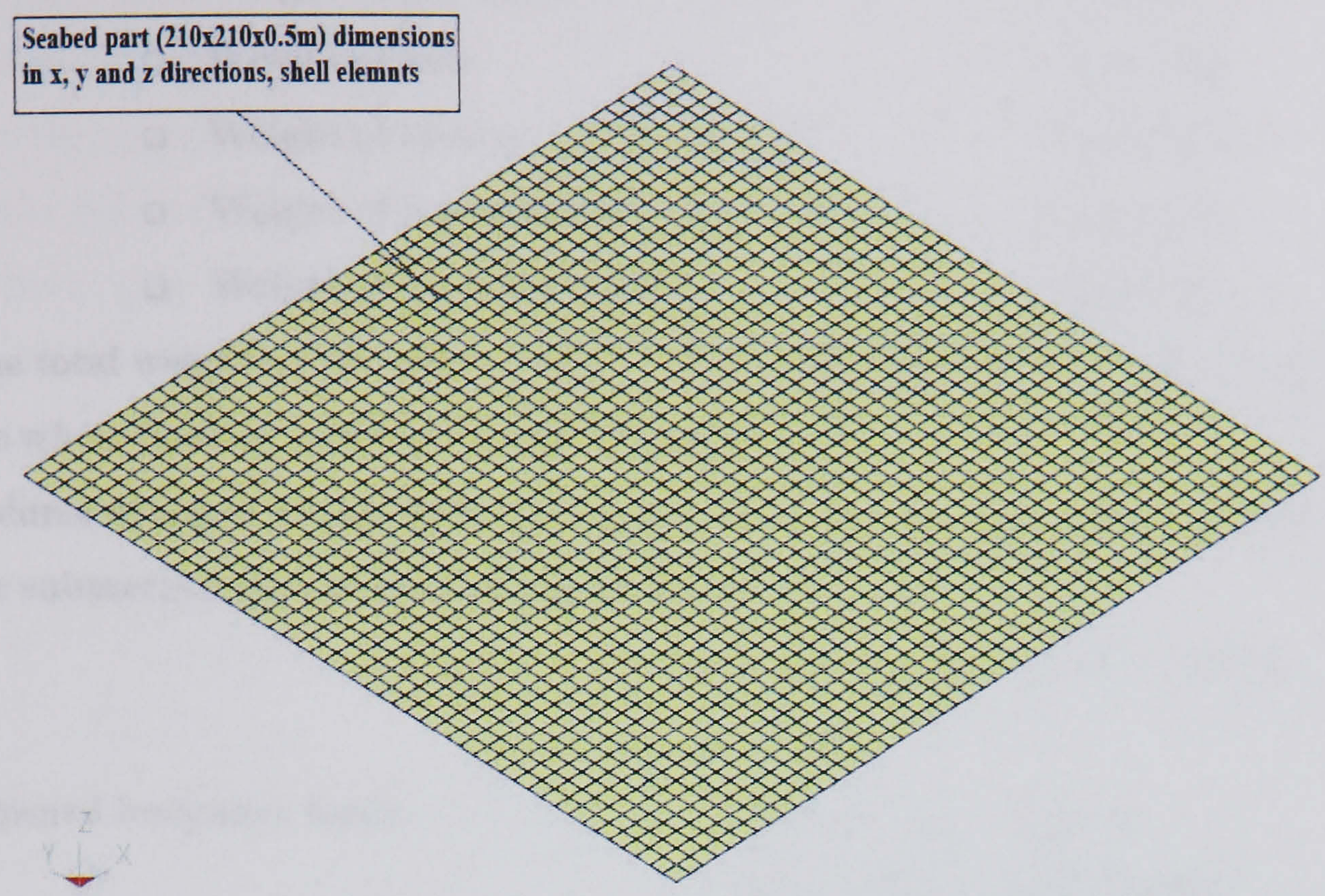

Figure (5.23) Seabed part (forming boundary at the model base)

5.2 Summary of Gravity Loads:

Concrete volume = hull volume + concrete filling volume

+ Concrete base disk volume.

$$= (6.25)^2 \times \pi \times 0.4 + \{(6.25)^2 - (6)^2\}\ \pi\ (28.1) + (6)^2 \pi\ (1.80)$$

$$+ (6)^2\ \pi\ (2.2) + (9.5)^2\ \pi\ (2.5)$$

$V_{concrete} = 1{,}480.7\ m^3$

Foam volume $= (6)^2\ \pi\ (24.1)$

$V_{foam} = 2{,}725.6\ m^3$

Foam density $= 120000 \div 2725.6 = 44\ kg/m^3$

Therefore density of 44.14 kg/m^3 is used to compensate for the non circular boundary in the geometry and the weights as calculated by the code are:

- **Total foam weight = 119,997 kg**
- **Steel tower weight = 88,091 kg**
- **Weight of yaw ring = 1,647 kg**
- **Weight of bearing ring = 1,600 kg**
- **Weight of nacelle box = 10,088 kg**
- **Weight of gear = 12,717 kg**
- **Weight of drive = 75 kg**

- Weight of generator = 23,819 kg
- Weight of hub = 3,592 kg
- Weight of blades = 11,667 kg
- Weight of transmission = 1,495 kg
- Weight of mooring cables = 9205 kg

The total weight of the above parts = 283,993 kg this represents the weight of the whole floating structure except concrete part.

Volume of water displaced by concrete = volume of concrete disk + volume of the submerged part of the hull (up to 22.5m) =

$$= (9.5)^2\ \pi\ (2.5) + (6.25)^2\ \pi\ (22.5)$$

$$= 3{,}470\ m^3$$

Upward buoyancy force $= V_{\text{displaced water}} \times \gamma_{\text{sea water}}$

$$= 3470 \times 1025 = 3{,}556{,}750\ kg$$

Weight of concrete used in the structure = 3,556,750 – 283,993 =3,272,757 kg

Volume of concrete material used $= 1{,}480.7\ m^3$

Density of concrete used $= \dfrac{3272757}{1480.7} = 2{,}210\ kg/m^3$

A value of 2218 kg/m^3 is used for density to substitute for geometry approximation (actual concrete volume as calculated by the code = 1,475.4 m^3).

5.3 Design Features:

The choice of 60m diameter, rotor blades was selected to be as large as possible within the reach of proven wind technology in the past decade, today much larger blades are available and most likely at no extra weight or strength penalty.

Mainly driven by yaw system design, a downwind 10 degrees coned three bladed configuration of the rotor blades is used, free yaw mode operation will contribute to system stability and more energy yield due to better alignment with wind directions, (as well as offsetting the extra weight for power yaw control).

Free from noise restrictions typical of on land sites, the rotor will operate at a higher tip speed, the benefits from this being less tower height and less weight

for the same energy capture. However, this high tip speed needs to be controlled to protect generators.

For the course of this model work, the typical design values used are listed in Table 5-1 sea state values are extracted from Nobel Denton [142], Various Editors [22] and DNV [75] they typically represent British North Sea moderate depth water parameters. Wind speed assumed values are most widely used in wind energy with a return period of 50 years is considered here as discussed later in this Chapter:

Table 5-1 Typical values for the floating turbine analysis	
Description	**Value**
▪ Surface current speed	1.5 m/s
▪ Wind rated hub speed	12.5 m/s
▪ Cutting wind in	6 m/s
▪ Cutting wind out	26 m/s
▪ Angular rotor speed	22 rpm
▪ Drive speed for generator	1000 rpm
▪ Rated power	1.4 MW
▪ Maximum wave height	28 m
▪ Tidal and surface wind current	1.5 m/s
▪ Crest to crest wave period	17 sec
▪ Maximum (survival) wind speed	40.5 m/s

5.4 Load Curves:

Beside the gravity loads which are readily calculated by defining geometry and mass density for the material, other loads applied to the floating model include: (i) buoyancy upward pressure on base disk bottom, (ii) hydrostatic all round water pressure on base disk and hull sides, (iii) loads due to drive rotation and loads due to rotor rotational movement, (iv) wind loads on the rotor blades, (v) and hydrodynamic loads due to wave and current on the concrete base disk and the floating hull cylinder. Values and directions of these loads are the most crucial to the analysis; strength, structural stability

and economy are all dependant on good quantification of these loads which will be detailed in the next sections. Load curves are ramped over some time to avoid impact numerical noise generated by sudden load application.

5.4.1. All round water pressure:

Water pressure load due to all round pressure on the hull cylinder, this pressure is constant with time at certain depth. This pressure is acting normal to the surface at the point of application assumed to be at the centre of element inward normal to hull vertical axis.

Pressure is function of depth $P = \gamma_{water} \times h$

γ_{water} = Sea water density = 1025 kg/m^3 = 10,250 N/m^3

Therefore, these values are readily applied by LS-DYNA3D through gravity loads for both the floating structure and ALE fluid elements. The constraints and the coupling actions at the fluid structure interface are working towards a (build up) action of this pressure using the defined equation of state.

5.4.2 Load curve for rotor rotation:

This curve assumes a constant speed of rotor rotation of 22 rpm angular velocity, representing rotor rotation at a rated wind speed and to be applied to all rotor parts. Where, 22 rpm = 22 $\times$ 0.105 = 2.31 rad/sec, tangential tip speed for transmission = $\omega \times$ r = 2.31 $\times$ 0.25 = 0.58 m/sec. This is transformed to a tangential blade tip speed of $\omega \times$ r = 69.3 m/sec with r = 30m for blade radius. For the load curve the rotor rotation was ramped from zero to its maximum value of 2.31 radians per second over a time interval of 0.1 seconds which could be extended if necessary, after which it remains constant for the required run time as shown in Figure (5.24).

x	y
0	0
0.1	2.31
2	2.31

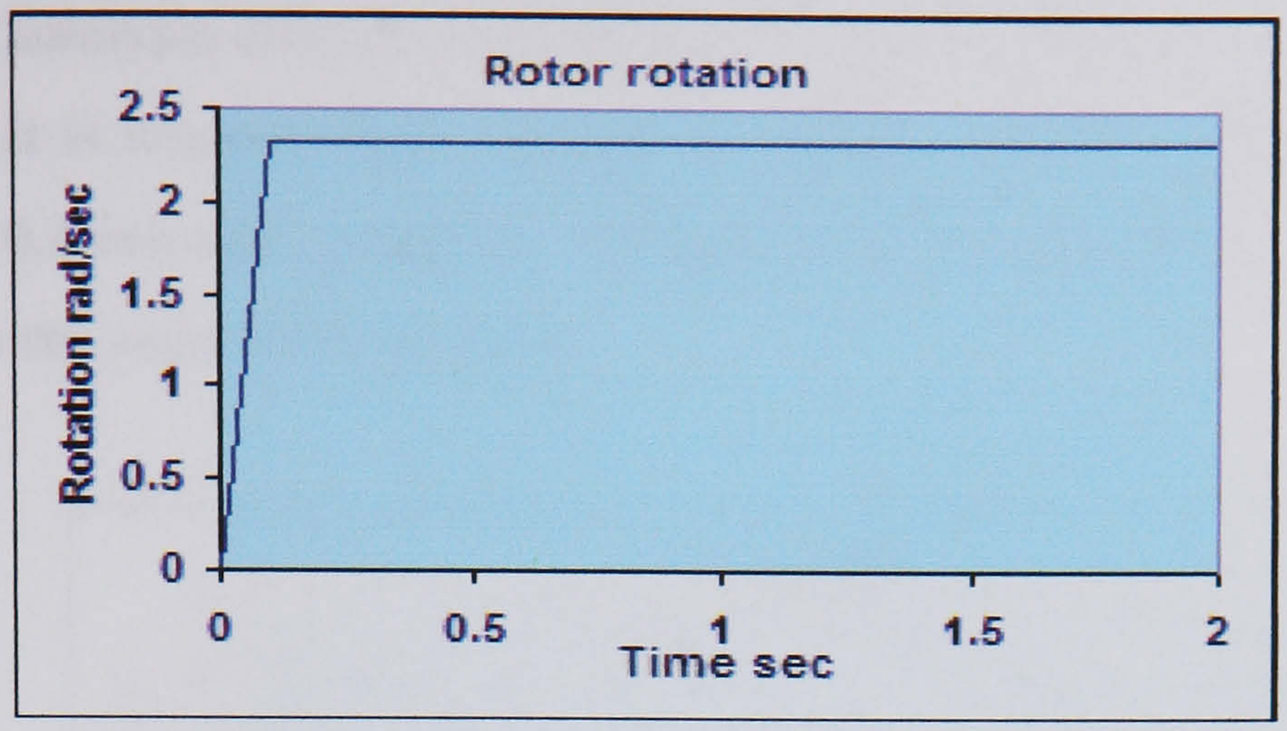

Figure (5.24) Load curve for rotor rotation

5.4.3 Load curve for drive rotation:

Assumed angular speed necessary for electrical generator is 1000 rpm, then $\omega = 1000 \times 0.105 = 105$ rad/sec and tangential tip speed = $\omega \times$ r = $105 \times 0.25 =$ 26.25 m/sec. The curve is shown in Figure (5.25) and is ramped from zero to its maximum value of 105 radians per second over a time of 0.1 seconds, after which it remains constant to the required time.

x	y
0	0
0.1	105
2	105

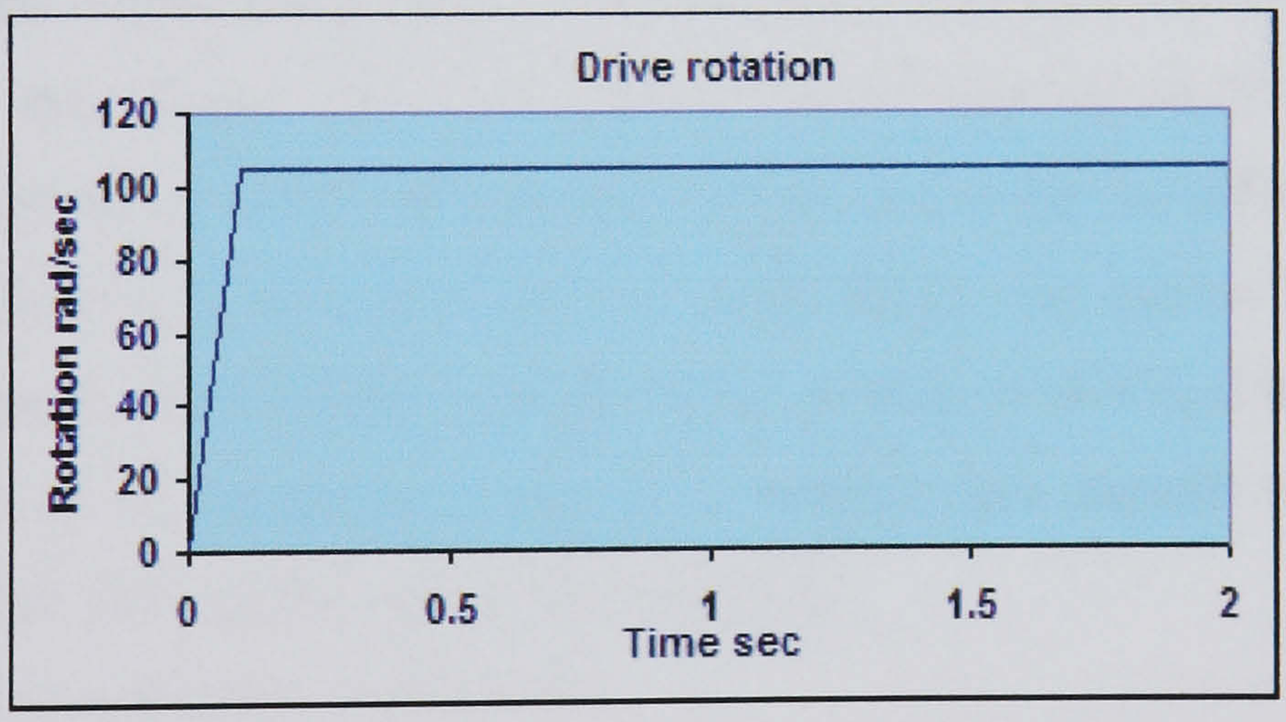

Figure (5.25) Load curve for drive rotation speed

5.4.4 Load curve for gravity:

This is applied via:

***LOAD_BODY_*Z*, part set containing either one part at a time or all parts together need be defined to use this function. With constant value of 9.81 m/sec^2 downwards along the vertical global coordinate, and a time values**

covers the whole analysis domain is defined. The gravity load curve is shown in Figure (5.26), it is ramped from zero to its maximum value of 9.81 m/sec^2 over a period of 0.1 seconds (could be changed if necessary) then continue to be constant up to the required run time.

x	y
0	0
0.1	9.81
2	9.81

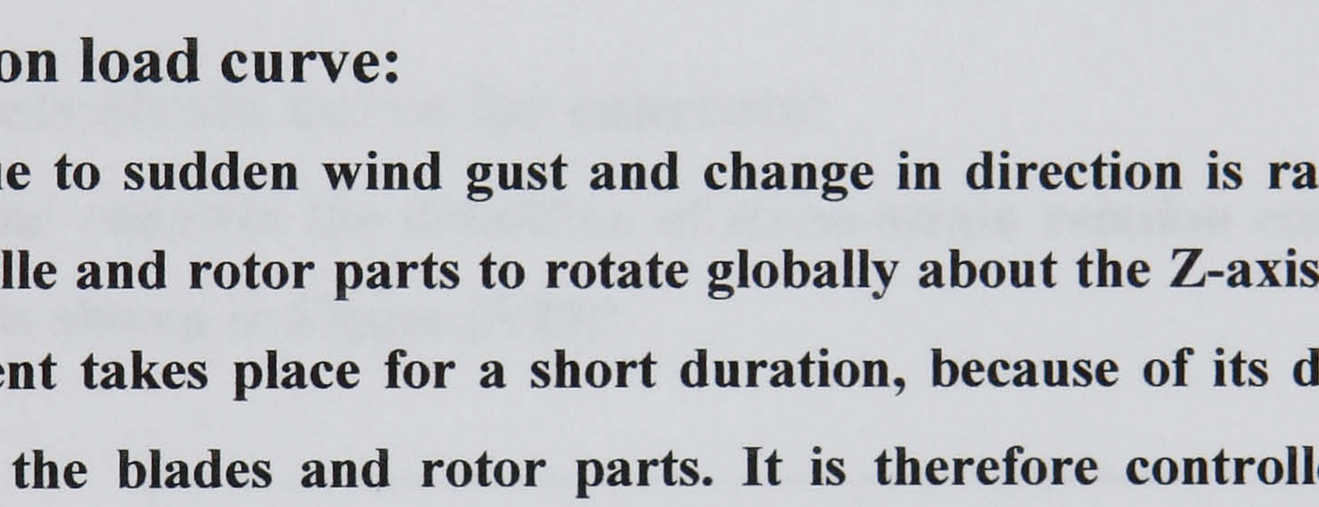

Figure (5.26) Load curve for gravity

5.4.5 Yaw rotation load curve:

Yaw movement due to sudden wind gust and change in direction is random and results in nacelle and rotor parts to rotate globally about the Z-axis. This alignment movement takes place for a short duration, because of its drastic negative effect on the blades and rotor parts. It is therefore controlled by reducing yaw speed to a very slow motion, thus reducing its effect to a negligible value. Should it be taken into consideration, the curve for this rotation against time need be defined and is shown in Figure (5.27), it is shown ramped from zero to its maximum value of 1 radians per second where it continue for 1 second and applied using the function:

*BOUNDARY_PRESCRIBED_MOTION

x	y
0	0
1	1
2	1

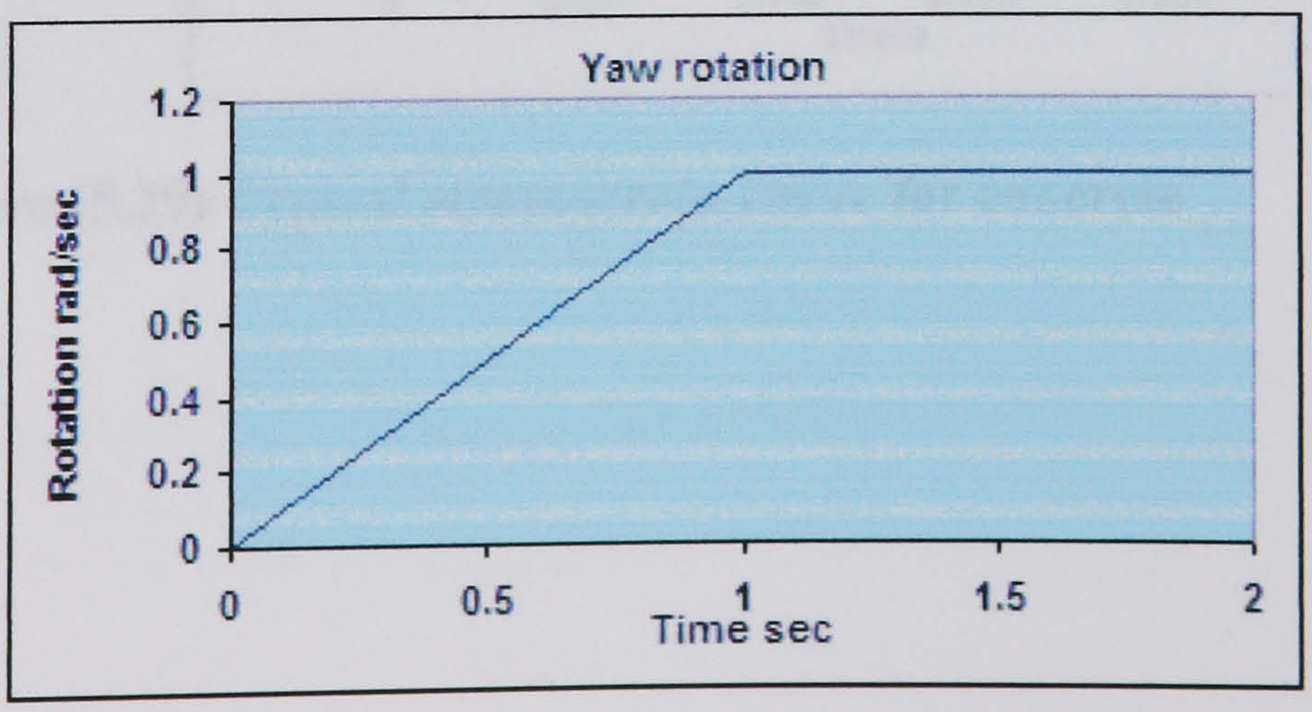

Figure (5.27) Load curve for yaw rotation

5.4.6 Typical stress-strain curve for steel:

As shown in Figure (5.28), these values are required for some functions and need be defined, ready for use.

X	y
0	0
0.0007	34
0.0013	150
0.0019	265
0.0057	394
0.012	463
0.0183	488
0.0246	483
0.0309	473

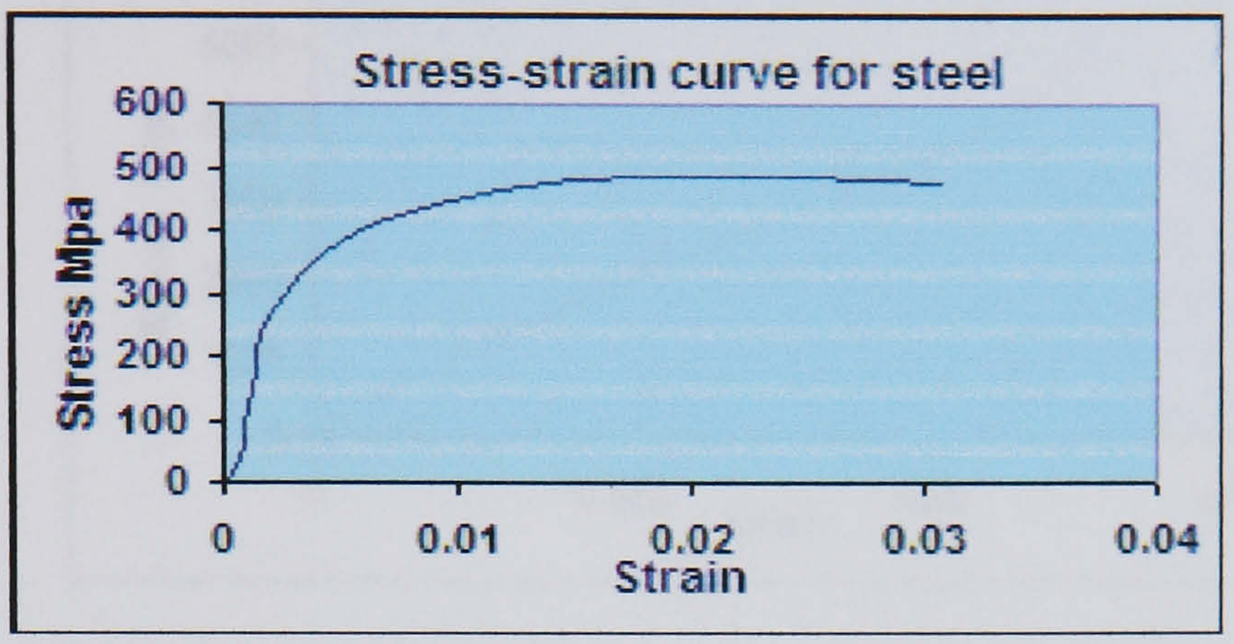

Figure (5.28) Typical stress-strain curve for steel

5.4.7 Typical stress-strain curve for concrete:

Some of the material requires the definition of stress-strain relation concrete stress-strain curve is shown in Figure (5.29):

x	y
0	0
0.00059	2.14E+01
0.00118	3.68E+01
0.00178	4.60E+01
0.00237	4.90E+01
0.00467	4.92E+01

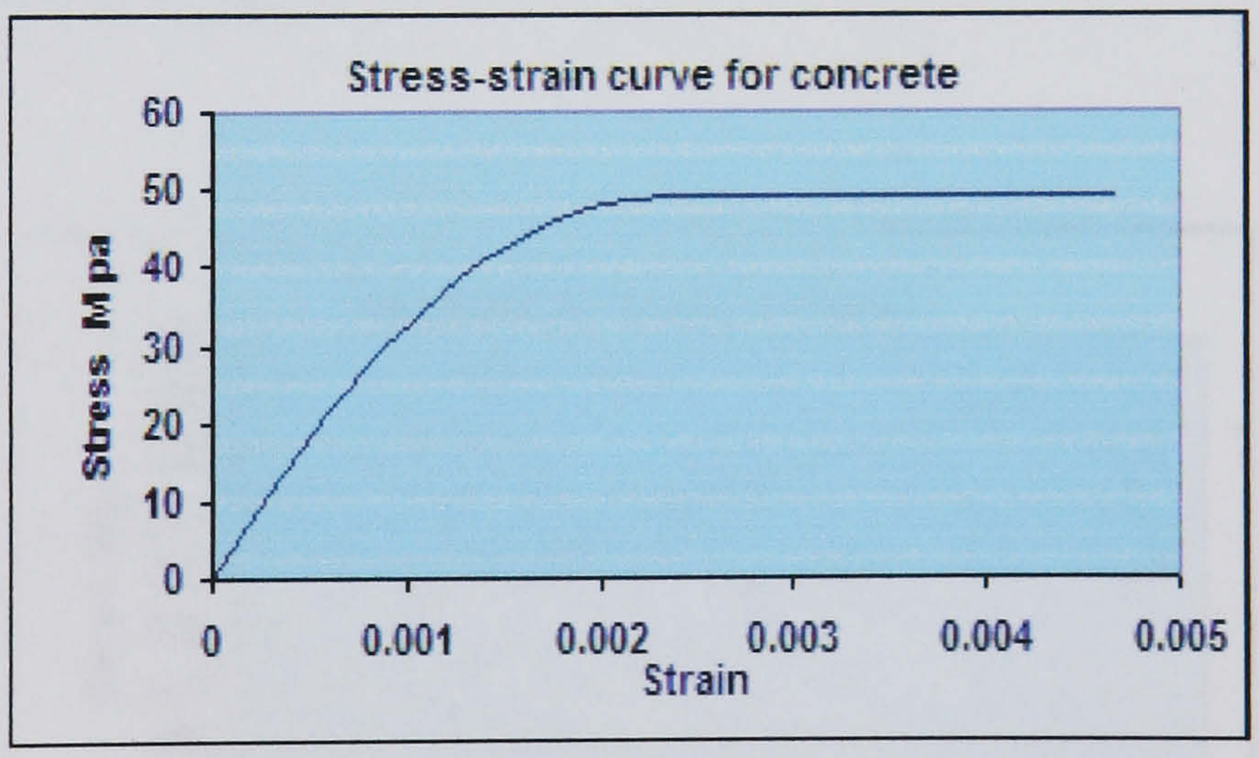

Figure (5.29) Typical stress-strain curve for concrete

5.4.8 Typical stress-strain curve for epoxy glass:

This is used for blades materials and this curve is shown in Figure (5.30).

x	y
0	0
0.0021	1.00E+03
0.005	2.00E+03
0.008	3.00E+03
0.011	4.00E+03
0.0125	5.00E+03
0.015	6.00E+03
0.018	7.00E+03
0.02	8.00E+03
0.022	9.00E+03

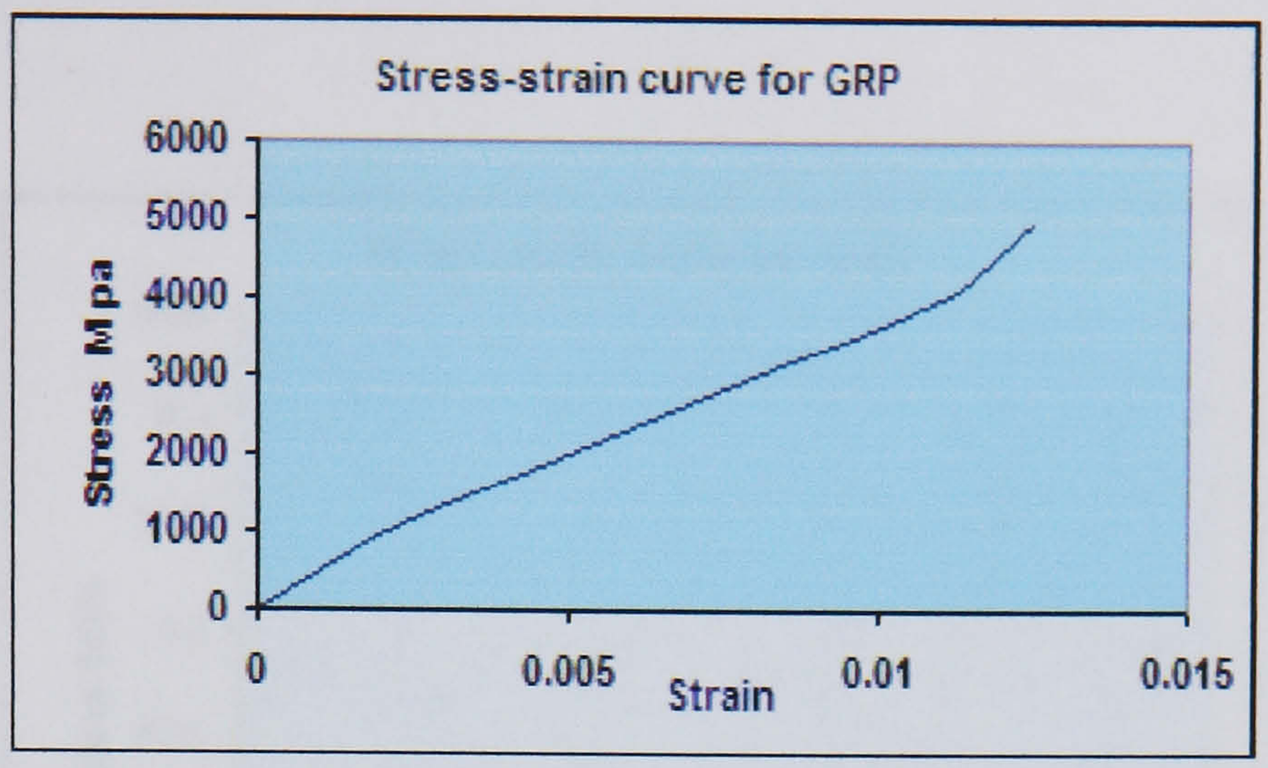

Figure (5.30) Typical stress-strain curve for epoxy glass

5.4.9 Typical stress-strain curve for copper:

Copper material properties are used for the generator, stress-strain curve is shown in Figure (5.31) mirror image of the compression test curve.

X	y
0	0
0.1	3.15E+02
0.2	4.38E+02
0.3	5.38E+02
0.4	6.30E+02
0.5	7.20E+02
0.6	8.13E+02

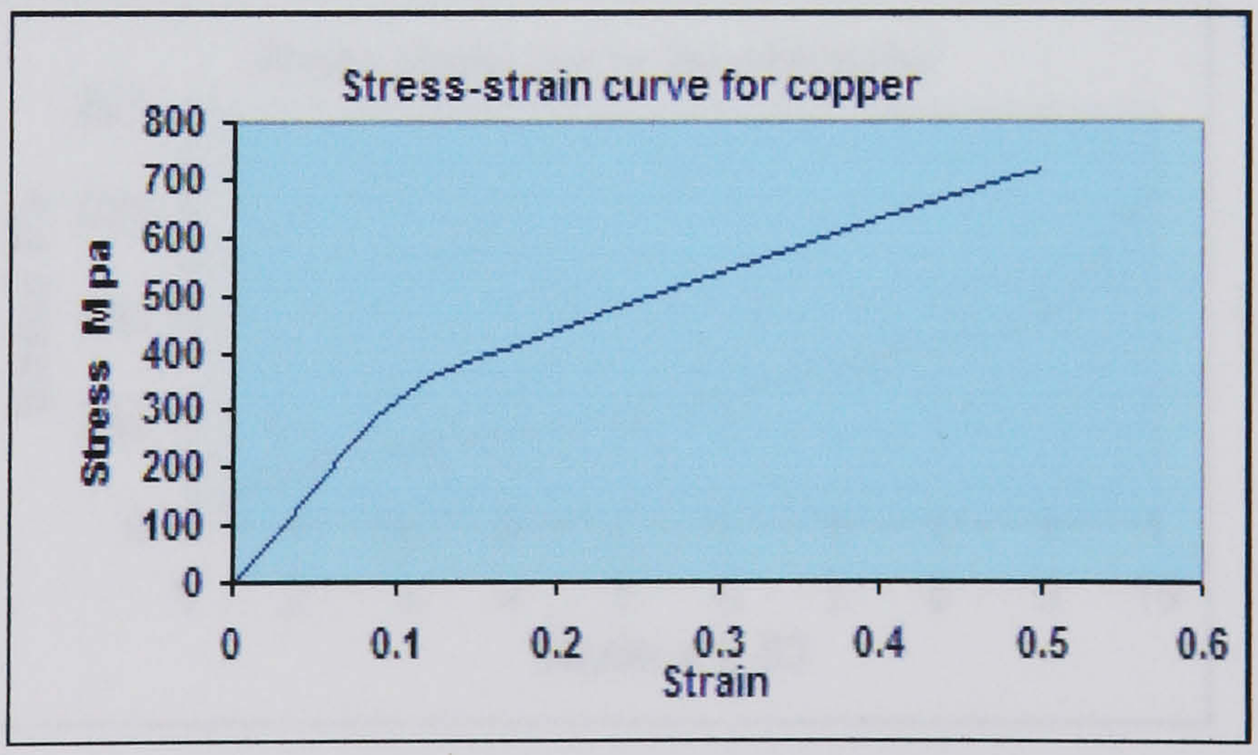

Figure (5.31) stress-strain curve for copper

5.4.10 Typical stress-strain curve for foam:

Synthetic low-density foam is used as filling inside the hull; stress-strain curve is shown in Figure (5.32).

x	y
0	0
0.05	2.17E-02
0.1	3.17E-02
0.15	3.67E-02
0.2	4.02E-02
0.25	4.33E-02
0.3	4.67E-02
0.35	5.04E-02
0.4	5.04E-02
0.45	6.04E-02
0.5	6.68E-02
0.6	9.09E-02
0.65	1.04E-01
0.7	1.41E-01
0.75	1.93E-01
0.8	2.90E-01

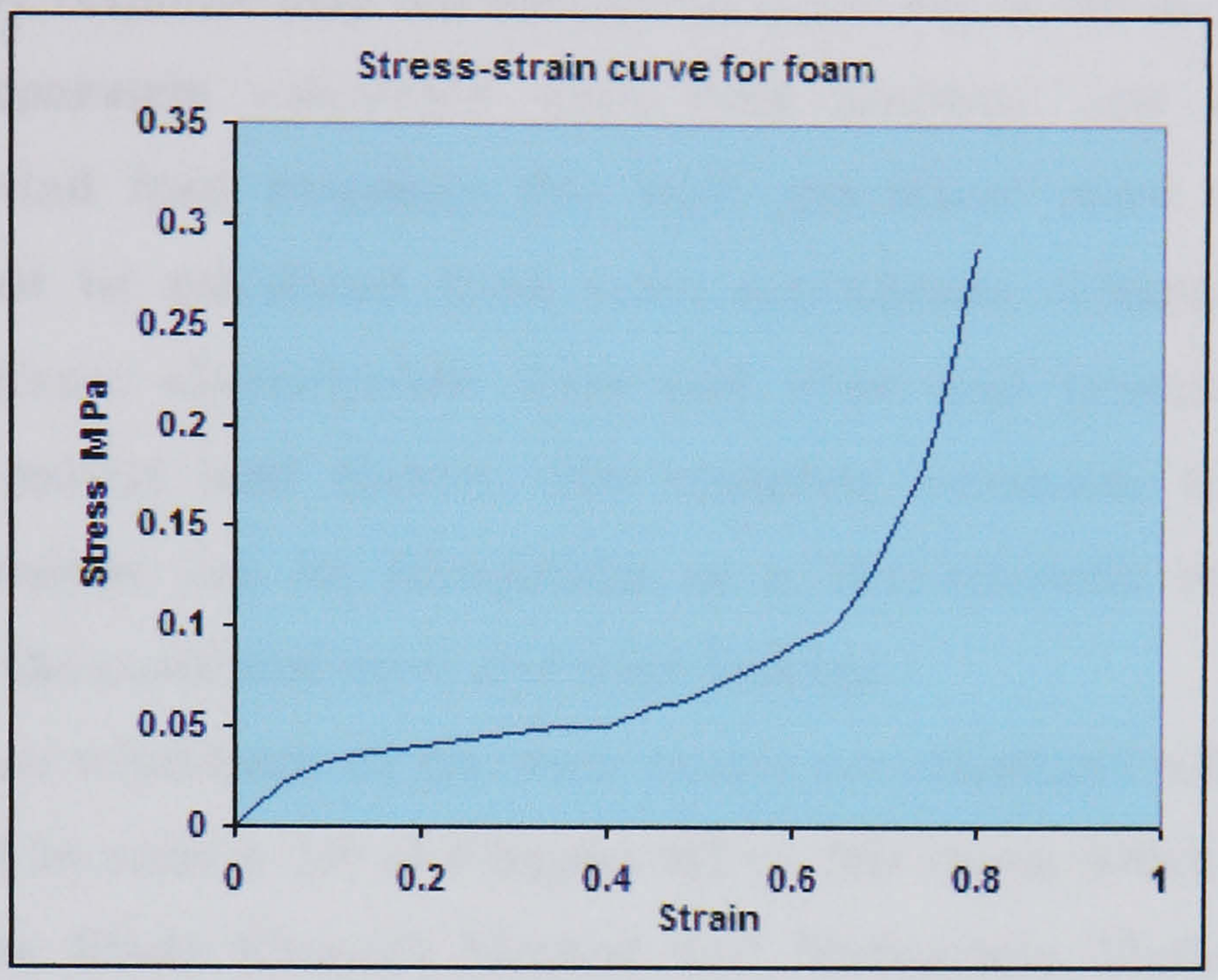

Figure (5.32) Typical stress-strain curve for foam

5.4.11 Typical stress-strain curve for polyester:

As required for taut mooring cables the curve is shown in Figure (5.33).

X	y
0	0
0.001	100
0.002	150
0.003	175
0.004	200
0.005	250
0.006	300
0.007	350
0.008	400
0.95	650

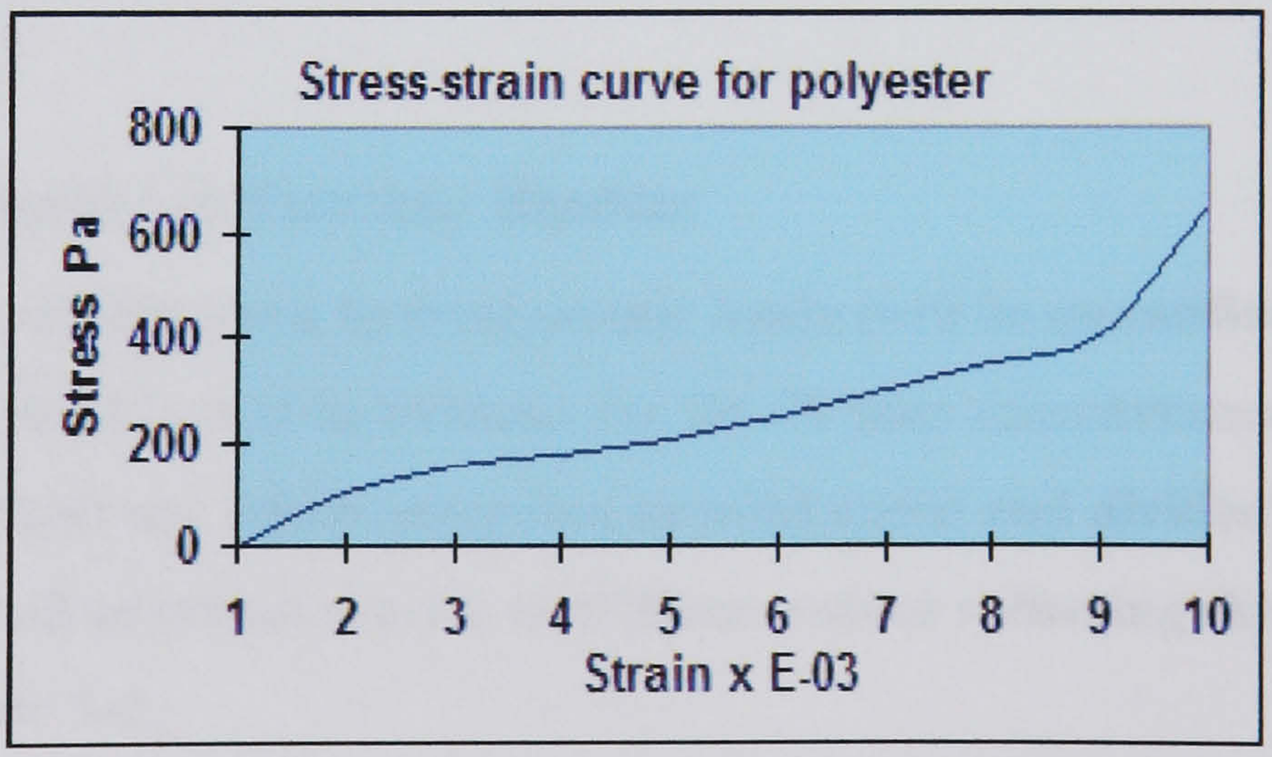

Figure (5.33) stress-strain curve for polyester

5.5 Load Combinations:

For a wind turbine structure, loads do not always combine linearly to give the sought after maximum load response as already discussed in Chapter IV of this thesis. Aero-elastic wind load calculations are likely non-linear, and the combined wind and wave response may not necessarily come out as the linear combination of the separately calculated wave load response and the separately calculated wind load response. For such non-linear cases the combined response must be calculated from some appropriate structural analysis, for the concurrent characteristic wave and wind load processes without applying any partial load factors. The resulting maximum load response from such analysis can be interpreted as a characteristic load response, which reflects the combined wave and wind loading.

In this work, aerodynamic wind loads on the rotor blades are calculated using the procedure discussed in section 3.8 of Chapter III of this thesis which is based on combining the Blade Element Method and Momentum Method theories. Meanwhile hydrodynamic effects of the sea condition on the supporting buoy are calculated by the Morison's equation also discussed in section 3.9 of Chapter III of this thesis based on linear superposition of wave and current actions. Quantification of these dominant environmental loads and their formulation for LS-DYNA3D solver is detailed in the sections to follow:

5.6 Aerodynamic Loads on Turbine Blades:

Throughout the course of this work hydrodynamic loads (will be quantified later) are assumed constant and at its extreme for the 50 year reoccurrence period. Aerodynamic loads are taken according to wind speed and divided to 5 cases believed to cover all practical service conditions, values reflecting these cases are shown in Table 5-2.

Following the methodology formulated in section 3.8 of Chapter III and Appendix-A3 both of this thesis, a MathCAD semi-automated worksheet was created to carry out the iteration process that will lead to pressure values per relative radius of blade. The outcome of the iteration for different radius 'r' values and corresponding airfoil chord length with pitch angle at a certain

angular rotor speed will be repeated for each of the above mentioned wind cases. Pressure values reflecting each wind speed calculated by the MathCAD sheet will be presented and simultaneously applied. This will represent wind pressure on the swept area nonlinearly changing over blade span. It is obvious that these values are unique to a certain blade with the defined airfoil family, radius, pitch angle and rotor angular speed. Therefore changing any of these parameters will result in a different nonlinear pressure profile distribution along the blade length.

Table 5-2 Service characteristics for the floating turbine analysis			
Case	Wind velocity m/s	Radial velocity rad/sec	Rotation rpm
1	5	1.78	17
2	12.5	2.31	22
3	22	2.52	24
4	26	Parked position	Parked position
5	40.5	Parked position	Parked position

Recalling the iterative technique mentioned before values for lift coefficient C_L and drag coefficient C_D defined for an angle of attack α for certain Reynolds' number (Re =1.6E06) are required to carry out the iteration process, therefore values for typical airfoil (Reso-1) are extracted from Jeppe Johansen [131]. This airfoil is purposely designed and tested for wind turbine blades and is used as input and shown in Table 5-3.

Table 5-3 Lift and drag coefficients for Reso-1 airfoil						
α	3	5	10	15	20	25
C_L	0.6	0.94	1.21	1.25	1.18	0.98
C_D	0	0	0.03	0.085	0.16	0.32

Furthermore application of the iteration technique requires an angle of twist for the blades airfoil, hence an optimum Betz (ideal) blade twist chord distribution against r/R (fraction of rotor radius) versus section pitch angle θ is readily taken from Manwell [78] and is presented in Table 5-4.

Table 5-4 Twist-chord distribution for optimum Betz blade		
r/R	Chord C in metres	Pitch angle
0.1	1.375	36.6
0.2	0.858	18.5
0.3	0.604	10.6
0.4	0.462	6.4
0.5	0.373	3.8
0.6	0.313	2.0
0.7	0.269	0.7
0.8	0.236	-0.2
0.9	0.210	-0.1
1	0.189	-1.6

In order to make use of this pressure scheme, constant pressure load curves are constructed at r/R values shown in Table 5-5, with intervals of the blade span i.e at 3, 6, 9, …….27m. Pressures at these distances are assumed to be the centre value of uniform load. These pressure ring load curves are input to LS-DYNA3D as nodal set loads where series of nodal sets coinciding with these relative radiuses are constructed in one node set then called to be acted upon by the relevant load curve. Dictated by the blade relative radius 'r' arbitrarily used in iteration to construct the pressure profile, a total of 9 load curves were extracted from the following table starting at 3m and ending at 27m blade radius. These load curves are different for each of the first 3 cases (non-zero rotational speed cases) shown in Table 5-2. The common characteristics between these nodes in each set is that they share the same radial location and hence the same pressure. Therefore a circumferential constant ring of pressure in the fashion shown in Figure (5.34) is used which is compatible with the assumptions used in attaining these pressure values. These constant pressure values are applied in the wind direction (negative y-direction) to simulate the downwind action and this direction is compatible with the action of the hydrodynamic loads (mentioned in the next section).

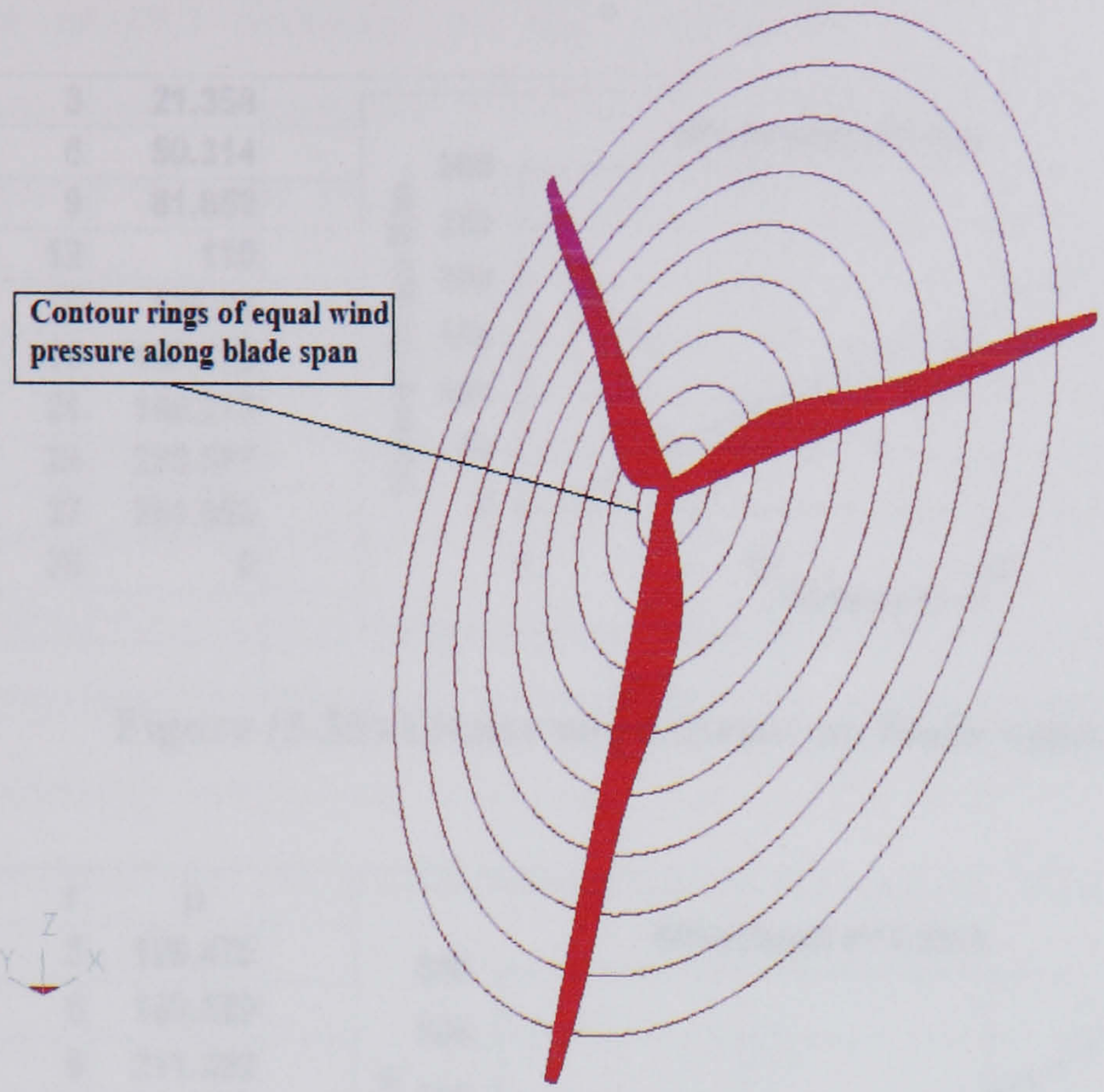

Figure (5.34) Equal radial wind pressure thrust rings

The above detailed procedure and with the use of the MathCAD routine iteration is valid for cases 1, 2 and 3 of Table 5-2 and results are detailed in Table 5-5.

Table 5-5 Equal wind pressure rings along blade span N/m

r m	Case1: V = 5 m/s	Case2: V = 12.5 m/s	Case3: V = 22 m/s
3	21.4	129.5	290.5
6	50.3	160.5	244.3
9	81.9	211.3	233.3
12	110.0	264.4	257.9
15	138.2	320.9	302.0
18	167.2	374.3	357.5
21	195.8	426.6	419.0
24	223.7	479.1	486.7
27	251.9	531.7	556.2
30	0	0	0

Linear pressure values summarized in Table 5-5 are presented in Figure (5.35) through Figure (5.37) for the 3 previous cases.

3	21.358
6	50.314
9	81.852
12	110
15	138.24
18	167.172
21	195.813
24	223.677
27	251.852
30	0

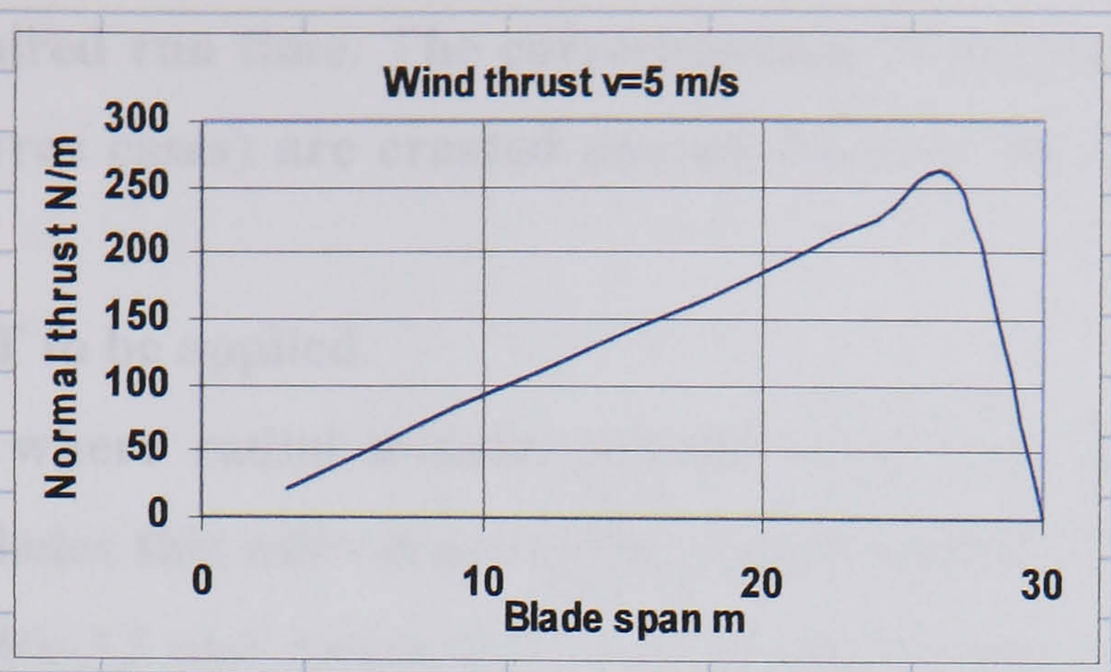

Figure (5.35) Linear wind thrust on blade span case 1

r	p
3	129.475
6	160.529
9	211.289
12	264.363
15	320.92
18	374.288
21	426.593
24	479.134
27	531.714
30	0

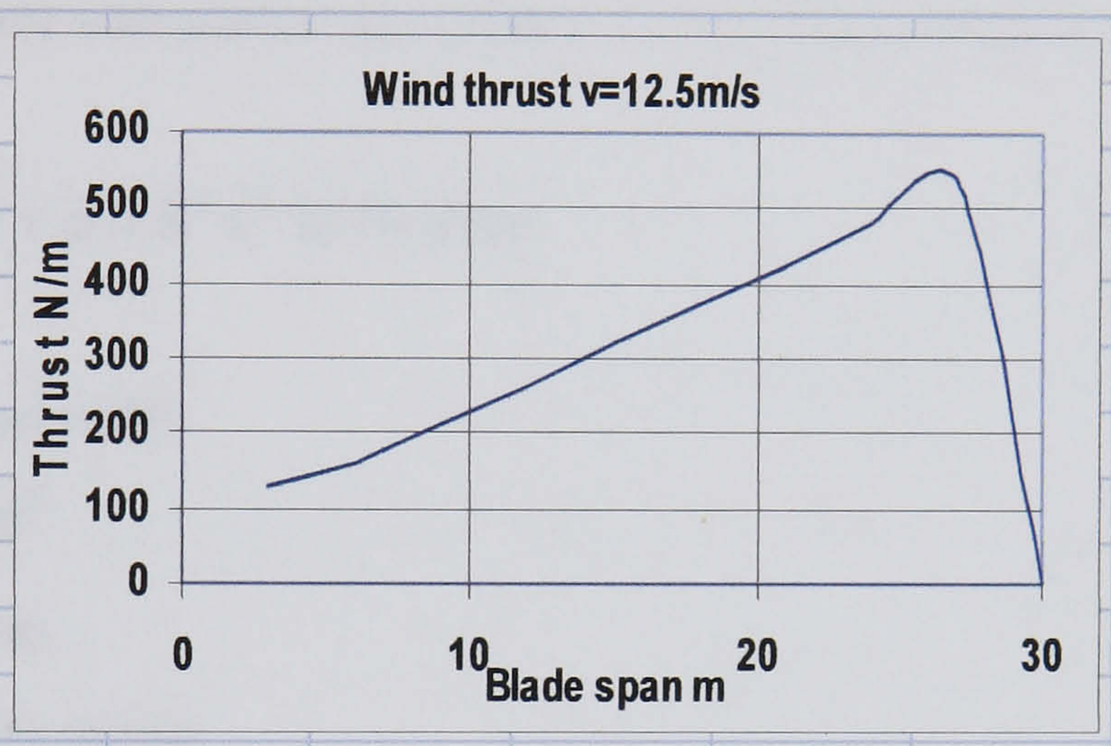

Figure (5.36) Linear wind thrust on blade span case 2

r	p
3	290.509
6	244.324
9	233.323
12	257.863
15	301.953
18	357.454
21	418.995
24	486.732
27	556.169
30	0

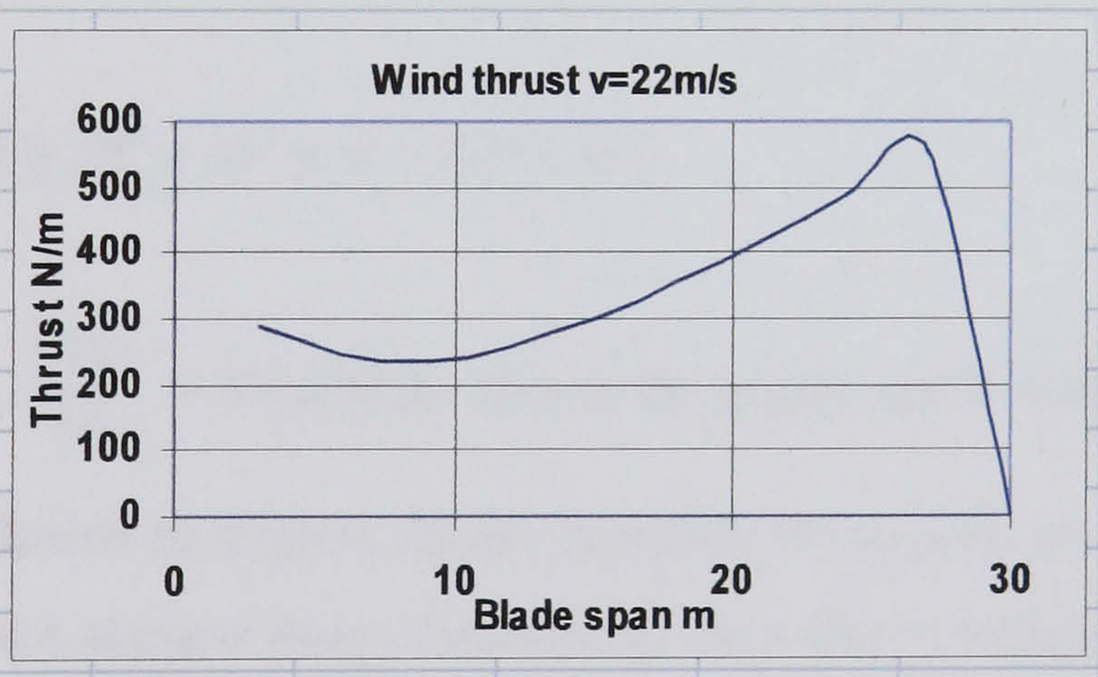

Figure (5.37) Linear wind thrust on blade span case 3

Therefore to feed these values in LS-DYNA3D, load curve for each of these 27 values shown in Table 5-5 (excluding zero values at 30m radius) are constructed ramped from zero to its maximum value shown in the previous

table at (0.1 seconds) or any required value then continuously applied throughout the required run time. The corresponding 27 nodal sets at radial distances (for the three cases) are created paving the way for the use of the load function:

*LOAD_NODE_SET to be applied.

For cases 4 and 5 where radial angular velocity ω is zero simulating the parked position of blades this will render angle φ (as discussed in section 3.8 of Chapter III, Appendix-A2 and Appendix-A3 all of this thesis) zero and hence parameters a and a' (also discussed in previous source) are undefined, and accordingly forces will show null values. Hence for these two cases constant wind thrust forces are calculated according to the formula (4.3.1) of Manwell [78] as follows:

Thrust $T = C_T \times 0.5 \times \rho \pi R^2 u^2$ in Newton 5.1

Where:

C_T = thrust coefficient = 8/9

ρ = air density kg/m^3

R = rotor radius in m

u = free wind velocity m/sec

Therefore:

For Case 4, which is the cut in wind (parked position wind speed) = 26 m/sec and thrust will be:

$T = 8/9 \times 0.5 \times 1.225 \times 30^2 \times 26^2 \times \pi = 1{,}041$ KN

Then:

The linear thrust is: $\frac{1041}{30} = 35$ KN/m, this is the value used in the load curve for this case and is shown in Figure (5.38) ramped from zero to its maximum value of 35 KN/m at 0.1 second then constant all over the remaining run time.

x	y
0	0
0.1	35
2	35

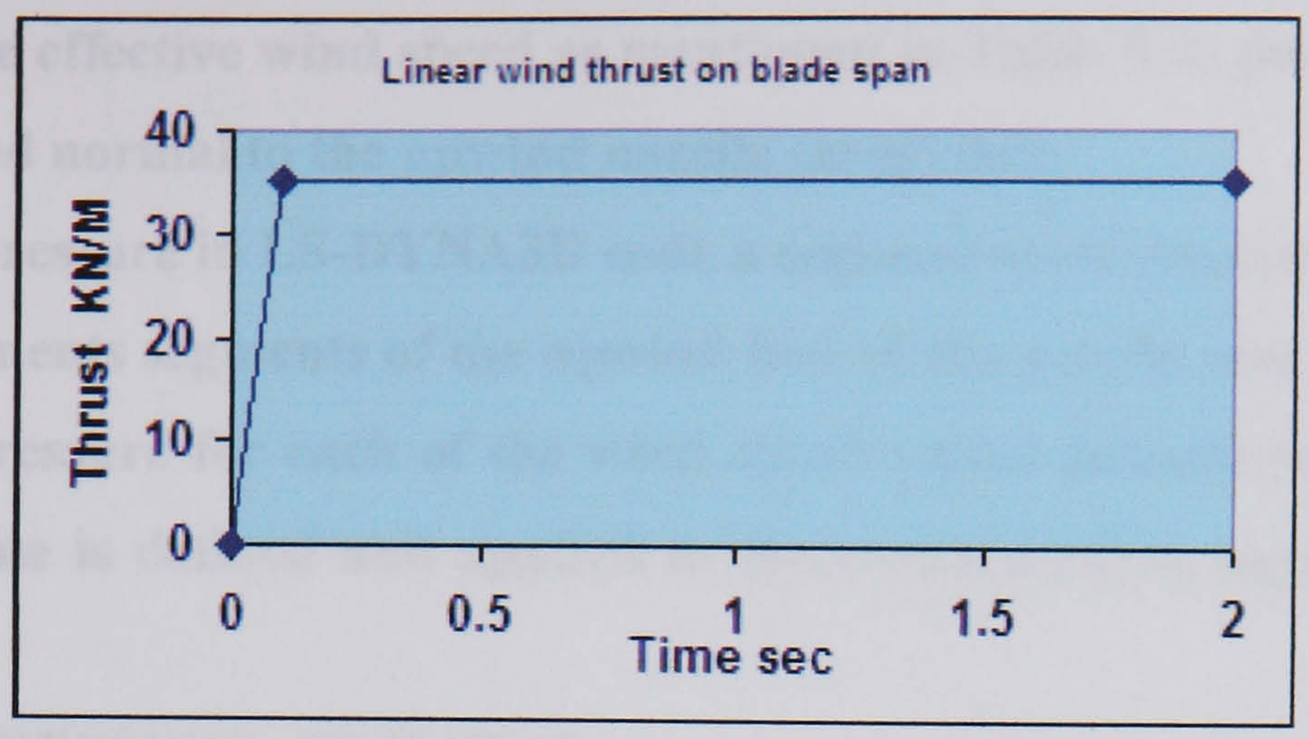

Figure (5.38) Linear wind thrust load curve for case 4

For Case 5: Which is the parked survival wind speed = 40.5 m/sec, thrust will be:

$\frac{1041}{26^2} \times 40.5^2 = 2526$ **KN and the linear thrust will be:**

$\frac{2526}{30}$ **= 84.2 KN/m and is shown for this case in Figure (5.39) ramped from zero to its maximum value of 84 KN/m at 0.1 second then constant afterward throughout the analysis.**

x	y
0	0
0.1	84
2	84

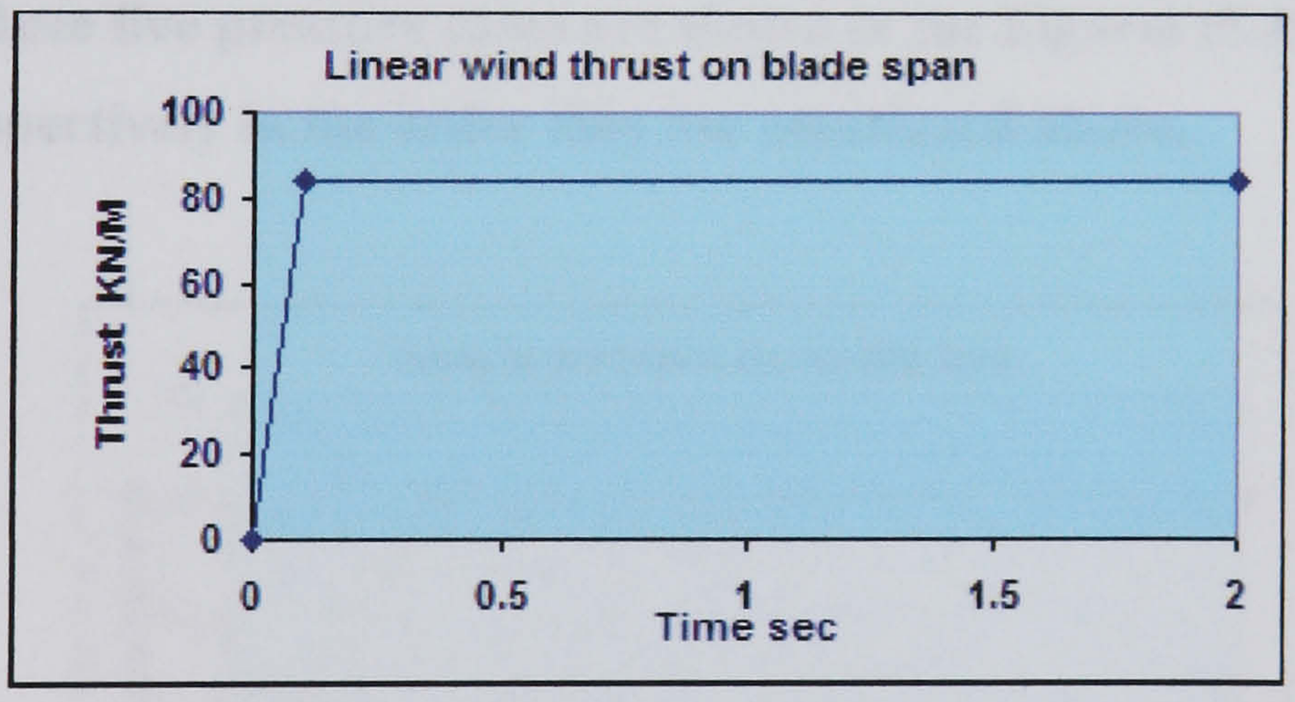

Figure (5.39) Linear wind thrust load curve for case 5

5.7 Wind Load on Nacelle Upwind Face:

The surface of the nacelle shell directly hit by wind suffers sustainable static pressure due to blowing wind, for the purpose of analysis the wind pressure (q_s) as defined by BS 6399-2:1997 [105] is used were:

$q_s = 0.613\, V_e^2$

Where V_e is the effective wind speed as mentioned in Table 5-2; pressure q_s in Pascal is applied normal to the upwind nacelle (area) face.

To apply this pressure in LS-DYNA3D code a segment set is created consisting of the shell elements segments of the upwind face of the nacelle and load curve representing pressure for each of the wind speed values (mentioned in Table 5-2) against time is defined and applied to the corresponding segment using the function:

***BC_LOAD_PRESSURE_SEGMENT**

For each of the 5 wind speed cases these pressures are calculated as follows:

Case 1:

$$q_s = 0.613\ (5)^2 = 15.325\ N/m^2$$

Case 2:

$$q_s = 0.613\ (12.5)^2 = 95.78\ N/m^2$$

Case 3:

$$q_s = 0.613\ (22)^2 = 296.69\ N/m^2$$

Case 4:

$$q_s = 0.613\ (26)^2 = 414.388\ N/m^2$$

Case 5:

$$q_s = 0.613\ (40.5)^2 = 1005.5\ N/m^2$$

Load curves for these five pressure cases are shown in the Figures (5.40) through (5.44) respectively in the order they are mentioned above.

x	y
0	0
0.4	15.3
2	15.3

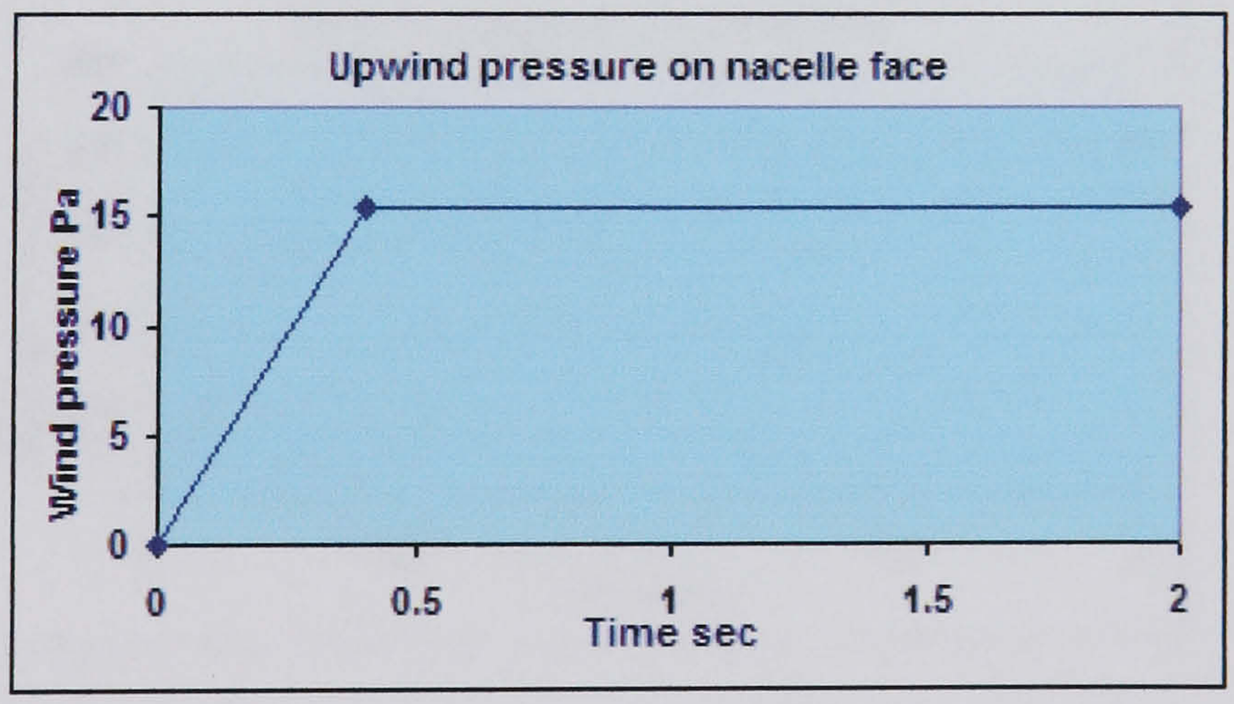

Figure (5.40) Upwind pressure on nacelle face for case 1

x	y
0	0
0.4	95.8
2	95.8

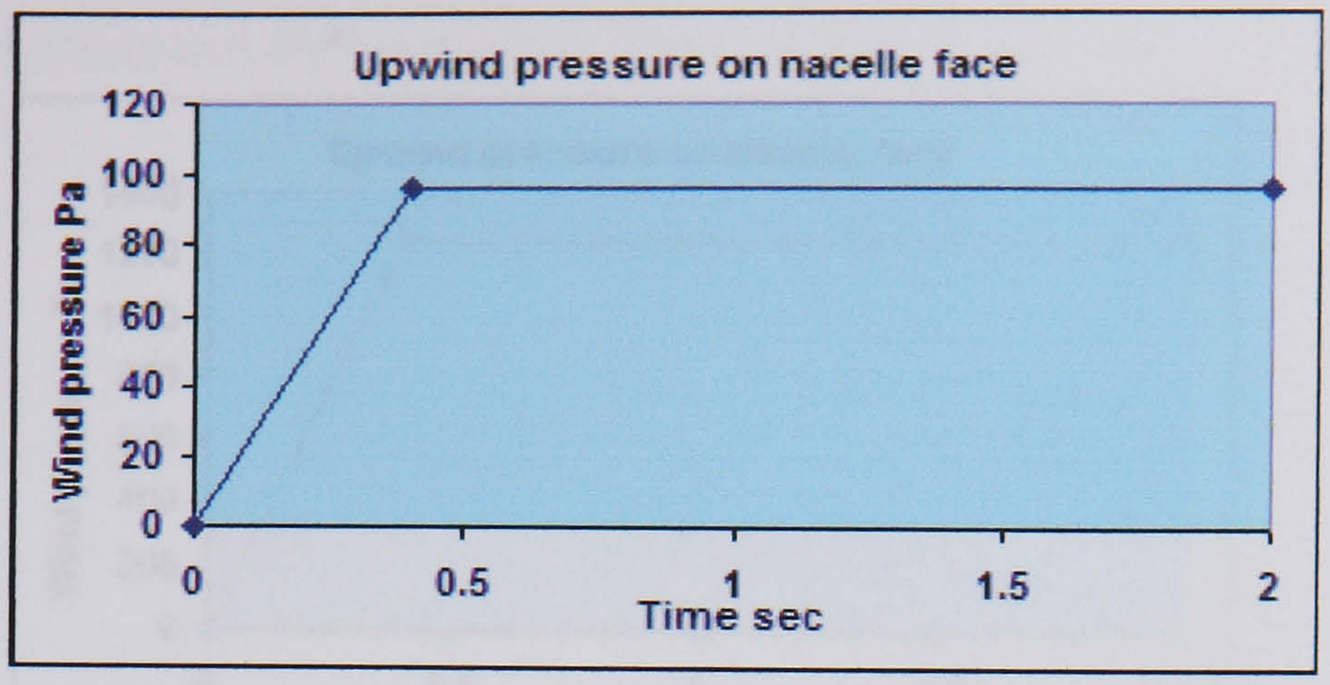

Figure (5.41) Upwind pressure on nacelle face for case 2

x	y
0	0
0.4	296.7
2	296.7

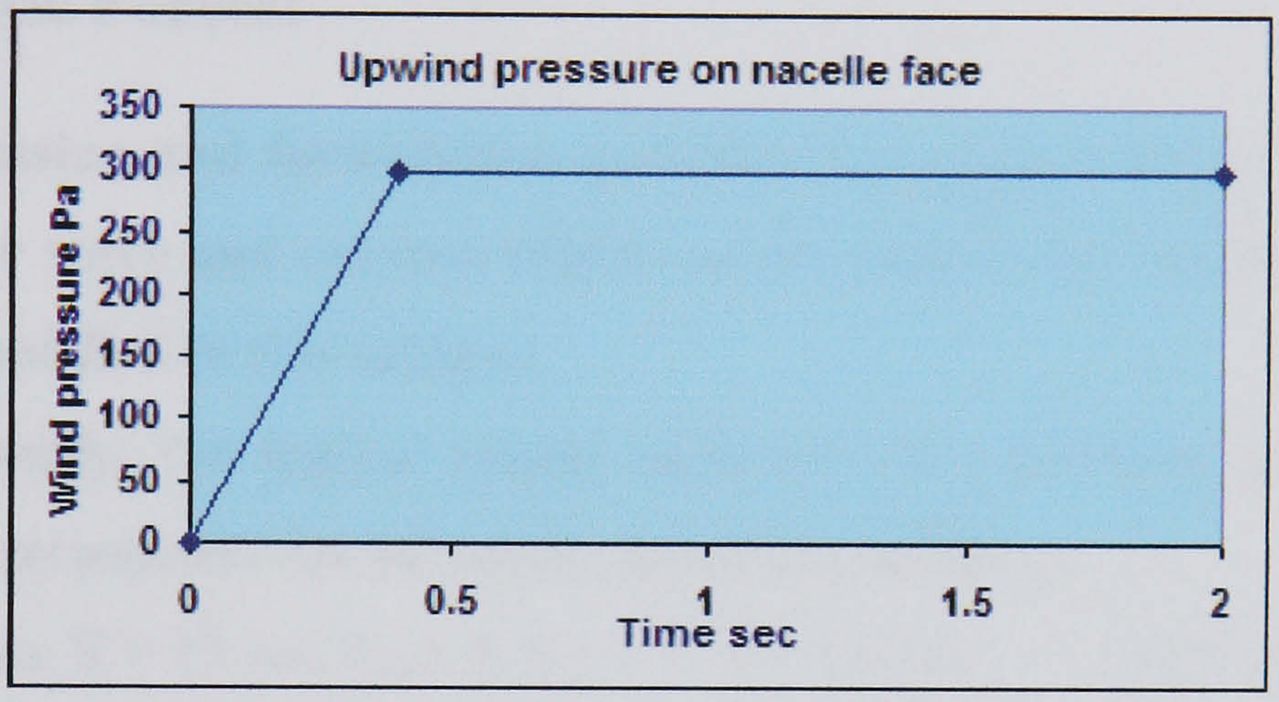

Figure (5.42) Upwind pressure on nacelle face for case 3

x	y
0	0
0.4	414.5
2	414.4

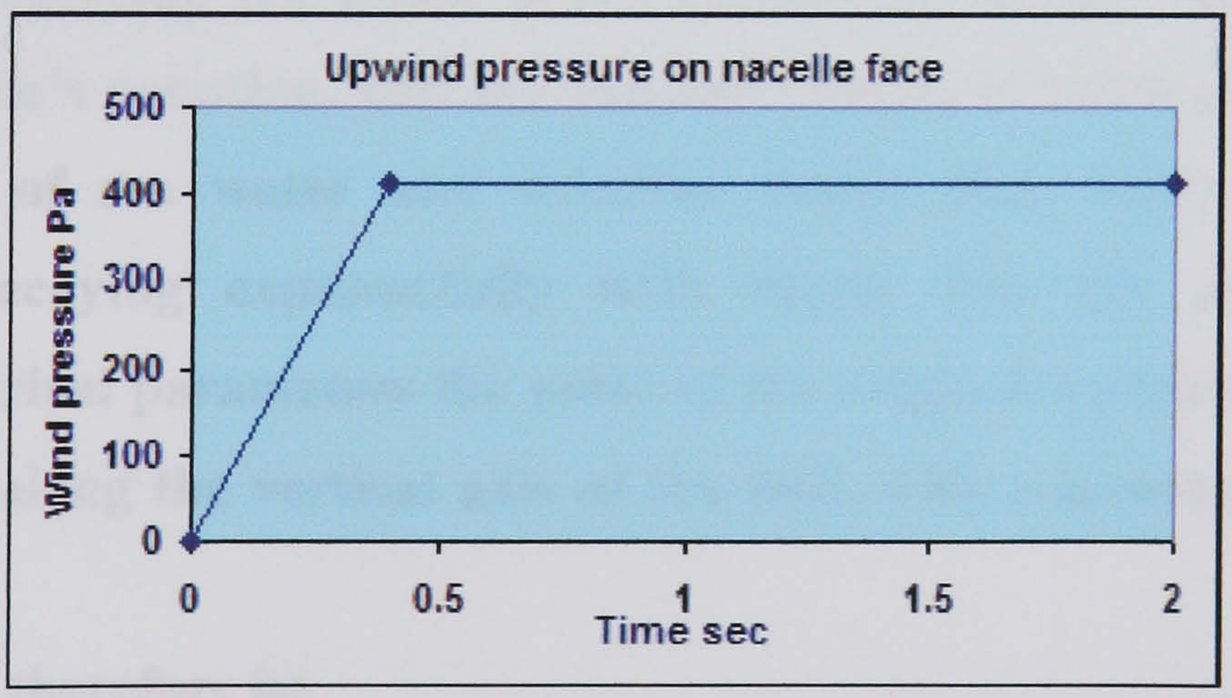

Figure (5.43) Upwind pressure on nacelle face for case 4

x	y
0	0
0.4	1005.5
2	1005.5

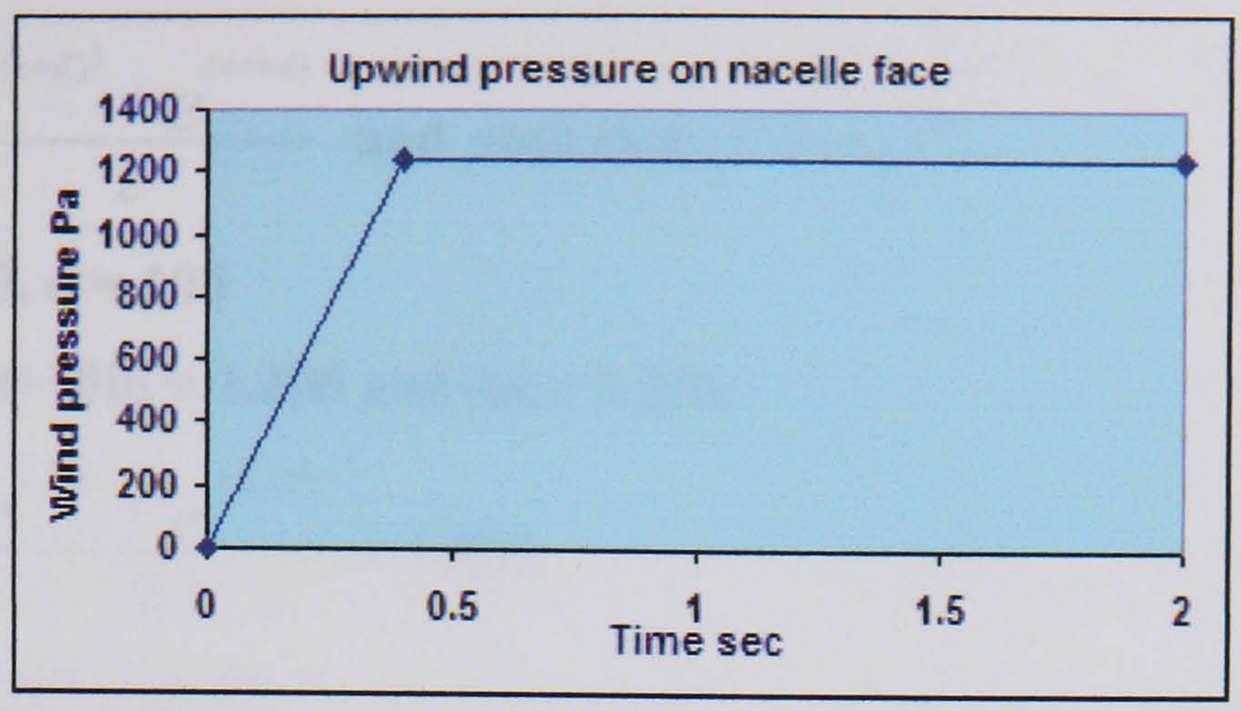

Figure (5.44) Upwind pressure on nacelle face for case 5

5.8 Hydrodynamic Forces:

Based on the discussion and formulation mentioned in section 3.9 of Chapter III of this thesis for wave and current effects on the supporting concrete hull, these loads are quantified in this section:

As stressed previously, the typical values used for sea conditions represent British North Sea parameters for 50 years extreme conditions:

H = 28 m, L = 500 m, T = 17 sec, C_d = 1, C_m = 2, d = 100 m, ρ = 1,025 kg/m^3

D = 12.5 m, surface and tidal current velocity = 1.5 m/sec

The wave number k = $\frac{2\pi}{L}$ = 0.01256, area (A) = $\frac{\pi D^2}{4}$ = 122.72 m^2

Surface and tidal currents are added to the kinematics velocity vector value used in the Morison's equation, and the current velocity is taken as 1.5m/sec for the top 10m of sea water and 0.5m/sec below that, water particles kinematics are decaying exponentially with depth. For the purpose of calculating geometrical parameters the point of the origin is assumed to be at the water surface along the vertical axis of the hull, with z assumed positive upward.

The Morison force therefore is:

$F = F_{drag} + F_{inertia}$

The Morison equation will be evaluated at the still water level (z = 0m) and at the bottom end of the concrete base disk (z = -25m) with a linear variation assumed in between. Therefore wave kinematics at these two levels is calculated using the above typical values.

The hyperbolic functions are defined using the exponent values as:

$$\cosh k(z+d) = \frac{e^{k(z+d)} + e^{k(z+d)}}{2} \quad \text{and} \quad \sinh(kd) = \frac{e^{kd} - e^{-kd}}{2}$$

At the surface z = 0, d = 100

k(z+d) = 0.01256 (0+100) = 1.256 and kd = 1.256

$$\therefore \cosh(1.256) = \frac{e^{1.256} + e^{-1.256}}{2} = 1.898$$

$$\sinh(1.256) = \frac{e^{1.256} - e^{-1.256}}{2} = 1.61$$

Wave kinematics velocity and acceleration at the water surface are:

$$V_c = \frac{\pi \times 28 \times 1.989}{17 \times 1.6} \times 1 = 6.12 \text{ m/sec}$$

Superimposing current velocity then V_c = 6.12 + 1.5 = 7.62 m/sec

$$a_c = \frac{2\pi^2 \times 28}{17} \frac{1.893}{1.6} \times 1 = 38.5 \text{ m/sec}^2$$

$$F_{drag} = 0.5 \times 1 \times 1025 \times 12.5(7.62)^2 = 371{,}975 \text{ N} = 372 \text{ KN}$$

$$F_{inertia} = 2 \times 1025 \times 122.72 \times 38.5 = 9{,}685{,}676 \text{ N} = 9{,}686 \text{ KN}$$

$$F_{surface} = 371975 + 9685676 = \underline{10{,}057{,}651 \text{ N}} = 10{,}058 \text{ KN}$$

These forces are evaluated at the bottom level of the circular concrete base disk where;

z = -25 m, d = 100 m

Therefore k(z+d) = 0.01256 (-25+100) = 0.9427 and kd = 0.0125 (100) = 1.256 then

$$\cosh(0.94275) = \frac{e^{0.94275} + e^{-0.94275}}{2} = 1.4783 \text{ and}$$

$$\sinh(1.256) = \frac{e^{1.256} - e^{-1.257}}{2} = 1.61$$

$$V_c = \frac{\pi \times 28}{17} \times \frac{1.4783}{1.61} \times 1 = 4.78 \text{ m/sec, superimposing current velocity at this}$$

depth it became

$$V_c = 4.78 + 0.5 = 5.28 \text{ m/sec and wave particles acceleration is}$$

$$a_c = \frac{2 \times \pi^2 \times 28}{17} \times \frac{1.478}{1.61} \times 1 = 30 \text{ m/sec and hence forces are}$$

$F_{drag} = 0.5 \times 1 \times 1025 \times 12.5(4.53)^2 = 131{,}462$ N = 131 KN and

$F_{inertia} = 2 \times 1025 \times 122.72 \times 30 = 7{,}547{,}280$ N = 7,547 KN and the bottom level force is

$F_{bottom} = 131462 + 7547280 = \underline{7{,}678{,}742 \text{ N}} = 7{,}679$ KN

The underlined are the forces at the water level and at the base disk bottom level predicted by Morison's equation. As mentioned before the force between these two points is assumed to vary linearly, an assumption fairly close to the actual profile for analysis purposes. Noticeably, the inertia force is dominant at both points which was expected, the trapezoidal profile force is acting linearly normal to the concrete hull vertical surfaces in the negative y-direction coinciding with wind direction and measured in N/m schematic drawing of this load profile is shown in Figure (5.45).

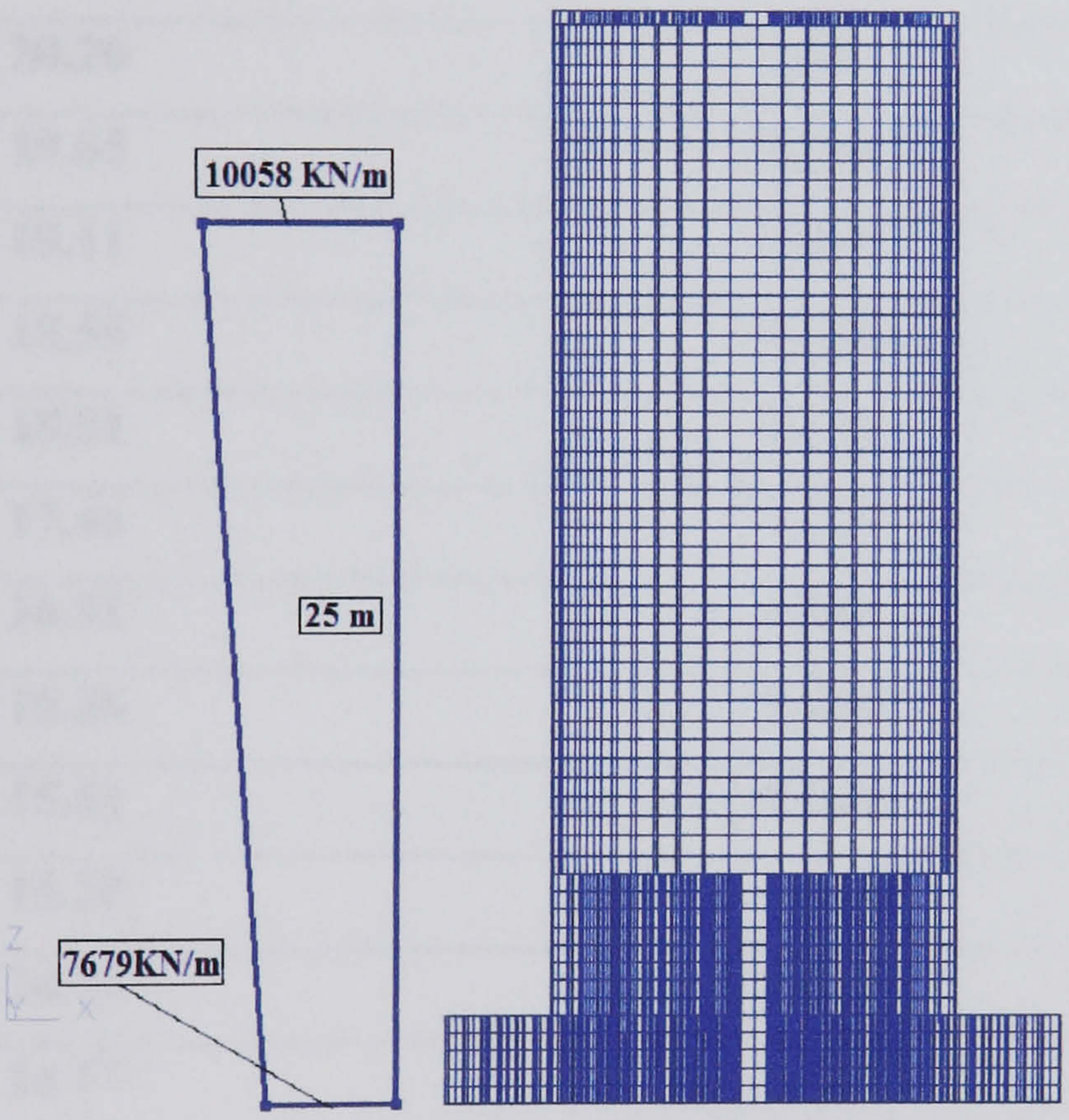

Figure (5.45) Hydrodynamic loads on supporting hull vertical side

To formulate these linear pressure forces to be readable by LS-DYNA3D, corresponding force values for all nodes located on the plane x = 0 and for the given elevation are used in creating constant load versus time curves, then applied as a point load on the relevant one node set. These loads at different elevations are tabulated in Table 5-6 are extracted from Figure (5.45). To be

compatible with downwind loading of the rotor, loads are considered in the negative global Y-axis.

Table 5-6 Horizontal hydrodynamic pressure on buoy vertical side	
Elevation m	**Normal force KN**
24.58	**10,018**
24.03	**9,966**
23.48	**9,913**
22.94	**9,861**
22.39	**9,809**
21.84	**9,757**
21.29	**9,705**
20.74	**9,653**
20.20	**9,601**
19.65	**9,548**
19.11	**9,496**
18.55	**9,444**
18.01	**9,392**
17.46	**9,340**
16.91	**9,288**
16.36	**9,236**
15.81	**9,184**
15.28	**9,131**
14.72	**9,080**
14.17	**9,027**
13.62	**8,975**
13.07	**8,923**
12.53	**8,871**
11.98	**8,819**
11.43	**8,766**
10.88	**8,714**
10.34	**8,662**
9.79	**8,610**

9.24	8,558
8.69	8,506
8.14	8,454
7.60	8,401
7.05	8,349
6.50	8,297
6.0	8,250
5.5	8,202
5.0	8,155
4.5	8,107
4.0	8,059
3.5	8,012
3.0	7,964
2.5	7,917
2.0	7,870
1.5	7,821
1.0	7,774
0.5	7,726
0.0	7,679

5.9 Summary of Employed Contacts and Constraints:

One of the very specific features of the LS-DYNA3D code is its wide range of available constraints and its ability to model complicated contacts between different parts to simulate the physical behaviour of the integrated model. Due to the generality of the code certain tricks some times are needed to apply certain constraint or contact, e.g. some of the constraints are only available to rigid material parts, therefore such part need to be defined as rigid material. The employed constraints and contacts are summarised here:

i) **Cable part termination nodes at top and bottom are firmly fixed for translation and not rotation through boundary condition constrained linear interpolation, where end nodes of the cables are constrained to the surrounding nodes of the seabed part, more than**

one node of the surrounding seabed part is constrained to the cable end node to minimize local stress effects.

ii) Seabed part is defined as finite rigid wall and hence it is given rigid material, all parts nodes are slaved to it. A gap equals half of the seabed shell thickness is left between water part bottom and seabed line to accommodate proper contact.

iii) Water part side and bottom nodes are constrained against movement as one set in the three translations, this is necessary to prevent the flow of the ALE material, thus initiating pressure build up within it.

iv) Water part side segments are given non-reflecting boundary to model the indefinite domain through the absorption of the travelling wave rather than reflecting it.

v) Hull and cables are coupled to ALE parts (water and air) via constrained Lagrange in solid, with penalty type 4 for hull and type 2 for cables.

vi) Hull and foam are contacted through automatic surface to surface in which the foam part (the softer material) segments are the slave.

vii) Contact interior is applied to foam (soft material) to combat negative volume error initiation in foam elements.

viii) Hull is contacted to cable part via contact automatic nodes to surface in which all cable nodes are slaved to all hull segments to prevent cable elements overlapping with hull elements in case of large distortion.

ix) Top cable nodes are constrained to the surrounding hull nodes at the interface points this is done through constrained interpolation, to avoid local high stress and probable (local) failure more than one hull node is constrained to neighbouring cable end node.

x) A set containing hull, foam and tower nodes are constrained as extra nodes to the bearing ring (rigid part) to model full integrity.

xi) Bearing and yaw rings are connected via 'joint revolute' to allow relative rotational movement necessary for the yaw system.

xii) Nacelle box is slaved to gear, generator, transformer and yaw ring using merged rigid bodies feature, hence all need be rigid this

action guarantees solid connection between nacelle and its internal parts and assures the common yaw action for all parts above the bearing.

xiii) Driver is linked to gear via 'joint revolute' to model rotational connection but no relative displacements of the two parts.

xiv) Transmission part is constrained to nacelle part via 'joint revolute' to join full fixity coupled with rotation ability about local axis of the transmission, this requires both parts to be rigid.

xv) Hub and nacelle flat faces are defined to each other by contact automatic surface to surface appropriate gap is assured between the two shell meshes to account for the sum of half of both sections to guard against penetration numerical noise.

xvi) All blades nodes are constrained as extra nodes to the transmission part to assure full fixity of the rotor parts.

xvii) All hub nodes are constrained to the transmission part as extra nodes to assure full integrity of the rotor action.

xviii) Blades root segments and hub internal segments are contacting each other by contact automatic surface to surface, the automatic contact found to be more robust in prevention of the warning messages which might be source of numerical noise. A proper gap between the two meshes to account for the sum of half of both shells is maintained to avoid penetration problems.

xix) A gap equals half the hollow tubular section diameter used in the tower part is left above and below the tower geometry to account for necessary offset required by contact to avoid penetration problems.

5.10 Analysis Phase:

Now at this stage all necessary data have been established to create the input data file using the pre-processor. Exporting it to the LS-DYNA3D solver for running the model for analysis is the next step in this direction. Changing the model geometry, material properties, loading and or boundary conditions for any reason (if needed) is straight forward process that can be incorporated in

the analysis at any stage. Considering changing important environmental parameters to simulate extreme conditions and different critical load cases and occurrences will be the first priority. The probability of integrating different environmental conditions to simulate the actual situation has been done through application of hydrodynamic loads at its maximum 50 year period while wind loads are changed according to the 5 service conditions mentioned in this chapter.

The outcome of the analysis is expected to yield quantities such as stresses, strains, bending moments, forces, velocities, displacements and kinetic energies. All these values will be attained and presented by the post-processors attached to the LS-DYNA3D analysis code. Values may be presented for the whole structure, certain materials, parts or a set of parts, elements or nodes giving good flexibility for representing such information. Experience obtained from running the verification models in Chapter IV of this thesis and from preliminary analysis on the full scale model have led to the conclusion that both time and memory capacity resources required are beyond that of single personal computer currently employed. With time step in the order of '10^{-7}' the number of time steps involved in the solution will be well beyond half a million cycles necessitating the use of double precession version of the code to combat the numerical round off errors and parallel cluster of hardware arrangements to fulfil memory and time requirements. Both features are not currently available, therefore left as further future suggested work.

CHAPTER VI

Discussions, Conclusions and Future Work

6.1 Discussions:

The main questions which invariably need to be answered preferably before any detailed model is constructed are:

- **What level of detail is sufficient to model the structure appropriately for its intended purpose?**
- **Does the modelling philosophy and techniques adopted achieve this?**

Validation and verification work was carried out at Chapter IV of this thesis and its objective was to answer these questions for use in a detailed model of Chapter V. The aim was to push the finite element analysis to its limit so the latest techniques were investigated and employed, however this highlighted potential problems both in complexity, formulation difficulties in some aspects of the modelling and the level of detail adopted. Whilst the validation work was being carried out the 'detailed' model was being constructed and was subject to analysis runs under straightforward load cases such as gravity and transverse wind loading.

A considerable degree of debugging was carried out on the detailed model. Analysis runtime was significantly longer than those models adopted for verification, so it was important that as many issues were addressed as possible before embarking on each run.

The detailed study of buoyancy indicated that the ALE formulation was working as expected, and indeed yielded more insight into the real behaviour than at first had been anticipated. As the dynamics of the structure are captured in the finite element modelling, there are always certain issues when comparing with a 'pseudo-static' hand calculation for the purposes of verification. However these are more concerned with the shortcomings of the calculation based on statics rather than any real problems with the finite element formulation. As buoyancy is

fundamental in capturing the real behaviour of the structure, this part of the work gives confidence that the behaviour of the anchored structure under the action of external loading from wind etc would be captured correctly. It would be difficult to verify and validate to any great degree that behaviour under external loading was being modelled correctly, however the confirmation that buoyancy effects are working allows the modelling techniques to proceed to this next phase.

It was evident from the buoyancy study that there are many features associated with the more detailed models which would merit further parametric investigation. To probe further into these areas would required dedicated studies and expand the work beyond its current limitations.

The output of 'time-histories' such as pressures/stresses at interfaces, displacements etc. and general observations of the model behaviour were validated and verified against calculations where possible. Referring to the time histories, anomalous results where high frequency 'noise' was captured was shown to have little global effect on the model behaviour once filtering had taken place. Although the source of the 'noise' either from internal reflection or fluid-structure interfaces is still open for debate, this give little cause for concern as its effects do not appear to be influencing the model in any way. Frequency analysis was inconclusive, so this will provide a point of discussion for future detailed analysis regarding fluid-structure interfaces and energy absorbing boundaries.

In terms of results from the three dimensional models, the two main issues were the size of the model and the formulation of the cable mooring system. The immense size of the final model was constricting in the lengthy run-time required before each set of results could be processed. Once the problems with the cable modelling was discovered in the validation models it was evident that this was still going to be a problem with the detailed model so the value of the results would be limited by this.

In answering the first question above with regard to detailing, it could be argued that the level of detail in certain parts of the model are not necessarily required, i.e. the level of detail for the parts above the tower. However the only issue with the formulation of these parts is really the increased analysis runtime with an increase in element provision. Therefore the decision was made to leave these parts as detailed as possible, and the validation work would highlight any potential difficulties with this area of the model.

6.2 Conclusions:

- **The LS-DYNA3D code is for sure capable of modelling the floating offshore wind turbine in terms of geometry, constrains, different loads applied and boundary conditions that need be employed to capture complications involved in contacts.**

- **There is no rapid solution to the long time required to run explicit analysis for such a big structure, the application of the time reducing techniques employed in the LS-DYNA3D code thought expected to reduce run time but may not do so significantly.**

- **Load regime based on simple combination of all service loads using well established combination criteria is possible and its results are fed to LS-DYNA3D code as load curves in the input file.**

- **The downwind blades and free yew system seems to be a good choice for the offshore wind turbines, also the avoidance of constant speed gear or generators will contribute to the economy of the wind turbine through producing power in as many operational speeds as possible.**

- **Due to the nature of the high stresses at the maximum survival wind speed, some sort of control (pitch, stall or blades deflect as a rush in the**

wind) must be applied to adjust blades orientation thus reducing these stresses at the extreme conditions.

- **Rotor and nacelle vertical loads must be evenly distributed around the vertical axis to reduce moments arising from non-symmetry.**

- **Catenaries mooring or steel cable mooring are deficient compared to taut polyester mooring both in their gravity loads, fatigue properties and footprint this is however needs further investigation.**

- **Overall structural stability is the main structural concern for the floating wind turbine especially in the survival wind speeds, therefore the blades control mentioned earlier should help addressing these concerns.**

- **Minimizing the lateral movement of the floating structure will increase energy capture and reduce fatigue effects but will increase local stress.**

- **Improving the aerodynamics of both the supporting structure and the superstructure is vital in reducing the effects of the applied loads and hence cheaper design.**

- **Because the centre of mass of a horizontal axis wind turbine is quite high a massive structure is necessary to support the wind turbine. Hydrodynamic stability is achieved by moving the centre of mass as low as possible through placing the ballast in the lowest possible location this will lead to further elongation of the support structure which minimize the heave motion due to wave action.**

- **The location of some parts e.g. the transformer part (if needed) does not need to be in the nacelle, therefore locating such parts some where**

either at the seabed or at the floating surface of the turbine will contribute good deal to reducing the weight of the superstructure thus lowering the centre of gravity of the whole assembly and consequently increasing the restoring moment and improving the buoyancy stability.

6.3 Future Work

There is no doubt that LS-DYNA3D provides a state of the art approach to modelling complex dynamic problems, but with this comes increased validation and verification work, debugging, and analysis runtimes. This project has certainly highlighted these aspects, and although some problems have not been resolved, there is much value in the work achieved so far.

- **The ALE formulation appears to have worked for simple float models, however, further comparison to other simulations for fluid-structure interaction such as spring and damper analogies or normal Lagrangian formulations can definitely highlight its superiority, providing the way forward in this field. Complex dynamic load regimes may be used to simulate the real cases once workable models are achieved.**

- **The work has identified areas which warrant further investigation and parametric study. The effects of buoyancy were dealt with in a detailed study, but this forms only one of a number of important issues to ensure that the global model behaviour is captured correctly. For example, the fluid-cable interaction problems were not resolved fully and could form an extension of the buoyancy study. Also the correct representation for the loading on the wind turbine blades may be investigated through fixed base models, thus verifying this part of the model is working correctly. Until these are studied in depth, the full extent of the issues is still**

unquantifiable at this stage, but this report has gone some way to addressing some of the issues and highlighting others.

- **A distinction is now made between the needs of industry and research. Turbine aerodynamics technology and design is well known so there is probably very little that work such as this can offer in this focussed area. However the global behaviour of the structure and forces as a whole, especially when floating is subject to conservative design rules and it is this aspect which the research is attempting to give insight to.**

- **Much of industry is concerned with 'fit-for-purpose' solutions so the fact that many products are governed by conservative designs may be of little consequence in some areas. However offshore wind farming is big business and it is likely that this industry will be interested in economic design which may be demonstrated through FE analyses such as that performed within this study.**

- **For the future, it is suggested that the ALE approach be pursued further. Potential problems with the mooring systems will require debugging to further the workability of the model, and further studies should pay heed to the latest finite element technology, as this is a very forward moving area (new techniques are always just around the corner in the present climate). This is also true of the available computing power which will decrease the analysis runtimes.**

- **There ought to be better use of the advances in material technology in terms of good use of composite materials for different parts involved to assure safe integral functions of these parts combined with good energy production, less cost and less maintenance requirements.**

- **Applied loads estimations need be revolutionised, this is better established through more research being done in the field of long term collection of sea state and wind data both vertically and horizontally, analysing them and tabulate them to be readily available or incorporated in the design codes, atlases and guidelines if the conservatism in the design is to be avoided.**

- **More emphasis is required on the fatigue analysis of the floating wind turbine. This must include the assurance of the superiority of the polyester mooring in fatigue properties both in more research in its material properties as well as improvement and in long term observation of the fatigue action and durability to combine these advantages with its light weight positive effect.**

- **Further work need be established to close the gaps available in compatibility of both the LS-DYNA3D solver and its attached post and pre-processors, avoiding the formatted keyword, enhancement of the debugging and error reporting techniques, the use of the double precession, rewriting the manual in a more user friendly method and introduction of more complicated practical examples if this code is to attract more users and be competitive in its field.**

- **An automation of the calculation of the aerodynamic and the hydrodynamic service loads experienced by the floating turbine will contribute to the efficiency of the analysis process, allow for easier parametric investigations and help avoid human errors in load predictions. This automation will be better if incorporated in the code used for analysis.**

- **Further investigation is needed where the results of more than one explicit code or from a sequential analysis or field measurements on full scale floating turbine are calibrated against those of the LS-DYNA3D code.**

Finally the installation of floating offshore wind farms based on this concept will demonstrate the viability of the project and provide valuable data and experience for analysts and designers and will further highlight the issues of utmost priority for this industry. Such early installation will also pave the way for resolving just which agencies have jurisdiction over which activities and will push forward the resolution of ambiguities and legal rights both nationally and internationally.

REFERENCES

[1] Vugts J h et al "Design of the Support Structure of an Optimised Offshore Wind Energy Converter" Proc. EWEC' 99 (1999).

[2] Swift R H & Dixon J C 1982, "Design Wave Forces on Offshore Structures", BWEA 4th wind energy conference Cranfield UK.

[3] LSTC "FEMB (Finite Element Model Builder) versions 28" User's Manual, A pre-processor for use with LS-DYNA, PDF online file, LSTC website. http://www.lstc.com/, June 2003.

[4] Khün M et al "Opti-OWECS Structural and Economic Optimisation of Bottom-Mounted Offshore Wind Energy Converters" JOULE III project, Delft University of Technology, Delft, Netherlands, August 1998.

[5] Ivan Holland et al (Editors) "Design of Offshore Concrete Structures", publisher Spon Press.

[6] Martine C M "Physical and Numerical Modelling of Offshore Foundations Under Combined Loads" Ph. D. thesis New College Oxford University Trinity Term 1994.

[7] Cassidy M J "The Non-Linear Dynamic Analysis of Jack up Platforms Under Random Ocean Waves" Ph. D. thesis 1999, Oxford University, UK.

[8] Bell R W "The Analysis of Offshore Foundations Subjected to Combined Loading" M.Sc. thesis 1991, Civil Engineering, Oxford University, UK.

[9] de Santa Maria P E L (1988) "Behaviour of Footing for Offshore Structures Under Combined Loads" Ph.D. thesis, Civil Engineering, Oxford University, UK.

[10] K. C. Tong "Technical and economic aspects of a floating offshore wind farm" Journal of Wind Engineering and Industrial Aerodynamics 74-76 (1998) 399-410.

[11] LSTC "LSPOST A New Post Processor For LSDYNA", May 1999, Livermore Software Technology Corporation, PDF online file, LSTC website. http://www.lstc.com/ , April 2003.

[12] Weil Thomas G "Preliminary Design of Three Fixed Offshore Wind Generator Support Structures" 1949-publication: 1975 Doc. Type: Book libraries:1

[13] Ude Todd C 1994 "TFPOP: Program for Analysing Second-Order Load and Response Models of Offshore Structures", reliability of marine structures report No. RMS—15, Stanford University.

[14] Bjerager et al "Reliability Method for Marine Structures Under Multiple Environmental Load Processes" Proceedings of the 5th International Conference on Behaviour of Offshore Structures, Tronheim, Norway, June 1988, Vol. 3, pp. 1239–1254.

[15] Winterstein S R and Haver S "Statistical Uncertainties in Wave Heights and Combined Loads on Offshore Structures" Journal of Offshore Mechanics and Arctic Engineering, ASME, May 1991. Presented at the 9th International Conference on Offshore Mechanics and Arctic Engineering, Houston TX Feb. 1990.

[16] Freris L. L "Wind Energy Conversion Systems" Printice Hall 1996.

[17] Reuter A. and Borman A "New Concepts and Optimal Design of Steel Towers for Large Wind Turbines" Proceedings of the EUWEC Conference 1996, p. 231.

[18] Barthelmie R J et al "Prediction of Offshore Wind Speeds–a comparison of methods BWEA Conference p. 93 1985.

[19] D I Page editor, British Wind Energy Association "Prospects for Offshore Wind Energy: The state of the art and future opportunities", DTI / BWEA, ETSU report no. 126, June, 29th 1993.

[20] Patel M H "Dynamics of Offshore Structures" Butterworth 1989.

[21] Clause G F and Birk L "Design of Optimum Structures Based on Long Term Wave Statistics" 17th OMAE Conference 1998, paper 0521.

[22] Various editors "Advanced Offshore Engineering" Benthham press 10/ 1994

[23] Winterstein et al "Reliability of Floating Structures: Extreme Response and Load Factor Design" Journal of Waterway Port and Coastal Engineering ASCE July/ august 1999.

[24] Houlsby G T et al "Research on Offshore Foundations: Papers at Offshore Technology Conference 1999" OUEL report no. 2197/ 98 Department of Engineering Science, Oxford University, UK.

[25] Anderson O V "Design Regulations for Offshore Wind Farms– specification for concrete and steel structures" OWEMES 2000 conference proceedings Rome: ENEA, 2000.

[26] Gud P "Offshore Wind Turbine Foundation Concepts–Monopiles" OWEMES 2000 conference proceedings Rome: ENEA 2000.

[27] Boccotti P "Wave Mechanics for Ocean Engineering" Elsevier Science 2000 ISBN: 0-444-50380-3.

[28] Boss "Behaviour of Offshore Structures" Elsevier Science 1997.

[29] de Rider H A J "Design and Construct" of complex civil engineering systems: A new approach to organizations and contracts Ph D thesis DUT Netherlands 1996.

[30] Kühn M et al "Opti–OWECS final report Vol.0: Executive Summary" Delft University of Technology (DUT), Netherlands 1998.

[31] Kühn M et al "Opti–OWECS final report Vol. 1: Integrated Design Methodology for Offshore Wind Energy Conversion Systems" DUT Netherlands 1998.

[32] Kühn M et al "Opti–OWECS final report Vol.2: Methods Assisting the Design of Offshore Wind Energy Conversion Systems" DUT Netherlands 1998.

[33] Cockerill T T et al "Opti–OWECS final report Vol.3: Estimates of Costs of Offshore Wind Energy at European Sites" DUT Netherlands 1998.

[34] Ferguson (editor) M C "Opti-OWECS Final Report Vol. 4: Atypical Design Solution for an Offshore Wind Energy Conversion System" DUT Netherlands 1998.

[35] Cockerill T T "Opti–OWECS Final Report Vol. 5: User Guide OWECS cost model" DUT Netherlands 1998.

[36] Kühn M "Technology Reference Systems and Conventions to be Used Within Opti–OWECS project" DUT Netherlands 1996.

[37] Mathies H G et al "Study of Offshore Wind Energy in the EC–OULE 1 (JOUR 0072)" Verlag Naturlich Engergien, Brekendorf, Germany 1995.

[38] Kühn M et al "Towards a Mature Offshore Wind Energy Technology"– guidelines for the Opti–OWECS project, Wind Energy, issue April 1999.

[39] Henderson A R et al "Floating Offshore Wind Energy" Presented at the BWEA Conference 20, Cardiff University UK September 1998.

[40] Kühn M et al "Structural and Economic Optimisation of Bottom-Mounted Offshore Wind Energy Converters" overview on final results of the Opti–OWECS. http://www.windenergy.citg.tudelft.nt/content/research/pdfs/ew99mk1.pdf, March 2003.

[41] Zaaijer M B et al "Towards Selection of Concepts for Offshore Support Structures for Large Scale Wind Turbines" July 2003. http://www.ct.tudelft.nl/windenergy/ca-wee/info/MAREC2001_Support.pdf,

[42] Ferguson M "Support Structure for Offshore Wind Turbines" Kvaerner Oil and Gas http://www.owen.eru.rl.ac.uk/papers&Articles.html, June 2003.

[43] Henderson A R et al "Prospects for Floating Offshore Wind Energy" European Wind Energy Conference, Copenhagen, 2–6 July 2001.

[44] Jhon O Halliquist "LS-DYNA Theoretical Manual" May 1998 Livermore Software Technology Corporation, online PDF file LSTC website.

[45] LSTC "LS-DYNA Keywords User's Manual" April 2003, Version 970 Livermore Technology Corporation, PDF online, LSTC website.

http://www.lstc.com/ , July 2003.

[46] LSTC "LS-DYNA Keyword User's Manual Volume II (Material Models, References and Application)" March 2001, version 960 Livermore Software Technology Corporation, PDF file online, LSTC website. http://www.lstc.com/, January 2003.

[47] Peter S Tromans and Luc Vanderscuren "Response Based Design of Floaters" http://www.info.ogp.org.uk/metocean/floatingSystems/presentations/Tromans, June 2003.

[48] John D. Reid Ph. D "LS-DYNA Examples Manuel" March 1998, Livermore Software Technology Corporation, online PDF LSTC website. http://www.lstc.com/ , June 2003.

[49] The Steel Construction Institute and The British Constructional Steelwork Association Limited, "Steelwork Design Guide to BS 5950-1: 2000, Volume 1, Section Properties, Member Capacities, 6th edition".

[50] Department of Energy "Probability Distributions for Environmental Loads on Offshore Structures" report prepared by Lloyd's Register of Shipping for the Department of Energy, offshore technology report OTI 88 504 HMSO publication 1988 UK.

[51] Department of Energy "INFOIL 2 THESAURUS TERMINOLOGY FOR THE OFFSHORE INDUSTRY" offshore technology information OTI 88 505 HMSO publication 1988 UK.

[52] Department of Energy "Metocean Parameters–Parameters Other Than Waves" offshore technology report OTH 89 299 HMSO publication 1990 UK.

[53] Department of Energy "Guidance on the Design and Construction of Offshore Installations" HMSO publication 1974 UK.

[54] Department of Energy "Metocean Parameters–Wave Parameters" Offshore Technology Report OTH 89 300 HMSO publication 1990 UK.

[55] Department of Energy "Fluid Loading on Fixed Offshore Structures Volume I" Offshore Technology Report OTH 90 322 HMSO Publication 1990 UK.

[56] Department of Energy "Fluid Loading on Fixed Offshore Structures Volume II" Offshore Technology Report OTH 90 322 HMSO publication 1990 UK.

[57] Department of Energy "Development of a Method to Make use of Sensitivity Studies and its Application to Analysis of Uncertainties in Environmental Loading on Offshore Structures" Offshore Technology Information OTI 88 537 report HMSO publication 1989 UK.

[58] Sore Krohn "Offshore Wind Energy: Full Speed Ahead" Danish Wind Industry Association www.WINDPOWER.org, February 2003.

[59] Rehfeldt Knud Dr and Matthias S Dr "North Sea Offshore Wind–A Powerhouse for Europe" study prepared for Greenpeace October 2000 Greenpeace website online PDF file.

[60] Khün M (editor) "Structural and Economic Optimisation of Offshore Wind Energy Converters" Overview of the Second Phase of the Joule III Project Opti-OWECS (idem: Wind Engineering Vol.21 No.4 1997).

[61] Kühn M "DESIGN OTIMISATION OF AN OFFSHORE WIND ENERGY CONVERTER BY MEANS OF TAILORED DYNAMICS" 1999 European Wind Energy Conference and Exhibition (EWEC 99) March 1–5 1999 Nice France.

[62] Henderson A R "Analysis Tools for Large Floating Offshore Wind Farms" Ph D thesis University College London UK June 2000, interlibrary loan.

[63] S. K. Chakrabarti "Hydrodynamics of Offshore Structures" Computational Mechanics Publication Springer-Verlag ISBN 0-905451-66-X.

[64] Necholas Pincott "Offshore Wind Farms–Construction and Operational Issues" Norton Rose Seminar: 12 June 2001

http://www.nortronrose.co./Wind%20Farm/Wind%20Farm/Papers.html , January 2002.

[65] Metoc Plc Contractor "An Assessment of the Environmental Effects of Offshore Wind Farms" ETSU W/35/00543/REP report prepared for Trade and Industry Department UK Crown Copyright 2000.

[66] Unknown author, http://europe.eu.int/comm/research/energy/nn/nn_rt/nn_rt_wind/artticle_1101_en.html, May 2005.

[67] N. Aquelet and M Souli, "Damping effect in fluid-structure interaction: application to slamming problem" http://www.univ-lille1.fr/gdr-ifs/cv/aquelet/damp3.pdf, 05/2005

[68] European Commission Directorate-General for Energy "Wind Energy-The Facts" 5 volumes http://www.ewea.org/doc/ewea.pdf , April 2003.

[69] Lee E. Harris and Jose Enrique Chacon Gonzalez "Stability Analysis of the Submerged Reef Ball Breakwater Proposed for the <Undisclosed Hotel>" Resort Quintana Roo Mexico. 25/06/2003 http://www.artificialreefs.org/ScientificReports/CancunHotelRBstability.htm , March 2003.

[70] Watson Gillian Final Report OWEN workshop on "Structure and Foundation Design of Offshore Wind Installations" Wednesday 1 March 2000 http://www.owen.org.uk/workshop_3/ws3_final.pdf, August 2003.

[71] Unknown author, web site: http://www.offshorewindenergy.org/text2html.php?textfile=expert_guides/technology_of_OWE#3, August 2004.

[72] Ove Ditlevsen "Stochastic Wave Loads on Tubular Offshore Structures-Models for dynamics and reliability analysis" 25 April 2001 online website. http://www.mek.dtu.dk/staff/od/books.htm , August 2001.

[73] Walker F. J and Jenkins N "Wind Energy Technology" John Wiley & Sons UK 1997.

[74] Bowes W H and Russel L T "Stress Analysis by the Finite Element Method for Practicing Engineers" D. C. Heath and Company 1975.

[75] DET NORSKE VERITAS (DNV), Offshore Standard, DNV-OS-E301, Position Mooring, 2004, http://www.dnv.com, October 2004.

[76] Bathe K J "Finite Element Procedures in Engineering Analysis" Prentice-Hall Inc. USA 1982.

[77] Hartwig Dobesch and Goerge Kury "Basic Meteorological Concepts and Recommendations for the Exploitations of Wind Energy in the Atmospheric Boundary Layer" Report http:/www.wmo.ch/web/wcp/wcasp/cclcc/rapp_full_rpts/dobesch_rpt.pdf, June 2003.

[78] J F Manwell, J G McGowan and A L Rogers "Wind Energy Explained" Theory, Design and Application, John Wiley & Sons Ltd. ISBN 0-470-84612-7.

[79] R D Coock et al "Concepts and Applications of Finite Element Analysis" John Wiley & Sons 2002.

[80] Ir. Dr. Iberahin Jusoh "Consideration of Environmental Loading in Design Codes for Offshore Structures" Jurutera June 2001 http://www.jaring.my/iem/june01/contents.htm, August 2002.

[81] Andrew R. Henderson, Minoo H. Patel "Multible Turbine Floating offshore Windfarms", European Wind Energy Conference, 1-5 March Nice, France.

[82] O. C. Zienkiewicz and R.E Taylor "The Finite Element Method" 4th edition McGraw Hill London 1989.

[83] American Bureau of Shipping "Guidance notes on Safehull-Dynamic Loading Approach for floating production, storage and offloading (FPSO) systems http://www.eagle.org/rules/downloads.html, June 2002.

[84] M. A. Crisfield "Non-linear Finite Element Analysis of Solids and Structures" volume 1 1997 John Wiley & Sons Ltd.

[85] M. A. Crisfield "Non-linear Finite Element Analysis of Solids and Structures" volume 2-1997 John Wiley & Sons Ltd.

[86] Emil Simiu and Robert H Scanlan "Wind Effects on Structures-Fundamentals and Applications to design" 1996 John Wiley & Sons Inc. third edition.

[87] Michiel B Zaaijer "Comparison of monopole, tripod, suction bucket and gravity base design for a 6 MW turbine" Delft University of Technology Netherlands http://www.owemes.it/articoli/pdf/Zaaijer.doc, April 2003.

[88] Det Norske Veritas "Guidelines for Design of Wind Turbines" second edition 2002, printed by Judsk Centraltrykkeri, Denmark ISBN 87-550-2870-5

[89] British Standard BS 302-7:1989 "Standard Steel Wire Ropes"—part 7: Specification for large diameter ropes for general purposes British Standard online website, March 2003.
http://www.tionestop.com/tionestop/where/bs.htm

[90] Hans Christian Soerensen & Lars Kjeld Hansen, Concerted Action on Offshore Wind Energy in Europe "Social Acceptance, Environmental Impact and Politics" Draft Report June 2001 EMU Blegdamsvej 4 1tv DK-2200 Copenhagen Denmark.
http://www.emu-consult.dk/includes/c5appendix.pdf, March 2002.

[91] Group of Companies "Offshore Wind Energy Ready to Power a Sustainable Europe" final report, December 2001, Report Ref.: Duwind 2001.006 available online website.

[92] Tomas Petru "Modelling of Wind Turbines for Power System Studies" thesis, Chalmers University of Technology, Göteberg Sweden 2001.

[93] International Organization for Standardization "Wind Actions on Structures" International Standard ISO 4354:1997(E), British Library via interlibrary loan.

[94] Peter Hauge Madsen "Predicting Ultimate Loads for Wind Turbine Design" presented at AIAA/ASME Wind Energy Symposium, Reno, Nevada January 11-14, 1999.
http://www.nrel.gov/docs/fy99osti/25787.pdf, June 2002.

[95] National Renewable Energy Laboratory "Guideline DG01 Wind Turbine Design Loads Analysis" NWTC–Certification Team, June 23 2002. http://www.nrel.gov/wind/pdfs/dg04_000203.pdf, July 2003.

[96] British Standard "Wind turbine generator systems-Part 13: Measurement of Mechanical loads, DD IEC TS 61400-13, first edition, 2001-06, British Standards online. http://www.tionestop.com/tionestop/where/bs.htm, January 2003.

[97] British Standard "Wind turbine generator systems-Part 23: Full-scale structural testing of rotor blades, technical specification, DD IEC TS 61400-23:2002 first edition 2001-04, British Standards online. http://www.tionestop.com/tionestop/where/bs.htm, June 2003.

[98] British Standard "Wind turbine generator systems Part 2: safety of small wind turbines" BS EN 61400-2:1996 IEC 1400-2:1996, IEC online British Standards website. http://www.tionestop.com/tionestop/where/bs.htm, July 2003.

[99] British Standard "Wind turbine generator systems-Part 11: Acoustic noise measurement techniques" BS EN 61400-11:1999, IEC 61400-11:1998, November 1998, British Standards online. http://www.tionestop.com/tionestop/where/bs.htm, June 2002.

[100] British Standard "Wind turbine generator systems- Part 12: Wind turbine power performance testing" BS EN 61400-12:1998, IEC 61400-12:1998, April 1998, British Standards online. http://www.tionestop.com/tionestop/where/bs.htm, August 2002.

[101] Gunner Char. Larsen, Kent Ronald, Hans E. Jorgensen, Kimono Agrarianism and Jalap de Boer "Ultimate Loading of Wind Turbines" Rios National Laboratory, Rescaled Denmark April 1999. http://www.risoe.dk/vea-vim/projects/prodeto/reports/r1111.pdf, June 2003.

[102] British Standard "Lattice towers and masts- Part 4: Code of practice for loading of guyed masts" BS 8100-4: 1995, British Standards online. http://www.tionestop.com/tionestop/where/bs.htm, January 2003.

[103] British Standard "Lattice towers and masts-Part 3: Code of practice for strength assessment of members of lattice towers and masts" BS 8100-3:1999, Incorporating Corrigendum No. 1, British Standards online. http://www.tionestop.com/tionestop/where/bs.htm, August 2002.

[104] British Standard "Lattice towers and masts- Part 2: Guide to the background and use of Part 1-Code of practice for loading" BS 8100-2:1986, British Standards online. http://www.tionestop.com/tionestop/where/bs.htm, January 2002.

[105] British Standard "Loading for buildings-Part 2: Code of practice for wind loads" BS 6399-2:1997 British Standards online. http://www.tionestop.com/tionestop/where/bs.htm, March 2002.

[106] Bomel Ltd "Environmental considerations" Health and Safety Executive, Offshore Technology Report 2001/010 HMSO London.

[107] R W Robinson and J Hamilton "A Criterion for Assessing Wind Induced Crossflow Vortex Vibrations in Wind Sensitive Structures" OTH 92 379, Health and Safety Executive- Offshore Technology Report, London: HMSO

[108] Hiroshi Imamura "Aerodynamics of Wind Turbines" http://ibis.mach.me.ynu.ac.jp/Private/imamura/paper/Wind_Aero.pdf, April 2003.

[109] Gunjit S Bir and Michael Robinson "Code Development for Control Design Applications" Phase I: Structural Modelling Presented at AIAA/ASME Wind Energy Symposium, Reno Nevada January 11-14 1999. http://www.nrel.gov/docs/fy99osti/25792.pdf, August 2002.

[110] Tony Gibbs "B1.1 Determination of Wind Loads for Use in Analysis" http://www.oas.org/pgdm/document/mhbdc/b1_text.doc, March 2003.

[111] International Standard "Wind turbine generator systems- Part 1: Safety requirements IEC 61400-1 second edition 1999-02, IEC, BS online

website. http://www.tionestop.com/tionestop/where/bs.htm, January 2002.

[112] Bomel Ltd "Loads" Offshore Technology Report 2001/013, Health and Safety Executive HMSO London.

[113] Guanpeng Xu "Computational Studies of Horizontal Axis Wind Turbines" Ph. D thesis, Georgia Institute of Technology, May 2001, word document online. http://www.ae.gatech.edu/people/lsankar/NREL/Xu-RENO2000.doc, August 2002.

[114] Harri Vihrala "Control of Variable Speed Wind Turbines" Ph. D thesis Tamber University of Technology October 29 2002.

[115] The Danish Energy Agency's Approval Scheme for Wind Turbines, "Recommendation for Technical Approval of Offshore Wind Turbines" December 2001. http://www.vindmoellegodkendelse.dk/UK/RekomOffshore12UK.pdf, April 2003.

[116] P.W Carlin, A.S. Laxson, and E.B. Muljadi "The History and State of the Art of Variable-Speed Wind Turbine Technology" Technical Report, NREL /TP-500-28607 February 2001. http://www.nrel.gov/docs/fy01osti/28607.pdf, June 2002.

[117] Subramani Balasubranyam "Head Impact Characterization of Generic A-Pillar Of An Automobile" MSc thesis, Morgantown, West Virginia 1999 http://etd.wvu.edu/ETDS/E699/finalThesis6.PDF, August 2003.

[118] Dayton A. Griffin "Blade System Design Studies Volume I: Composite Technologies for Large Wind Turbine Blades" SAND 2002-1879 Unlimited Release Printed July 2002 Washington USA.

[119] Raymond Hunter et al "European Wind Turbine Testing Procedure Developments" Task 1, Riso National Laboratory, Roskilde Denmark, January 2001. http://www.risoe.dk/rispubl/VEA/veapdf/ris-r-1209.pdf, June 2002.

[120] Lance Manuel et al "Parametric Models for Estimating Wind Turbine Fatigue Loads for Design", Department of Civil Engineering, University of Texas at Austin USA, March 2003.
http://www.rms-group.org/RMS_Papers/pdf/lance/aiaa01.pdf

[121] Holger Soker et al "Offshore Wind Energy in the North Sea" A study for Greenpeace, October 2000, Greenpeace website.

[122] Peter Fuglsang, Kenneth Thomsen, "Cost Optimisation of Wind Turbines for Large–Scale Offshore Wind Farm" Riso National Laboratory Roskilde Denmark February 1998.
http://www.risoe.dk/rispubl/VEA/veapdf/ris-r1000.PDF, October 2002.

[123] Don W Lobitz "A Nastrran-Based Computer Program For Structural Dynamic Analysis of Horizontal Axis Wind Turbines" Proceedings of the Horizontal Axis Wind Turbines Technology Workshop, department of Energy and NASA-Lewis, Cleveland, May 1984.

[124] LeRoy M. Fitzwater and Steven R. Winterstein "Predicting Design Wind Turbine Loads from Limited Data: Comparing Random Process and Random Peak Modeles"AIAA-2001-0046 USA.
http://www.sandia.gov/Renewable_Energy/wind_energy/asme/AIAA-2001-0046.pdf, November 2002.

[125] Anders Ahlström "Simulating Dynamic Behaviour of Wind Power Structures" Licentiate Thesis Royal Institute of Technology, Department of Mechanics Stockholm2002.
http://www2.mech.kth.se/~andersa/thesis/Licthesis.pdf, January 2003.

[126] Donghoom Lee, Dewey H. Hodges and Mayuresh J. Patel "Multi-flexible-body Dynamic Analysis of Horizontal Axis Wind Turbines" Wind Energy 2002;5:281-300 (DOI: 10.1002/we.66)
http://www.ae.gatech.edu/~dhodges/papers/JWE.pdf, April 2003.

[127] Osamu KIYOMIYA Tatsuomi RIKIJI Pieter H.A.J.M. van GELDER "Dynamic Response Analysis of Onshore Wind Energy Power Units during Earthquakes and Wind" proceedings of the 12th (2002)

International Society of Offshore and Polar Engineering Conference, Kitakyushu Japan May 26-31 2002.

[128] Paul S Veers and Sandy Butterfield "Extreme Load Estimation for Wind Turbines: Issues and Opportunities for Improved Practice" AIAA-2001-0044.

http://www.sandia.gov/Renewable_Energy/wind_energy/asme/AIAA-2001-0044.pdf, March 2003.

[129] Yutaka Hasegawa, et al "Numerical Analysis of Yawed Inflow Effects on HAWT Rotor" FEDSM 99-S295-9, Proceedings of the 3rd ASME/JSME Joint Fluids Engineering Conference July 18-23 1999, Sanfrancisco California.

[130] Y. Hasegawa, K. Kikuyama and K. Karikomi "Effects of Turbulent Characteristics on Aerodynamic Behaviour of HAWT rotor" http://www.hdl.mech.nagoya-u.ac.jp/research/wind/EWEC.pdf, October 2002.

[131] Jeppe Johansen "Unsteady Airfoil Flows with Application to Aeroelastic Stability" Riso National Laboratory, Roskilde Denmark October 1999. http://www.risoe.dk/rispubl/VEA/veapdf/ris-r-1116.pdf, July 2004.

[132] Dayton A. Griffin "Blade System Design Studies Volume I: Composite Technologies for Large Wind Turbine Blades", October 2003. http://www.sandia.gov/Renewable_Energy/wind_energy/other/021879.pdf

[133] Richard Eppler "Airfoil Design and Data" Berlin 1990, ISBN 0-387-52505-X.

[134] Abbot and Ira Herbert "Theory of Wing Sections-Including Summary of airfoil Data, New York: Dover 1959.

[135] JØrgen et al "Prediction of Dynamic Loads and Induced Vibrations in Stall" Riso-R-1045(EN) Riso National Laboratory, Roskilde May 1998. http://www.risoe.dk/rispubl/VEA/veapdf/ris-r-1045.pdf, January 2003.

[136] O. M. Faltinsen "Sea Loads on Ships and Offshore Structures" Cambridge University Press 1998 ISBN 0 521 45870 6 paperback.

[137] David M. Eggleston and Forrest S. Stoddard "Wind Turbine Engineering Design" 1987 Van Nostrand Inc. New York, ISBN 0-442-22195-9.

[138] A.R. Henderson, R. Leutz and T. Fujii "Potential For Floating Offshore Wind Energy in Japanese Waters" ISOPE Conference, Katakyushu, Japan, 26-31, 2002.

[139] Po Wen Cheng "A reliability Based Design Methodology for Extreme Response of Offshore Wind Turbines" Ph. D. thesis DUWIND Delft University Wind Energy Research Institute, ISBN 90-79468-08-7

[140] Jerry I Lin "DYNA3D: A Nonlinear, Explicit, Three-Dimensional Finite Element Code for Solid and Structural Mechanics" User Manual, October 1999 http://www.llnl.gov/eng/mdg/Codes/DYNA3D.pdf , April 2003.

[141] Klaus Weimar "LS-DYNA User's Guide" Rev. 1.19, September 2001, CAD-FEM GmbH, www.cadfem.de or PWS www.p-w-s.com, June 2002.

[142] Noble Denton for the Department of Energy "Environmental Parameters on the United Kingdom Continental Shelf" Offshore Technology Report OTH 84 201.

APPENDICES

Appendix-A1 LS-DYNA3D Code

A1.1 Introduction:

The LS-DYNA3D is an explicit '3-D' finite element code for analyses of the large deformation dynamic response of elastic, inelastic solids and structures, Halliquist [44]. The program is extensively used by (i) aerospace, including effects of birds striking airplanes, aircraft analysis, improved methods of manufacturing aircraft wings (ii) analysis of shipping containers for radioactive materials and ship collision (iii) automobile design crash tests, and human effects (iv) biomedical studies, including brain impact studies, human response to balloon angioplasty, spinal region surgical procedures and artificial implants, and development of a new machine to break kidney stones using shock waves (lithotripter) (v) aluminium can and metal forming production (vi) train accident analysis (vii) structural analysis, Halliquist [44], Subramani [117]. A wide range of material types and interfaces enable the efficient mathematical modelling of wide spectrum of complex engineering problems, Jerry [140] and Klaus [141].

LS-DYNA3D (dynamics in three dimensions) is a non-linear structural dynamics code that can analyze the complex structural response of mechanical and geometrical systems subjected to high-rate of loadings and impacts. The program simulates the effect of stress and displacements on structures. Like most engineering codes LS-DYNA3D is based on finite element method, a technique of examining physical systems by breaking them into discrete but interconnected elements. What makes this program different is its ability to span a broad spectrum of engineering problems and computing environments. Developed in the second half of the 1970s mainly for supercomputer applications to study the effects of weapons systems, the rapidly improving program became extremely versatile. The parallel development in computing hardware enables the use of the program on personal pc.

A1.2 Basic Formulation of LS-DYNA3D:

The finite element method is a numerical procedure for analyzing structures and continua. The finite element method involves descretizing differential equations into simultaneous algebraic equations. The advances made in the computational efficiency of digital computers have increased the use of the finite element method as an analysis tool since large number of the equations generated by the finite element method can be solved very efficiently. Discussions to follow are intended to give attention to some important features rather than to cover the whole topic they are extracted from Halliquist [44], Subramani [117], Jerry [140] and Klaus [141].

Based on the momentum conservation principle, the basic formulation could be derived as follows, Halliquist [44];

$$\sigma_{ij,j} + \rho f_i = \rho \ddot{x}_i \qquad \text{(A1.1)}$$

Equation A1.1 should satisfy the traction boundary conditions

$$\sigma_{ij} n_i = t_i(t) \qquad \text{(A1.2)}$$

On boundary δ_{b1}, while the displacement boundary conditions

$$x_i(X_\alpha, t) = D_i(t) \qquad \text{(A1.3)}$$

On boundary δ_{b2}, the contact discontinuity

$$(\sigma^+_{ij} - \sigma^-_{ij})\, n_i = 0 \qquad \text{(A1.4)}$$

Along an interior boundary δ_{b3} when $x^+_i = x^-_i$, here σ_{ij} is the Couchy stress, ρ is the density, f_i is the body force density, $\ddot{x}$ is the acceleration, and n_j is the unit vector normal to the boundary δb

Equations of global energy balance and state evaluations can be obtained by integrating the energy equation in time. The energy equation is given as

$$\dot{E} = V s_{ij} \dot{\varepsilon}_{ij} - (p+q)\dot{V} \qquad \text{(A1.5)}$$

s_{ij} is the deviatoric stresses and p represents the pressure. Deviatoric stress is

$$S_{ij} = \sigma_{ij} + (p+q)\,\delta_{ij} \qquad \text{(A1.6)}$$

Where

$$P = -\tfrac{1}{3}\,\sigma_{ij}\,\delta_{ij} - q = -\tfrac{1}{3}\,\sigma_{kk} - q \qquad \text{(A1.7)}$$

Respectively, q is the bulk viscosity, δ_{ij} is the Cronecker delta (δ_{ij} =1 if i =j; otherwise δ_{ij} =0) and $\dot{\varepsilon}_{ij}$ is the strain rate tensor. The weak form of the equilibrium equation when δx_i satisfies all the boundary conditions on δb_2 is given By:

$$\int_{v}(\rho\ddot{x}_i - \sigma_{ij,j} - \rho f_i)\delta x_i dv + \int_{\delta b1}(\sigma_{ij}n_j - t_i)\delta x_i ds + \int_{\delta b3}(\sigma_{ij}^{+} - \sigma_{ij}^{-})n_j \delta x_i ds = 0 \qquad \text{(A1.8)}$$

Application of $(\sigma_{ij}\delta x_i), j - \sigma_{ij,j}\delta x_i = \sigma_{ij}\delta x_{i,j}$ this to the divergence theorem, leads to the statement of principle of virtual work, which can be given as

$$\delta\pi = \int_{\upsilon}\rho\,\ddot{x}_i\,\delta x_i\,dv + \int_{\upsilon}\sigma_{ij,j}\,\delta x_{i,j}\,dv - \int_{\upsilon}\rho f_i\delta_{xi}\,dv - \int_{\partial b1}t_i\,\delta_{xi}\,ds = 0 \qquad \text{(A1.9)}$$

Superimposing a mesh of finite elements, interconnected at nodal points on a reference configuration and track particles through time, i.e.

$$x_i(X_\alpha, t) = x_i(X_\alpha(\xi,\eta,\zeta), t) = \sum_{j=1}^{k} \Phi_j(\xi,\eta,\zeta)\, x_i^j(t) \qquad \text{(A1.10)}$$

Where Φ_j are shape interpolation functions of the parametric coordinates (ξ,η,ζ) ,k is the number of nodal points defining the element, and x_i^j is the nodal coordinate of the j^{th} node in the i^{th} direction. One of the widely used 8-noded mesh solid element typically shown in Figure (A1.1). The node definition for this element is shown after the solid element.

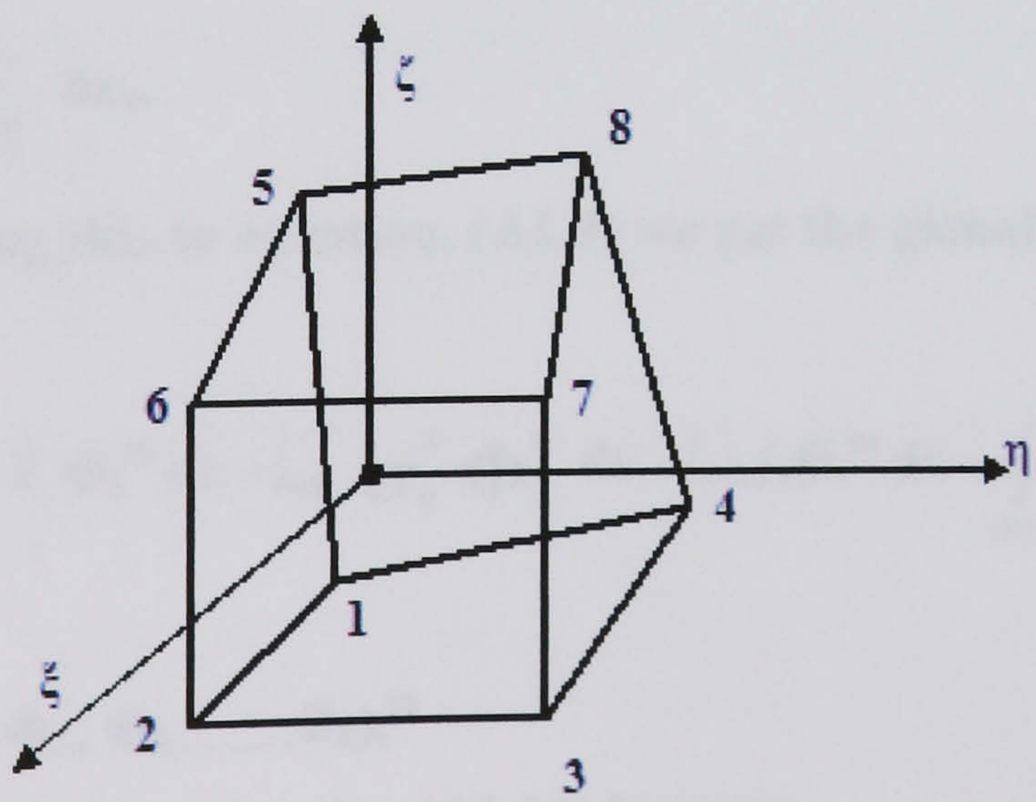

Figure (A1.1) Solid element

node	ξ	η	ζ
1	-1	-1	-1
2	1	-1	-1
3	1	1	-1
4	-1	1	-1
5	-1	-1	1
6	1	-1	1
7	1	1	1
8	-1	1	1

For a mesh with a 8-node hexahedron solid element, equation (A1.10), becomes

$$\mathbf{x_i}(X_\alpha, t) = \mathbf{x_i}(X_\alpha(\xi,\eta,\zeta), t) = \sum_{j=1}^{8} \Phi_j(\xi,\eta,\zeta)\, x_i^j(t) \qquad \text{(A1.11)}$$

and the shape function

$$\phi_j = \frac{1}{8}(1+\xi\xi_j)(1+\eta\eta_j)(1+\zeta\zeta_j) \qquad \text{(A1.12)}$$

where ξ_j, η_j, ζ_j take their nodal values of $(\pm 1, \pm 1, \pm 1)$ as shown in the previous figure.

Summing over the n elements δπ may be approximated to

$$\delta\pi = \sum_{m=1}^{n} \delta\pi_m \qquad \text{(A1.13)}$$

And applying this to equation, (A1.9) we get the global finite element equilibrium as

$$\sum_{m=1}^{n} \{ \int_{v_m} \rho\, \ddot{x}_i\, \Phi_i^m\, dv + \int_{vm} \sigma_{ij}^m\, \Phi_{i,j}^m\, dv - \int_{vm} f_i \Phi_i^m\, dv - \int_{\partial b1} t_i \phi_i^m\, ds \} = 0 \qquad \text{(A1.14)}$$

Where:

$$\Phi_i^m = (\Phi_1, \Phi_2, \Phi_3, \ldots\ldots \Phi_k)_i^m \qquad \text{(A1.15)}$$

In matrix notation equation (A1.14) becomes

$$\sum_{m=1}^{n} \{ \int_{vm} \rho N^t N a\, dv + \int_{vm} B^t \sigma\, dv - \int_{vm} \rho N^t b\, dv - \int_{\partial b1} N^t t\, ds \}^m = 0 \qquad \text{(A1.16)}$$

Where N is an interpolation matrix, σ is the stress vector

$$\begin{bmatrix} \ddot{x}_1 \\ \ddot{x}_2 \\ \ddot{x}_3 \end{bmatrix} = \mathbf{N} \begin{bmatrix} a_{x1} \\ a_{y1} \\ . \\ . \\ a_{yk} \\ a_{zk} \end{bmatrix} = \mathbf{N}\,\mathbf{a}$$

$$\sigma^t = (\sigma_{xx}, \sigma_{yy}, \sigma_{zz}, \sigma_{xy}, \sigma_{yz}, \sigma_{zx}) \qquad \text{(A1.17)}$$

B is the strain-displacement matrix, a is the nodal acceleration vector

b is the body force load vector, and t are applied traction loads

$$b = \begin{bmatrix} f_x \\ f_y \\ f_z \end{bmatrix}, \text{ and } \mathbf{t} = \begin{bmatrix} t_x \\ t_y \\ t_z \end{bmatrix} \qquad \text{(A1.18)}$$

For an 8-node hexahedron solid, B is 6 x 24 strain-displacement matrix and N is 3x 24 rectangular interpolation matrix and is given by:

$$\mathbf{B} = \begin{bmatrix} \frac{\delta}{\delta x} & 0 & 0 \\ 0 & \frac{\delta}{\delta y} & 0 \\ 0 & 0 & \frac{\delta}{\delta z} \end{bmatrix} \text{ and } \mathbf{N}(\xi,\eta,\zeta) = \begin{bmatrix} \phi_1 & 0 & 0 & 0 & \phi_2 & 0 & - & - & 0 & 0 \\ 0 & \phi_1 & 0 & 0 & 0 & \phi_2 & - & - & \phi_8 & 0 \\ 0 & 0 & \phi_1 & 0 & 0 & 0 & - & - & 0 & \phi_8 \end{bmatrix}$$

By summing the rows we can obtain a diagonal mass matrix and the k^{th} diagonal term is given as:

$$m_{kk} = \int \rho \phi_k \sum_{i=1}^{8} \phi_i dv = \int_v \rho \phi_k dv \qquad \text{(A1.19)}$$

Terms in the strain-displacement matrix are calculated instantly, the above matrixes:

$$\frac{\delta \phi_i}{\delta \xi} = \frac{\delta \phi_i}{\delta x}\frac{\delta x}{\delta \xi} + \frac{\delta \phi_i}{\delta y}\frac{\delta y}{\delta \xi} + \frac{\delta \phi_i}{\delta z}\frac{\delta z}{\delta \xi}$$

$$\frac{\delta \phi_i}{\delta \eta} = \frac{\delta \phi_i}{\delta x}\frac{\delta x}{\delta \eta} + \frac{\delta \phi_i}{\delta y}\frac{\delta y}{\delta \eta} + \frac{\delta \phi_i}{\delta z}\frac{\delta z}{\delta \eta} \qquad \text{(A1.20)}$$

$$\frac{\delta\phi_i}{\delta\zeta} = \frac{\delta\phi_i}{\delta x}\frac{\delta x}{\delta\zeta} + \frac{\delta\phi_i}{\delta y}\frac{\delta y}{\delta\zeta} + \frac{\delta\phi_i}{\delta z}\frac{\delta z}{\delta\zeta}$$

or in matrix form

$$\begin{bmatrix} \frac{\delta\phi_i}{\delta\xi} \\ \frac{\delta\phi_i}{\delta\eta} \\ \frac{\delta\phi_i}{\delta\zeta} \end{bmatrix} = \begin{bmatrix} \frac{\delta x}{\delta\xi} & \frac{\delta y}{\delta\xi} & \frac{\delta z}{\delta\xi} \\ \frac{\delta x}{\delta\eta} & \frac{\delta y}{\delta\eta} & \frac{\delta z}{\delta\eta} \\ \frac{\delta x}{\delta\zeta} & \frac{\delta y}{\delta\zeta} & \frac{\delta z}{\delta\zeta} \end{bmatrix} \begin{bmatrix} \frac{\delta\phi_i}{\delta x} \\ \frac{\delta\phi_i}{\delta y} \\ \frac{\delta\phi_i}{\delta z} \end{bmatrix} = J \begin{bmatrix} \frac{\delta\phi_i}{\delta x} \\ \frac{\delta\phi_i}{\delta y} \\ \frac{\delta\phi_i}{\delta z} \end{bmatrix} \qquad \textbf{(A1.21)}$$

Hence the desired terms can be obtained by inverting the Jacobean matrix J as

$$\begin{bmatrix} \frac{\delta\phi_i}{\delta x} \\ \frac{\delta\phi_i}{\delta y} \\ \frac{\delta\phi_i}{\delta z} \end{bmatrix} = J^{-1} \begin{bmatrix} \frac{\delta\phi_i}{\delta\xi} \\ \frac{\delta\phi_i}{\delta\eta} \\ \frac{\delta\phi_i}{\delta\zeta} \end{bmatrix} \qquad \textbf{(A1.22)}$$

A similar formulation could be reached for other elements; they are detailed in the theoretical manual, Halliquist [44].

A1.3 Volume Integration:

Gaussian quadrature is used to carry the volume integration. For some functions g defined over with n integration point then:

$$\int_v g dv = \int_{-1}^{1}\int_{-1}^{1}\int_{-1}^{1} g|j| d\xi d\eta d\zeta \qquad \textbf{(A1.23)}$$

Which may be approximated by,

$$\sum_{j=1}^{n}\sum_{k=1}^{n}\sum_{l=1}^{n} g_{jkl}\left|J_{jkl}\right| w_j w_k w_l \qquad \textbf{(A1.24)}$$

Where w_j, w_k, w_l **are weighting factors and** $g_{jkl}=g(\xi_j, \eta_k \zeta_l)$ **and** $|J|$ **is the determinant of the Jacobean matrix. For one point quadrature n=1,** $w_i = w_k = w_l = 2$ **and** $\xi_1 = \eta_1 = \zeta_1 = 0$ **from which it follows**

$$\int g dv = 8g(0,0,0)|J(0,0,0)| \qquad \textbf{(A1.25)}$$

Note that $8|J(0,0,0)|$ give an approximation to the element volume.

The biggest advantage of one point integration is a substantial saving in the computer time. An anti-symmetry property of the strain matrix

$$\frac{\partial \phi_1}{\partial x_i} = -\frac{\partial \phi_7}{\partial x_i}\frac{\partial \phi_3}{\partial x_i} = \frac{-\partial \phi_5}{\partial x_i}$$

$$\frac{\partial \phi_2}{\partial x_i} = -\frac{\partial \phi_8}{\partial x_i}\frac{\partial \phi_4}{\partial x_i} = -\frac{\partial \phi_6}{\partial x_i} \qquad \textbf{(A1.26)}$$

At $\xi = \zeta = \eta = 0$ reduces the amount of effort to compute strain matrix given by equation (A1.26) by 25 times over the 8–point integration Halliquist [44], Klaus [141]. This cost savings extends to strain and element nodal forces calculations where the number of multipliers is reduced by a factor of 16, Subramani [117]. Because only one constitutive evaluation is needed, the time spent determining stresses is reduced by a factor of 8. However 8-point integration has another disadvantage in addition to cost. When fully integrated elements used in the solution of plasticity problems and problems with Poisson's ratio approaching 0.5 get locked up in the constant volume bending modes, Halliquist [44]. An average pressure must be applied to all elements to avoid the locking up of elements in the constant volume bending modes; consequently the hourglass modes are resisted by the deviatoric stresses. If these deviatoric stresses become negligible, when compared to the pressure or if the material failure causes loss of this stress state component, then hourglass will still occur without any means to resist it.

A1.4 Control of Hourglass:

Any explicit time integration scheme calls for what is called "economic" element, which can reduce the overall time. This can be done when a reduced one (Guass) point integration is used. One point integration however gives rise to "zero energy modes" called the "hourglass modes" as already been discussed. These undesirable hourglass modes are often observed to be oscillatory and they tend to have periods that are typically much shorter than the periods of the structural response. If these hourglass modes tend to have periods that are comparable to

the structural response periods it forms a stable kinematics component of the global deformation and they are admissible. A viscous damping or small elastic stiffness capable of stopping the anomalous modes while having a negligible affect on the state global deformation modes can in a way resist the formation of the undesirable hourglass modes. To understand the formation of the undesirable hourglass modes, the following strain rate for an 8-node solid element is considered:

$$\dot{\varepsilon}_{ij} = \frac{1}{2}\left(\sum_{k=1}^{8} \frac{\delta\phi_k}{\delta x_i}\dot{x}_j^k + \frac{\delta\phi_k}{\delta x_j}\dot{x}_i^k\right) \qquad \text{(A1.27)}$$

If diagonally opposite nodes have identical velocities, then the strain energy rates (due to the asymmetries in equation (A1.26) are identically zero ($\dot{\varepsilon}_{ij} = 0$) that is when the following "hourglass" condition occur (diagonally opposite nodes have identical velocities):

$$\dot{x}_i^1 = \dot{x}_i^7, \dot{x}_i^2 = \dot{x}_i^8, \dot{x}_i^3 = \dot{x}_i^5, \dot{x}_i^4 = \dot{x}_i^6 \qquad \text{(A1.28)}$$

It is possible to prove the orthogonality of the hourglass shape vectors with the derivatives of shape functions as follows:

$$\sum_{k=1}^{8} \frac{\partial\phi_k}{\partial x_i}\Gamma_{\alpha k} = 0 \qquad i=1,2,3 \qquad \alpha=1,2,3,4 \qquad \text{(A1.29)}$$

Hourglass modes are avoided by the use of artificial resisting forces consistent with the orthogonal nature of the modes Γ_k and related to the element volume, material sound speed. The product of the base vectors with the nodal velocities for these modes are given by

$$h_{i\alpha} = \sum_{k=1}^{8} \dot{x}_i^k \Gamma_{\alpha k} = 0 \qquad \text{(A1.30)}$$

If hourglass modes are present then equation (A1.30) becomes nonzero. And the resisting 12 hourglass force vectors are:

$$f_{i\alpha}^k = a_h h_{i\alpha}\Gamma_{\alpha k} \text{ and } a_h = Q_{hg}\rho v_e^{2/3}\frac{c}{4} \qquad \text{(A1.31)}$$

Where Q_{hg} is an empirical constant defined between 0.05 and 0.15

Refined finite element meshing of components tends to reduce the hourglass modes which otherwise produce artificial energies in excess of the initial energy of the system.

Thus in conclusion, the biggest disadvantage to one-point integration is the need to control the zero energy modes, which arise, called hourglass modes. Undesirable hourglass modes tend to have periods that are typically much shorter than the periods of the structural response, and they are often observed to be oscillatory. However, hourglass modes that have periods that are comparable to the structural response periods may be a stable kinematics component of the global deformation modes and must be admissible. One way of resisting undesirable hourglass is with viscous damping or small elastic stiffness capable of stopping the formation of the anomalous modes but having a negligible effect on the stable global modes.

Since the hourglass deformation modes are orthogonal to the strain calculations, work done by the hourglass resistance is neglected in the strain energy equation. This may lead to a slight loss of energy; however, hourglass control is always recommended for the under-integrated solid elements. The energy dissipated by the hourglass forces reacting against the formations of the hourglass modes is tracked and reported in the output files.

A1.5 Time Step Control:

A new time step size is determined by taking the minimum value over all elements as follows

$$\nabla t^{n+1} = \alpha_{\min}\left(\nabla t_1, \nabla t_2, ..., \nabla t_N\right) \qquad \textbf{(A1.32)}$$

Where N is the number of elements. For stability reasons the scale factor α is typically set to a value of 0.9 (default) or smaller value.

For a solid element, a critical time step size ∇t_e is computed as follows:

$$\nabla t_e = \frac{Le}{\left(\left[Q + (Q^2 + c^2)^{1/2}\right]\right)} \qquad \textbf{(A1.33)}$$

Where $L_e = \frac{v_e}{A_{e\max}}$ for 8-node solid element and Q (C_0, C1) and C_0, C_1 are the bulk viscosity coefficients and Q is given by

$$Q = \frac{C_1 c + C_0 v_c \left|\dot{\varepsilon}_{kk}\right|}{A_{e\max}} \quad \text{for } \dot{\varepsilon}_{kk} < 0 \qquad \textbf{(A1.34)}$$

$$Q = 0 \text{ for } \dot{\varepsilon}_{kk} \geq 0$$

L_e Is the characteristic length:

8-nodes: $L_e = \frac{v_e}{A_{e\max}}$

4-node tetrahedras: $L_e =$ **minimum altitude**

Where v_e is the element volume, $A_{e\max}$ is the area of the largest side, and c is the adiabatic sound speed given by

$$c = \left[\left(\frac{4G}{3\rho_0} + \frac{\delta p}{\delta \rho} \right)_s \right]^{1/2} \qquad \textbf{(A1.35)}$$

And ρ is the specific mass density.

For an isentrope sound speed, c is given by

$$c = \left[\frac{4G}{3\rho_0} + \frac{\delta p}{\delta \rho} \right)_E + \frac{pV^2}{\rho_0} \frac{\delta p}{\delta E} \right)_\rho \Bigg]^{1/2} \qquad \textbf{(A1.36)}$$

For the incremental energy, E in the units of pressure is the product of pressure p and the incremental relative volume dv:

$$\frac{\delta p}{\delta \rho}\Big)_s = \frac{\delta p}{\delta \rho}\Big)_E + \frac{\delta p}{\delta E}\Big)_\rho \frac{\delta E}{\delta \rho}\Big)_S \qquad \textbf{(A1.37)}$$

and

dE = -pdv

Sound speed for elastic materials with constant bulk modulus is given by

$$c = \sqrt{\frac{E(1-\nu)}{(1+\nu)(1-2\nu)\rho}} \qquad \textbf{(A1.38)}$$

Where E is the Young's modulus and ν is the Poisons ratio.

This is the approach for solid elements, while reference is made to the LS-DYNA3D theoretical manual Halliquist [44] for time step calculation of beam and truss elements, shell elements and discrete elements. Explicit methods are based on time integration; therefore time step factors in the time step control cards are of utmost importance.

A1.6 Time Integration:

The equations of equilibrium for a nonlinear finite element system in motion are nonlinear differential equations for which numerical solutions much easier to obtain in general than analytical solution. The procedure used to solve the equations of equilibrium can be divided into two methods: direct integration and mode superposition.

In direct integration, equations of equilibrium are integrated using a numerical step-by-step procedure. The term 'direct' is used because the equations of equilibrium are not transformed into any other form before the integration process is carried out. Some of the few commonly used direct integration methods are the *central difference method*, *Houbolt method*, *Wilson-theta method*, and *Newmark method* Halliquist [44], Subramani [117], Jerry [140] and Klaus [141].

LS-DYNA3D is based on the *central difference method* of direct integration therefore; the description of the direct integration method will concentrate on the central difference method.

Considering the single degree of freedom damped system as shown below, the equilibrium equations for the given system are obtained from d'Alembert's principle

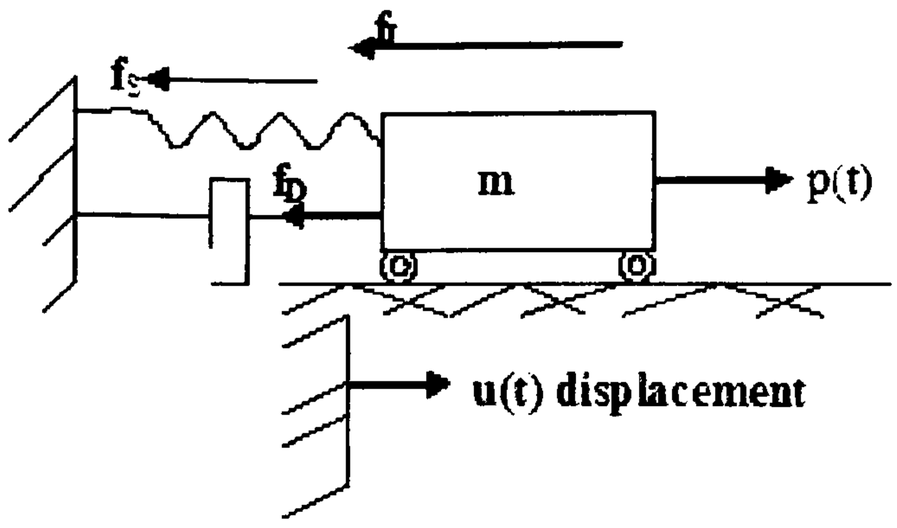

f_I = inertia force

f_S = elastic force

f_D = damping force

Forces acting on damped mass m

$$f_I + f_D + f_{int} = p(t) \quad f_I + f_D + f_{int} = p(t) \qquad \text{(A1.39)}$$

f_I = mü; ü = $\frac{d^2u}{dt^2}$ **is acceleration**

f_D = c $\dot{u}$ **;** $\dot{u} = \frac{du}{dt}$ **is velocity, and c is the damping coefficient**

$f_{int} = k.u$ **; u displacement and k is the linear stiffness**

For a linear behaviour the equations of motion lead to linear ordinary differential equations given by $m\ddot{u} + c\dot{u} + k.u = p(t)$ **and for a nonlinear case the inertial force varies as a nonlinear function of the displacement which leads to a nonlinear ordinary differential equation given by** $m\ddot{u} + c\dot{u} + f_{int}(u) = p(t)$

Analytical solutions of such equations is available, considering the dynamic response of a linear system subjected to a harmonic loading, with the knowledge of the common used terms

Harmonic loading: $P(t) = P_o \sin \varpi t$

Circular frequency: $\omega = \sqrt{\frac{k}{m}}$ **for single degree of freedom**

Natural frequency: $f = \frac{\omega}{2\pi} = \frac{1}{T}$ **, T is the period**

Damping ratio: $\zeta = \frac{c}{c_{cr}} = \frac{c}{2m\omega}$

Damped vibration: $\omega_0 = \omega\sqrt{1-\zeta^2}$

Applied load frequency: $\beta = \frac{\varpi}{\omega}$

The closed form solution with initial conditions u_0 = initial displacement, $\dot{u}_0$ = initial velocity and $\frac{p_0}{k}$ = static displacement is given by;

$$u(t) = u_0 \cos \omega t + \frac{\dot{u}_0}{\omega} \sin \omega t + \frac{p_0}{k} \frac{1}{1-\beta^2} (\sin \varpi t - \beta \sin \omega t) \qquad \textbf{(A1.40)}$$

For nonlinear problems, only numerical solutions are possible. LS-DYNA3D uses the explicit central difference method to integrate the equations of motion.

The semi-discrete equations of motion at time n are:

$$\mathbf{Ma^n = P^n - F^n + H^n} \qquad \textbf{(A1.41)}$$

Where M is the diagonal mass matrix, P^n is the external and body force loads, F^n is the stress divergence vector, and H^n is the hourglass resistance. The central difference time integration method is used to advance time t^{n+1} as follows:

$$a^n = M^{-1}(P^n - F^n + H^n) \qquad \textbf{(A1.42)}$$

$$v^{n+1/2} = v^{n-1/2} + a^{''} \nabla t^n \qquad \textbf{(A1.43)}$$

$$u^{n+1} = u^n + v^{n+1/2} \nabla t^{n+1/2} \qquad \textbf{(A1.44)}$$

Where $\nabla t^{n+1/2} = \frac{(\nabla t^n + \nabla t^{n+1})}{2}$

And v and u are the global nodal velocity and displacement vectors, respectively.

Initial geometry can be updated by adding the displacement increments

$$\mathbf{X^{n+1} = x^o + u^{n+1}} \qquad \textbf{(A1.45)}$$

The stability of the central difference method is determined by looking at the stability of the linear system. The equations of a linear system is uncoupled into the model equations where the model matrix of eigen vectors, Φ, are normalized with respect to the mass matrix M, and linear stiffness matrix K. The decoupling of damping matrix, C for viscous proportional damping is obtained from the normalization as

$$\mathbf{\Phi^T C \Phi = 2\xi\omega} \qquad \textbf{(A1.46)}$$

The equations of motion in the modal coordinates x are:

$$\ddot{x} + \dot{2}\zeta\omega\dot{x} + \omega^2 x = \underbrace{\phi^T p}_{=y} \qquad \textbf{(A1.47)}$$

With central differences we obtain for the velocity and acceleration

$$\dot{x}_n = \frac{x_{n+1} - x_{n-1}}{2\nabla t} \quad \textbf{and} \quad \ddot{x}_n = \frac{x_{n+1} - 2x_n + x_{n-1}}{\nabla t^2} \qquad \textbf{(A1.48)}$$

Substituting equation (A1.43) into equation of motion at time t^n leads to

$$x_{n+1} = \frac{2 - \omega^2 \nabla t^2}{1 + 2\zeta\omega\nabla t^2} x_n - \frac{1 - 2\zeta\omega\nabla t}{1 + 2\zeta\omega\nabla t} x_{n-1} + \frac{\nabla t^2}{1 + 2\zeta\omega\nabla t^2} y_n \qquad \textbf{(A1.49)}$$

And equation (A1.48) in the matrix form is given by

$$\begin{bmatrix} X_{n+1} \\ \\ X_n \end{bmatrix} = \begin{bmatrix} \frac{2-\omega^2\nabla t^2}{1+2\zeta\omega\nabla t} & \frac{1-2\zeta\omega\nabla t}{1+2\zeta\omega\nabla t} \\ \\ 1 & 0 \end{bmatrix} \begin{bmatrix} X_n \\ \\ X_{n-1} \end{bmatrix} + \begin{bmatrix} \frac{\nabla t^2}{1+2\zeta\omega\nabla t^2} \\ \\ 0 \end{bmatrix} \qquad \textbf{(A1.50)}$$

Or

$$[X_{n+1}] = [A][X_n] + [L]Y_n \qquad \textbf{(A1.51)}$$

Where A is the time integration operator for discrete equations of motion. After m time steps with L = 0 the value $[X_m] = [A_m][X_0]$

The spectral radius ρ (A) is the largest eigen value of A the solution will be stable if and only if $|\rho(A) \le 1|$. The condition that $|\rho(A) \le 1|$ for an undamped equation of motion gives the value of time step ∇t as

$$\nabla t \le \frac{2}{f_{\max}}$$

Thus the time step size is bound by the largest natural frequency in the model, which in turn is bound by the highest natural frequency of any element in the model.

The time step size is always limited by the single element in the model. The disadvantage of this method is that even if only one element has a time step much less, then all other elements should also be calculated for the same step size. Hence, 'sub-cycling' called as mixed time integration has to be introduced. This method employs in grouping the elements based on their step size and individual

time integration should be carried out for each group. This method could be helpful as it reduces the time for solving. However the use of mass scaling to preserve a reasonable time step size works better than subcycling and hence the later is turned off.

A1.6.1 Central Difference Method:

Considering dynamic system, represented mathematically by a system of ordinary differential equations with constant coefficients. The central difference method is an effective solution scheme for such a system of equations. The velocity and acceleration are approximated, Figure (A1.2) as follows:

$$\dot{u}_n = \frac{1}{(\Delta t)^2}(u_{n+1} - u_{n-1}) \qquad \textbf{(A1.52)}$$

$$\ddot{u}_n = \frac{1}{(\Delta t)^2}(u_{n+1} - 2u_n + u_{n-1}) \qquad \textbf{(A1.53)}$$

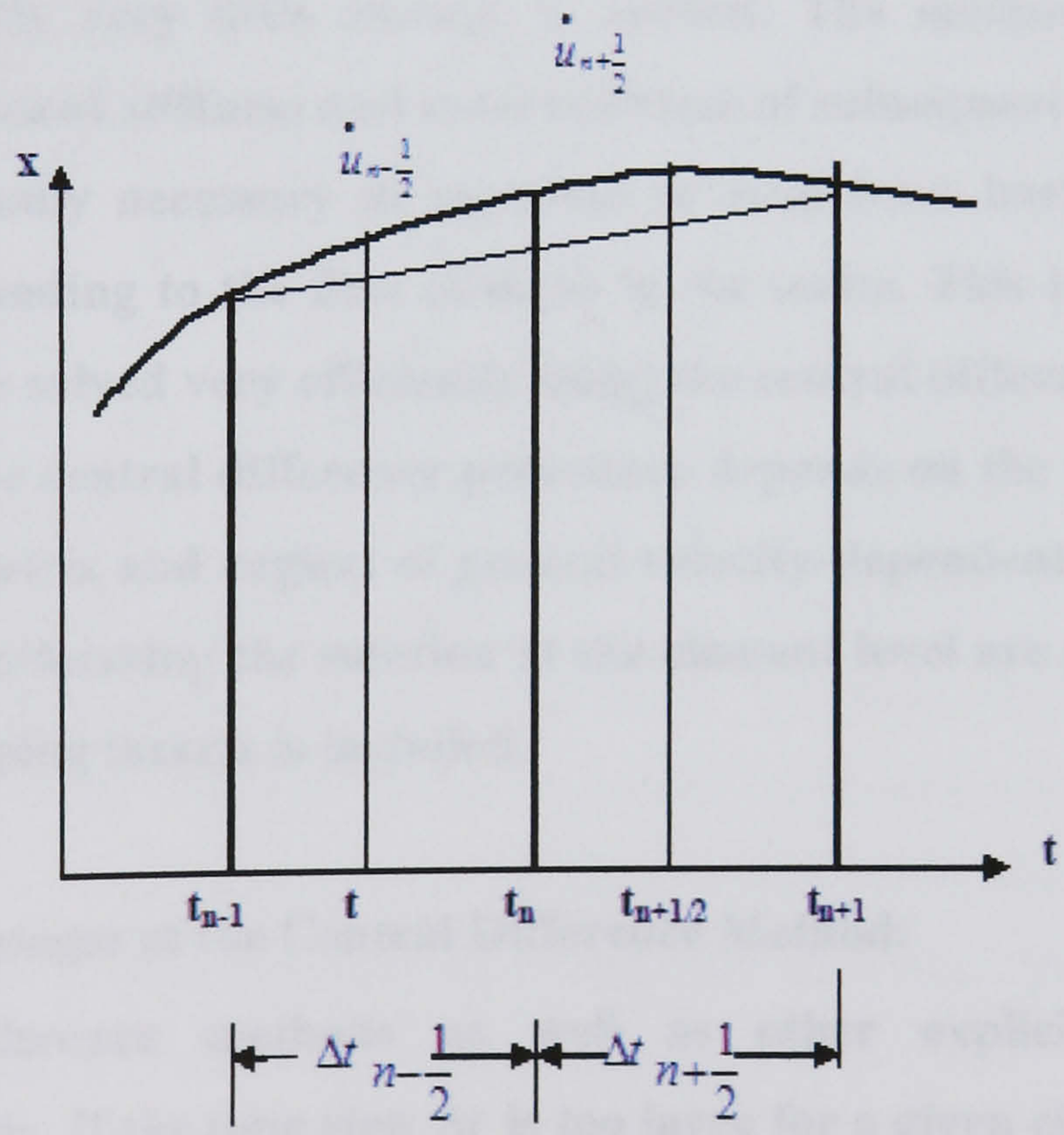

Figure (A1.2) Central difference method representation

Substituting the approximate values for the velocity and acceleration from the central difference scheme in the equations of equilibrium, to get

$$\left(m+\frac{1}{2}\Delta tc\right)u_{n+1}=\Delta t^2 p_n-(\Delta t^2 k-2m)u_n-\left(m-\frac{\Delta t}{2}c\right)u_{n-1} \qquad \textbf{(A1.54)}$$

Where p_n is the external body force loads, the solution for u_{n+1} can be determined. Since the solution for u_{n+1} is based on conditions at time t_{n-1} and t_n, the central difference integration procedure is called the explicit integration method. Also this method does not require the factorization of the effective stiffness matrix in the step-by-step solution. On the other hand, other methods like Newmark, Wilson and Houbolt does not involve conditions at time t_{n+1} hence called implicit integration methods, Halliquist [44], Subramani [117] and Jerry [140]

- **Advantages of the Central Difference Method:**

The main advantage of the central difference method is that no stiffness and mass matrices of the complete element assemblage are calculated, Bath [76], Coock [79] and Klaus [141]. The solution can be essentially carried out on an element level and relatively very little storage is needed. The method becomes more effective if the element stiffness and mass matrices of subsequent elements are the same, since it is only necessary to calculate or read from back-up storage the matrices corresponding to the first element in the series. This is why systems of large order can be solved very efficiently using the central difference scheme. The effectiveness of the central difference procedure depends on the use of a diagonal (lumped) mass matrix and neglect of general velocity-dependent damping forces. The benefits of performing the solution at the element level are preserved only if the diagonal damping matrix is included.

- **Disadvantages of the Central Difference Method:**

The central difference methods as well as other explicit methods are conditionally stable. If the time step Δt is too large for a given element size L the method fails and if Δt is smaller than required the solution time becomes very expensive losing the effectiveness of the method. Therefore, it is necessary to determine the critical time for the given problem. For central difference method, critical Δt is governed by the following equation.

$$\Delta t = \frac{L}{C} \qquad \textbf{(A1.55)}$$

Where, $C =$ **light wave speed** $= \sqrt{\frac{E}{\rho}}$ **, E= Material Young's Modulus**

ρ =Material Density. The above equation is called the CFL (Courant, Friedrichs and Lewy) condition, Bath [76], Coock [79]. The physical interpretation of the condition is that the time step Δt must be small enough that the information does not propagate across more than one element per time step. In some structural analysis depending on the material properties and dimensions of the geometry the time step required could be very small resulting in a longer computational time.

A1.7 Numerical Analysis:

The numerical analysis attempts to solve the differential equations by numerical procedures, which can be easily programmed using a standard programming language. The higher time step values from the initial boundary values can be programmed by the differential equations. This is done by splitting the differential equation into numerical components in the time axis using the forward, central or the backward differentiation methods. The numerical methods can be broadly classified as the explicit and implicit methods. In the explicit method, the previous time step is used to calculate the next time step. On the other hand, the implicit method calculates the next time step values by solving a matrix of the present and the previous time step values. The explicit method gives an accurate solution for a shorter time step and is conditionally stable, whereas the implicit method requires larger time steps for correct results, as already been discussed in the previous section.

A1.8 Contact-Impact Algorithm:

LS-DYNA3D uses three approaches for dealing with the impact contact and sliding interfaces of the models. The methods are known as the "kinematics constraint method", the "penalty method", and the "distributed parameter method", Subramani [117], Jerry [140]. The kinematics constraint method is used only for tying surfaces. In this method, constraints are imposed in the global equations by a transformation of the nodal displacement components of the "slave" nodes along the contact interfaces. This way only the global degrees of freedom of each master node are coupled. This method requires "consistent" zoning of the interfaces. In the penalty method, artificial interface springs are placed normal to the contacting surfaces on all the penetrating nodes. These artificial spring elements are assembled in the global stiffness matrix and their modulus is determined based on the elements in which the nodes reside. This method is stable and produces less noise for hourglass modes. However, for relatively large interface pressures, the stiffness has to be scaled up and the time step reduced. In such cases the third method "distributed parameter" is more appropriate. This last method is mainly used for "sliding interfaces" in which the internal stress in each element in contact determines the pressure distribution for the corresponding master surface. Accelerations are updated after mass and pressure distributions on the master surface are completed. With these three algorithms, an array of contacting interfaces is available in LS-DYNA3D, which allows the simulation of most contact conditions.

Treatment of sliding and impact along interfaces are very critical in simulating the correct load transfer between components in an analysis. Contact forces generated influence the acceleration of the body. Contact algorithms employed in finite element codes divide the nodes of bodies involved in contact into slave and master nodes. After the initial division, each slave node is checked for penetration against master nodes for an element face. Therefore, using a robust contact algorithm that can efficiently track and generate appropriate forces to the slave nodes without generating spurious results is very important. A brief discussion of the three methods used by LS-DYNA3D with merits and demerits follows:

A1.8.1 Kinematics constraint method:

This method uses the impact and release conditions of Hughes et al, Halliquist [44]. Constraints are imposed on the global equations by a transformation of the nodal displacement components of the slave nodes along the contact surface. This transformation has the effect of eliminating the normal degree of freedom of nodes. Since computational efficiency of the explicit time integration needs to be preserved, the mass is lumped to the extent that only the global degrees of freedom of each master node are coupled. Impact and release conditions are imposed to ensure momentum conservation. This method is advantageous to use when materials in contact have very different material properties. The nodes are constrained to stay on or very close to the surface without causing penetrations due to the difference in the stiffness. However, problems arise when the master surface zoning is finer than the slave surface zoning. Certain master nodes can penetrate through the slave surface without resistance and create a kink in the slide line.

A1.8.2 Penalty method:

This method consists of placing normal interface springs between all penetration nodes and the contact surface. With the exception of the spring stiffness matrix, which must be assembled in the global stiffness matrix, the implicit and explicit methods are similar. Momentum is conserved without the necessity of impact and release conditions. The equations involving the stiffness of the contact spring are as follows:

$k = f_s * Area^2 K \Big/$ **minimum diagonal length for shell elements** **(A1.56)**

$$k = \frac{f_s * Area^2 * K}{Vlume}$$ **for solid elements** **(A1.57)**

Area = Area of contact segment

K = Bulk modulus of contacted element

f_s **= penalty factor (0.1 by default)**

The interface stiffness k is chosen to be approximately the same order of magnitude as the stiffness of the interface element normal to the interface. Consequently the computed time step size is unaffected by the existence of the interfaces. However, if interface pressure becomes large, unacceptable penetration may occur. By scaling up the stiffness f_s and scaling down the time step Δt, this may be overcome. K for a contact segment is calculated based on the material properties of the component involved in the contact. If two different materials with varying stiffness such as foam and steel come in contact, the stiffness of the lesser magnitude is taken as the contact stiffness. This causes penetration problems as the force generated by foam is small compared to that generated by steel. This is overcome by scaling f_s until the forces generated by the two materials are in equilibrium. Determining the appropriate value of f_s is important so that the forces are in equilibrium.

A1.8.3 Distributed parameter method:

This method is derived from TENSOR programs, Halliquist [44], which displaced fewer mesh instabilities compared to the nodal constraint algorithm. In this method one half the slave element mass of each element in contact is distributed to the covered master surface area. Also, the internal stress in each element determines a pressure distribution for the master surface area that receives mass. After the distribution of mass and pressure the acceleration of the master surface is updated.

A1.9 Contact Energy Calculation:

The contact energy $E_{contact}$ is incrementally updated from time n to n+1 for each contact interface. $E_{contact}$ is determined using the following equation,

$$E_{contact}^{n+1} = E_{contact}^{n} + \left[\sum_{i=1}^{nsn} \Delta F_i^{slave} * \Delta dist_i^{slave} + \sum_{i=1}^{msn} \Delta F_i^{master} * \Delta dist_i^{master} \right]^{n+1/2} \quad \textbf{(A1.58)}$$

where

nsn = number of slave nodes

msn = number of master nodes

ΔF_i^{slave} **= interface force between the ith slave node and the contact segment**

ΔF_i^{master} **= interface force between the ith master node and the contact segment**

$\Delta dist_i^{slave}$ **= is the incremental distance the ith slave node has moved during the current time step.**

$\Delta dist_i^{master}$ **= is the incremental distance the ith master node has moved during the current time step.**

Monitoring the contact energy calculated is very important to ensure proper calculation made by the contact algorithm. In the absence of friction, the slave and master side energies should be close in magnitude but opposite in sign. The sum $E_{contact}$ should equal the stored energy. Large negative contact energy is a sign of undetected nodal penetrations.

Appendix-A2 The Floating Wind Turbine Construction:

A2.1 Introduction:

In this appendix, supplemented to the main text, a pre-processor, FEMB-28 LSTC [3], the Keyword User's Manuals LSTC [45] and [46], the Theoretical Manual, Halliquist [44], Reid LSDYNA Examples Manual [48] and Klaus [141] are used and frequently consulted for preparing the input file for the LS-DYNA3D non-linear dynamic explicit code. In this appendix, the use of this pre-processor is shown to produce the seventeen parts used in the developed detailed model presented in Chapter V of this thesis.

Before starting to digitise a model, a drawing has to be sketched, with dimensions intended to be used in the analysis, these drawings should represent different parts, and on the same global reference axis for the whole parts and does not need to be scaled. These parts will coincide or interact as one body once activated together and given the right materials, properties, contact and boundary conditions. The database file is opened in which a certain set of dimensions are readily picked and defined to be the default dimensions. These have to be strictly followed for a consistent set of units throughout the model till the stage of analysis. All parameters in this work follow SI units as follows; mass (kg), length (m), stress (MPa), force (N), time (second), pressure (Pa), temperature (deg. C), modulus of elasticity (Pa) and mass (kg/m^3).

Most FEM models require certain steps procedure or pre-process, in order to create the keywords input file which would be readily imported to the main solver for analysis. Obviously the code must be capable of reading this file. In this work, the solver is LS-DYNA3D code, version 970, of LSTC, and the pre-processor is FEMB-28, these mentioned steps are:

1. Modelling: or digitising drawings to form nodes then elements, either directly through nodes or via creating lines or surfaces then elements.

In the modelling stage, the structure is merely translated to lines or surfaces, then finally to elements. Checked for model integrity and coincident nodes, the named functions of nodes, lines and surfaces could or must be deleted once they have

served their purpose, and are no longer needed. However, if a geometrical change is required, this data is stored and could be recalled back. The aim of this stage is to interpret the structure into compatible elements and nodes.

2. Materials: have to be defined for each part(s) or elements.

This is the next stage, implemented through the material menu, and chosen from the ready material library (could also be user defined). Before material is created and assigned to a part, this part has to be current, parts are displayed in material colour once they have been assigned a material, otherwise will be displayed in grey.

3. Property: has to be defined and assigned to appropriate parts to simulate the desired behaviour or boundary conditions. All model parts need to be turned on and displayed in either property colour or in grey if property is not assigned. All elements should be assigned their intended geometrical properties.

4. Contact: this is for interaction of coupling surfaces in the model, specifically when modelling integral actions of parts.

5. Boundary conditions: this is the final formulation of the actual behaviour of a part or material to simulate the intended action to be analysed, most of the common boundary conditions are recognised by LS-DYNA3D and can be readily introduced. Mainly restraints of rotations translations and loads reflecting the intended action need be simulated.

The definition of a database is a precondition for creating parts; the code does not allow creation of parts in an empty database. Parts are created at the beginning and called when needed or created promptly when required once created they can be switched on and off for updating and modification, or to perform any operation that involve such parts. Materials and properties can either be defined upon creation of a part or assigned at a later stage.

As already stated, the model consists of seventeen parts; these will be mentioned in some detail in this appendix with an emphasis on pre-processor use of preparing the input file. The basic emphasis here will be on the keyword cards related to materials, properties, boundary conditions, contact, constraints and load applications and will be discussed as follows:

A2.2.1. Blades part:

As mentioned in the main text they are made of shell elements, element formulation 16 is chosen to guard against hourglass modes material and property keyword cards are:

Modelled by shell elements, *SECTION_SHELL, two keyword cards required for defining property and material with the ID numbers appearing are arbitrary (but unique) and follows part successive order as in Chapter V of this work:

SEC ID	**Section ID**	**15**
ELFORM	**Element Formulation**	**16**
SHRF	**Shear Factor**	**0.83333**
NIP	**Number of Integration Points**	**4**
PROPT	**Print out Option**	**3**
QR/IRID	**Quadrature Rule**	**0**
ICOMP	**Layered Composite Flag**	**0**
SETYP	**2D Solid Element Type**	**1**
T1	**Shell Thickness at Node1**	**0 .030**
T2	**Shell Thickness at Node2**	**0.030**
T3	**Shell Thickness at Node3**	**0.030**
T3	**Shell Thickness at Node4**	**0.030**
NLOC	**Location of Preference Surface**	**0**
MAREA	**Non-Structural Mass per**	**0**

And material card is:

***MAT_PLASTIC_KINEMATIC**

MID	**Material ID**	**15**
RO	**Mass Density**	**976.3**
E	**Young's Modulus**	**$2.9x10^{11}$**
PR	**Poisson's Ratio**	**0.30**
N	**MADYMO3D Couple Flag**	**0**
SIGY	**Plastic Hardening modulus**	**0**
BETA	**Hardening parameter**	**0.1**
SRC	**Strain Rate Parameter**	
SRP	**Strain Rate Parameter**	
FS	**Failure Strain Eroding Elements**	**1.0**
VP	**Local Coordinate System or X-comp.**	**0**

A2.2.2. Hub part:

Modelled by plate shells, *SECTION_SHELL, with property inputs:

SEC ID	**Section ID**	**14**
ELFORM	**Element Formulation**	**16**
SHRF	**Shear Factor**	**0.83333**
NIP	**Number of Integration Points**	**4**
PROPT	**Print out Option**	**3**
QR/IRID	**Quadrature Rule**	**0**
ICOMP	**Layered Composite Flag**	**0**
SETYP	**2D Solid Element Type**	**1**
T1	**Shell Thickness at Node1**	**0.032**
T2	**Shell Thickness at Node2**	**0.032**
T3	**Shell Thickness at Node3**	**0.032**
T3	**Shell Thickness at Node4**	**0 .032**
NLOC	**Location of Preference Surface**	**0**

MAREA	**Non-structural Mass per**	**0**

And material card is: *MAT-PLASTIC_KINEMATIC

MID	**Material ID**	**14**
RO	**Mass Density**	**5148**
E	**Young's Modulus**	**$2.1x10^{11}$**
PR	**Poisson's Ratio**	**0.30**
SIGY	**Plastic Hardening modulus**	**$3.6x10^{6}$**
BETA	**Hardening parameter**	**0.4**
SRC	**Strain Rate Parameter**	
SPR	**Strain rate parameter**	
FS	**Failure Strain Eroding Elements**	**1.0**
VP	**Local Coordinate System or X-comp.**	**0**

A2.2.3 Transmission part:

Section property is solid brick element or *SECTION_SOLID with parameters:

SEC ID	**Section ID**	**13**
ELFORM	**Element Formulation**	**3**
AET	**Ambient Element Type**	**0**

Modelled with material type 20 or *MAT_RIGID with factors:

MID	**Material ID**	**3**
RO	**Mss Density**	**7850**
E	**Young's Modulus**	**$2.1x10^{11}$**
PR	**Poisson's Ratio**	**0.28**
N	**MADYMO3D Couple Flag**	**0.0**
COUPLE	**Coupling Option**	**0.0**
M	**MADYMO/CAL3D Couple**	**0.0**

ALIAS	VDA Surface ALIAS	0.0
CMO	Centre of Mass Constraint	
CON1	Translation Constraint	
CON2	Rotational Constraint	
LCO OR	Local Coordinate System or X-comp.	13
A_2	Y-comp. Vector 1	0
A_3	Z-comp. Vector 1	0
V_1	X-comp. Vector 2	0
V_2	Y-comp. Vector 2	0
V_3	Z-comp. Vector 2	0

A2.2.4 Nacelle part:

Modelled with shell elements or *SECTION_SHELL and parameters:

SEC ID	Section ID	8
ELFORM	Element Formulation	16
SHRF	Shear Factor	0.83333
NIP	Number of Integration Points	2
PROPT	Print out Option	3
QR/IRID	Quadrature Rule	0
ICOMP	Layered Composite Flag	0
SETYP	2D Solid Element Type	1
T1	Shell Thickness at Node1	0.02
T2	Shell Thickness at Node2	0.02
T3	Shell Thickness at Node3	0.02
T4	Shell Thickness at Node4	0.02
NLOC	Location of Reference Surface	0
MAREA	Non-structural mass per	0

And of material type 20 or *MAT_RIGID with parameters:

MID	**Material ID**	**8**
RO	**Mss Density**	**7850**
E	**Young's Modulus**	**$2.1x10^{11}$**
PR	**Poisson's Ratio**	**0.28**
N	**MADYMO3D Couple Flag**	**0.0**
COUPLE	**Coupling Option**	**0.0**
M	**MADYMO/CAL3D Couple**	**0.0**
ALIAS	**VDA Surface ALIAS**	**0.0**
CMO	**Centre of Mass Constraint**	
CON1	**Translation Constraint**	
CON2	**Rotational Constraint**	
LCO OR A_1	**Local Coordinate System or X-**	**8**
A_2	**Y-comp. Vector 1**	**0**
A_3	**Z-comp. Vector 1**	**0**
V_1	**X-comp. Vector 2**	**0**
V_2	**Y-comp. Vector 2**	**0**
V_3	**Z-comp. Vector 2**	**0**

A2.2.5 Gear part:

Modelled with brick solid elements, *SECTION_SOLID with input values:

SEC ID	**Section ID**	**9**
ELFORM	**Element Formulation**	**3**
AET	**Ambient Element Type**	**0**

And material type 20 or *MAT_RIGID with input values:

MID	**Material ID**	**9**
RO	**Mss Density**	**7850**

E	**Young's Modulus**	**$2.1x10^{11}$**
PR	**Poisson's Ratio**	**0.28**
N	**MADYMO3D Couple Flag**	**0.0**
COUPLE	**Coupling Option**	**0.0**
M	**MADYMO/CAL3D Couple**	**0.0**
ALIAS	**VDA Surface ALIAS**	**0.0**
CMO	**Centre of Mass Constraint**	
CON1	**Translation Constraint**	
CON2	**Rotational Constraint**	
LCO OR A_1	**Local Coordinate System or X-**	**9**
A_2	**Y-comp. Vector 1**	**0**
A_3	**Z-comp. Vector 1**	**0**
V_1	**X-comp. Vector 2**	**0**
V_2	**Y-comp. Vector 2**	**0**
V_3	**Z-comp. Vector 2**	**0**

A2.2.6 Drive part:

Modelled with solid brick elements, *SEC_SOLID with input values:

SEC ID	**Section ID**	**10**
ELFORM	**Element Formulation**	**3**
AET	**Ambient Element Type**	**0**

And material type 20, *MAT_RIGID with inputs:

MID	**Material ID**	**10**
RO	**Mss Density**	**7850**
E	**Young's Modulus**	**$2.1x10^{11}$**
PR	**Poisson's Ratio**	**0.28**
N	**MADYMO3D Couple Flag**	**0.0**

COUPLE	**Coupling Option**	**0.0**
M	**MADYMO/CAL3D Couple**	**0.0**
ALIAS	**VDA Surface ALIAS**	**0.0**
CMO	**Centre of Mass Constraint**	
CON1	**Translation Constraint**	
CON2	**Rotational Constraint**	
LCO OR	**Local Coordinate System or X-comp.**	**10**
A_2	**Y-comp. Vector 1**	**0**
A_3	**Z-comp. Vector 1**	**0**
V_1	**X-comp. Vector 2**	**0**
V_2	**Y-comp. Vector 2**	**0**
V_3	**Z-comp. Vector 2**	**0**

A2.2.7 Generator part:

Also modelled with solid brick elements, *SEC_SOLID of parameters:

SEC ID	**Section ID**	**11**
ELFORM	**Element Formulation**	**3**
AET	**Ambient Element Type**	**0**

And material type 20, *MAT_RIGID with parameters:

MID	**Material ID**	**11**
RO	**Mss Density**	**8900**
E	**Young's Modulus**	**$1.25x10^{10}$**
PR	**Poisson's Ratio**	**0.25**
N	**MADYMO3D Couple Flag**	**0.0**
COUPLE	**Coupling Option**	**0.0**
M	**MADYMO/CAL3D Couple**	**0.0**
ALIAS	**VDA Surface ALIAS**	**0.0**
CMO	**Centre of Mass Constraint**	

CON1		Translation Constraint	
CON2		Rotational Constraint	
LCO	OR	Local Coordinate System or X-comp.	11
A_2		Y-comp. Vector 1	0
A_3		Z-comp. Vector 1	0
V_1		X-comp. Vector 2	0
V_2		Y-comp. Vector 2	0
V_3		Z-comp. Vector 2	0

A2.2.8 Yaw ring part:

Modelled with solid bricks, *SECTION_SOLID and parameters:

SEC ID	Section ID	7
ELFORM	Element Formulation	3
AET	Ambient Element Type	0

And material type 20, *MAT_RIGID, with input values:

MID	Material ID	7
RO	Mss Density	7850
E	Young's Modulus	$2.1x10^{11}$
PR	Poisson's Ratio	0.28
N	MADYMO3D Couple Flag	0.0
COUPLE	Coupling Option	0.0
M	MADYMO/CAL3D Couple	0.0
ALIAS	VDA Surface ALIAS	0.0
CMO	Centre of Mass Constraint	
CON1	Translation Constraint	
CON2	Rotational Constraint	
LCO	OR Local Coordinate System or X-comp.	7
A_2	Y-comp. Vector 1	0

A_3	Z-comp. Vector 1	0
V_1	X-comp. Vector 2	0
V_2	Y-comp. Vector 2	0
V_3	Z-comp. Vector 2	0

A2.2.9 Bearing part:

Modelled with brick elements, *SECTION_SOLID of parameters:

SEC ID	Section ID	6
ELFORM	Element Formulation	3
AET	Ambient Element Type	0

And material rigid type 20, *MAT_RIGID of inputs:

MID	Material ID	6
RO	Mss Density	7850
E	Young's Modulus	$2.1x10^{11}$
PR	Poisson's Ratio	0.28
N	MADYMO3D Couple Flag	0.0
COUPLE	Coupling Option	0.0
M	MADYMO/CAL3D Couple	0.0
ALIAS	VDA Surface ALIAS	0.0
CMO	Centre of Mass Constraint	
CON1	Translation Constraint	
CON2	Rotational Constraint	
LCO OR	Local Coordinate System or X-comp.	6
A_2	Y-comp. Vector 1	0
A_3	Z-comp. Vector 1	0
V_1	X-comp. Vector 2	0
V_2	Y-comp. Vector 2	0

V_3	Z-comp. Vector 2	0

A2.2.10 Tower part:

Modelled with beams, *SECTION_BEAM of inputs:

SEC ID	Section ID	5
ELFORM	Element Formulation	3
SHRF	Shear Factor	
QR/IR ID	Quadature Rule	2
CST	Cross Section Type	1
SCOOR	Location of TRIAD	2
A	Cross Sectional Area	$307x10^{-4}$
Iss	Inertia in S-dir	$9.14x10^{-4}$
Itt	Inertia in T-dir	$9.14x10^{-4}$
Irr	Inertia in R-dir	$18.3x10^{-4}$
SA	Shear Area	$307x10^{-4}$

And material type 98, *MAT_SIMPLIFIED_JOHNSON_COOK, with inputs:

MID	Material ID	11
RO	Mss Density	7850
E	Young's Modulus	$2.1x10^{11}$
PR	Poisson's Ratio	0.28
VP	Formulation Rate Effect	1.0
A	Parameter	$7.9200x10^{8}$
B	Parameter	$5.0951x10^{8}$
N	Parameter	0.26
C	Parameter	0.014
PSFAIL	Plastic Strain Failure	0.05
SIGMAX	Maximum Stress	$4.5x10^{8}$

SIGSAT	**Saturation Stress**	**$4.5x10^8$**
EPSO	**Plastic Strain Rate**	**1.0**

A2.2.11 Hull part:

Modelled with solid bricks, *SECTION_SOLID with inputs:

SEC ID	**Section ID**	**3**
ELFORM	**Element Formulation**	**3**
AET	**Ambient Element Type**	**0**

And material type 1, *MAT_ELASTIC with inputs:

MID	**Material ID**	**3**
RO	**Mass Density**	**2213.4**
E	**Young's Modulus**	**$2.4x10^{10}$**
PR	**Poisson' ratio**	**0.25**
DA	**Axial Damping Factor**	**0**
DB	**Bending Damping Factor**	**0**

The coupling card for hull fluid part set is as follows:

***CONSTRAINED_LAGRANGE_IN_SOLID**

SlAVE	**Slave part ID**	**3**
MASTER	**Master part ID**	**1**
SSTYPE	**Slave type**	**1**
MSTYP	**Master type**	**0**
NQUAD	**Quadrature rule for coupling**	**2**
CTYPE	**Coupling type**	**4**
DIREC	**Coupling direction**	**2**
MCOUP	**Multi-material option**	**-1**
START	**Start time for coupling**	
END	**End time for coupling**	

PFAC	**Penalty factor**	**0.01**
FRIC	**Coefficient of friction**	
FRCMIN	**Minimum volume fraction**	
NORM	**Normal orientation**	**0**
NORMTYP	**Penalty coupling spring direc…**	**0**
DAMP	**Damping factor**	**0.6**
CQ	**Heat transfer coefficient**	
HMIN	**Min air gap**	
HMAX	**Max air gap**	
ILEAK	**Leakage control**	**0**
PLEAK	**Leakage control penalty factor**	**0.01**
LCIDPOR	**Load curve for porous flow**	

A2.2.12 Foam part:

Modelled with solid bricks, *SECTION_SOILD with parameters:

SEC ID	**Section ID**	**4**
ELFORM	**Element Formulation**	**3**
AET	**Ambient Element Type**	**0**

And material type 57, *MAT_LOW_DENSITY_FOAM with inputs:

MID	**Material ID**	**4**
RO	**Mass density**	**44.14**
E	**Young's Modulus**	**$1.6x10^9$**
LCID	**Stress-strain LCID**	**5**
TC	**Tension cut-off stress**	**0**
HU	**Hysteretic unloading**	**1.0**
BETA	**Creep decay constant**	
DAMP	**Viscous coefficient**	**0.1**

SHAPE	**Shape factor**	**0.5**
FAIL	**Failure stress cut-off**	**0**
BVFLAG	**Bulk viscosity flag**	**1**
ED	**Young's relaxation**	**0**
BETA1	**Optional decay constant**	**0**
KCON	**Interface stiffness coefficient**	**200**
REF	**Reference geometry flag**	**1**

A2.2.13 Moorings part:

The mooring cables consists of gripping corbels fixed at the hull deck outer circumference, 10m vertically below them are the shoe guides, firmly attached to hull outer surface, allowing cables to pass through. From there cables extend to mooring points at a piled seabed anchor, shared by more than one cable in the floating farm.

Section properties are defined by beams, *SECTION_BEAM with inputs:

SEC ID	**Section ID**	**16**
ELFORM	**Element Formulation**	**6**
SHRF	**Shear Factor**	
QR/IRID	**Quadature Rule**	**2**
CST	**Cross Section Type**	**1**
SCOOR	**Location of TRIAD**	**3**
NSM	**Non structural mass per**	**8.7**
VOL	**Volume of Discrete Beam**	**1.716324×10^{-3}**
INER	**Inertia of Discrete Beam**	**1.4221×10^{-4}**
CID	**Coordinate System ID optional)**	**0**
CA	**Cable Area**	**4.2274×10^{-2}**
Offset	**Cable Offset**	
RCON	**R-rotational Constraint**	**0.0**
SRCON	**S-rotational Constraint**	**0**

TRCON	**T-rotational Constraint**	**0**

And modelled with material type 71, *MAT_CABLE_DISCETE_BEAM with inputs:

MID	**Material ID**	**16**
RO	**Mass Density**	**1**
E	**Young's Modulus**	**$9x10^9$**
LCID	**Load Curve ID (stress-strain) optional**	**3**
FO	**Inertial Tensile Force**	**0**

The coupling card for cables and water is:

***CONSTRAINED_LAGRANGE_IN_SOLID**

SlAVE	**Slave part ID**	**17**
MASTER	**Master part ID**	**1**
SSTYPE	**Slave type**	**1**
MSTYP	**Master type**	**1**
NQUAD	**Quadrature rule for coupling**	**0**
CTYPE	**Coupling type**	**2**
DIREC	**Coupling direction**	**1**
MCOUP	**Multi-material option**	
START	**Start time for coupling**	
END	**End time for coupling**	
PFAC	**Penalty factor**	
FRIC	**Coefficient of friction**	**0.01**
FRCMIN	**Minimum volume fraction**	
NORM	**Normal orientation**	**0**
NORMTYP	**Penalty coupling spring direc…**	**0**
DAMP	**Damping factor**	**0.05**

CQ	Heat transfer coefficient	
HMIN	Min air gap	
HMAX	Max air gap	
ILEAK	Leakage control	0
PLEAK	Leakage control penalty factor	0.01
LCIDPOR	Load curve for porous flow	

And the coupling card for cable and air is:

*CONSTRAINED_LAGRANGE_IN_SOLID

SlAVE	Slave part ID	17
MASTER	Master part ID	2
SSTYPE	Slave type	1
MSTYP	Master type	1
NQUAD	Quadrature rule for coupling	0
CTYPE	Coupling type	4
DIREC	Coupling direction	2
MCOUP	Multi-material option	
START	Start time for coupling	
END	End time for coupling	
PFAC	Penalty factor	
FRIC	Coefficient of friction	0.001
FRCMIN	Minimum volume fraction	
NORM	Normal orientation	0
NORMTYP	Penalty coupling spring direc…	0
DAMP	Damping factor	
CQ	Heat transfer coefficient	
HMIN	Min air gap	
HMAX	Max air gap	
ILEAK	Leakage control	0

PLEAK	**Leakage control penalty factor**	**0.01**
LCIDPOR	**Load curve for porous flow**	

A2.2.14 Water part:

Modelled with solid ALE element, *SECTION_SOLID_ALE

SEC ID	**Section ID**	**1**
ELFORM	**Element Formulation**	**11**
AET	**Ambient Element Type**	**0**
AFAC	**Smoothing W.F. –simple ave.**	**0**
BFAC	**Smoothing W.F. –volume w..**	**0**
CFAC	**Smoothing W.F. –Isoparam.**	**0**
DFAC	**Smoothing W.F. –Equipoten.**	**0**
STAR	**Start time for smoothing**	**0**
END	**End time for smoothing**	**0**
AAFAC	**ALE Advection factor**	**0**

While material for water part is modelled using material type 9, *MAT_NULL with parameters and equation of state as:

MID	**Material ID**	**15**
RO	**Mass density**	**1025**
PC	**Pressure cut-off**	**-1.0132×10^{3}**
MU	**Viscosity coefficient**	**8.684×10^{-4}**
TEROD	**Relative volume in tension**	**0**
CEROD	**Relative volume in compression**	**0**
YM	**Young's modulus**	**0**
PR	**Poisson's ratio**	**0**

This requires the definition of equation of state,*EOS_GRUNEISEN as:

EQSID	**Equation of state ID**	**1**
C	**Equation constant**	**$1.647x10^3$**
S_1	**Equation constant**	**1.921**
S_2	**Equation constant**	**$-9.6x10^{-2}$**
S_3	**Equation constant**	**0**
GAMA0	**Equation constant**	**0.35**
A	**Equation constant**	
EO	**Initial internal energy**	
V0	**Initial relative volume**	**1.0**

A2.2.15 Air part:

Also modelled with solid ALE elements, *SECTION_SOLID_ALE with input values:

SEC ID	**Section ID**	**2**
ELFORM	**Element Formulation**	**11**
AET	**Ambient Element Type**	**4**
AFAC	**Smoothing W.F. –simple ave.**	**0**
BFAC	**Smoothing W.F. –volume w..**	**0**
CFAC	**Smoothing W.F. –Isoparam.**	**0**
DFAC	**Smoothing W.F. –Equipoten.**	**0**
STAR	**Start time for smoothing**	**0**
END	**End time for smoothing**	**0**
AAFAC	**ALE Advection factor**	**0**

And material type 9, *MAT_NULL with inputs:

MID	**Material ID**	**2**
RO	**Mass density**	**1.1845**
PC	**Pressure cut-off**	**$-1.0132x10^2$**
MU	**Viscosity coefficient**	**$1.8444x10^{-5}$**

TEROD	**Relative volume in tension**	**0**
CEROD	**Relative volume in compression**	**0**
YM	**Young's modulus**	**0**
PR	**Poisson's ratio**	**0**

This material requires an equation of state as, *LINEAR POLYNOMIAL as:

EQSID	**Equation of state ID**	**2**
C0	**Equation constant**	**0**
C_1	**Equation constant**	**0**
C_2	**Equation constant**	**0**
C_3	**Equation constant**	**0**
C_4	**Equation constant**	**0.4**
C_5	**Equation constant**	**0.4**
EO	**Initial internal energy**	**253307.82**
V0	**Initial relative volume**	**1**

A2.2.16 Seabed part:

Modelled with shell element, *SECTION_SHELL with input values:

SEC ID	**Section ID**	**17**
ELFORM	**Element Formulation**	**16**
SHRF	**Shear Factor**	**0.83333**
NIP	**Number of Integration Points**	**4**
PROPT	**Print out Option**	**3**
QR/IRID	**Quadrature Rule**	**0**
ICOMP	**Layered Composite Flag**	**0**
SETYP	**2D Solid Element Type**	**1**
T1	**Shell Thickness at Node1**	**0 .050**
T2	**Shell Thickness at Node2**	**0.050**

T3	**Shell Thickness at Node3**	**0.050**
T3	**Shell Thickness at Node4**	**0.050**
NLOC	**Location of Preference Surface**	**0**
MAREA	**Non-Structural Mass per**	**0**

And material type 20, *MAT_RIGID defined by parameters:

MID	**Material ID**	**17**
RO	**Mss Density**	**1800**
E	**Young's Modulus**	**$9x10^9$**
PR	**Poisson's Ratio**	**0.25**
N	**MADYMO3D Couple Flag**	**0.0**
COUPLE	**Coupling Option**	**0.0**
M	**MADYMO/CAL3D Couple**	**0.0**
ALIAS	**VDA Surface ALIAS**	**0.0**
CMO	**Centre of Mass Constraint**	**-1**
CON1	**Translation Constraint**	**2**
CON2	**Rotational Constraint**	**111111**
LCO OR	**Local Coordinate System or X-comp.**	**17**
A_2	**Y-comp. Vector 1**	**0**
A_3	**Z-comp. Vector 1**	**0**
V_1	**X-comp. Vector 2**	**0**
V_2	**Y-comp. Vector 2**	**0**
V_3	**Z-comp. Vector 2**	**0**

***INITIAL_VOLUME_FRACTION_GEOMETRY**

Defining the concrete cylinder disk geometry in water as:

Variable	Description	Value(s)
SID_ALE	Part or part set ID	1
ST_ALE	Set type	1
GROUP	Group ID	1
GEOTPE	Geometry type	4
IN_OPT	Set type	0
GR_FILL	Group ID	2
X0	x-coordinate of special point	0
Y0	y-coordinate of special point	0
Z0	z-coordinate of special point	0
X1	x-coordinate of normal vector	0
Y1	y-coordinate of normal vector	0
Z1	z-coordinate of normal vector	2.5
R1	Radius of lower base of cone	9.5
R2	Radius of upper base of cone	9.5

***INITIAL_VOLUME_FRACTION_GEOMETRY**

Defining the concrete cylinder part geometry in water:

Variable	Description	Value(s)
SID_ALE	Part or part set ID	1
ST_ALE	Set type	1
GROUP	Group ID	1
GEOTPE	Geometry type	4
IN_OPT	Set type	0
GR_FILL	Group ID	2
X0	x-coordinate of special point	0
Y0	y-coordinate of special point	0
Z0	z-coordinate of special point	2.5

X1	x-coordinate of normal vector	0
Y1	y-coordinate of normal vector	0
Z1	z-coordinate of normal vector	2.5
R1	Radius of lower base of cone	6.25
R2	Radius of upper base of cone	6.25

***INITIAL_VOLUME_FRACTION_GEOMETRY**

Defining the concrete cylinder geometry part in air:

Variable	Description	Value(s)
SID_ALE	Part or part set ID	2
ST_ALE	Set type	1
GROUP	Group ID	2
GEOTPE	Geometry type	4
IN_OPT	Set type	0
GR_FILL	Group ID	2
X0	x-coordinate of special point	0
Y0	y-coordinate of special point	0
Z0	z-coordinate of special point	25
X1	x-coordinate of normal vector	0
Y1	y-coordinate of normal vector	0
Z1	z-coordinate of normal vector	31
R1	Radius of lower base of cone	6.25
R2	Radius of upper base of cone	6.25

A2.3 Control Cards:

These are for instructing the code for certain tasks to modify the default values concerning dynamic relaxation time, starting, ending, cpu time, termination time, ...etc. These tasks are readily defined by the code, some of them are compulsory, while others are optional. Due to the importance of defining these cards, compulsory cards and some optional cards used are detailed:

***CONTROL_ACCURACY**

OSU	**Objectives Stress Update**	**1**
INN	**Invariant Node Numbering**	**2**

***CONTROL_CPU**

CPUTIM	**Seconds of CPU Time**	**00**

***CONTROL_ENERGY**

HGEN	**Hourglass Energy Calcu**	**1**
RWEN	**Stone Wall Energy Dissipat**	**2**
SLNTEN	**Sliding Interface Energy Dis**	**1**
RYLEN	**Damping Energy Dissipation**	**2**

***CONTROL_HOURGLASS**

IHQ	**Hourglass Viscosity Type**	**4**
HQ	**Hourglass Coefficient**	**0.0001**

***CONTROL_OUTPUT**

NPOPT	**Input Phase Print Suppressi**	**0**
NEECHO	**Input phase Echo Suppressi**	**0**
NREFUP	**Beam Reference Node Update**	**0**
IACCOP	**Averaged Accelerations**	**1**
OPIFS	**Interface Output Inter**	**0**
IPNINT	**Initial Time Step Print Option**	**0**
IKEDIT	**Problem Status Output Option**	**0**
IFLUSH	**Number of Time Steps Interval**	**0**
IPRIF	**Default Print Flag for Rbdo**	**0**

***CONTROL_SHELL**

WRPANG	**Shell Warpage Angle [degrees]**	**020**

IRIST	Triangular Shell Sorting	1
IRNXX	HUGES_LIU Shell Normal up	-1
ISTUPD	Shell Thickness Change Option	1
THEORY	Shell Theory	2
BWC	Warping Stiffness Belytsch	2
MITER	Plane Stress Plasticity Option	1
PROJ	Projection Method	1

*CONTROL_SOLUTION

SOLN	Analysis Solution Procedure	0

*CONTROL_TERMINATION

ENDTIM	Termination Time	5
ENDCYCL	Termination Cycle	
DTMIN	Initial Time Step S.F	
ENDENG	Percent Energy Change	
ENDMAS	Percent Mass Change	

*CONTROL_TIMESTEP

DTINIT	Initial Time Step Size	
TSSFAC	Computed Time Step	0.9
ISDO	Time Step Formula	0
ISLMIT	Shell Element Minimum Time Step	0
DT2MS	Mass Scaling	0
LCTM	Time Step Load Curve	0
ERODE	Errosion Flag	0
MSIST	Mass Scaling Limit	0

DATABASE Cards:

***DATABASE_GLSTAT**

DT	**Time Interval Output**	**1**

***DATABASE_MATSUM**

DT	**1**	

***DATABASE_BINARY_D3PLOT**

DT/CYCL	**Time Interval of Output**	**1**
LCDT	**Time Interval Load Curve**	**0**
BEAM	**Convergence Flag**	**0**
NOLTC	**Overrides on "DT" field**	**0**

***DATABASE_BINARY_D3THDT**

DT/CYCL	**Time Interval of Output**	**1**
LCDT	**Time Interval Load Curve**	**0**

A2.4 Analysis Phase:

The procedure started with a drawing using known dimensions, nodes, lines or surface, then elements. From there, materials, properties, boundary conditions, constraints, loads, contact, control cards, title, load curves, coordinate system….-. With all these are now defined, the next step is the analysis. First: the input file is exported by FEMB 28 (written in Notepad format) then edited for checking the format or inserting required data that are not supported by the pre-processor. The input file is either given a user defined name or saved as a default (file.dyn) to be recalled for running with LS-DYNA3D solver. Second: the LS-DYNA3D is activated (via solver function) the programme is run and database files defined will be automatically created, to be read by the attached post-processors, LSTC [11].

Appendix-A3 Blades Aerodynamics Formulations

A3.1 Rotor Aerodynamics:

Various methods are used to calculate the aerodynamic forces acting on the blades of a wind turbine. The most advanced are numerical methods solving Navier-Stokes equations for the compressible flow as well as the flow near the blades.

The two major approaches to calculating the forces are the Actuator Disk Model and the Blade Element Model. In the appendix to follow a brief introduction to these methods will be presented which extracted from Freris [16], Walker [73], Manwell [75], Det Norske [88], Andres [125] and Eggleston [137].

A3.1.1 Actuator disc model:

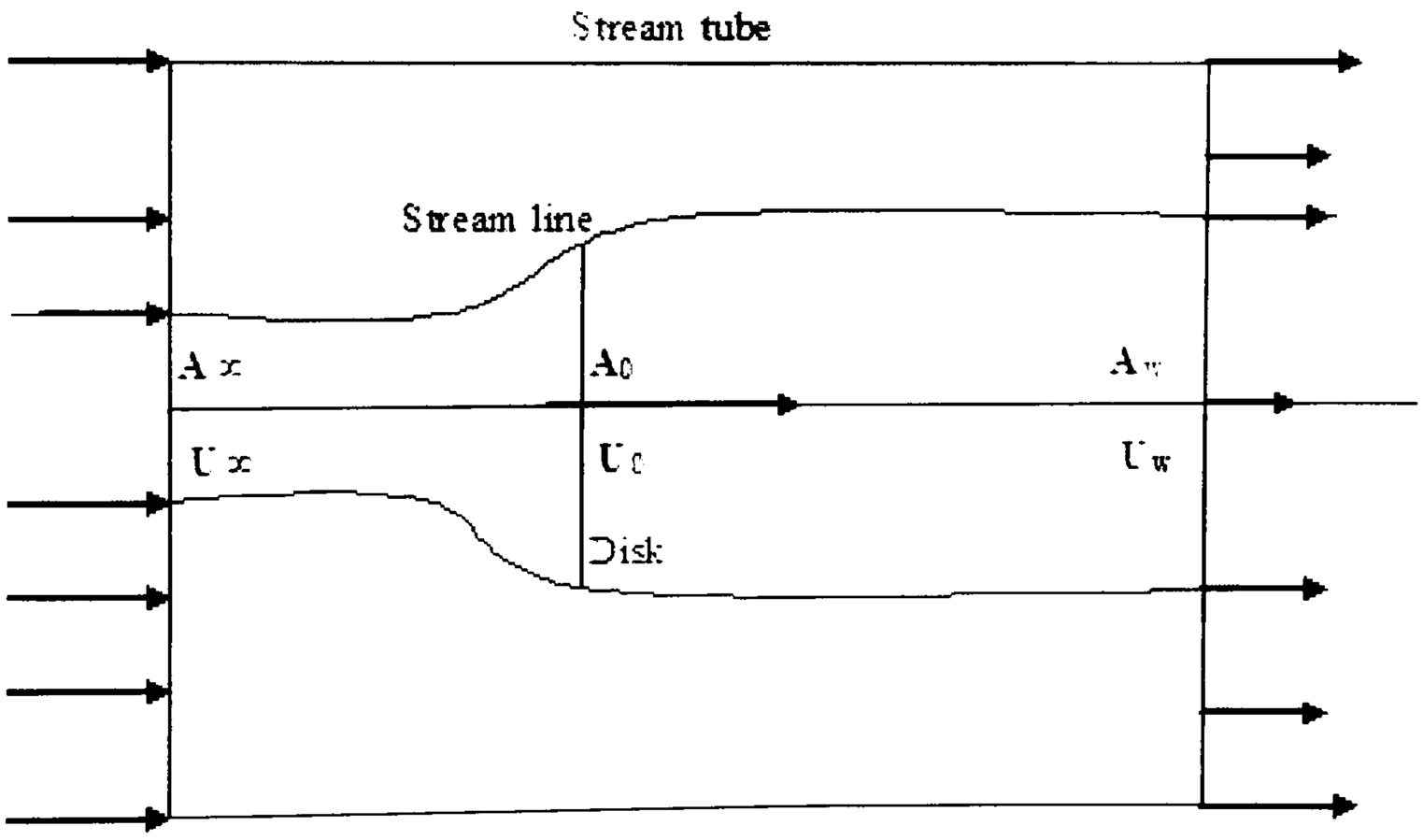

Figure (A3.1) Actuator disk

It is based on Bernoulli's equation and energy balances Andres [125], Eggleston [137] and Det Norske [88]. It is assuming that, the rotor is replaced by an actuator disc, through which the static pressure decreases discontinuously. By examining the flow through a control volume the extractable power from the turbine can be calculated Figure (A3.1).

The stream tube has a cross-sectional area larger than the cross-sectional area for the upstream disc and a smaller area than the downstream disc. Within the stream tube, continuity is required and the rate of the mass flow must be constant.

$$\dot{m} = \left| \rho_\infty A_\infty U_\infty \right| = \left| \rho_o A_o U_o \right| = \left| \rho_w A_w U_w \right| \qquad \text{A3.1}$$

By introducing an axial interference factor, a, as the fractional decrease in wind velocity between the free stream and the rotor plane represented by

$$a = \frac{v}{U_\infty} \qquad \text{A3.2}$$

It is found that

$$U_o = U_\infty (1 - a) \qquad \text{A3.3}$$

The air, which passes through the disk, undergoes an overall change in velocity. The velocity multiplied by the flow rate gives the rate of change of momentum, more known as a force

$$T = \dot{L} = \dot{m}(U_\infty - U_w) \qquad \text{A3.4}$$

Combining the equations above with the fact that the change of momentum comes entirely from the pressure difference across the actuator disc, it is obtained that

$$p_o^+ - p_o^- = (U_\infty - U_w)\rho_o A_o (1 - a) U_\infty \qquad \text{A3.5}$$

To obtain the pressure difference, the Bernoulli's equation is applied separately to the upstream and downstream sections of the stream tube. For the upstream section it becomes

$$\frac{1}{2}\rho U_\infty^2 + p_\infty = \frac{1}{2}\rho U_o^2 + p_o^+ \qquad \text{A3.6}$$

Similarly, downstream

$$\frac{1}{2}\rho U_w^2 + p_\infty = \frac{1}{2}\rho U_o^2 + p_o^- \qquad \text{A3.7}$$

Subtracting A3.6 from A3.7 yields

$$p_o^+ - p_o^- = \frac{1}{2}\rho (U_\infty^2 - U_w^2) \qquad \text{A3.8}$$

Equations A3.8 and A3.5 gives

$$U_w = (1-2a)U_\infty \qquad \textbf{A3.9}$$

Substituting A3.9, A3.3, and A3.1 into A3.4 obtains the force, T, which gives

$$T = 2\rho A_o U_\infty^2 a(1-a) \qquad \textbf{A3.10}$$

Combining A3.3, A3.9 and the rate of work done by the force; $P = T U_o$ **the power extraction from the air is obtained as:**

$$P = 2\rho A_o U_\infty^3 a(1-a)^2 \qquad \textbf{A3.11}$$

Or, by introducing the dimensionless power coefficient, $C_p = 4a(1-a)^2$

$$P = \frac{1}{2}\rho A_o U_\infty^3 C_p \qquad \textbf{A3.12}$$

The power coefficient represents the efficiency of the turbine, which depends on variables like the wind speed, the rotor speed and the pitch angle. The coefficient shows how much of the kinetic energy in the air stream that is transformed into mechanical energy. The maximum C_p **as a function of** a **is** $C_p = {}^{16}\!/_{27} \cong 0.59$ **, at** $a = {}^{1}\!/_{3}$ **(obtained by taking the first derivative of the power coefficient** $C_p = 4a(1-a)^2$ **with respect to 'a' and equating it to zero).**

The maximum value of C_p **= 0.59 is called the Betz limit and applies to all types of wind turbines. Intuitively there must be a wind speed change at which the conversion efficiency is maximum. If there were no change in wind speed, no energy would be extracted, and the power of the wind turbine would be zero. If the air were brought completely to rest, all its energy would dissipate. However, a rotating wind turbine will not completely prevent the flow of air, so it can only extract a proportion of the kinetic energy in the wind. Hence in terms of force exerted by wind on rotor area based on this assumption pressure is underestimated on blades. Therefore, its use for predicting these forces is in decline. Modern wind turbines operate at performance coefficient of about 0.4.**

A3.1.2 Blade Element Theory:

For the use of aeroelastic codes in design calculations, the aerodynamic method has to be very time efficient. The Blade Element Momentum (BEM) theory has been shown to give good accuracy with respect to time cost.

In this method, the turbine blades are divided into a number of independent

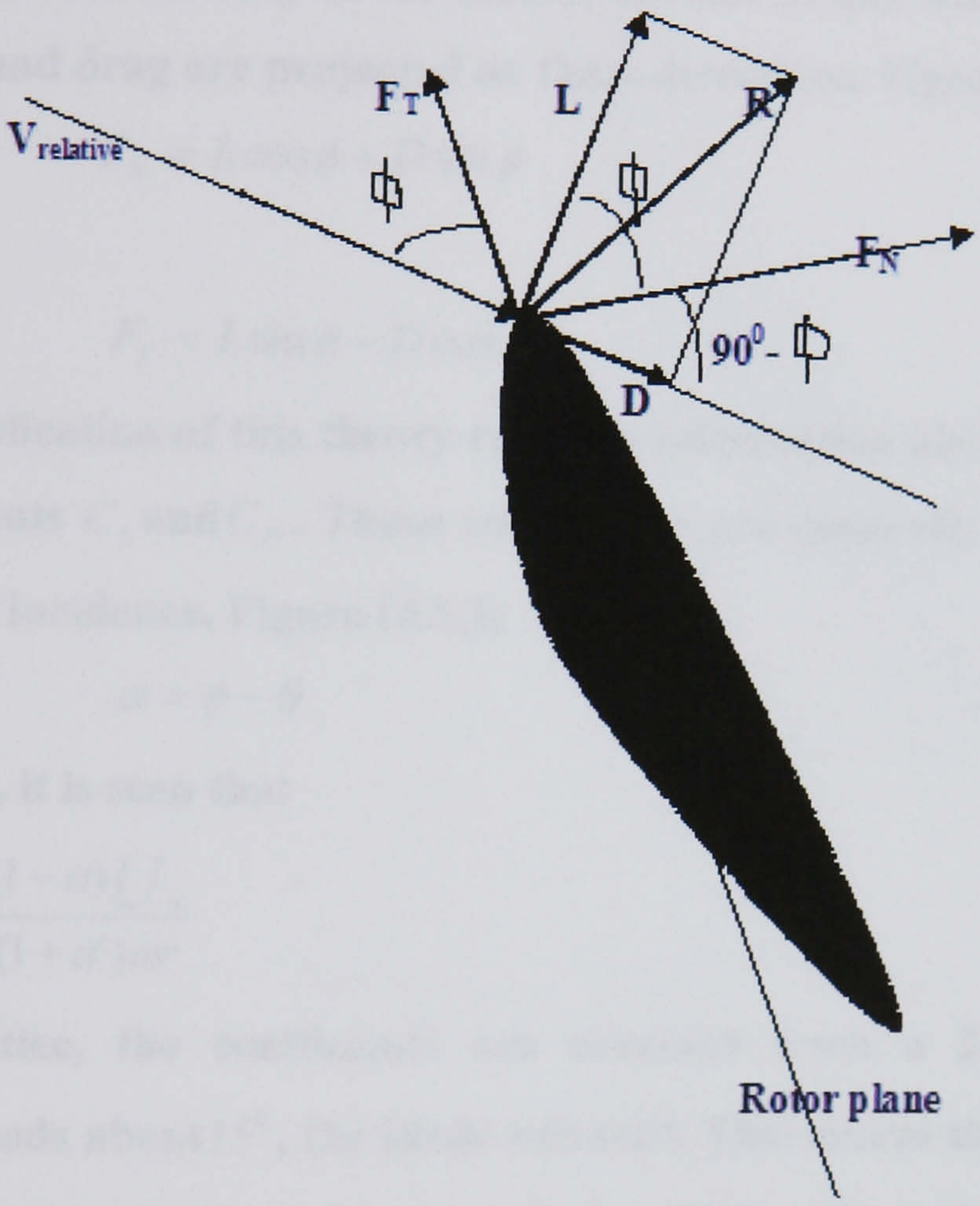

Figure (A3.2) Load forces on blade section

elements along the length of the blade. At each section, a force balance is applied involving 2-D section lift and drag with the thrust and torque produced by the section. At the same time, a balance of axial and angular momentum is applied. This produces a set of non-linear equations, which can be solved numerically for each blade section, the presented discussion follows Andres [125] and Det Norske [88], only the force in the flow direction was regarded. The BEM theory, also takes notice of the tangential force due to the torque in the shaft. The left force L per unit length is perpendicular to the relative speed V_{rel} of the wind and equals:

$$L = \frac{\rho c}{2} V_{rel}^2 C_L \qquad \text{A3.13}$$

Where c is the blade chord length. The drag force D per unit length, which is parallel to V_{rel} is given by

$$D = \frac{\rho c}{2} V_{rel}^2 C_D \qquad \text{A3.14}$$

Since the interest only in the forces, normal to and tangential to the rotor-plane, the lift and drag are projected on these directions, Figure (A3.2).

$$F_N = L\cos\phi + D\sin\phi \qquad \text{A3.15}$$

And

$$F_T = L\sin\phi - D\cos\phi \qquad \text{A3.16}$$

The application of this theory requires information about the lift and drag airfoil coefficients C_L and C_D. Those coefficients are generally given as functions of the angle of incidence, Figure (A3.3)

$$\alpha = \phi - \theta \qquad \text{A3.17}$$

Further, it is seen that

$$\tan\phi = \frac{(1-a)U_\infty}{(1+a')\omega r} \qquad \text{A3.18}$$

In practice, the coefficients are obtained from a 2D wind tunnel tests. If α exceeds about 15^0, the blade will stall. This means that the boundary layer on the upper surface becomes turbulent, which will result in a radical increase of drag and a decrease of lift. The lift and drag coefficients need to be projected onto the normal and tangential directions.

$$C_N = C_L\cos\phi + C_D\sin\phi \qquad \text{A3.19}$$

And

$$C_T = C_L\sin\phi - C_D\cos\phi \qquad \text{A3.20}$$

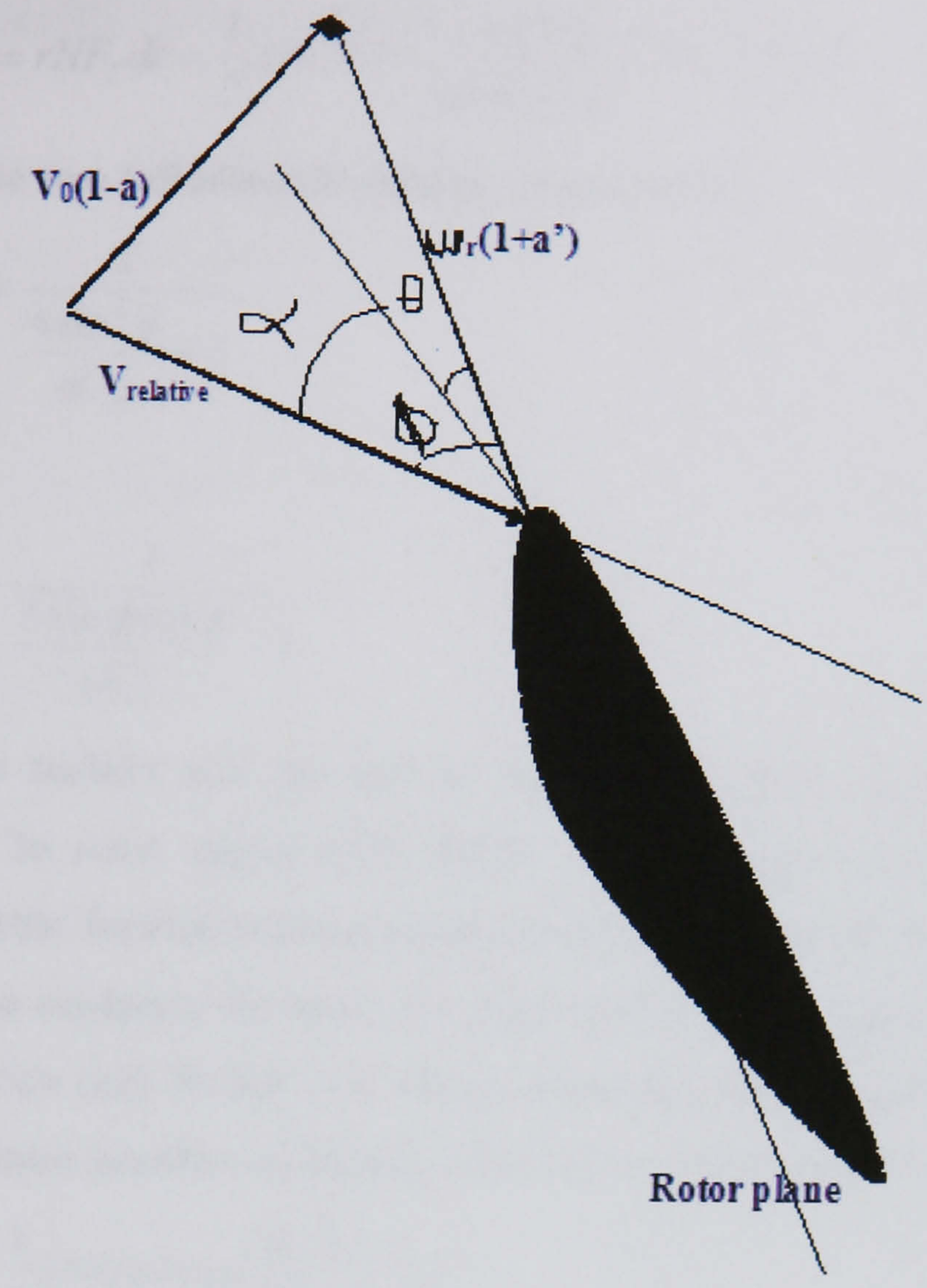

Figure (A3.3) Velocities at rotor plane

Further, a solidify σ is defined as the fraction of the annular area in the control volume, which is covered by the blades

$$\sigma(r) = \frac{c_r B}{2\pi r} \qquad \text{A3.21}$$

Where B denotes the number of blades.

The normal force and the torque on the control volume of thickness dr since $F_N and F_T$ are forces per length

$$dT = NF_N dr = \frac{1}{2}\rho N \frac{U_\infty^2 (1-a)^2}{\sin^2 \phi} c C_N dr \qquad \text{A3.22}$$

And

$$dQ = rNF_T dr = \frac{1}{2}\rho N \frac{U_\infty (1-a)\omega r(1+a')}{\sin\phi\cos\phi} cC_L r dr \qquad \textbf{A3.23}$$

Finally, the two influence factors are declared by

$$a = \frac{1}{\frac{4\sin^2\phi}{\sigma C_N} + 1} \qquad \textbf{A3.24}$$

And

$$a' = \frac{1}{\frac{4\sin\phi\cos\phi}{\sigma C_T} - 1} \qquad \textbf{A3.25}$$

These two factors are the key to establish a value for the forces normal and tangential to rotor plane using BEM. These factors are partially empirical and solution could be attained via iteration for each value of r/R.

To increase accuracy tip loss correction factor need be applied, this is to allow for the velocities and forces not being circumferentially uniform due to the rotor having a finite number of blades. This factor is expressed as:

$$F = \frac{2}{\pi}\arccos(\exp(\frac{B}{2}\frac{R-r}{r\sin\phi})) \qquad \textbf{A3.26}$$

This reduction factor is called Prandtl's tip loss factor Det Norske [88].

This is yields:

$$a = \frac{1}{\frac{4F\sin^2\phi}{\sigma C_N} + 1} \qquad \textbf{A3.27}$$

$$a' = \frac{1}{\left(\frac{4F\sin\phi\cos\phi}{\sigma C r} - 1\right)} \qquad \textbf{A3.28}$$

All terms as defined before.

More practical implementation of this method is further detailed in Chapter V of this thesis. Results of the iteration done using the MathCAD software to arrive at linear pressure profile for typical one case blade parameters are shown next to this paragraph.

A.3.1.3 MathCAD sheet for blade wind load typical iteration:

Calculation of Forces on Blades

$kN := 1000 \cdot N$

Initialise Variables $a := 0$ $a_1 := 0$ $V_0 := 12.5 \cdot m \cdot sec^{-1}$ $\omega := 2.31 rad \cdot sec^{-1}$

$B := 3$ $R := 30 \cdot m$

Rotor Blade Chosen : RISΦ-1 airfoil

$Re := 1.6 \cdot 10^6$

Input parameters

$r := 10 \cdot m$ $\theta := 10.6 \cdot deg$ $c := 0.604 \cdot m$

Iteration No 1

$$\phi := \operatorname{atan}\left[\frac{(1-a)\cdot V_0}{(1+a_1)\cdot\omega\cdot r}\right] \qquad \phi = 28.419\,\text{deg}$$

Pitch Angle $\alpha := \phi - \theta$ $\alpha = 17.819\,\text{deg}$

Using alpha, calculate Lift and Drag coefficients:

$\alpha lpha_1 := 3\cdot\text{deg}$ $\alpha lpha_2 := 5\cdot\text{deg}$ $\alpha lpha_3 := 10\cdot\text{deg}$ $\alpha lpha_4 := 15\cdot\text{deg}$

$\alpha lpha_5 := 20\cdot\text{deg}$ $\alpha lpha_6 := 25\cdot\text{deg}$

$CL_1 := 0.6$ $CL_2 := 0.94$ $CL_3 := 1.21$ $CL_4 := 1.25$ $CL_5 := 1.18$ $CL_6 := 0.98$

$CD_1 := 0$ $CD_2 := 0$ $CD_3 := 0.03$ $CD_4 := 0.085$ $CD_5 := 0.16$ $CD_6 := 0.32$

$C_L := \text{linterp}(\alpha lpha, CL, \alpha)$ $C_L = 1.211$

$C_D := \text{linterp}(\alpha lpha, CD, \alpha)$ $C_D = 0.127$

Normal Force Coeffiecient $C_N := C_L\cdot\cos(\phi) + C_D\cdot\sin(\phi)$ $C_N = 1.125$

Tangential Force Coefficient $C_T := C_L\cdot\sin(\phi) - C_D\cdot\cos(\phi)$ $C_T = 0.464$

$\sigma_r := \frac{c\cdot B}{2\cdot\pi\cdot r}$ $\sigma_r = 0.029$

$F := \frac{2}{\pi}\cdot\operatorname{acos}\left(e^{-B\cdot\frac{R-r}{2\cdot r\cdot\sin(\phi)}}\right)$ $F = 0.999$

$a := \frac{1}{\frac{4\cdot F\cdot\sin(\phi)^2}{\sigma_r\cdot C_N} + 1}$ $a = 0.035$

$a_1 := \frac{1}{\frac{4\cdot F\cdot\sin(\phi)\cdot\cos(\phi)}{\sigma_r\cdot C_T} - 1}$ $a_1 = 8.069\times 10^{-3}$

Iteration No 2

$$\phi := \operatorname{atan}\left[\frac{(1-a)\cdot V_0}{(1+a_1)\cdot\omega\cdot r}\right] \qquad \phi = 27.394\,\text{deg}$$

Pitch Angle $\alpha := \phi - \theta$ $\alpha = 16.794\,\text{deg}$

Using alpha, calculate Lift and Drag coefficients:

$alpha_1 := 3\cdot\text{deg}$ $alpha_2 := 5\cdot\text{deg}$ $alpha_3 := 10\cdot\text{deg}$ $alpha_4 := 15\cdot\text{deg}$

$alpha_5 := 20\cdot\text{deg}$ $alpha_6 := 25\cdot\text{deg}$

$CL_1 := 0.55$ $CL_2 := 0.9$ $CL_3 := 1.2$ $CL_4 := 1.25$ $CL_5 := 1.2$ $CL_6 := 1.0$

$CD_1 := 0$ $CD_2 := 0$ $CD_3 := 0.03$ $CD_4 := 0.085$ $CD_5 := 0.18$ $CD_6 := 0.31$

$C_L := \text{linterp}(alpha, CL, \alpha)$ $C_L = 1.232$

$C_D := \text{linterp}(alpha, CD, \alpha)$ $C_D = 0.119$

Normal Force Coeffiecient $C_N := C_L\cdot\cos(\phi) + C_D\cdot\sin(\phi)$ $C_N = 1.149$

Tangential Force Coefficient $C_T := C_L\cdot\sin(\phi) - C_D\cdot\cos(\phi)$ $C_T = 0.461$

$$\sigma_r := \frac{c\cdot B}{2\cdot\pi\cdot r} \qquad \sigma_r = 0.029$$

$$F := \frac{2}{\pi}\cdot\operatorname{acos}\left(e^{-B\cdot\frac{R-r}{2\cdot r\cdot\sin(\phi)}}\right) \qquad F = 0.999$$

$$a := \frac{1}{\frac{4\cdot F\cdot\sin(\phi)^2}{\sigma_r\cdot C_N} + 1} \qquad a = 0.038$$

$$a_1 := \frac{1}{\frac{4\cdot F\cdot\sin(\phi)\cdot\cos(\phi)}{\sigma_r\cdot C_T} - 1} \qquad a_1 = 8.213\times 10^{-3}$$

Iteration No 3

$$\phi := \operatorname{atan}\left[\frac{(1-a)\cdot V_0}{(1+a_1)\cdot\omega\cdot r}\right] \qquad \phi = 27.316\,\text{deg}$$

Pitch Angle $\alpha := \phi - \theta$ $\alpha = 16.716\,\text{deg}$

Using alpha, calculate Lift and Drag coefficients:

$\alpha lpha_1 := 3\cdot\text{deg}$ $\alpha lpha_2 := 5\cdot\text{deg}$ $\alpha lpha_3 := 10\cdot\text{deg}$ $\alpha lpha_4 := 15\cdot\text{deg}$

$\alpha lpha_5 := 20\cdot\text{deg}$ $\alpha lpha_6 := 25\cdot\text{deg}$

$CL_1 := 0.55$ $CL_2 := 0.9$ $CL_3 := 1.2$ $CL_4 := 1.25$ $CL_5 := 1.2$ $CL_6 := 1.0$

$CD_1 := 0$ $CD_2 := 0$ $CD_3 := 0.03$ $CD_4 := 0.085$ $CD_5 := 0.18$ $CD_6 := 0.31$

$C_L := \text{linterp}(\alpha lpha, CL, \alpha)$ $C_L = 1.233$

$C_D := \text{linterp}(\alpha lpha, CD, \alpha)$ $C_D = 0.118$

Normal Force Coeffiecient $C_N := C_L\cdot\cos(\phi) + C_D\cdot\sin(\phi)$ $C_N = 1.149$

Tangential Force Coefficient $C_T := C_L\cdot\sin(\phi) - C_D\cdot\cos(\phi)$ $C_T = 0.461$

$$\sigma_r := \frac{c\cdot B}{2\cdot\pi\cdot r} \qquad \sigma_r = 0.029$$

$$F := \frac{2}{\pi}\cdot\operatorname{acos}\left(e^{-B\cdot\frac{R-r}{2\cdot r\cdot\sin(\phi)}}\right) \qquad F = 0.999$$

$$a := \frac{1}{\frac{4\cdot F\cdot\sin(\phi)^2}{\sigma_r\cdot C_N} + 1} \qquad a = 0.038$$

$$a_1 := \frac{1}{\frac{4\cdot F\cdot\sin(\phi)\cdot\cos(\phi)}{\sigma_r\cdot C_T} - 1} \qquad a_1 = 8.231\times 10^{-3}$$

FINAL FORCES

$$K := \frac{4 \cdot F \cdot \sin(\phi)^2}{\sigma_r \cdot C_N} \qquad a_c := 0.2$$

$$a := \text{if}\left[a < 0.2, a, 0.5 \cdot \left[2 + K \cdot \left(1 - 2 \cdot a_c\right) - \sqrt{\left[K \cdot \left(1 - 2 \cdot a_c\right) + 2\right]^2 + 4 \cdot \left(K \cdot a_c^{\,2} - 1\right)}\right]\right]$$

$$\rho := 1.025 \cdot kg \cdot m^{-3} \qquad r = 10\,m$$

$$F_N := 0.5 \cdot \rho \cdot \frac{V_0^{\,2} \cdot (1 - a)^2}{\sin(\phi)^2} \cdot \left(c \cdot C_N\right) \qquad F_N = 244.45\,N \cdot m^{-1}$$

$$F_T := 0.5 \cdot \rho \cdot \frac{V_0 \cdot (1 - a) \cdot \omega \cdot r \cdot \left(1 + a_1\right)}{\sin(\phi) \cdot \cos(\phi)} \cdot c \cdot C_T \qquad F_T = 98.102\,N \cdot m^{-1}$$

$$\lambda := 10 \cdot deg$$

Resolve Forces

$$F_{res} := \sqrt{F_N^{\,2} + F_T^{\,2}} \qquad F_{res} = 263.4\,N \cdot m^{-1}$$

$$FORCE_N := F_N \cdot \cos(\lambda) + F_T \cdot \sin(\lambda) \qquad FORCE_N = 257.771\,N \cdot m^{-1}$$

$$FORCE_T := -F_N \cdot (\sin(\lambda)) + F_T \cdot \cos(\lambda) \qquad FORCE_T = 54.163\,N \cdot m^{-1}$$

$$F_{res} := \sqrt{FORCE_N^{\,2} + FORCE_T^{\,2}}$$

$$F_{res} = 263.4\,N \cdot m^{-1}$$

$$Forces_0 := FORCE_N$$

$$Forces_1 := FORCE_T$$

$$Forces = \begin{array}{|c|c|} \hline & 0 \\ \hline 0 & 257.771 \\ \hline 1 & 54.163 \\ \hline \end{array} \; N \cdot m^{-1}$$

Appendix-A4 MathCAD sheet for Grüneisen equation for water:

Gruneisen Equation of State for Fluid pressure:

$p := 0$ $\rho_o := 1025$

$C := 1647$ $\mu := 1.002 \cdot 10^{-03}$ $\gamma_0 := 0.35$ $a := 0$

$S_1 := 1.921$ $S_2 := -0.096$ $S_3 := 0$

$$k := \frac{\rho_o \cdot C^2 \cdot \mu \cdot \left[1 + \left(1 - \frac{\gamma_0}{2}\right) \cdot \mu - \frac{a}{2} \cdot \mu^2\right]}{\left[1 - (S_1 - 1) \cdot \mu - S_2 \cdot \frac{\mu^2}{\mu + 1} - S_3 \cdot \frac{\mu^3}{(\mu + 1)^2}\right]^2}$$

$k = 2.793 \times 10^6$

$$\frac{p - k}{\gamma_0 + a \cdot \mu} = -7.981 \times 10^6$$